การประเมินค่าแหล่งกำเนิดแสงแอลอีดีด้วยวิธีการวิเคราะห์แบบไทรโครแมติกโดยใช้กล้องดิจิทัล

นายธีศิษฏ์ วราภาสกุล

วิทยานิพนธ์นี้เป็นส่วนหนึ่งของการศึกษาตามหลักสูตรปริญญาวิทยาศาสตรดุษฎีบัณฑิต
สาขาวิชาเทคโนโลยีทางภาพ ภาควิชาเทคโนโลยีทางภาพและการพิมพ์
คณะวิทยาศาสตร์ จุฬาลงกรณ์มหาวิทยาลัย
ปีการศึกษา 2557

EVALUATING LED LIGHT SOURCES BY MEANS OF TRICHROMATIC ANALYSIS USING A DIGITAL CAMERA

Mr. Teesit Varapaskul

A Dissertation Submitted in Partial Fulfillment of the Requirements
for the Degree of Doctor of Philosophy Program in Imaging Technology
Department of Imaging and Printing Technology
Faculty of Science
Chulalongkorn University
Academic Year 2014

Thesis Title	EVALUATING LED LIGHT SOURCES BY MEANS OF TRICHROMATIC ANALYSIS USING A DIGITAL CAMERA
By	Mr. Teesit Varapaskul
Field of Study	Imaging Technology
Thesis Advisor	Associate Professor Pichayada Katemake, Ph.D.
Thesis Co-Advisor	Dipl.Eng. Razvan Ion Preda, Ph.D.

Accepted by the Faculty of Science, Chulalongkorn University in Partial Fulfillment of the Requirements for the Doctoral Degree

.....Dean of the Faculty of Science
(Professor Supot Hannongbua, Ph.D.)

THESIS COMMITTEE

.....Chairman
(Assistant Professor Chawan Koopipat, Ph.D.)
.....Thesis Advisor
(Associate Professor Pichayada Katemake, Ph.D.)
.....Thesis Co-Advisor
(Dipl.Eng. Razvan Ion Preda, Ph.D.)
.....Examiner
(Associate Professor Aran Hansuebsai, Ph.D.)
.....Examiner
(Associate Professor Pontawee Pungrassamee)
.....External Examiner
(D.Eng. Thananchai Piroonpan)

ธีศิษฏ์ วราภาสกุล : การประเมินค่าแหล่งกำเนิดแสงแอลอีดีด้วยวิธีการวิเคราะห์แบบไทรโครแมติกโดยใช้กล้องดิจิทัล (EVALUATING LED LIGHT SOURCES BY MEANS OF TRICHROMATIC ANALYSIS USING A DIGITAL CAMERA) อ.ที่ปรึกษาวิทยานิพนธ์หลัก: รศ. ดร. พิชญดา เกตุเมฆ, อ.ที่ปรึกษาวิทยานิพนธ์ร่วม: ดร. ราสวัน อิออน เปรดา, 245 หน้า.

งานวิจัยนี้มีจุดมุ่งหมายเพื่อสาธิตว่ากล้องดิจิทัลชนิดสะท้อนแสงเลนส์เดี่ยว (DSLR) สามารถใช้เป็นอุปกรณ์ทางเลือก สำหรับประเมินคุณภาพแหล่งกำเนิดแสงชนิดแอลอีดี ในด้านการแสดงสีให้เหมือนกับแหล่งแสงอ้างอิง กระบวนการทดลองได้ออกแบบจากสมมติฐานที่ว่า สาเหตุของการตอบสนองที่มีความสัมพันธ์ไม่เป็นเส้นตรงกับค่าสีในกล้องดิจิทัล ทำให้เกิดข้อผิดพลาดที่ยังยอมรับได้ เฉพาะกับสีที่อยู่ในขอบเขตที่กำหนดภายใต้ปริภูมิสีเอสอาร์จีบี (sRGB) เท่านั้น หรืออาจกล่าวได้ว่า เมื่อภาพถูกถ่ายภายใต้สภาวะที่จำกัดสภาวะหนึ่ง พฤติกรรมของกล้องดิจิทัลสามารถถูกพิจารณาว่ามีความสัมพันธ์ใกล้เคียงกับความเป็นเส้นตรงสำหรับจำนวนสีและขอบเขตสีที่กำหนดเท่านั้น และให้ค่าสีเชิงคำนวณ (colorimetric results) ของภาพดิจิทัล ที่บันทึกภายใต้แหล่งแสงทดสอบ และแหล่งแสงอ้างอิงที่มีความหมาย การสาธิตในงานวิจัยนี้ใช้ตัวอย่างสีที่อยู่ในปริภูมิสีที่กำหนด (color-space regions) และแหล่งกำเนิดแสงที่นำมาใช้ในการทดลองนี้ประกอบด้วยหลอดไฟ 4 ชนิด แหล่งกำเนิดแสงชนิดฟลูออเรสเซนต์ (fluorescent lamp) 2 ชนิด นำมาใช้ในการทดลองนี้เพื่อเป็นแหล่งกำเนิดแสงอ้างอิง และแหล่งกำเนิดแสงชนิดแอลอีดี 2 ชนิด นำมาใช้ในการทดลองนี้เพื่อเป็นแหล่งกำเนิดแสงทดสอบ นอกจากนี้กล้องดิจิทัลที่ใช้นั้น เป็นกล้องดิจิทัล 5 ชนิด ที่มีความแตกต่างกันทั้งในด้านผู้ผลิตและโครงสร้างของตัวรับแสง (CMOS = 3, CCD = 2) การถ่ายภาพในการทดลองนี้ถ่ายภาพตัวอย่างสีในตำแหน่ง 45 องศา ภายใต้แหล่งกำเนิดแสงที่ถูกติดตั้งให้อยู่ในตำแหน่งกึ่งกลางของตู้ทดลองที่มีสีดำ ตัวอย่างสีที่ใช้ในการทดลองนี้ เป็นตัวอย่างสีที่มีสีสันจำนวน 24 ตัวอย่าง และตัวอย่างสีชนิดไม่มีสีสัน 6 ตัวอย่าง โดยตัวอย่างชนิดที่ไม่มีสีสันนั้น นำมาใช้เพื่อคำนวณหาสมการเส้นตรงที่เหมาะสมและเป็นตัวแทนของข้อมูล (best fit function) ในแต่ละค่าสีทั้ง 3 ชนิด แดง เขียว และ น้ำเงิน (RGB channels) ของภาพถ่าย กระบวนการหาความสัมพันธ์เชิงเส้นตรง (linearization) ของค่าสีชนิดสี แดง เขียว น้ำเงิน นั้นคำนวณจากความสัมพันธ์ของค่าการสะท้อนแสงของตัวอย่างสีเทา (N2, N3.5, N5, N6.5, N8, และ N9.5) ที่ความยาวคลื่น 640, 530, และ 480 นาโนเมตร กับค่าสี แดง เขียว น้ำเงิน (RGB) ของตัวอย่างสีเทา กระบวนการในการคัดเลือกตัวอย่างสีที่ใช้ในการทดลองนี้ ใช้วิธีหาความแตกต่างสี (ΔE_{00}) ของตัวอย่างสีภายใต้แหล่งกำเนิดแสงทั้งสองชนิดที่วัดด้วยเครื่องวัดสีชนิด สเปกโตรโฟโตมิเตอร์ (spectrophotometer) และกล้องดิจิทัล ที่อุณหภูมิสี 6500 เคลวิน ถ้าค่าความแตกต่างสีระหว่าง 2 อุปกรณ์วัดสี มีค่ามากกว่า 6 ตัวอย่างสีนั้นจะถูกเปลี่ยนทดแทนด้วยตัวอย่างสีที่มีสีสันเดิม แต่ค่าความอิ่มตัวสีน้อยลง ผลการทดลองพบว่าค่าเฉลี่ยของความแตกต่างสีระหว่างค่าสีที่วัดด้วยเครื่องสเปกโตรเรดิโอมิเตอร์ (spectroradiometer) และกล้องดิจิทัล มีค่าน้อยกว่า 2.16 สำหรับกล้องที่มีตัวรับแสงชนิดซีซีดี (CCD) และมีค่าน้อยกว่า 3.82 สำหรับกล้องชนิดตัวรับแสงชนิดซีมอส (CMOS) ภายใต้แหล่งกำเนิดแสงทั้งสองชนิด ถึงแม้ว่าค่าเฉลี่ยของความแตกต่างสีระหว่างสองอุปกรณ์ทั้งสองนั้นจะมีค่าน้อยมาก แต่ยังไม่สำคัญเท่าค่าความแตกต่างระหว่างความต่างสีระหว่างอุปกรณ์ทั้งสองชนิด เนื่องจากจุดประสงค์ของงานวิจัยนี้ต้องการใช้กล้องดิจิทัลเป็นทางเลือก เพื่อวัดสีของวัตถุในเชิงเปรียบเทียบ และประเมินคุณภาพของแหล่งกำเนิดแสง

ภาควิชา	เทคโนโลยีทางภาพและการพิมพ์	ลายมือชื่อนิสิต	.....
สาขาวิชา	เทคโนโลยีทางภาพ	ลายมือชื่อ อ.ที่ปรึกษาหลัก	.....
ปีการศึกษา	2557	ลายมือชื่อ อ.ที่ปรึกษาร่วม	.....

5273929723 : MAJOR IMAGING TECHNOLOGY
KEYWORDS: TRICHROMATIC / LED / DIGITAL CAMERA

TEESIT VARAPASKUL: EVALUATING LED LIGHT SOURCES BY MEANS OF TRICHROMATIC ANALYSIS USING A DIGITAL CAMERA. ADVISOR: ASSOC. PROF. PICHAYADA KATEMAKE, Ph.D., CO-ADVISOR: DIPL.ENG. RAZVAN ION PREDA, Ph.D., 245 pp.

This research aimed to demonstrate that digital single lens reflex cameras (DSLR) could be used as an alternative device for evaluating the quality of LED light sources in terms of color rendering performance. The methodology presented in this work is developed from the assumption that the causes for non-linear response to color signals in digital cameras produce acceptable errors in some defined color-regions across the sRGB color-space, under determined conditions. In other words, it is assumed that when pictures are taken under particular constrained conditions, the digital cameras' behavior can be considered linear for a variable but determined number of colors within color-space volumes of the sRGB color-space, which could be properly distributed for obtaining meaningful colorimetric results of the color-shifts calculated from digital images recorded under the reference and test light sources. The demonstration for the existence of these color-space regions was carried out with 4 artificial light sources: 2 fluorescent lamps (reference source) and 2 LED bulbs (test source), 5 DSLR cameras: 2 with CCD sensors and 3 with CMOS sensors with specific settings, a black box, a 6-neutral-wheel for determining the best shooting position and a final 30-color-wheel, which has been used throughout the color selection process. The color-wheel has 24 colors and 6 neutrals for calculating the best fit functions on the red, green and blue channels of each individual captured image. The color samples selection process was carried out for minimizing the ΔE_{00} between spectrophotometric CIE $L^*a^*b^*$ and camera calculated CIE $L^*a^*b^*$ to less than 6 units under both types of light sources having color temperatures of 6500 Kelvin. The linearization of R, G and B values was done by using reflectance factors of the N2, N3.5, N5, N6.5, N8 and N9.5 Munsell samples at 640nm, 530nm and 480nm respectively. The average CIE color difference 2000 formula (ΔE_{00}) between spectroradiometric CIE $L^*a^*b^*$ and calculated CIE $L^*a^*b^*$ from testing and verifying cameras is less than 2.16 for CCD sensor camera and less than 3.82 for CMOS sensor camera under 2 types of light sources. However, the difference of ΔE_{00} across reference and test light source for spectroradiometer and camera are more important. The differences of the color shifts between reference light source and test light source, calculated from the digital pictures, in this study were close enough to the colorimetric measured ones in order to allow the alternative selection of digital cameras over colorimetric devices in the light quality assessment process.

Department:	Imaging and Printing Technology	Student's Signature .....
		Advisor's Signature .....
Field of Study:	Imaging Technology	Co-Advisor's Signature .....
Academic Year:	2014	

ACKNOWLEDGEMENTS

Above all, I wish to express my sincere appreciation to my advisor, Associate Professor Dr. Pichayada Katemake and co-advisor, Dr. Eng. Razvan Ion Preda for their invaluable suggestions and help throughout five years of work.

I would like to thank my wife Duangkamol Thanomsaksri and my beloved daughter and son for their constant support and unconditional love at all time.

I would like to acknowledge the financial support of Chulalongkorn University, especially THE 90th ANNIVERSARY OF CHULALONGKORN UNIVERSITY FUND (Ratchadaphiseksomphot Endowment Fund) for funding source of materials and expense related to this Ph.D. research and the fund from Chulalongkorn graduation school titled Dussadee Bundit Pue Pattana-Sat for my study.

I would like to thank the member of my Ph.D. committee, Assistant Prof. Dr. Chawan Koopipat, Associate Prof. Pontawee Pungrassamee, Associate Prof. Dr. Aran Hansuebsai and Dr. Thananchai Piroonpan for their suggestions.

CONTENTS

Page

Page

List of Figures

List of Tables

FORWARD

LED (Light Emitting Diode) light properties are evaluated today using colorimetric devices, generally spectroradiometers and illuminance spectrophotometers. This work aims to demonstrate that digital single lens reflex camera (DSLR) can be used as an alternative device for evaluating the quality of LED light source in terms of color rendering performance. The evaluation process of LED light quality according to the limited reliability of colour output obtained from digital pictures taken in constrained environment. This new way could be used as a cost-effective alternative method to the classic evaluation method.

The thesis has 7 chapters divided into 2 parts. The first 3 chapters consist of literature review and the last 4 chapters represent the original contributions and conclusions.

Chapter 1 presents introductory notions: light, light properties, light sources focusing on Light Emitting Diodes and light quality. It explains briefly the science fields reflected in this work: photometry, colorimetry and describes the main difference of colorimetric equipments versus digital image acquisition devices.

Chapter 2 shows how colour systems appeared and why. It presents how several colour systems evolved into the ones we know today describing in more detail the Munsell colour system and the CIELAB system, which are integrating part of the experiments and calculation processes of the original contribution section.

Chapter 3 shows light quality assessment methods, focusing on existing and proposed ways evaluate LED light sources. It describes the Colour Rendering Index (CRI) in detail, as the only accepted way for evaluating light at the moment of writing this thesis, mentioning its weaknesses and summarizing the research that is done for addressing the problems arising from using CRI. It summarizes the chromatic adaptation transform, setting weight on the Von Kries transform, which is used in the calculation of the Colour Rendering Index.

Chapter 4 presents the proposed methodology for using SLR digital cameras as an alternative device for light quality assessment. It enumerates the principles and the assumptions that govern the possibility of emitting such a method. The reasoning is explained and proven by an experimental process that is described in detail. Two

technically modest commercial lamps were used in the experiment (one fluorescent, one LED) to be sure that results would only improve by using better ones. For the same reason, the selected cameras were inexpensive and not completely new, entry levels in their series at the time they were produced.

Chapter 5 describes in detail the calculation processes that are part of the proposed method with many references to chapter 4, which is the backbone of the mathematical formulations and numerical solutions presented here. Parts of the algorithms are shown directly in Visual Basic code.

Chapter 6 presents the results. This chapter is divided in 2 sections. The first section describes the intermediary results obtained in the development of the proposed method, resuming the experimental steps that led to these results. The second part presents light quality assessments for the light sources presented in chapter 4.

Chapter 7 is a short list of conclusions regarding the method, calculations and results.

Appendices contain additional data sets for intermediary results and the results obtained with a 3 verifying SLR digital cameras. It is important to understand that the colours printed in this work cannot be accurate renditions of the actual hues due to the unexpected colour output of the printing process combined with the unpredictable influence of the paper support on the printed colour.

I wish to thank to my scientific coordinators Assoc. Prof. Dr. Pichayada Katemake and Dr. Eng Razvan I. Preda for their immense support.

CHAPTER 1

INTRODUCTION

1.1 Light

"Light" is a notion familiar to everyone but what is light exactly and since when is it studied?

The first source of light has been the sun, without which, life as we know it would not exist. Light has been studied throughout history, starting with the ancient Greek scientists and is still an object of study today. In the beginnings light was not distinguished from sight.

Plato mistakably believed that vision issued of out from the eye (Gross 1999). Empedocles correctly assumed that light travels with finite speed (Sarton 1952). Aristotle explained rainbows as a sort of reflection off of raindrops (Caes 2001). Euclid harnessed light through mirror reflection. Ptolemy is the first known scientist to experiment with optics and collect data (Riley 1995). His work was further developed by the Egyptian scientist Alhazen, who was the first to draw ray diagrams and to discount Plato's theory (Zewail and Thomas 2010). All these studies of ancient philosophers on light are referenced from English translations of published materials (Stratton 1917, Diels and Kranz 1949, Stratton 1964, Kirk, Raven et al. 1983). Each of these philosophers are supposed to have written whole books, but none of them were preserved. Ptolemy's "Optics", written 7 centuries after Plato, from which parts survived as a Latin version might not be identical to original. View of these ancient philosophers surface in the writings of authors, some of whom had lived nearly a millennium after the writers in question. Many advances were made after the 16^{th} century by scientists such as Galileo Galilei, Johannes Kepler, René Descartes, Willebrord Snell. The last two developed independently the law of refraction, based on the earlier work of Alhazen (Hog 2008). Robert Hooks developed a "pulse theory" and compared the spreading of light to that of waves in water. He suggested that light's vibrations could be perpendicular to the direction of propagation.

Sir Isaac Newton, based on the work of Pierre Gassendi, emitted the theory that light is composed of particles. During his life was a growing debate over whether light behaved as a particle or a wave, but due to Newton's prestige, the particle theory was accepted for almost a century (Hooke 1757). One of Newton's arguments against the wave nature of light was that waves bend around obstacles while light travels only in straight line. Newton published his theory in his treatise "Opticks" (Newton 1730) 17 years after his work "Principia" and after Robert Hook's death.

In 1801 to 1803, depending on source (Schneider 1986, Andrew 2006) Thomas Young reported his double-slit experiment that clearly showed light to diffract and thus travel as a wave. Fizeau and Foucault showed in 1850, through measurements, that light traveled slower through dense media (Michelson 1878). Augustin Fresnel and James Clerk Maxwell, working later within a wave theory of light, explained phenomena that Newton has been unable to explain in terms of a particle theory of light, such as polarization, interference, and diffraction. Maxwell is considered the father of modern perception of light (Yanoff and Duker 2013).

Maxwell created simplified model of Faraday's works on electricity and magnetism and shared how the two phenomena were related. Around 1862 Maxwell calculated that the speed of propagation of an electromagnetic field is approximately that of the speed of light, essentially proving that light was an electromagnetic wave (Marion 1981).

Although Maxwell's work seemed to have finally demonstrated that light was a wave, Albert Einstein, who described the Doppler effect for light, brought the particle theory back into the picture with Max Planck's quantum theory (Stoll 2003). Max Planck suggested that although light was a wave, these waves could gain or lose energy only in finite amounts related to their frequency. These amounts he called "quanta". Einstein postulated that light itself consists of located particles (quanta). Originally rejected, this idea became universally accepted in 1919 with Robert Millikan describing experiments on the photoelectric effect and with the measurement of Compton Scattering (Montwil and Breslin 2008).

The modern theory of quantum mechanics defines light in one sense as both a particle and a wave and in another sense as a phenomenon that is neither a particle nor a wave. Modern physics sees light as something that can be described with

mathematics appropriate to wave theory at lower frequencies and with mathematics appropriate to particle theory at higher frequencies.

Visible light, which occupies a middle ground frequency, can be described using either a wave or particle model or sometimes both.

1.2 Light's place in the electromagnetic spectrum

One of the greatest achievements of science was separating light from sight.

Until recently, visible light was the only known part of the electromagnetic spectrum. Ancient Greeks recognized that light traveled in straight lines and studied some of its properties, but it was just in 1800 when William Herschel discovered the first electromagnetic waves other than visible light. He was moving a thermometer through light split by a prism, studying in this way the temperature of light refracted in different colours. He noticed that the highest temperature was beyond red and concluded that the temperature change was due to a type of light rays that could not be seen. He called them "calorific rays" and they were named later infrared radiation (Lardner 1846). Johann Ritter noticed invisible rays that induced certain chemical reactions. They behaved similar to visible violet light rays but they are not in the spectrum. He called them "chemical rays" (Enloe 2001). Later they were named ultraviolet radiation. Michael Faraday was the first who linked electromagnetic radiation to electromagnetism in 1845 when he noticed that the polarization of light traveling through a transparent material responded to a magnetic field (Faraday effect) (Collett 2003). In 1860 James Maxwell developed four partial differential equations for the electromagnetic field, two of them predicting the possibility and the behavior of waves in the field. Analyzing, the speed of these theoretical waves, he realized that they travel at a speed close to the known speed of light (Silver 2008).

Electromagnetic waves are described by frequency (υ), wavelength (λ) or photon energy (E) (Figure 1.1), physical properties that relate to each other through the following equations (Montwil and Breslin 2008):

$$\upsilon = c / \lambda ; \upsilon = E / h ; E = hc / \lambda \qquad \text{Eqn.1-1}$$

where: c=299,792,453 m/s (speed of light in vacuum); h = 6.62606836(33) x 10^{-34} J s (Plank's constant)

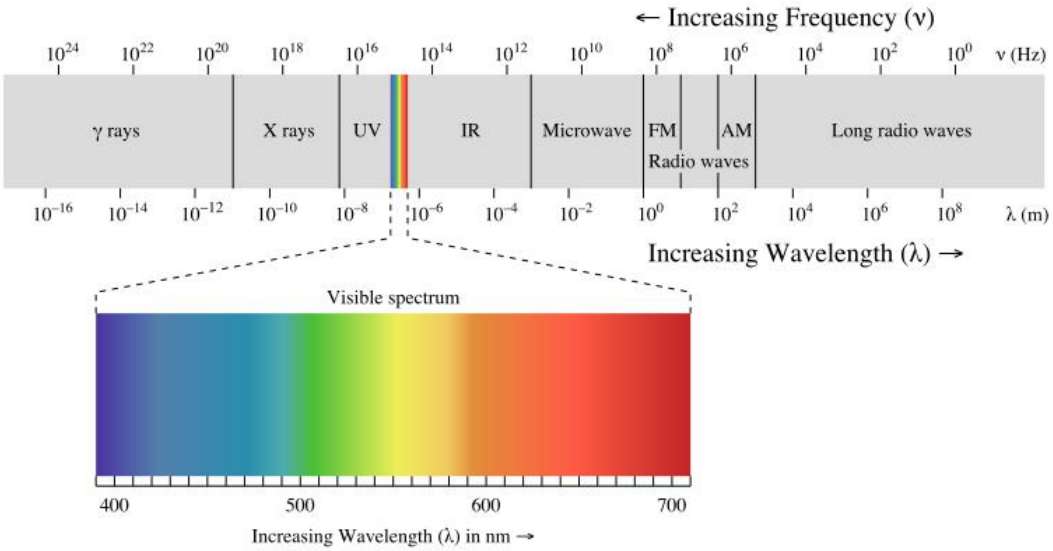

Figure 1.1 Electromagnetic spectral band.

Only a small portion of the electromagnetic spectrum, radiation with wavelengths between 380 and 760 nm, excites the human visual system and can be perceived as visible light.

1.3 Early development of artificial light sources

A typical "light source" emits electromagnetic radiation in the visible spectrum. Artificial light sources do not belong to one kind of science but embody most of them being the result of development in vacuum techniques, research of particular glasses, studies of the purification of gases, the refinement of metals, the elaboration of fluorescent substances, and other countless engineering features that allowed the making and improvement of all lamps we know today.

Mankind relied solely on sunlight and fire for lighting needs until 1802 when Sir Humphry Davy set the foundations of the lighting industry with his simultaneous

discoveries of light emission from incandescent metal wires and from electrical areas, same time with W. Petrov (Okamura 1994).

But their discoveries had to wait 50 years the development of steam powered dynamos and the refinement of Volt's battery before becoming a practical reality. Between 1850-1855, Leon Foucault built the first carbon arc lamp that was used for theoretical lighting (Hearnshaw 2014) and Heinrich Goebel made the first practical incandescent lamps, using carbonized bamboo filaments enclosed in evacuated perfume bottles (Dyer and Martin 2010).

Carbon arc systems were further improved by Serrin, in 1859, who designed a mechanical system to keep the arc at a given portion despite the unequal burning rate of the cathode and the anode (Bowers 2009). Compton and Wallace Farmer made later an arc lamp that was regulated in voltage, which permitted their use in series circuits (Dyer and Martin 2010). Paul Jablochoff invented a self-regulating arc lamp made of 2 close graphite rods separated by a plaster layer (DiLaura 2008). The major drawbacks of these lamps were the short lifetime, of 90 minutes, and the fact that the used set of electrodes could not be re-ignited. Despite these drawbacks, the lamps were used for the first practical electric arc street lighting in Paris (1878). In 1880, Compton and Pochin, along with Hefner Alteneck, invented the differential carbon arc lamp that superseded Jablochoff's lamp in street and industrial lighting (Fenna 2002). The harsh light, noisiness, high electric power consumption made these lamps unsuitable for home lighting.

Incandescent lamps were further improved by several scientists but their lifetime remained too short for being commercially viable. Francis Jehl and Thomas Edison found the reason for this in 1879 when they discovered that gases occluded in lamp materials are released in vacuum over time (Dyer and Martin 2010). They patented an effective outgoing method which consisted of heating the lamp during the pump-down pressure. Eight months before Edison made his successful low-resistance carbon filament lamp, Joseph Swan demonstrated a working incandescent graphite rod lamp before the Royal Institution in Newcastle, England (Gendre 2003).

Researchers increased filament temperature for obtaining higher luminous efficacies and colour temperatures but this led to a shortening of the lifetime of lamp bulbs and to severe blackening, as carbon has a high vapor pressure. Several metals

were investigated by Lodyguine for replacing the carbon filament (De Lodyguine 1897). Carl Auer Von Welsbach succeeded at making an Osmium filament lamp that started to be marketed in 1902 (Poljanc, Steinhauser et al. 2007). Haus Kuzel made the first Tungsten filament in 1905 which extended the lifetime of the lamps to 1000 hours and increased their luminous efficacy (Schade 2010). Incandescent lamps were improved throughout the first half of last century but their efficacies as light sources remained low. However, their advantage resided in small production cost and simplicity of use.

Another way of electric lightening resulted from the discovery of the electric glow discharge in rarefied gasses made by Michael Faraday between 1831 to 1835. Julius Plicker and Eurich Geissler investigated electrical discharges in evacuated glass tubes provided with electrodes at each end, Hittorf, Crooks and Goldstein revealed that the light colour of discharge changed upon addition of other gases and vapors (Porter 1965). Robert Bunsen and Gustav Kirchhoff explained the phenomenon in 1859 by showing that each chemical element emits a specific set of light colours, or spectral lines, which set the foundation of spectroscopy (Thomas 1991). The inner wavelength principles of these tubes were not understood until 1920 when Irving Langmuir, from General Electric, studied the physics of ionized gases and coined the term “plasma” to describe them (Langmuir and Kingdom 1925).

In the beginning, improvement of lamps had the aim to increase lighting efficacy and lifetime while reducing production costs and while making them easy to use. Later, another aim was added: the quality of light emitted by the light sources.

1.4 Quality of light

The quality of light emitted by a light source is given by how well we can see shapes and colours in it. This is strictly dependent upon the light source’s spectral power distribution, which is a representation of the emitted radiant power as a function of wavelength. Natural daylight is the only light source that will not distort our colour judgement, however its appearance and spectral characteristics can change dramatically during the day from day to day, season to season, being affected by

atmospheric conditions, pollution, altitude, surroundings, position of the sun, etc (Helmut 2013).

The International Commission on Illumination (CIE) has thoroughly defined natural light as having specific characteristics. The ability to simulate these characteristics, when producing an artificial light source, is critical in providing light of high quality. The evaluation consists in establishing the ability of the light source to render colours accurately. This requires colour measurements with highly specialized equipment known as spectroradiometers (Gulrajani 2010).

CIE established ideal curves for 3 daylight spectral power distributions (SPD), as shown in Figure 1.2(b). These kinds of curves represent profiles of imaginary light sources, called illuminants. Illuminants standardized by CIE are marked by a letter or by a letter-number combination, as the example shown in Figure 1.2(a), 1.2(b).

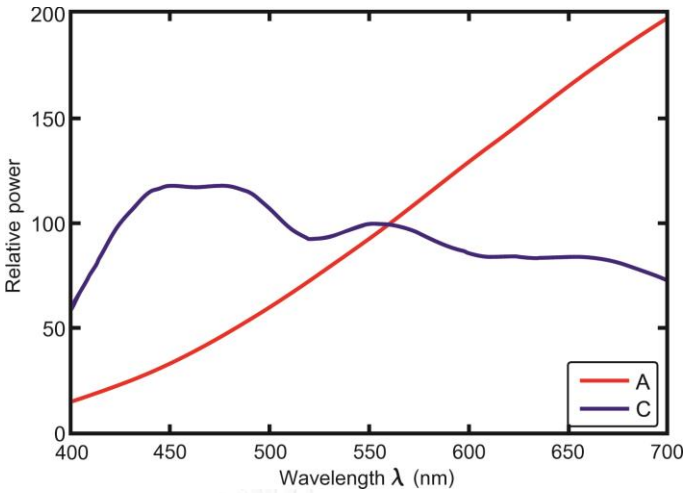

(a)

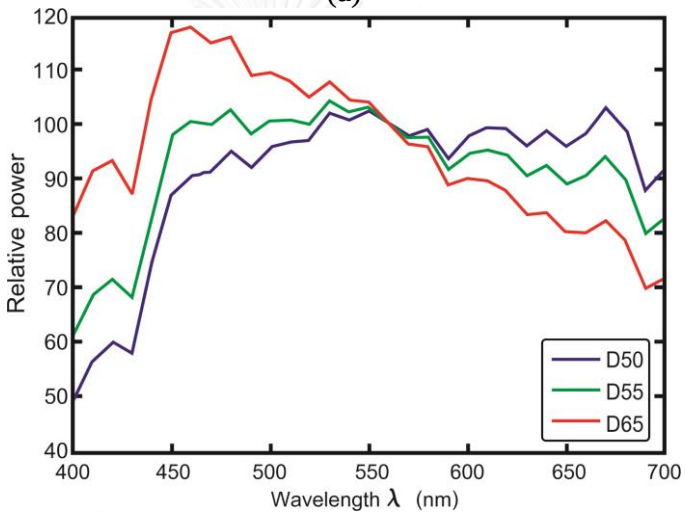

(b)

Figure 1.2 Spectral power distribution of three ideal daylight curves, (a) CIE standard illuminant A and C (b) CIE standard illuminant D50, D55 and D65.

Opposed to the standardized SPD shown in Figures 1.2(a), 1.2(b), some SPD curves of artificial light sources are shown in Figure 1.3. All sources from Figures 1.3(a),(b),(c),(d) have a correlated colour temperature of 6500K, but their SPDs differ strongly. Although the daylight standard illuminants have uneven curves, all of the colours of the spectrum are present in relative equal proportion and this is why sets of colours that match under one phase of daylight will also match under the other phase of daylight. However this does not happen in respect to the artificial light sources represented in Figure 1.3.

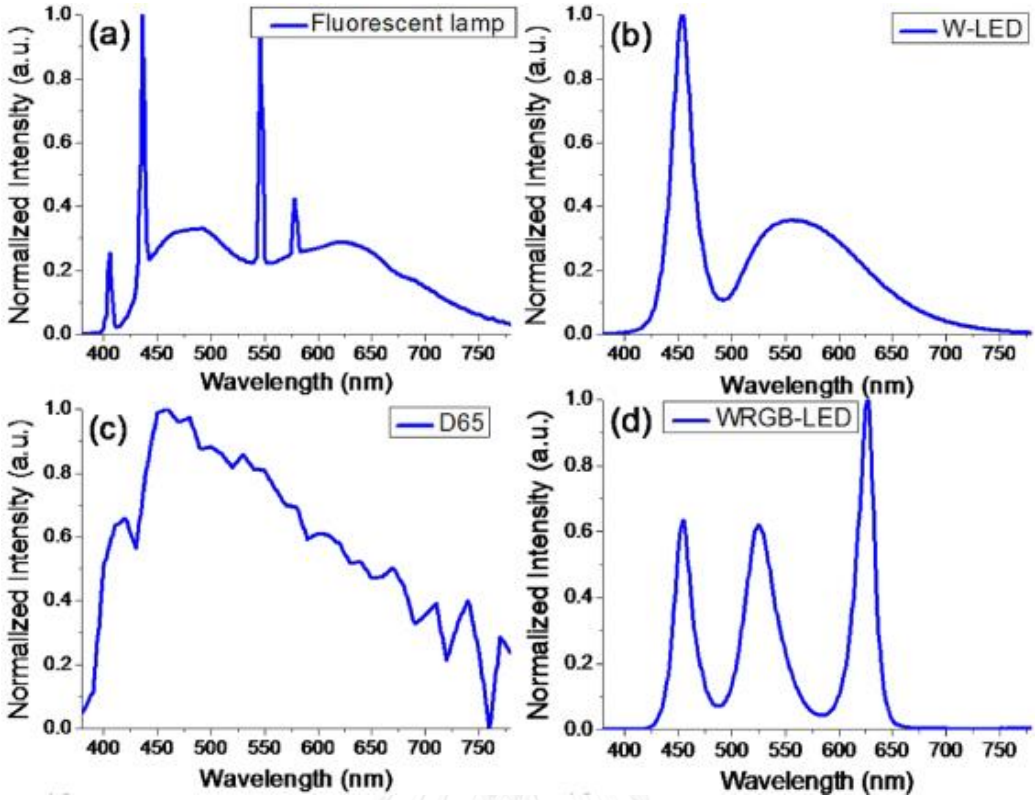

Figure 1.3 Spectral curves representing 6500K CCT.

Because the correlated colour temperature cannot be used in evaluating the quality of light, an index has been established scaled from 0 to 100, for calculating how well a light source can render colour. This index is called colour rendering index, (CRI) (Ohta and Robertson 2005).

1.5 LED Light sources

1.5.1 General description

LED stands for Light Emitting Diode. This is a low voltage electronic device that permits current to flow in only one direction. The diode consists of 2 slightly different materials brought together to form a PN junction. P stands for positive charge and N stands for negative charge. In fact the positive charge shows the absence of electrons while the negative charge shows the presence of electrons in excess. For this reason, the positive part of the junction is considered to be populated with holes while the negative part of the junction is populated with electrons. When a forward

voltage is applied to the semiconducting element, electrons move from the N side toward the P side, the holes move from the P side toward the N side and they combine near the junction. During this process, energy is released in term of light that is emitted by the LED (Wyszecki and Stiles 2000).

As seen in Figure 1.4 LED requires a specific electrical polarity. If voltage is applied in reverse polarity it can be destroyed.

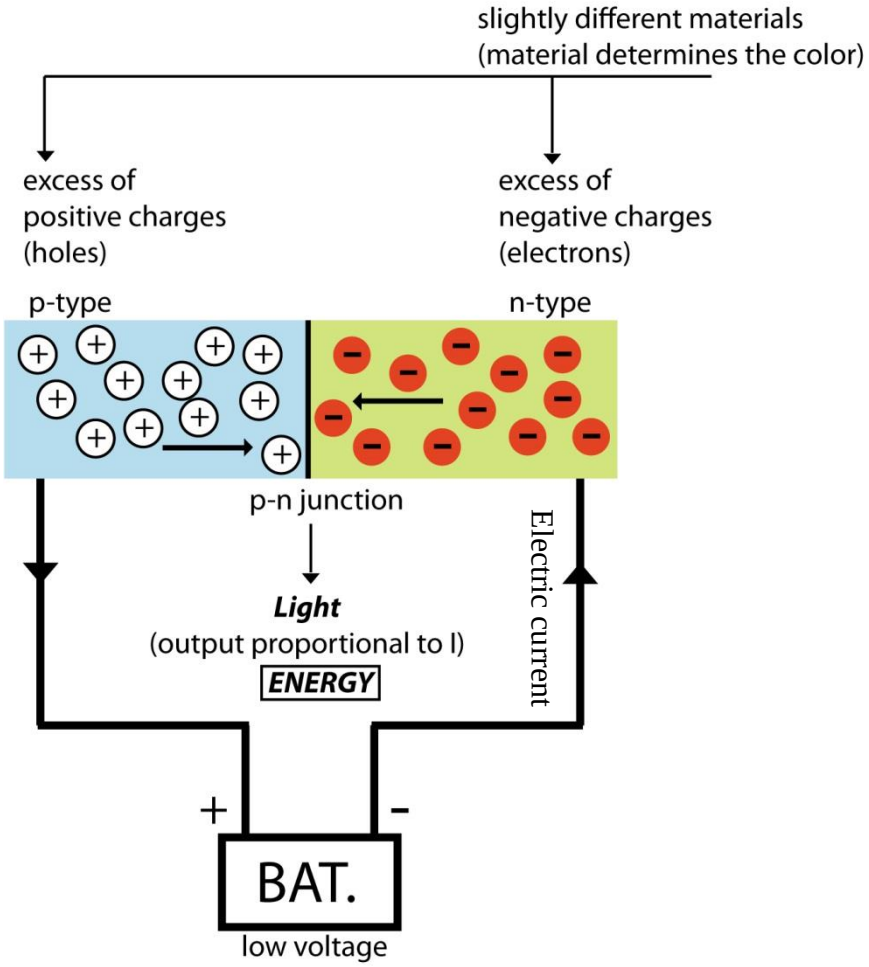

Figure 1.4 Principle of LED light source emission.

Small charges in the applied voltages can determine sharp increases of the forward currents as seen in Figure 1.5.

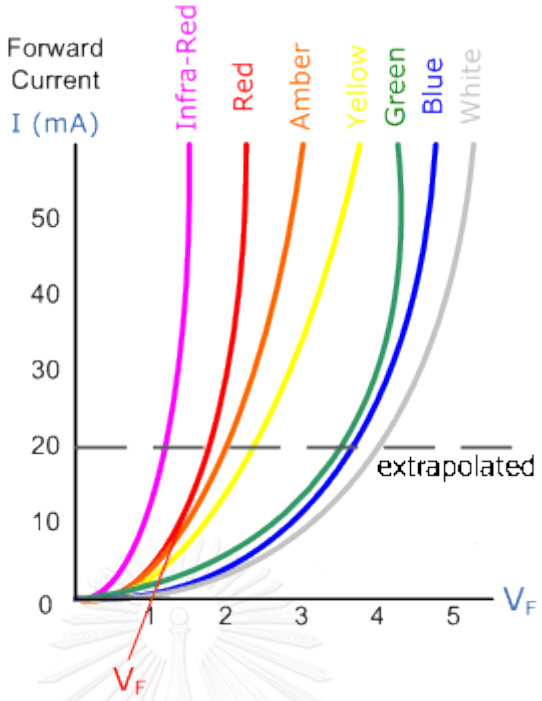

Figure 1.5 Characteristic of LEDs.

One single LED produces light of a single colour (monochromatic light). The colour is determined by the material used in the semiconducting element of an LED. A list of main types of LEDs used in lighting systems is shown in Table 1.1. Slight changes in the composition of the presented alloys change the colour of the emitted light (Yam and Hassan 2005).

Table 1.1 Colour emitted by various LEDs depending on material used to produce them.

Colour regions in spectrum	Substrates
Infrared	Gallium arsenide (GaAs) Aluminium gallium arsenide (AlGaAs)
Red	Aluminium gallium arsenide (AlGaAs) Gallium arsenide phosphide (GaAsP) Aluminium gallium indium phosphide (AlGaInP) Gallium(III) phosphide (GaP)
Orange	Gallium arsenide phosphide (GaAsP) Aluminium gallium indium phosphide (AlGaInP) Gallium(III) phosphide (GaP)

Colour regions in spectrum	Substrates
Yellow	Gallium arsenide phosphide (GaAsP) Aluminium gallium indium phosphide (AlGaInP) Gallium(III) phosphide (GaP)
Green	**Traditional green:** Gallium(III) phosphide (GaP) Aluminium gallium indium phosphide (AlGaInP) Aluminium gallium phosphide (AlGaP) **Pure green:** Indium gallium nitride (InGaN) / Gallium(III) nitride (GaN)
Blue	Zinc selenide (ZnSe) Indium gallium nitride (InGaN) Silicon carbide (SiC) as substrate Silicon (Si) as substrate—under development
Violet	Indium gallium nitride (InGaN)
Purple	Dual blue/red LEDs, blue with red phosphor, or white with purple plastic
Ultraviolet	Diamond (235 nm) Boron nitride (215 nm) Aluminium nitride (AlN) (210 nm) Aluminium gallium nitride (AlGaN) Aluminium gallium indium nitride (AlGaInN)—down to 210 nm
Pink	Blue with one or two phosphor layers: yellow with red, orange or pink phosphor added afterwards, or white with pink pigment or dye.
White	Blue/UV diode with yellow phosphor

1.5.2 Early developments

Henry Joseph Round observed in 1907 that silicon carbide emits light in response to the passage of an electric current. This phenomenon is called electroluminescence. The emitted light was yellow and dim. Bernhard Gudden and Robert Wichard Pohl used phosphor materials made from Zinc Sulphide doped with Copper and George Destriau wrote a report on the emission of light by Zinc Sulphide powders in 1936, being credited with the invention of "electroluminescence"

Doping is the process of adding other elements to the semiconductor material for changing its properties, creating this way two separate type of semiconductors in

the same crystal, bounded through the p-n junction that allows current to pass only one way. The light emitted by the electrons that combine with holes, while passing the p-n junction, escapes the semiconductor through a narrow light cone under a certain angle, for which reason LED displays have been always best viewed from one angle. Phosphors have the property to alter the light output of the LED creating a more pure harsh colour.

Gary Pittman started working with Gallium Sulphide in 1953 for creation of early solar cell which lead him into a group of scientists that worked on tunnel diodes (lasers). A failed attempt to create a laser leads Gary Pittman and Bob Biard in 1961 to the infrared LED (Figure 1.6). These LEDs, patented by Texas Instruments, were first used by IBM computers to replace the tungsten bulbs that controlled punch card readers (Brusso and Author 2008, Dudda 2013).

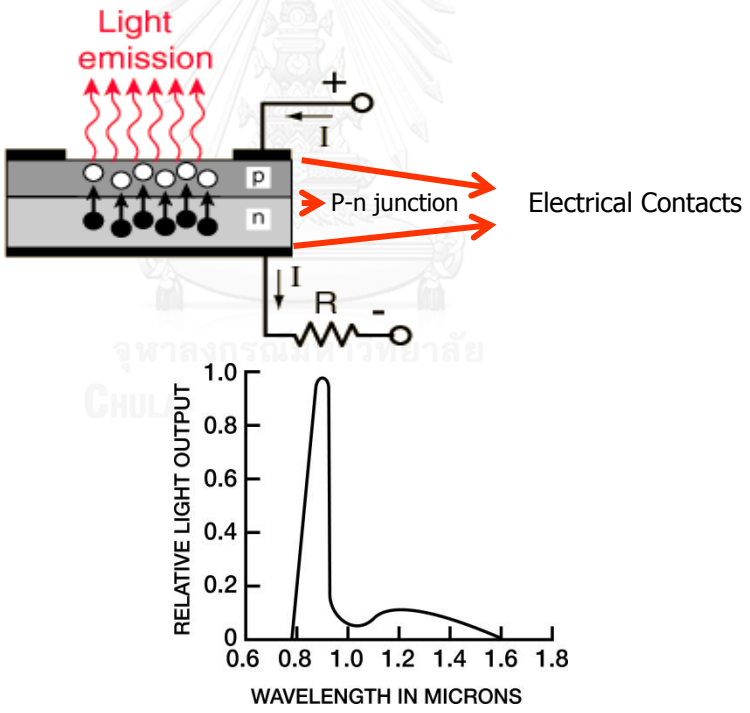

Figure 1.6 Characteristic of infrared LED created by Gary Pittman and Bob Biard.

1.5.3 LED types

In 1962 Nick Holonyak developed the first visible light LED, using Gallium Arsenide Phosphide on a Gallium Arsenide substrate (Held, 2007). The LED was emitting red light. Ten years later, M. George Craford created the first yellow LED

using Gallium Arsenide Phosphide and also developed a brighter red LED. In 1976 Thomas P. Pearsall developed special high brightness LEDs for fiber optic use, improving communications technology worldwide (Schubert 2002).

The first very bright LEDs appeared in the 1980s, first in red, then yellow and green. They were using Gallium Aluminium Arsenide Phosphide. Ultrabright LEDs producing orange-red, orange, yellow and green were made in the 1990 using Indium Gallium Aluminium Phosphide. At the end of 1990s ultrabright blue Gallium Nitride LEDs were created and shortly thereafter high intensity green and blue LEDs were produced using Indium Gallium Nitride. The ultrabright blue chips become the basis of white LEDs. The light emitting chip is coated with fluorescent phosphors that absorb the blue light from the chip and then re-emit it as white light as shown in Figure 1.7 (Kim, Luo et al. 2005).

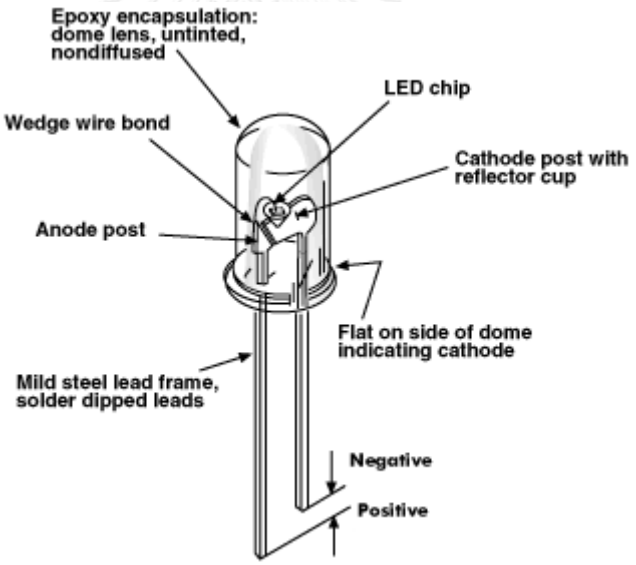

Figure 1.7 LED chip.

1.5.4 White light emitted by diode

There are 2 ways to create white light using light emitting diodes: one way is to mix the coloured light from several LEDs in order to obtain a spectral power distribution that produces a certain white light as shown in Figure 1.8 (Tsuei and Sun

2011). The appearance of white can be given by several SPDs. The LEDs are organized in clusters, intensity of the white light being dependent on the number of LEDs in the cluster.

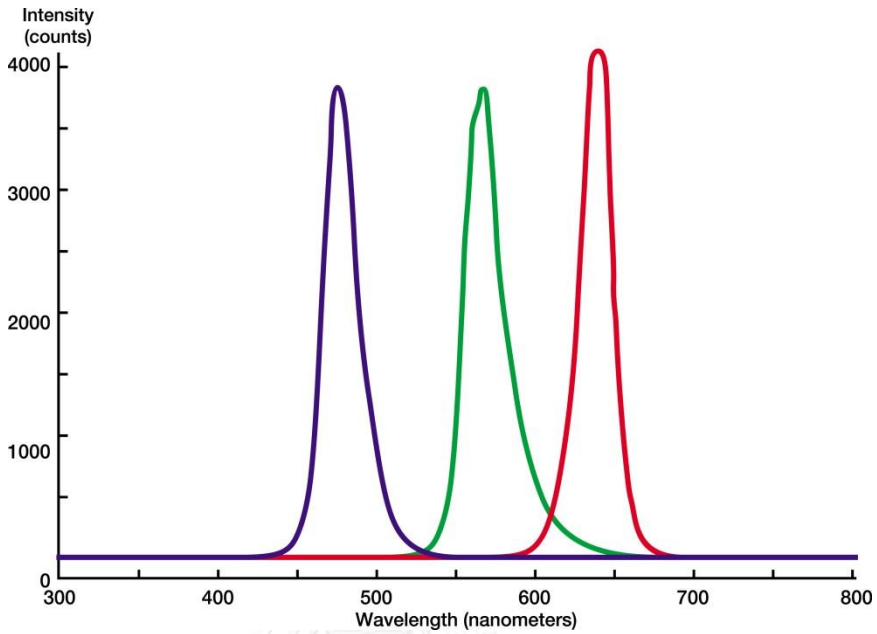

Figure 1.8 Spectral Power Distribution of RGB LEDs clustered for producing white light.

The advantage of using multicoloured LED clusters are: higher luminous efficacy, good colour rendering properties, complete flexibility for achieving any desired colour property. The disadvantages are difficulty to completely mix light, difficulty to maintain colour stability in different operating condition and during life time.

The multicoloured white LEDs can be di-, tri-, and tetra- chromatic. Higher luminous efficiency will often mean lower colour rendering, thus lower quality of light. The dichromatic white LEDs have the highest efficiency but lowest colour rendering capability in the series. At the other end are the tetrachromatic white LEDs with very good colour rendering capabilities but very low luminous efficiency (Lui, Xia et al. 2007).

The most common method to produce white light this way is by mixing the red, green, and blue primary colours, resulting the RGB LEDs. This allows precise

dynamic colour control. But one major problem is that emission power decays exponentially with rising temperature, which determines a substantial change in colourstability. Colour value output is affected over usage period and by temperature changes (Meneghini, Vaccari et al. 2014).

Another way is to coat with phosphorus a short wavelength Indium Gallium Nitride (InGaN) LED that emits blue light. If the peak wavelength of the LED is 450-470 nm, some of the blue light will be converted to yellow light by phosphorus, which will combine itself with the rest of blue light resulting white light (Yang, Lin et al. 2013).

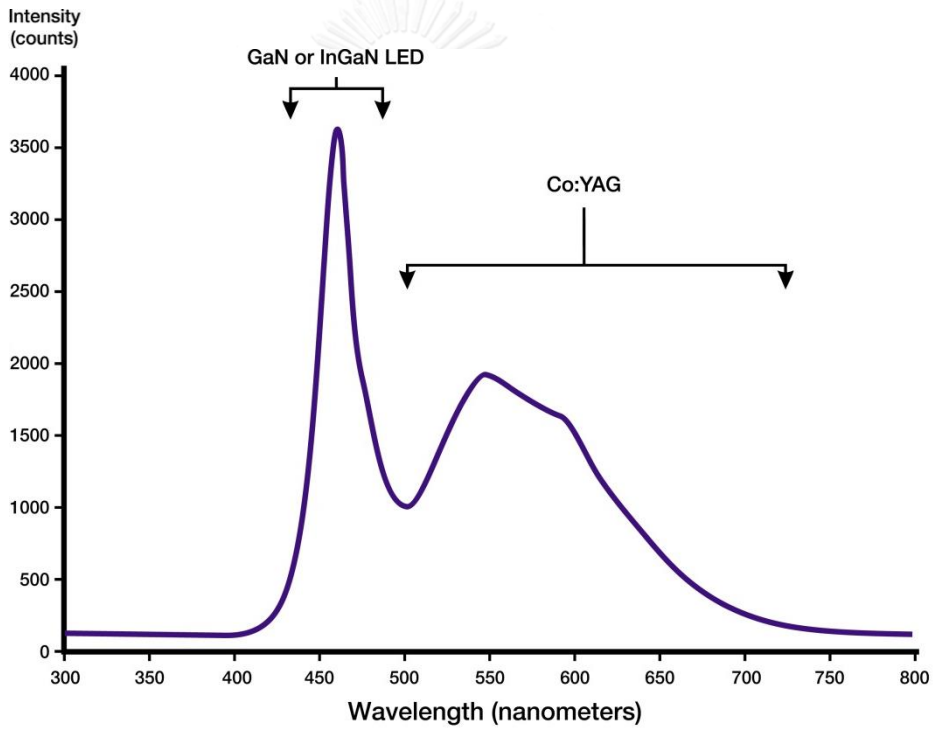

Figure 1.9 SPD of a white LED with improved phosphorus.

The advantage of phosphor converted white LEDs is mostly the fact that they represent a simple and compact white light source. The great disadvantages are related to the phosphor. Its uniform application is difficult to control and the limited options in phosphor availability results in limited range of available colour properties (Ma and Wang 2010).

InGaN technology results in superior reliability and colour integrity. The brightness and colour purity of InGaN white LEDs depend on the amount of phosphor coating, which determines a cool white shade, in small amount, pale white in higher amount and incandescent white if the amount is very high. Cool white is the brightest and incandescent is the dimmest. Figure 1.9 shows the spectral power distribution of a white LED light source with improved phosphorus (Lago, Meneghini et al. 2012).

White LEDs can be used only behind a clear or milky white lens or panel because the red colour is missing from their SPD. If a white LED is placed behind a red lens the resulted light is pink. An orange lens will turn its light to yellow and yellow lens will turn its light to lemon-lime.

1.6 Photometry

Photometry is the measurement of light, seen as electromagnetic radiation, weighted by spectral response of the eye. It is therefore restricted to the wavelength interval 360-830 nm which is detectable by the human eye. Photometry can be classified in:

a.) Visual photometry, which uses the eye as a comparison detector;

b.) Physical photometry, which uses either optical radiation detectors made to simulate the spectral response of the eye, or spectroradiometry combined with eye-response weighting calculations.

The measurement units of the photometric system are: luminous intensity, illuminance, and luminance, illustrated in Figure 1.10 (Poynton 2012).

Luminous intensity (cd), is defined by the power of light (lumen) per unit solid angle (steradian) as in the equations 1-2, 1-3:

$$I = \frac{F\,(lumen)}{\omega} \qquad \text{Eqn. 1-2}$$

$$\omega = \frac{Area}{r^2} \qquad \text{Eqn. 1-3}$$

Illuminance (lm/m^2 *, lux)* is a measurement defined by the amount of visible light incident on surface area (lumen per square meter) as in equation 1-4. This photometric unit is well recognized in measuring the illuminated object (Blitzer, Ferguson et al. 2008).

$$E = \frac{F\,(lumen)}{Area} \qquad \text{Eqn. 1-4}$$

Luminance (cd/m^2) is a photometric unit that refers to a luminous intensity consistently reflecting from a surface area of 1 m^2.

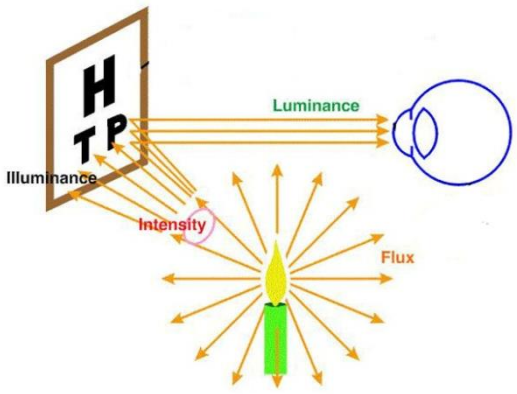

Figure 1.10 Photometric quantities illustrating Flux, Intensity, Illuminance, and Luminance.

The strength of different light sources can be compared by measuring the illumination they give on a surface under identical geometrical conditions. When the illuminations are exactly equal, the edge between the two half fields of the surface illuminated with different light sources virtually disappears. If the geometrical conditions on both sides are identical, the two light sources have the same strength.

A system for measuring the strength of sources can consist of some defined sources as standard unit, their strength considered to be 1 (Wolf 2013). Applying the

principle of superposition of illuminations, which says that the illumination resulting from two independent sources is the sum of illumination from both of them, two identical sources will give an illumination twice as strong as just one of them. If a considered light source is balanced by X unit sources, then it can be said that the considered source has a strength of X. Studying how the illumination varies with distance to the source by applying the inverse square law $\left(Intensity \propto \frac{1}{distance^2}; \frac{I_1}{I_2} = \frac{d_2^2}{d_1^2} \right)$, ratios of measured distances can be used to get the source strength, when it is not a multiple of the given unit (Wright 2010).

The above described way works only for measuring the strength of sources that give illuminations of the same colours in term of hue and saturation. In all the other cases, a number of standard sources of different hues must be used, building a system that is object of study for colorimetry.

1.7 Colorimetry

Colorimetry can be regarded as an advancement of photometry. When light sources of different hues are necessary for determining the strength of a light, as exemplified before, it was established that 3 standard light sources emitting light of well determined wavelength are sufficient this being referred to as the principle of trichromaticity. This principle is governing the human colour vision. Choosing 3 well-defined wavelengths as reference, light of a number of other wavelengths can be measured and as result, 3 matching functions are obtained, one for each of the reference lights. Using these three matching functions the colorimetric coordinates of an arbitrarily given light of any spectral composition can be calculated by weighted integration over wavelength.

A light source may vary considerably in term of strength, while maintaining hue and saturation constant. The absolute level of illumination is proportional to the distance from source to illuminated surface, while the remaining two dimensions, called chromaticity, are related to the particular kind of light source involved and the kind of media the radiation has to pass on its way from the source (Ware 2013).

Chromaticity (x,y) is defined by the formula:

$$x = \frac{X}{X+Y+Z}; y = \frac{Y}{X+Y+Z} \qquad \text{Eqn. 1-5}$$

and can be graphically shown in the chromaticity diagram (Figure 1.11)

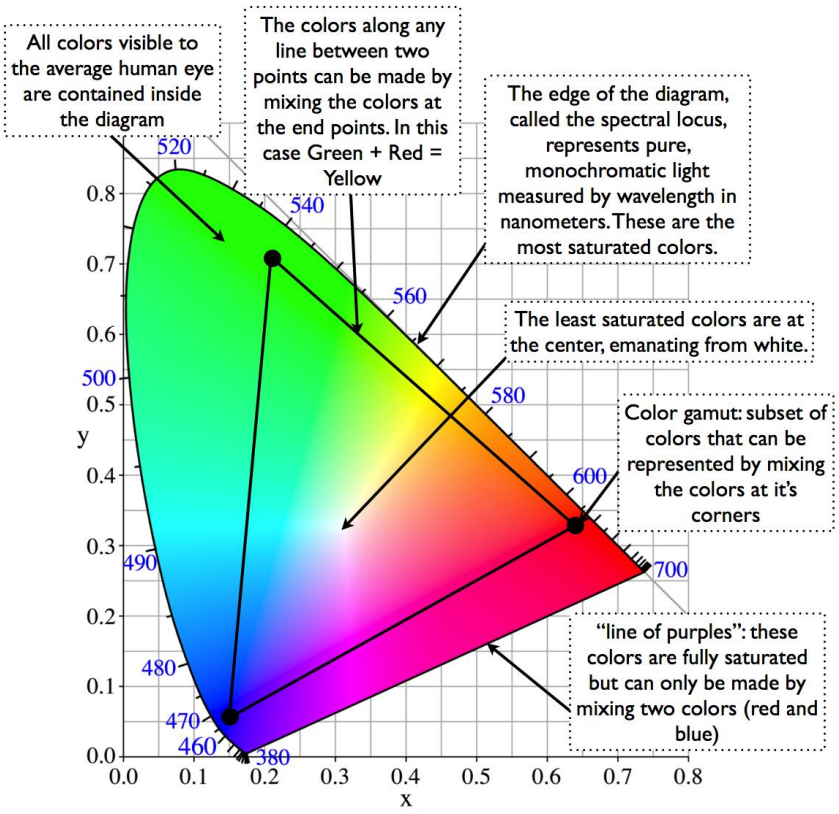

Figure 1.11 CIE chromaticity diagram.

Y is used as dimension of light strength and was defined in such a way as to correspond to photometry, giving illumination in units of lux.

Based on empirical matching performed by observers at 2 degrees of visual angle in the test field, CIE determined three matching functions for the 2^o standard observer, shown in Figure 1.12 (Poynton 2012).

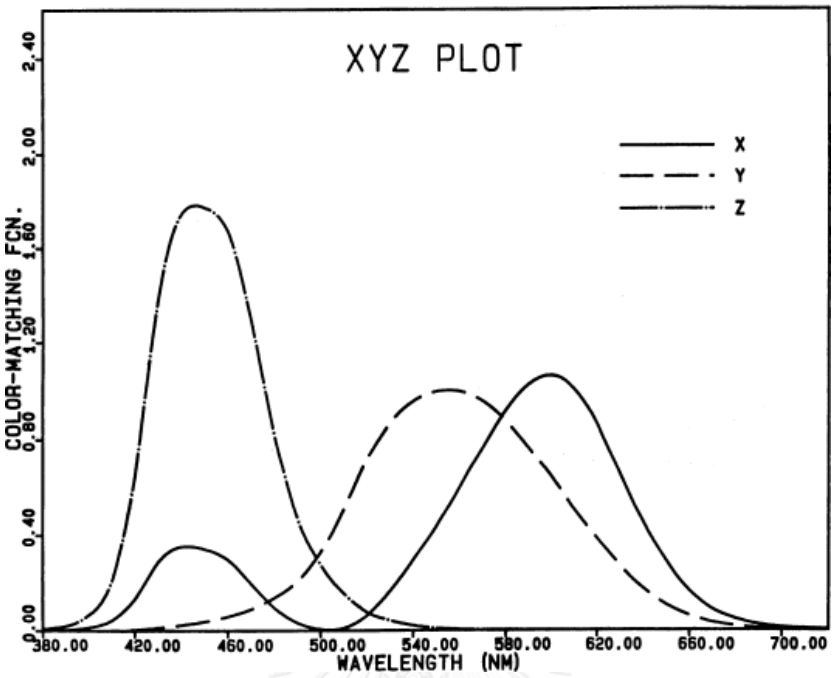

Figure 1.12 Colour matching functions at 2 degrees observer.

Summing the information written until here, colorimetry can be defined as a method of specifying, in numerical terms, the optical properties of light sources and materials considering their capacity to create our coloured environment, being based on the fundamental insights about human colour vision researched by Isaac Newton, Thomas Young and others, summed up by James Clerk Maxwell and standardized by an international optical committee (Commission Internationale de l'Eclairage)

Colours are measured in term of colorimetry systems, but only a colour sample in conjunction with a given illumination can be characterized by a certain X, Y, Z triplet. Once the sample is illuminated with another light source, the X, Y, Z values will change. X, Y, Z will depend also on the orientation of the surface relative to the light source and the observer.

1.8 Colorimetric equipment

"Colorimetric" refers to the usually built-in technical property of a device to measure colour in numerical terms that are meaningful in relation to the standards established by CIE (Randall 1983). Some colorimetric equipment measures the spectral composition of light or of the light reflected by materials or transmitted through materials. These devices are usually calculating automatically the tristimulus values. Other colorimetric equipments measure directly the tristimulus value, using a different measuring technique.

Depending on how they measure colour, colorimetric devices are called:

1. Tristimulus colorimeters, if they measure the tristimulus values of colours;
2. Spectroradiometers, if they measure the spectral composition of light or the spectral reflectance from sample without direct contact;
3. Spectrophotometers, if they measure the spectral reflectance, transmittance or relative irradiance of a colour in direct contact with the sample;
4. Densitometers, if they measure the degree of light passing through or reflected;
5. Colour temperature meters, if they measure the colour temperature of an incident illumination.

Spectrophotometers and spectroradiometers that calculate tristimulus values are called usually, but not necessarily, spectrocolorimeters.

1.9 Digital image acquisition devices

Digital image devices are non-colorimetric equipments that can record still or motion picture through a process that includes processing, compression and storage. The first digital image was produced by Harry G. Bartholomew and Maynard D. McFarlane through a system that generated at both transmitter and receiver end a punched data card or tape that was recreated as an image. The system is known as Bartlane cable picture transmission system (Jones 2012). The main type of digital imaging devices today are scanners and digital cameras.

Scanner evolved from devices that operated on telephotography technique which used a rotating drum with a photo detector attached to it. These techniques

were later applied for building photocopiers. The first scanners were drum copiers in which the original item was placed on a rotating drum that passed the original item in front of the optical equipment which captured its image and produced a copy, the method being similar to that of a photocopy machine. These different scanning ideas were the basis of the first designs of digital cameras. The first digital cameras needed a long time to capture an image, were difficult to use and very expensive. After the appearance of the charge coupled device sensor (CCD), shown in Figure 1.13, digital image acquisition started to develop quickly (Woods 2012).

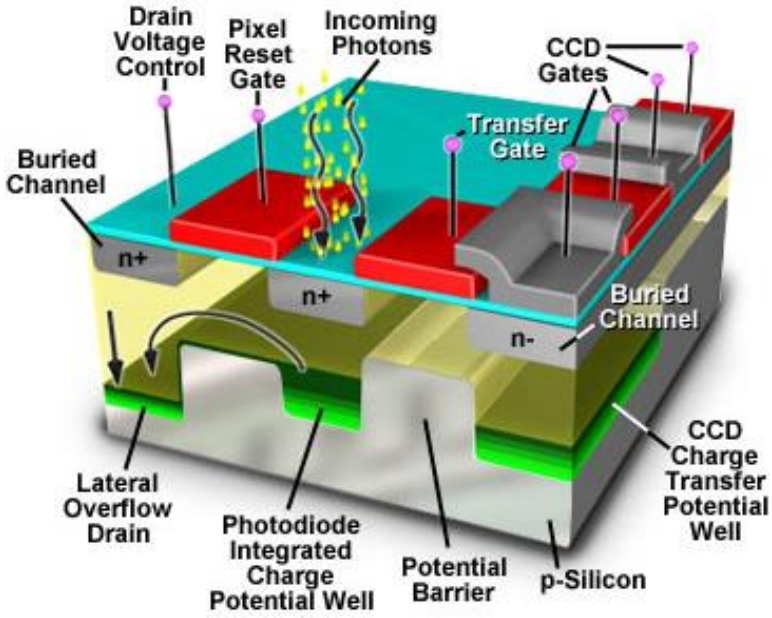

Figure 1.13 Charge-Coupled Device (CCD).

CCD became part of the imaging system used in scanners, digital cameras, telescopes, and camcorders. Other type of sensors were developed later, such as contact image sensor (CIS) for scanners and charged metal oxide sensor (CMOS) for digital cameras Figure 1.14 (Dhanani and Parker 2013).

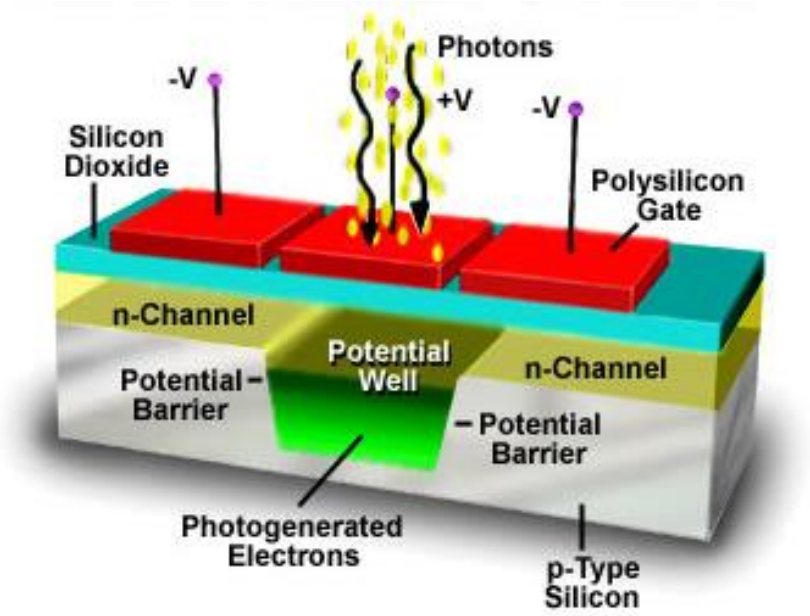

Figure 1.14 Complementary Metal Oxide Sensor (CMOS).

Digital image devices acquire the tristimulus values of colour through sensors and filters, being comparable with colorimeters from this point of view, but their colour output is not colorimetric. However, because dedicated colorimetry systems typically yield only spot measurements, due to their fixed aperture of the measurement port, the wide areas that digital imaging system can capture, make them very attractive for colour measurements and therefore many studies have been made for correcting their colour output in order to obtain colorimetric colour values.

CHAPTER 2

COLOUR SYSTEM

2.1 Early studies

Philo of Alexandria was the first to notice that we see and produce an apparently endless abundance of colours. He stated that the abundance of colour is so rich and plentiful that we cannot name all its shades and tones. His observation led to the conclusion that colours need a systematic order. There have been many attempts to create colour systems (Alesse 2008).

The basic assumption, which still persists in many people's minds, was to represent colours as characteristics of the surface bodies and not as subjective phenomena produced by the eye and in the brain as result of light's properties. From Aristotle who was probably the first to investigate colour mixtures until Newton, a base line of seven colours was applied to all colour systems: white, yellow, red, violet, green, blue, and black. Grosseteste translated the works of Aristotle in the 13th century and became aware that colours were not only defined according to their brilliance or saturation but that their brightness or whiteness also seemed to play a part (Huxtable. 2013). He retained the black-white axis but he removed them from the classical 7 colour straight line and turned them through a right angle, opening up a new dimension for colour systems. His colour system was the first one to distinguish between the two colour types known today as: 1.) achromatic (black, grey and white) and 2.) chromatic (all other colours). In 1310 the Dominican monk Dietrich von Freiberg linked many of his observations to his recognition that four colours are spread across the sky in front of dark clouds and he named them red, yellow, green, and blue, speaking of primary median colours, all of which can be mixed together (Topdemir and Kamal 2007). Davinci included white and black to the list of four primary colours red, yellow, green, and blue (Hullfish 2013).

The oldest colour system known today worth mentioning originate from Forsius, who concluded in a manuscript written in 1611, that colours could be brought

into a special order (Nassau 1997). The manuscript layed undiscovered in the Royal Library in Stockholm until 1969 when it was presented before the first congress of the "International Colour Association" (Küller 1997). Forsius had the ideas of introducing four basic chromatic colours applying for each colour a gray scale along the central axis of sphere. The colours on the sphere are arranged so that three opposing pairs are created: red versus blue, yellow versus green, white versus black. With the colour diagrams shown in chapter VII of his manuscript, Forsius paved the way for modern colour systems.

The forerunner of systems that use three basics colours is Aguilonius system that used the triplet red, yellow, and blue (Barth, Deutsch et al. 2012). Only 20 years after Forsius published his colour diagrams, containing also the first hand - drawn colour circle, in 1630, Fludd prints the first colour circle. This colour-wheel contained seven areas around the circumference containing the seven colours from Aristotle's line (Kuehni and Schwarz 2007).

Kircher observed that when light is split in colours by a glass, the brightest one occurs after passing through the thinnest side of the glass and the darkest after passing through the thicker side of the glass. The ordering of colours from bright to dark, as in his system, emerged again only during the 20th century (Kuehni and Schwarz 2007).

The idea that colours do not result from changes imposed to white light by mixing it with darkness, but are original components of light, resulted from the experiments with a prism. The first to experiment with a prismatic glass was Marci who allowed sunlight to enter through a small opening in a darkened room, directing the resulting ray through a prism (Mach 2003). He observed a series of colours and remarked that the resulted coloured light cannot be subjected to further separation. Grimaldi discovered that small opening leave a trail of coloured light traces, a phenomenon known today as diffraction (Renner 2008). Newton repeated Marci's experiments directing the rays refracted by the first prism through a second prism. He observed that the rays were deflected more but not further separated into colours by the second prism. This proved that colours are not modifications of white light but are its original components. The 7 colours resulted from Newton's experiment, red, orange, yellow, green, cyan, ultramarine, violet, are pure colours, meaning that each one of these

colours is not a mixture of other colours (Shevell 2003). They can be mixed to produce secondary colours and mixed in the right proportions to produce white. Newton placed the 7 colours on a circle, assigning the vacant centre to white, in order to symbolize that the sum of the seven colours is white. Newton's colour circle inspired many colour systems of the 18th and 19th centuries. The first one based on Boutet's painter circle of 1708 shown in Figure 2.1 but the colorist evidently misread orange and violet (Kuehni 2004). Scientists argue today that 7colours can be actually seen and it is believed that Newton added the 7th colour only in order to associate light's component colours to the musical octave (Allen 1999). Newton's colour circle completed the transition from the one dimensional to the two-dimensional colour system.

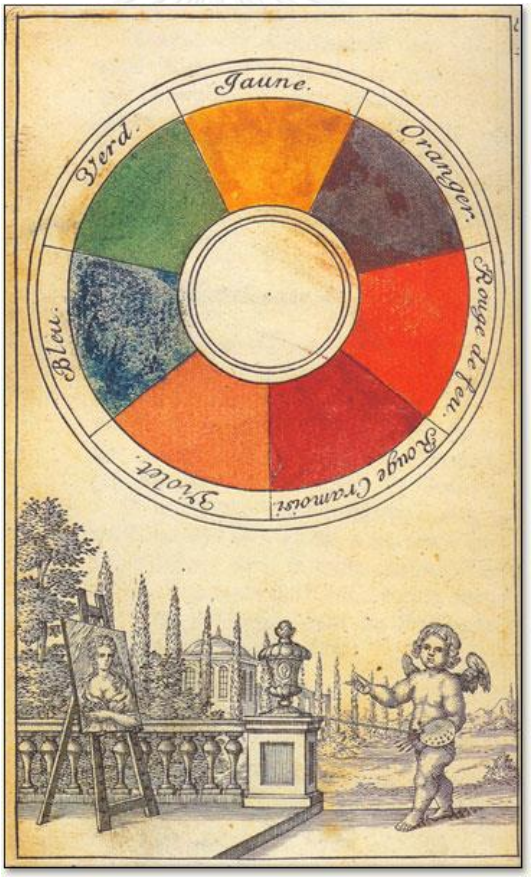

Figure 2.1 Newton's Circle (Shevell 2003).

Mayer realized that very small variations in colour are not noticed by the eye and therefore, difference between mixtures cannot be selected freely (Kuehni 2008). He tried to identify the exact number of colours that human eye can perceive, choosing red, yellow and blue as basic colours and vermillion, massicot and azurite as their representatives amongst the pigments, while black and white were considered to lighten or darken the colours. Jacques Cristophe Le Bon, who is credited with the invention of colour printing, observed that three paints of red, yellow and blue are sufficient to produce all other colours (Lowergard 2006). Although he invented the fundamental three colour system and demonstrated it with many dyes, he did not create a properly organized colour system. Such a colour system was made later by Harris (Harris 1766) shown in Figure 2.2 He introduced the first printed colour circle in 1766 specifying the way of producing the primary colours (red, yellow, blue) exactly. In Harris circle these 3 colours are placed at the greatest distance. Their mixture is represented by orange, green and purple. In his six- colour system Harris recommends mixing each adjacent colour so that 18 colours result to complete the circle in the sequence: red, orange-red, red-orange, orange, yellow-orange, orange-yellow, yellow, green-yellow, yellow-green, green, blue-green, green-blue, blue, purple-blue, blue-purple, purple, red-purple, purple-red. Each of the 3 initial colours is divided with the aid of concentric circles into 20 saturation levels resulting 360 hues. Harris defines a total of 660 colours with only 33 names. He showed that black is obtained through the superimposition of the 3 basic colours: red, yellow and blue. While Newton mixed light rays, Harris mixed pigments, the difference between their colour systems, expressed with today's knowledge, being that Newton's colour system is additive, while Harris's colour system is subtractive. We know today that a surface reflects the wavelengths of the incident light rays that correspond to one colour, while it absorbs the rest. Harris progressively removes (subtracts) a component of radiation by superimposing one colour upon another.

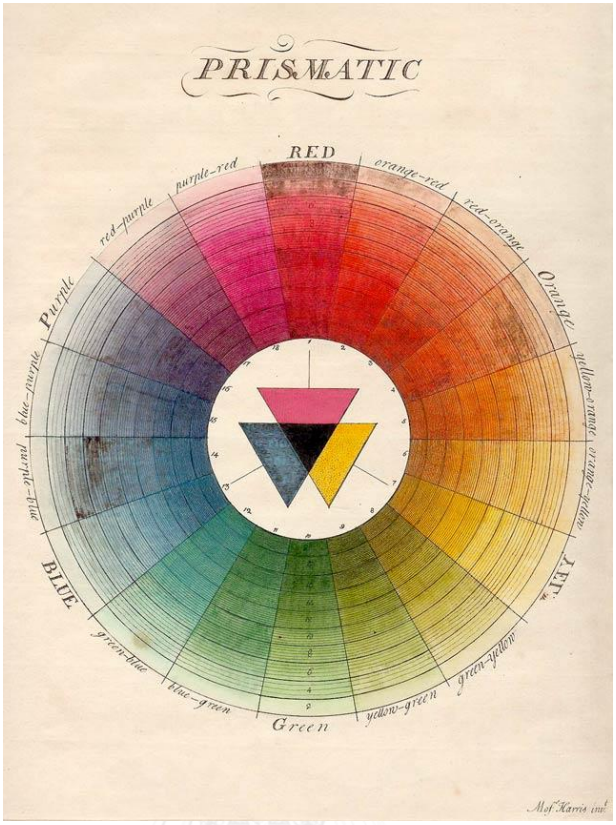

Figure 2.2 Moses Harris colour system (Harris 1766).

Johann Heinrich Lambert (Lambert 1772), the founder of light measurement (photometry) became aware of Mayer's colour triangle, while studying his astronomical works, and recognized that Mayer found the means of constructing and naming many of the possible colours but observed that in order to include their full abundance, one more element had to be added to Mayer's colour system: depth. Lambert carried out his own experiments and suggested a pyramid constructed from a series of triangles that differed from Mayer's triangle in size as well as in the position of black. Lambert's pyramid incorporates the primary, secondary and tertiary colours into one geometrical form, logically linking them with the neutral gray values placed along its central axis as shown in Figure 2.3. Lambert emphasized that the colours of light and the colours of materials behave in a different way when mixed.

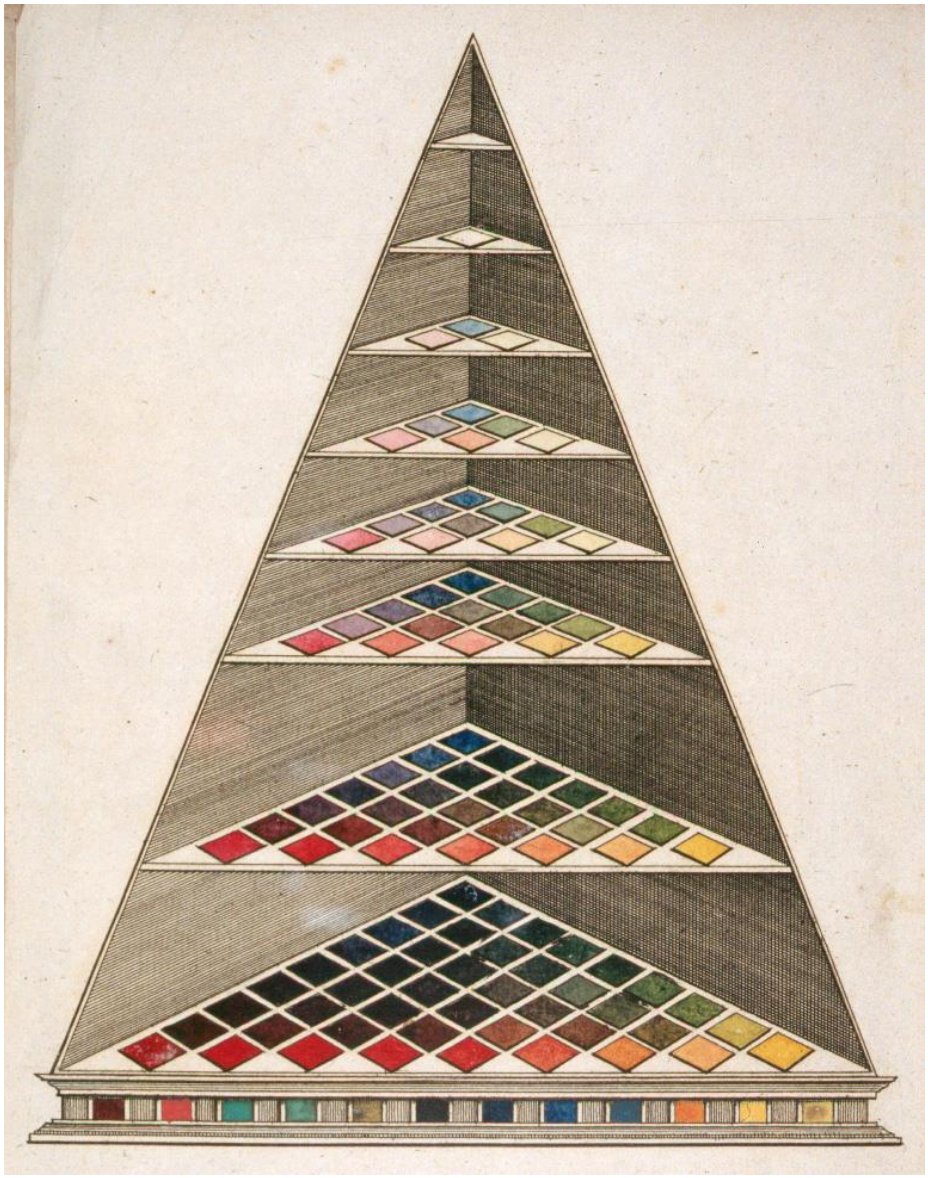

Figure 2.3 Lambert's pyramid (Lambert 1772).

At the same time when Lambert was demonstrating that a 3-dimensioned system can reproduce the complete fullness of colours, Schiffermüller was creating a colour circle with 12 colours: blue, sea-green, green, olive-green, yellow, orange-yellow, fire-red, red, crimson, violet-red, violet-blue, and fire-blue, with continuous transitions from one colour to the other (Parkhurst and Feller 1982). The 3 primary colours: red, yellow, and blue are not placed at equal distance from each other, as in the circle of Harris (Harris 1766). Schiffermüller was the first to arrange the complementary colours (two colours which additively neutralize each other and combine to give white, while subtractive their mixture will result in black) opposite

one another: blue opposite to orange, yellow opposite to violet, red opposite to sea-green. He felt that colours should be treated as a natural system and therefore be arranged in a natural order. His colour circle is shown in Figure 2.4.

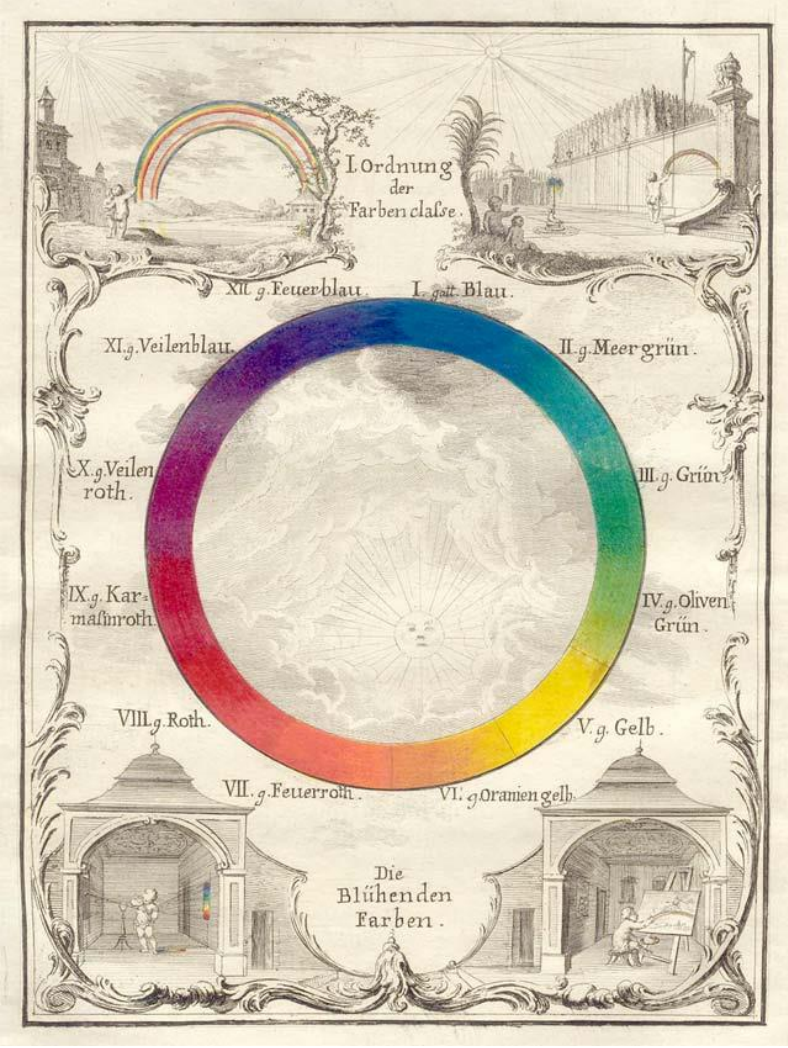

Figure 2.4 Ignaz Schiffermüller colour circle (Schiffermüller 1772).

In 1801, Young first arrived at his ideas for a trichromatic theory, explaining that human eye cannot record each of the infinite number of colours separately: “Since it is hardly possible to believe that each light sensitive point on the retina contains an infinite number of particles, which must all be in a position to oscillate with the respective wave in full agreement, it is therefore necessary to assume that this number is, for example, limited to the three main colours red, yellow, and blue”. Later, he wrote “It is necessary to modify the assumption which I made in my last paper

(Finger 2004) and to replace red, yellow, and blue with red, green, and violet". First his violet appeared to be more like blue and for this reason red, green, and blue have been associated with the "Trichromatic Theory of vision". His theory was confirmed in the 1960's when it was proved that 3 different type of sensitive cells (cones) exist on the human retina that contain pigments, which can absorb blue, green, and red light. In 1821 Fraunhofer used a diamond to scratch fine closely spaced parallel vertical line on a sheet of glass and succeeded in measuring with this diffraction grating the length of waves of which light consisted (Zappe 2010). Fifteen years later Schwerd could take exact measurements of the visible spectrum with this diffraction grating and showed that red light has a longer wavelength than blue light and that green light lies in the middle of the spectrum, between red and blue (Converse 1856).

Chevreul demonstrated in 1839 that a colour will lend its adjacent colour a complementary tinge and as a result, opposing complementary colours will brighten while non-complementary colours will appear contaminated. Da Vinci's and Goethe's observation that colours will influence each other when observed adjacently was formulated by Chevreul in a famous law: "Two adjacent colours, when seen by the eye, will appear as dissimilar as possible" (Chevreul 1858). He designed a 72-segment circle defining the colour hues on the basis of the various changes which a colour under goes in the direction of white (higher intensity) and black (lower intensity).His colour circle is shown in Figure 2.5. Chevreul failed in discovering a law of colour harmony, but his work was of great influence.

Figure 2.5 Michel Eugène Chevreul colour circle (Chevreul 1858).

Philip Otto Runge set his objective "to enquire into the mutual relationship of the given colours in order that our impressions of their compositions and the altered appearances arising out of their mixtures can be deduced in a definite way, and can each time be reliably repeated when using our materials"(Kuehni 2008). Runge designed a colour sphere wishing to record the harmonies of colours rather than to create a practical system for mixing colours as shown in Figure 2.6. He wanted to order all possible colours by other means than language and his sphere is considered the first attempt to create a genuine colour system.

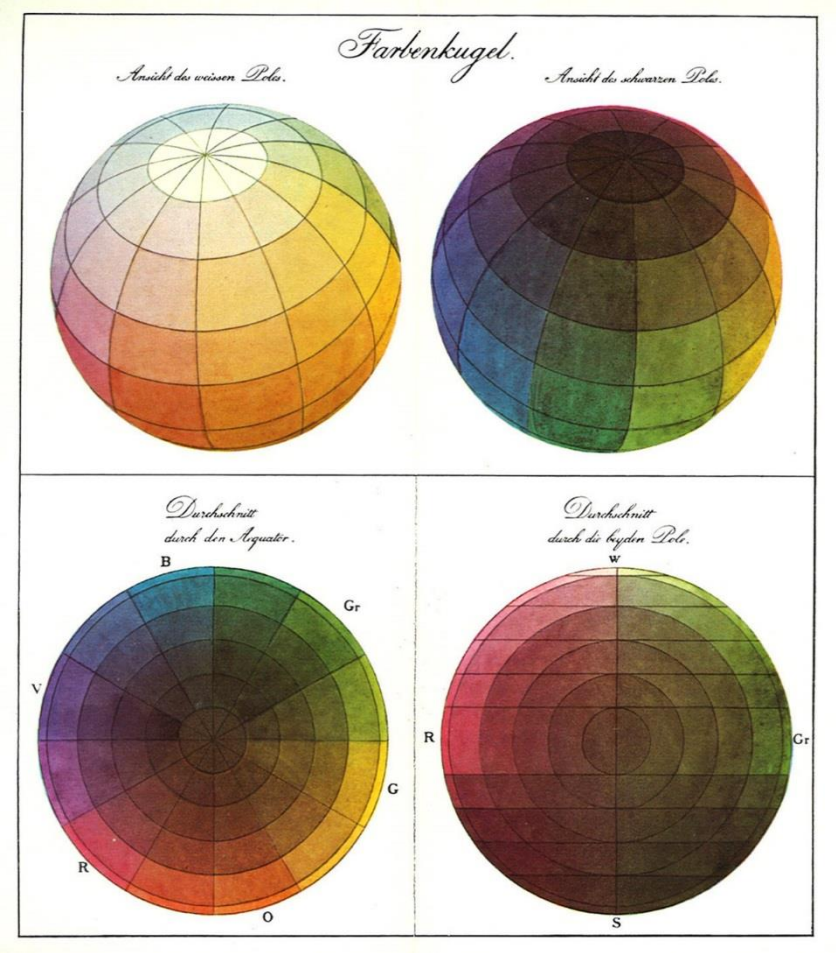

Figure 2.6 Philip Otto Runge colour sphere (Runge 1810).

2.2 Modern colour ordering methods

In 1859 Maxwell presented his theory of colour vision, acknowledged as being the origin of colorimetry. He demonstrated that all colours arise from mixtures of the red, green, blue spectral colours on the assumption that the light stimulus can be both added and subtracted. The three colours are allocated to the corners of a triangle into which a curve of spectral colours is placed that is provided with technical data. Before him, physicists determined wavelengths in the region of 10^{-7} m with the aid of microscopic diffraction gratings. Maxwell's observations of colours are based on Thomas Young observations that no more than three colours of the spectrum were required to produce the others. Young's theory gained credibility when George Wilson of Edinburgh presented the first statistical analysis on colour blindness

(Maxwell 1857). Maxwell showed that the statistical observations make sense if the concerned individuals were assumed to have 3 colour receptors out of which 1 or 2 were ineffective. Maxwell's colour measurement experiments involved test subjects who judged the colour of a sample by comparing it with a mixture of the red, green, blue basic colours. The mixture proportions, recorded as three numbers identified as R, V (verde=green), B are known since that time as tristimulus values.

Maxwell introduced new parameters: r = R/(R+V+B), v = V/(R+V+B) and b = B/(R+V+B), becoming aware that the brilliance of a multicoloured surface is relatively insensitive to change in brightness. The three parameters totally eliminate brilliance and their sum is always 1, which means that all their possible combinations can be represented as the points of an equivalent triangle, Maxwell's triangle. Within this triangle, the results of mixing two colours can be predicted. The combinations of any two colours will lie on the line connecting the 2 colours in Maxwell' triangle has a precise meaning, based on psychophysical measurements. Newton's circle of seven colours plus white implicitly satisfies the trichromatic theory since it equates to a model which allocates a point within a 3D space to each colour. By entering the experimental results into his colour triangle, Maxwell located a point for white. With the aid of this point, Maxwell could specify three new variables: hue, tint, and shade. He showed how these 3 variables can be linked and portray colours as the sum of red, green, and blue spectral colours. (Kuehni 2010)

Helmholtz introduced in his "Manual of Psychological Optic" the three variables still used today to characterize colours: hue, saturation, and brightness. He was the first to observe that spectral colours shine more intensely and possesses greater saturation than colours applied to a white base using pigments (Hatfield 1990). Helmholtz arranged the spectral colours on a curved line, an imaginary force field of colour with white in the middle, corresponding to Newton's gravitational center. In this arrangement, complementary colours required in greater amounts to produce white were given greater leverage. But the position of the spectral colours was only finally resolved at the end of the 19th century when König and Dietrici examined "the basic sensations in normal and anomalous colour system and the distribution of their intensities in the spectrum" (König 1886).

Benson (Benson 1868) created the first colour system that was based on a colour cube but a cube will be always confronted with the problem that it does not fully allow for the significance of brightness and as a result colour hues cannot be placed correctly. Wilhelm Von Bezold designed a colour cone and a colour circle (Figure 2.7) but his attempts to present a comprehensive colour system failed because he overemphasized the blue and violet hues. However he had an important contribution by observing electrical lamps through coloured filter and noting that when seen through a red filter, the brightness point of the lamp was discoloured green. In modern perceptual physiology this is known as the Bezold-Brucke phenomenon (Bezold 1876).

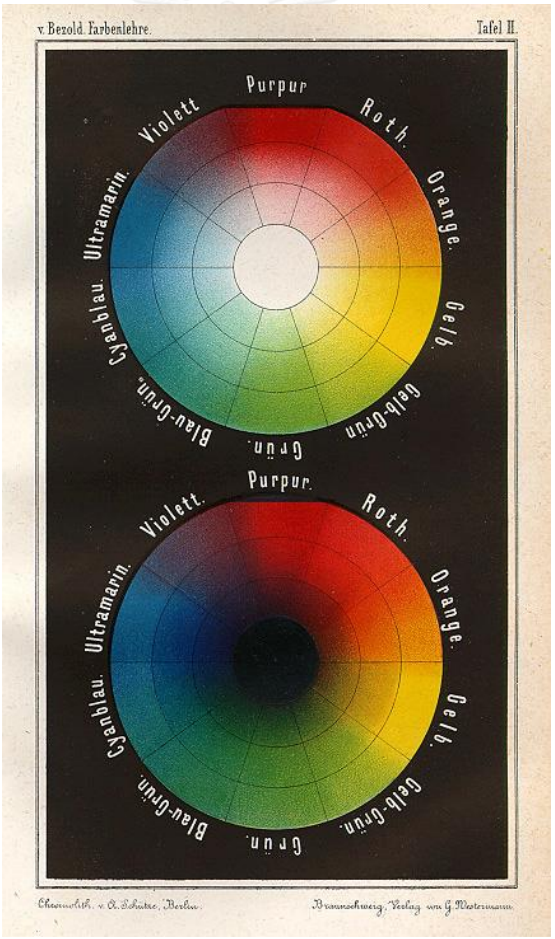

Figure 2.7 Wilhelm von Bezold Colour Circle (Bezold 1876).

Wilhelm Wundt introduced 2 colour systems (Figure 2.8) establishing the experimental branch of psychology and securing it as an empirical science (Kuehni and Schwarz 2007).

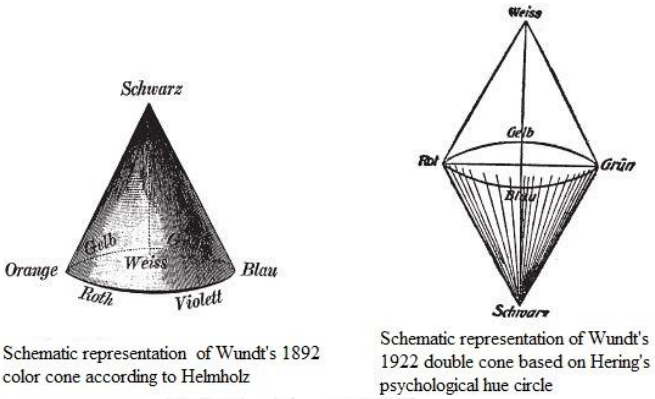

Figure 2.8 Wilhelm Wundt's colour systems (Kuehni and Schwarz 2007).

Charles Blanc was a French art critic who examined colour contrast and the possibilities for optical mixtures. His colour-system comprises a circle containing six opposing triangles in which the additive primaries of red, yellow, and blue alternate with the subtractive primaries of orange, green, and violet (Figure 2.9) (Blanc 1867).

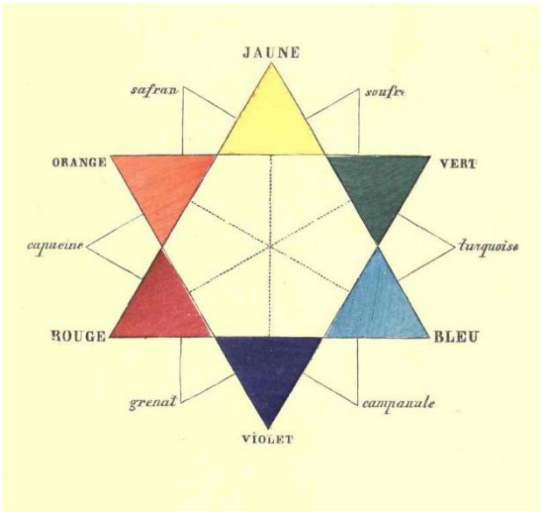

Figure 2.9 Charles Blanc (Blanc 1867).

Nicholas Ogden Rood had an interest in colour frame both artistic and scientific sides. His colour system proposes concentric colour-circles for the first hue. They are based on the primary colours red, green, and blue and possess 12 outer segments of equal size, having the colours: red, orange, orange-yellow, yellow, green-yellow, green, green-blue, cyan, blue, ultramarine-blue, violet, and purple. These circles became poles as they progress inwards, the center being white (Figure 2.10). Rood produced also a scientific version. The colours, with their precise angular positions, are these used by painters in their palettes. The basic of Rood's colour wheel is a laborious improvement on Maxwell's triangle (Rood 1892).

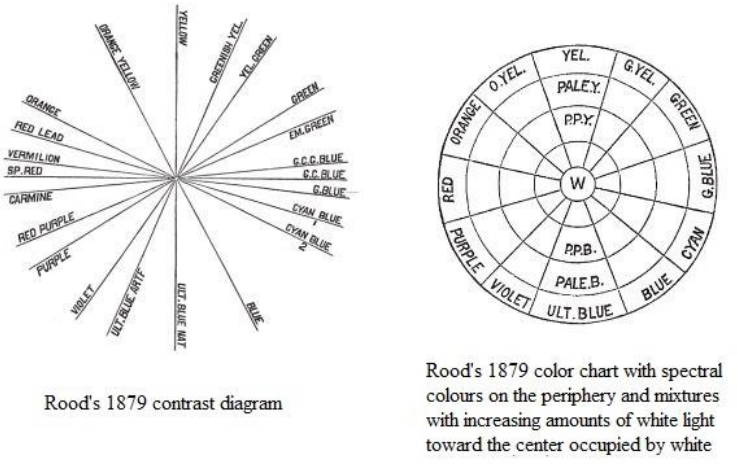

Rood's 1879 contrast diagram

Rood's 1879 color chart with spectral colours on the periphery and mixtures with increasing amounts of white light toward the center occupied by white

Figure 2.10 Nicolas Odgen Rood colour system (Rood 1892).

2.2.1 Munsell System

2.2.1.1 Introduction

Munsell system is considered to be the first successful attempt to create a genuine colour system after Runge's colour sphere. Albert Henry Munsell was an artist, not a scientist, but his system based on the principle of perceived equidistance provided standard samples according to a logically organized plan, which became the most widespread and commonly used. Munsell realized that a geometrically symmetrical solid as the sphere is unable to portray the opposing relationships between colours as human perceive them. Munsell made two important inventions to

help make measurements for organizing this system. One of these inventions was the photometer (Figure 2.11) that he used to measure the luminance of coloured objects, which helped him define how colour changes. Another invention was the Spinning Top, a rotating colour wheel, similar to the one developed by Maxwell, which he used for determining the relation between chroma and value and create templates for chroma- and value- steps in each hue. These steps, especially the value step, were created with regard to the sensitivity of human visual system (Kuehni 2002).

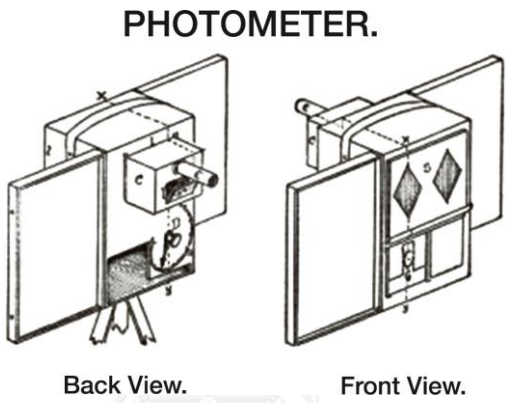

Figure 2.11 Munsell's photometer.

2.2.2.2. Hue, Value and Chroma

The hue of a colour shows how we perceive the colour of an object. Is it red, green, blue, orange? If we have a colour of same hue, such as red, it can be a vivid red or a dull red. This difference is described by chroma. For example, orange fruit and carrot have a colour described by the same hue but different chroma. Value gives the measure of colour's intensity. Brighter colours have higher value, darker colours have lower value. Munsell chose Red, Yellow, Green, Blue, and Purple as main hues and arranged them in a circle adding between each two hues the intermediate ones: yellow-red, green-yellow, blue-green, purple-blue, and red-purple. The circle had 10 segments of colours arranged at equal distances and placed so that opposing pairs compensate each other, resulting an achromatic mixture (Figure 2.12) (Whitcomb and Benson 1968).

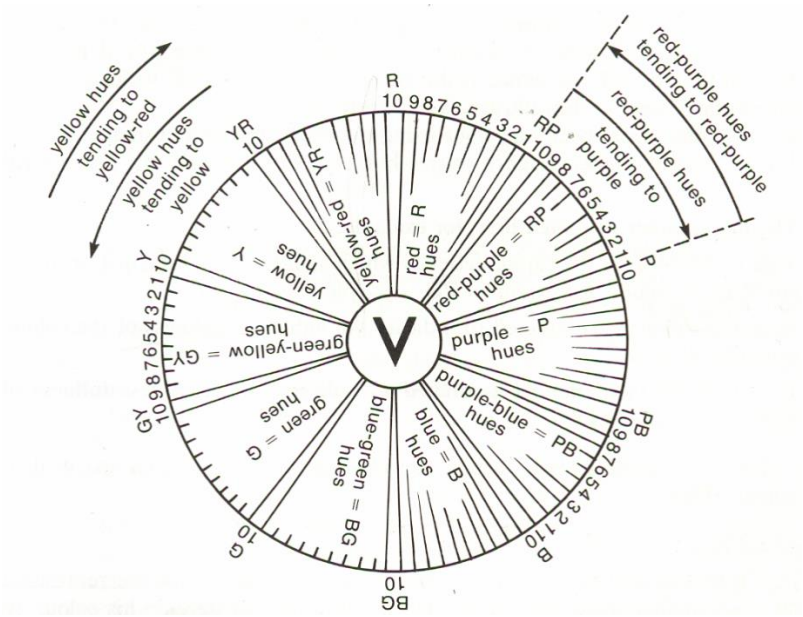

Figure 2.12 Munsell's circle.

Before Munsell 15 colour theory, the intensity of colour was defined as saturation but Munsell divided saturation in two different dimensions: value and chroma. He defined chroma as the difference between a pure hue and a pure grey. The human visual system is modeled through the Munsell colour theory in that a maximum chroma of a colour is defined by the hue of the colour, like for example a yellow hue will have less chroma values than a purple hue.

2.2.2.3. Munsell Colour Tree

Munsell organized the colours in a three dimensional space based on Hue, Value and Chroma, in which each dimension of a colour can be changed independently of the other dimensions and in which the distances between colours are visually uniform because the colour system was derived from vigorous testing of the human visual response to colour. Munsell created a total of 40 hues, first into 10 then 20 and finally into 40 segments so that they will be perceived as equidistant by the human eye. The colour system has the shape of a tree and is therefore called the Munsell Tree (Figure 2.13). In its center are the gray colours with black and white is divided into 10 steps by vertical value scale, determined with Munsell's own constructed photometer (Sharma 2004).

Figure 2.13 Munsell Colour Tree.

The Munsell Tree has many advantages:

a.) More colours can be added in between the existing colours without disturbing their order (every existing colour keep its dimension values after adding new colours);

b.) Each colour is given its own values, which can act as coordinates in a space that can be used for colour specification.

c.) It created a standard system of colour specification.

An example of how to read a colour in Munsell notation is given below:

5B 4/6 means hue of 5B, value of 4 and chroma of 6.

The main limitation of this system is that it has a discrete number of samples, therefore the space is not continuous. Also, the visually uniform spaced colours are at large distance from each other making it difficult to measure a threshold such as the just noticeable difference.

The Munsell Colour Tree was converted into a Colour Atlas containing the discrete number of samples painted on paper support. Two editions are used to this day: a matt and glossy edition, the later being produced in 1958 (Sharma 2004).

The Munsell book of colour appeared in 1929, after Munsell's death. A refinement of Munsell's notation was recommended by OSA, known as "renotation"

and later implemented in association with the Optic Society of America. The number of hues in the Munsell Book of colour doubled from 20 to 40 in 1950 (Blaszczyk 2012).

2.2.2 CIE LAB system

The groundwork for the CIE LAB system is the Munsell colour system. Its limitation inspired the “Commission internationale de l'éclairage” (CIE) to develop a uniform, continuous colour space for characterizing colour differences. This colour space is designed to approximate human vision, aspiring to perceptual uniformity, although it does not take into account the Helmholtz Kohlrausch effect (Woods 2012). The CIELAB system was derived from the CIE1931 RGB and CIE1931 XYZ colour spaces, which are the first mathematically defined colour spaces. Such colour spaces were needed for colour measurement. Some problems would arise because the quantification of either a sample or a light source comparative to a standard is a subjective procedure and dyed samples can also fade in time making them unreliable. Therefore, for objective colorimetric measurements (colorimetry) a colour system was required that did not make use of samples (Stroebel and Zakia 2008).

The CIE chromatic diagram already presented in the previous chapter (Figure 1.11) has its origins in Maxwell’s colour measurements and his triangle, described before. Colour of a certain wavelength with an additive mixture of three elementary colours (red, green, blue) produced by an apparatus with which the observer can adjust the red green blue proportions, recorded as three digits noted with R for red, G for green and B for blue.

Wright and Guild used a large number of normally sighted people to manipulate three monochromatic light sources of constant energy for achieving a match with the primary colours (Byrne and Hillbert 1997). They obtained sets of three values (tristimulus values), from which mean values were derived then were used to construct the colour matching functions by plotting their locus according to wavelength. These Figures were related by CIE to a hypothetical standard observer. CIE also stipulated that a colour sample had to be measured under average daylight conditions. These functions, called colour matching functions (Figure 2.14) were tweaked by CIE, so that only positive values would arise for any colour match,

therefore the notation of the old Maxwellian trichromatic values cannot be directly related to the primary colours any more (Fairman, Brill et al. 1997).

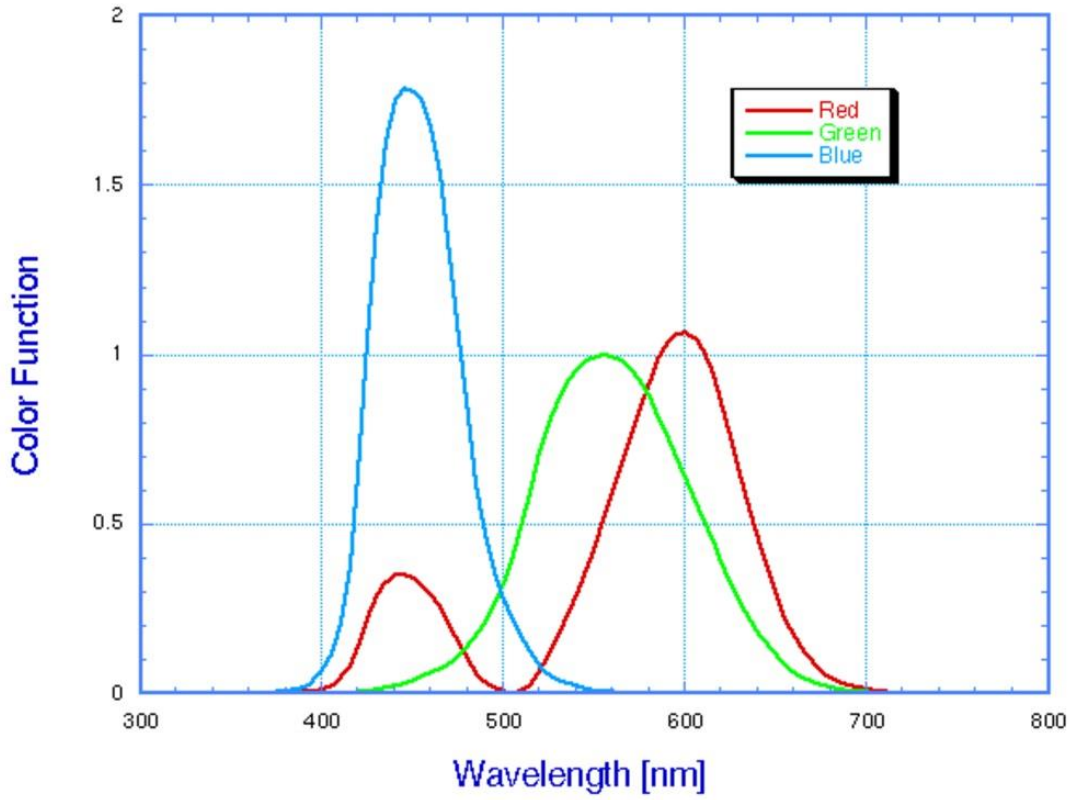

Figure 2.14 CIE Colour Matching Functions (Wyszecki and Stiles 2000).

In the desire of building a colour map, CIE eliminated one dimension by defining three new variables, named colour masses as shown in equation 2-1:

$$x = \frac{X}{X+Y+Z}; y = \frac{Y}{X+Y+Z}; z = \frac{Z}{X+Y+Z} \qquad \text{Eqn.2-1}$$

The 2 independent values that remain after these transformations can be shown on a 2-dimensional map.

The CIE diagram is a mathematical construction, based on the ability of human eye to match colours, which offers the possibility to calculate the position of each colour in relation to each of primary colours, by specifying the light sources.

Each CIE diagram plane represents colours of different brightness related to the other planes. Rösch constructed the “colour-mountain” by plotting the brightness-value of the corresponding optimal colours vertically above the colour points on plane of the CIE standard diagram (Figure 2.15) (Agoston 1989).

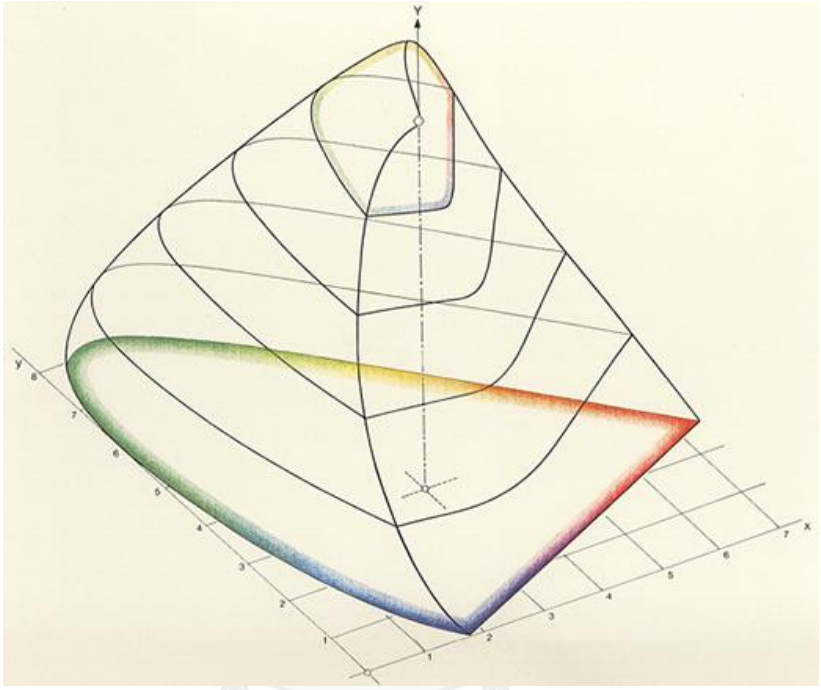

Figure 2.15 S. Rosch colour mountain (Agoston 1989).

McAdam placed around the base colours specified in the CIE diagram, ellipses that indicate their area of colour tolerance. The ellipses are determined experimentally and point to the position of those colours which can be distinguished from the nominal colour (Wyszecki and Stiles 2000). Mc Adam wrote "Analogous to Mercator charts and other kinds of maps of the world that misrepresent the ratios of distances, the chromaticity diagram does not represent perceptually equal colour differences by equal distances between points that represent equally luminous colours. The noticeability of colour differences was not considered - very little data was available - when the chromaticity diagram was devised and adopted. However, as soon as it came into use, anomalies were encountered in interpreting the points conFigured on the diagram. Inconsistencies between distances and perceived magnitudes of colour-

differences were evident. The analogy with geographical maps was quickly noted, and suggestions were made about changing the representation so that equal distances would represent equally noticeable colour-differences. A chromaticity diagram that possessed such properties came to be called 'uniform'. The search for such a diagram has extended over 50 years and is no nearer its goal. In fact, much of the evidence accumulated indicates that the goal is unattainable: a flat diagram cannot represent equal colour-differences by equal distances more than a flat map of the world can represent equal geographical distances by equal distances on the map."

The transformation from X, Y, Z to L, a, b is not a simple one. The first LAB space was the Hunter Lab. Today Lab is more often used as an informal abbreviation for the CIE 1976, marked as L^*, a^*, b^*. Both spaces derive from the same CIE 1931 XYZ colour space with the difference that Hunter coordinates are based on a square root transformation while CIE coordinates are based on a cube root transformation of the colour data. L^* has a scale of 0 to 100 and is defined by the appropriate function of a psycho-physical colour value selected in a way that uniform steps on the scale will reproduce closely the uniform differences, in terms of lightness, between colours. The a^* and b^* coordinates represent a colour's position between red-magenta and green (negative a^* values show green while positive a^* values indicate magenta), and between yellow and blue (negative b^* values show blue while positive b^* values indicate yellow) (Figure 2.16) (Hunter 1987). Red-green and yellow-blue opponent channels are calculated as differences of lightness transformations of cone responses in the eye. The uniform colour space based on these four basic colours was first described by Ewald Hering in his opponent colour theory mentioned earlier in this thesis. CIELAB space is relative to the white point of the XYZ data it has been converted from and attempts to be perceptually uniform, meaning that a change of the same amount in a colour value should produce a change of about the same visual importance.

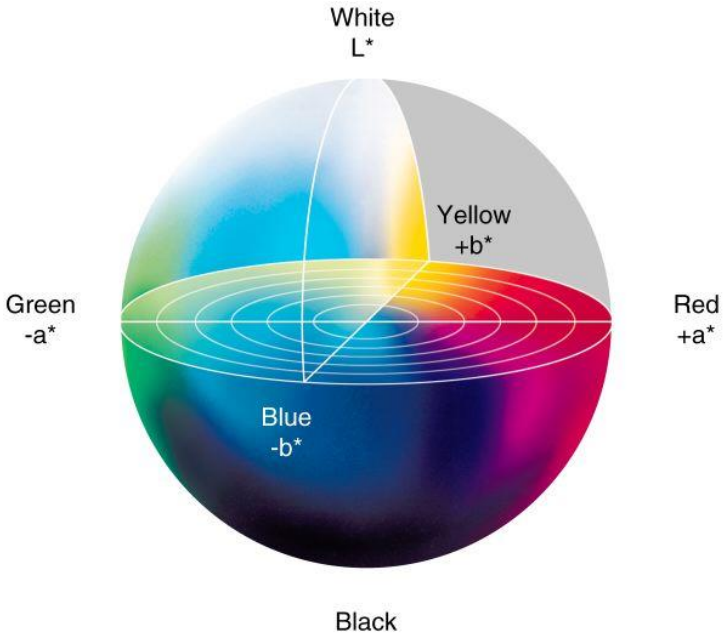

Figure 2.16 CIELAB space (Hunter 1987).

It results that the relative perceptual differences between any two colours in L^* a^* b^* can be approximated by treating each colour as a point in a 3-D space ($L^*a^*b^*$ space) and calculating the Euclidean distance between them. However, many of the colours within the $L^*a^*b^*$ space are purely imaginary, falling outside the gamut of human vision, and therefore cannot be reproduced in the physical world. $L^*a^*b^*$ values do not define absolute colours unless the white point is specified.

2.2.3 Other colour systems

2.2.3.1 Brief enumeration of some colour systems

Wilhem Ostwald a friend of Munsell, who received the Nobel Prize for his work on catalysis in chemistry, introduced a colour system devoted to colour harmonies (Hunter 1987). Michael Jacobs, a canadian sculptor and painter, built a colour system based on the peculiar combination of: red, green and violet. Max Becke's colour system objective was to examine the lows of material colouration and the effect of colours. The American psychologist Edwin G. Boring constructed a double pyramid having as central plane a rectangle, the corners occupied by Ewald Hering's four chromatic complementary colours (red, green, yellow, and blue), and the achromatic colours white and black at the tip of the pyramids.The psychologist

Dimmick returned to Boring's system in 1950 for investigating the capacity of subjects to differentiate between colours. Faber Birren constructed a colour system based on a colour circle that was in accordance with the practicalities of art and artist, differentiating between warm and cold colours. Johansson adopted Hering's ideas and promoted them in Sweden by suggesting a colour-solid. His system became very popular among teachers architects and designers. Hesselgren tried to give tangible forms to Johannsson's colour-solid, building a Colour Atlas with 507 standard colours arranged in planes of equal hues according to brightness and saturation, which provide the structure for a phenomenological based colour system that contributed to future NCS system (Silvestrini 1994).

2.2.3.2 Natural Colour System (NCS)

NCS has its origin in Hering's psychological approach and operates with the six primary colours proposed by Leonardo Da Vinci. In 1924 Arthur Pope constructed a colour system centered on a gray axis, divided into 9 gradations running between black and white, composed of a series of triangle that vary in shape and size, with a 2D projection resulting in a 12 segmented circle (Pope 2011).

The main variables of colour perception in this system are: hue, purity (saturation) and brightness. Johannson selected a similar layout for his colour system. His and Hesselgren's Colour Atlas are the references of the NCS system, a project initiated in 1965 by Anders Hard and Lars Sivik. NCS is a proprietary perceptual colour model usually used for matching colours rather than mixing. The geometrical shape of this colour system is a double-cone with yellow, red, blue, and green occupying the circular base. The colours are defined by three values: blackness, chromaticity (saturation), hue. The hue is expressed as percentage between opponent colour pairs: red-yellow and green-blue. Blackness, chromaticity and whiteness (not expressed as variable) must add up to 100%. An example of colour representation in the NCS system is given, below: S2010 R10B (Hardin and Maffi 1997).

2.2.3.3 OSA-UCS system

Wyszecki layed the foundation for the OSA-Uniform Colour Scale system by presenting a cuboctohedron constructed on the basis of perceived equidistance. The cuboctohedron is a geometrical Figure that results from slicing off all corners of a cube to the midpoint of each edge. This geometrical Figure gives the possibility of allocating 12 immediate neighbors to its central point. The Committee for Uniform Colour Scales of the Optical Society of America, founded in 1947 under Deane B. Judd, adopted the cuboctohedron for designing their colour order system. OSA's committee aim was to produce a set of samples such that the perceptual spacing between neighboring samples was equal, whether the samples differed in hue, saturation, chroma or a mixture of the three. Therefore the scaling judgments for this system are perceptual difference judgments. The system has three axes: L, j and g. Variation along the L axes changes the lightness, variation along the g axes, changes the ratio of redness to greenness content of the colour, while variation along the j axes changes the blueness/yellowness. The scaling was performed under CIE illuminant D65 against a nonselective background of 30% reflectance. The L j g coordinates can be computed from the CIE 1969 (10^{o}) xyz tristimulus coordinates. The L variable is specifically constructed to incorporate chromatic and achromatic colours. Positive values of L result for colours that have more brightness than the recommended background while darker colours will have negative values, going through zero when the colour's brightness corresponds to the background brightness (Kuehni 2003).

2.2.3.4 DIN system

The German Standard Institute created a perceptively equidistant colour system that operates with the variables: colour-hue, saturation and brightness. By means of colour-hue and saturation, the DIN system is not different than others but it achieves special status by means of its darkness scale, which can be regarded as the measure of the relative brightness of non-self-illuminating colours. 600 samples were included between 1961 to 1962 building the DIN Colour Chart 6169 (Fairchild 2013).

2.2.3.5 ISCC-NBS system

Inter Society Colour Council and the National Bureau of Standards proved through their system that colour identification itself can be the foundation of a colour system. The system's goal was to "a means of designating colours in the United States Pharmacopoeia, in the National Formulary, and in general pharmaceutical literature is desired; such designation to be sufficiently standardized as to be acceptable and usable by science, sufficiently broad to be appreciated and used by science, art, and industry, and sufficiently commonplace to be understood, at least in a general way, by the whole public." The system consists of a set of blocks within the Munsell colour system. Between 1955 to 1976, Kelly and Judd attempted to reduce colours into increasingly fine blocks. The colour names were selected independently from Munsell's system. The definitive source of this system is the publication: Colour: Universal Language and Dictionary of Names (Kelly and Judd 1955).

CHAPTER 3

LIGHT QUALITY ASSESSMENT METHODS

Light sources are traditionally characterized by their efficacy, correlated colour temperature and general colour rendering index (CRI). For new light sources, especially light emitting diodes (LEDs), the visual assessment correlates poorly with the traditional colour rendering index but no other alternative solution has been accepted until now. This chapter explains how the CRI is calculated presenting also the improvements brought to the original calculation process. It shows the weaknesses of the CRI method and describes briefly other proposed methods for assessing the quality of light.

3.1. Colour Rendering Index

Over the years, the International Commission on Illumination (CIE) has recommended assessing the quality of the light by using colour rendering index (CRI). This index measures how well light sources render the colours of a set of test samples by comparing with a reference source, better results being reflected in higher CRI values (CIE 1995). Figure 3.1 shows the 14 standard CRI test colours of which the first eight are those normally used for standard CRI. TCS01 to TCS08 are chosen to be mid-saturated colours, all having approximately the same lightness, and range in colour across the entire visible spectrum. The final six special colours, TCS09 to TCS14 include more saturated primary colours as well as simulated European skin tone and foliage. When CRI is calculated, it can be rated on a scale from 0-100. Generally, a CRI of 70 and above will be required for most lighting applications.

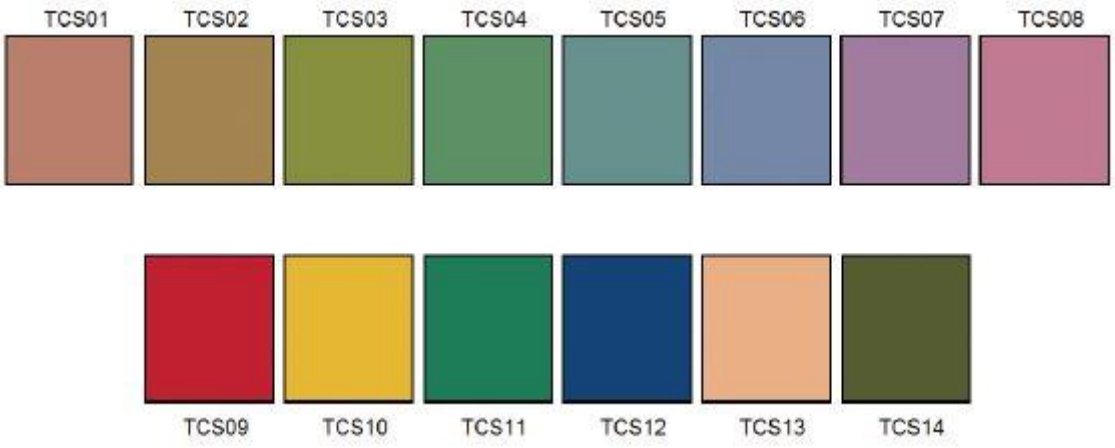

Figure 3.1 CRI test colours presented solely to give a general idea of the colours and range.

The CRI calculation proposed by CIE in 1974 can be schematically diagramed as in Figure 3.2.

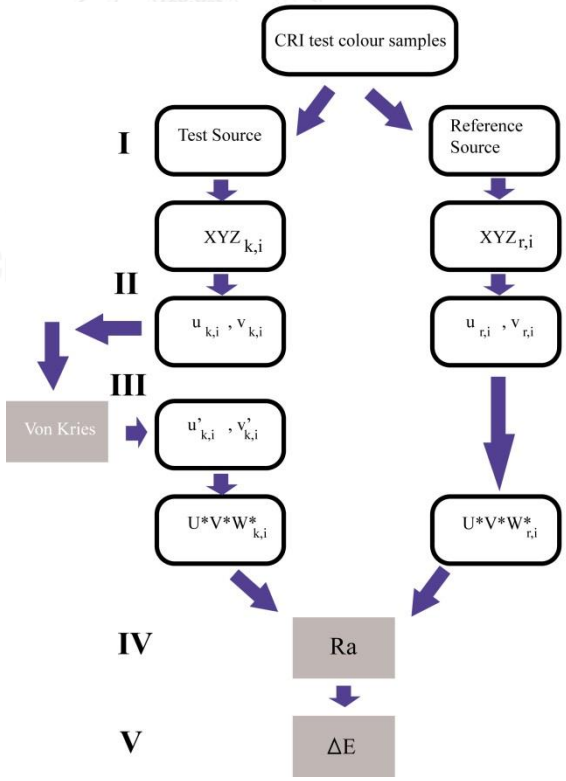

Figure 3.2 Schematic diagram for CRI calculation proposed by CIE.

The main steps, marked with Roman numbers in the diagram, are explained below.

I. CIE provides 8 test colour samples for calculating the CIE General Colour Index and 6 more for calculating the CIE Special Colour Index. The 14 samples are given through their approximate Munsell notation: 7.5R 6/4, 5Y 6/4, 5GY 6/8, 2.5G 6/6, 10BG 6/4, 5PB 6/8, 2.5P 6/8, 10P 6/8, 4.5R 4/13, 5Y 8/10, 4.5G 5/8, 3PB 3/11, 5YR 8/4, 5GY 4/4. The reference Illuminant is selected according to the correlated colour temperature (CCT) of the test source. If the CCT of the test source is under 5000K, the reference must be a Planckian radiator. If the CCT of the test source is above 5000K then the reference must be the CIE daylight illuminant (D65).

II. Colorimetric data must be transformed from CIE 1931 values (X, Y, Z, x, y) to the (u, v) coordinate of the 1960 diagram by means of the following equations:

$$u = 4X/(X + 15Y + 3Z) \quad \text{Eqn.3-1}$$

$$v = 6Y/(X + 15Y + 3Z) \quad \text{Eqn.3-2}$$

III. When the reference illuminant is changed to the test source which has different chromaticities, the change is called illuminant colour shift. The eyes adapt to the test source and this change in chromatic adaptation is called adaptive colour shift. CIE recommended the use of Von Krise linear transform for estimating the adaptive colour shift. The new colour coordinates after adaptive colour shift is called corresponding colour. The difference between the chromaticity of corresponding colour and chromaticity of refference source is called resultant colour shift. To account for the adaptive colour shift due to the different state of chromatic adaptation under the lamp to be tested, *k*, and under the reference illuminant, *r*, the following formula is used:

$$u'_{k,i} = \frac{10.872 + 0.404\frac{c_r}{c_k}c_{k,i} - 4\frac{d_r}{d_k}d_{k,i}}{16.518 + 1.481\frac{c_r}{c_k}c_{k,i} - \frac{d_r}{d_k}d_{k,i}} \qquad \text{Eqn.3-3}$$

$$v'_{k,i} = \frac{5.520}{16.518 + 1.481\frac{c_r}{c_k}c_{k,i} - \frac{d_r}{d_k}d_{k,i}} \qquad \text{Eqn.3-4}$$

The values $u'_{k,i}$ and $v'_{k,i}$ are the chromaticity coordinates of a test colour sample i, after the adaptive colour shift. The functions c and d for using in the equations 3.3 and 3.4 are calculated for the light source to be tested u_k, v_k, and the test colour samples i under the light source to be tested $u_{k,i}$, $v_{k,i}$, according to the following equations:

$$c = (4 - u - 10v)/v \qquad \text{Eqn.3-5}$$

$$d = (1.708v + 0.404 - 1.481u)/v \qquad \text{Eqn.3-6}$$

Colourimetric data must now be transformed into the 1964 Uniform Space coordinates using the following 2 sets of equations:

$$\begin{aligned} W^*_{r,i} &= 25(Y_{r,i})^{1/3} - 17; \\ U^*_{r,i} &= 13W^*_{r,i}(u_{r,i} - u_r); \\ V^*_{r,i} &= 13W^*_{r,i}(v_{r,i} - v_r) \end{aligned} \qquad \text{Eqn3-7}$$

$$\begin{aligned} W^*_{k,i} &= 25(Y_{k,i})^{1/3} - 17; \\ U^*_{k,i} &= 13W^*_{k,i}(u_{k,i} - u_k); \\ V^*_{k,i} &= 13W^*_{k,i}(v_{k,i} - v_k) \end{aligned} \qquad \text{Eqn3-8}$$

The values $u'_k = u_r$, $v'_k = v_r$ are the chromaticity coordinates of the light source to be tested after consideration of the adaptive colour shift. The values $Y_{r,i}$ and $Y_{k,i}$ must be normalized so that $Y_r = Y_k = 100$.

IV. The difference between the resultant colour shift of the test colour sample under the test lamp k and illuminated by the reference r is calculated with the following 1964 Colour Difference Formula:

$$\Delta E_i = \sqrt{(\Delta U_i^*)^2 + (\Delta V_i^*)^2 + (\Delta W_i^*)^2} \qquad \text{Eqn.3-9}$$

V. The Special Colour Rendering Index, R_i, for each test colour sample is calculated with the following equation:

$$R_i = 100 - 4.6\Delta E_i \qquad \text{Eqn.3-10}$$

The general Colour Rendering Index, *CRI*, is calculated with the following equation:

$$CRI = \frac{1}{8}\sum_{i=1}^{8} R_i \qquad \text{Eqn.3-11}$$

Although the CRI colours are specified as physical samples, the derivation of CRI can be completely computational, which means that light quality assessment does not have to be done by shining light on real colour chips. Instead of the light reflected by real colour chips, the measured spectra of the light source and the defined spectra of the CRI colour samples can be used. This is the way that illuminance spectrophotometers are working. An illuminance spectrophotometer has to be pointed only to the light source that has to be tested. The CRI is calculated based on built-in spectra of the CRI-colour samples, on the built in spectral power distribution (SPD) of illuminants and based on the measured SPD of the light that has to be tested. For a comparison based on perceived colour to be meaningful, the colour temperatures of both the test light source and the reference light source have to be the same. Spectral power distributions of several illuminants are shown in chapter 1. The reflectance curves of the main 8 CRI colour samples are presented in Figure 3.3.

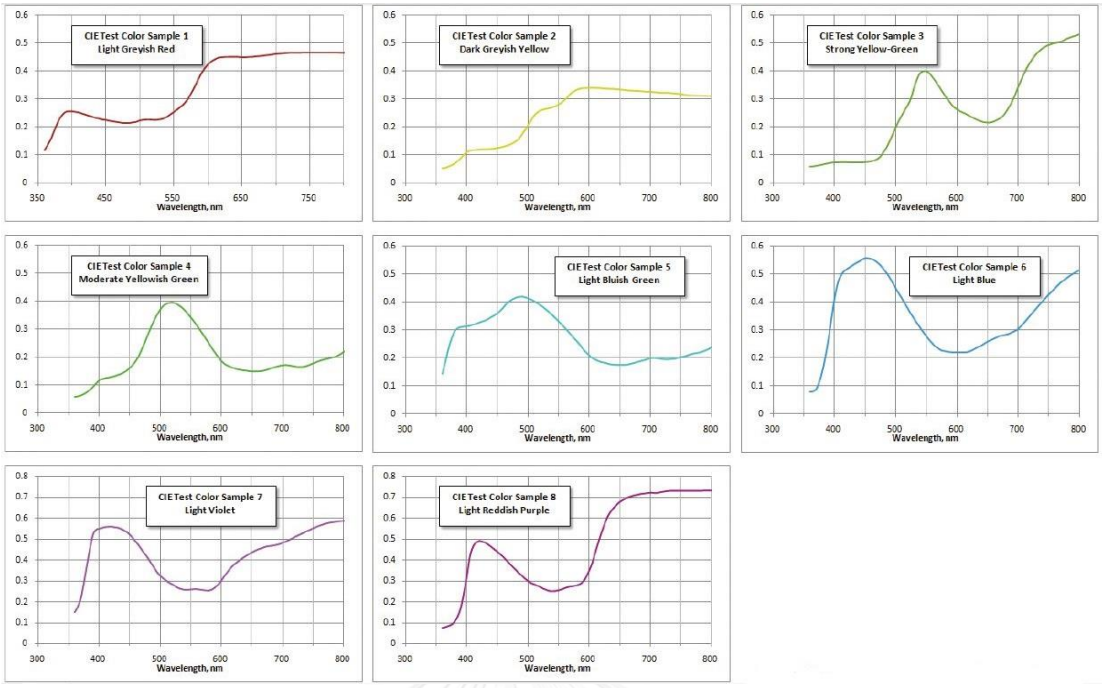

Figure 3.3 CRI test colour samples spectra.

The spectra of the CRI test colour samples can be mathematically combined with the spectra of the reference light source (illuminant) so that the test colours generate an ideal resultant colour point for each. The same is done for the test light, combining its measured SPD with the test colours, in order to produce a second set of colour points. Once these colour points are defined as trichromatic values, the calculation process is performed as shown before. The entire test can be run in software from the captured spectrum of the test light source as in illuminance spectrophotometer devices, which have such software integrated along with the necessary spectra database.

If the colour points from the test light source are identical to those from the reference light source then the colour rendering is identical and the CRI is 100. A perfect score of 100 represents no colour differences in any of the eight samples under the test source and reference illuminant. The CRI definition allows negative numbers that are usually rounded to zero.

3.2. Proposed light quality assessment method due to CRI's criticized weakness

One of the newest and most efficient light source types is the light emitting diode (LED). It is increasingly used in many applications because of its individual characteristics. LED overcomes incandescent light source in terms of high efficiency, easily adjustable intensity, chromaticity control, and attractiveness for highly sensitive materials, due to optical radiation (Taguchi 2006, Berns 2010) LED generates less heat than the cost effective halogen lamp and much less than the cost ineffective incandescent lamp.

Despite the fact that the CRI of LED light sources are generally lower than the ones calculated for incandescent sources, various visual assessment results suggest otherwise. It can be implied that the CRI may not be good enough for assessing the quality of LED sources. For solving this problem, The National Institute of Standard and Technology (NIST) created a new index for measuring the quality of light sources called the Colour Quality Scale (CQS). Many researchers agree upon a better communication in quality of LED light sources of CQS in terms of little variation in value which is highly relevant to more of a human perception (Davis and Ohno 2006).

Due to subjective matter, it is very difficult to explain human colour perception. There are various experimental techniques that can be used to measure it. The tool for estimating colour perception composes of three main techniques: the threshold, matching and scaling experiment. In addition, one-direction scaling techniques also have variety of common techniques for assessing colour perception as follows: rank order, partition scaling, paired comparison, rating and category scale, magnitude and ratio estimation (Fairchild 2013).

CQS is calculated differently from CRI, using the CIE $L^*a^*b^*$ colour space instead of the obsolete CIE $W^*U^*V^*$ colour space. A spectroradiometer is the favorite tool to obtain spectral reflective data from surface colours corresponding to the actual viewing condition.

Why is Colour Rendering Index inappropriate to assess the quality of LED light source?

The relationship between colour rendering property of various LED light sources and human colour preference using visual assessment method has been investigated by Narendran et al (Narendran and Deng 2002). The scene stimuli composing of many displayed objects were shown under various LED light source in comparison to incandescent light source at 200 lux. Observers then would estimate their preference of scene stimuli under both light sources. The result showed that using only white LED light source, observers could perceive human skin tone poorly whereas using blending RGB LED with white LED light source could observe the best preference stimuli at overall scene. Moreover, observer's preference of colour had no correlation to CRI value of light source. Therefore, they recommended that CRI value was inappropriate to assess the quality of LED light source.

Why is the Colour Quality Scale better than the Colour Rendering Index for expressing the quality of LED?

Boissard et al. studied whether blending LED source is possible to match stimuli with fluorescent and incandescent source or not. Moreover, they also investigated which index can represent the quality of light source that was as close as human visual perception. All illumination in their study was controlled at approximately 250 lux. From observer's estimation, RGB LED source blending with warm and cool white LED provided stimuli's perception as close to incandescent and fluorescent source respectively. With higher CRI value, it was meant to have a better quality of light source but the study proved that the CRI value of blending LED was definitely lower than a reference source. However, when using CQS, the value among them was not much different. It might therefore be implied that the CQS is better than the CRI for expressing the quality of LED source (Boissard and Fontoynont 2009).

Are there better methods than CRI and CQS for describing the quality of LED light sources?

CRI and CQS did not always describe visual colour correctly, Cheng et al. demonstrated that the modified method of both indices to be more in correlation with human vision. The magnitude estimation was used to assess the colour appearance

attribute of 60 textile samples in terms of lightness hue and saturation under the 3 light sources: white LED, fluorescent lamp, and blending 8 LEDs. Using CIE D65 as a reference source, the CRI and CQS value of blending 8 LED sources was close to that of fluorescent source but the value was much higher than that of the white LED. Both values of CRI and CQS did not have any conformity when comparing with magnitude estimation result. Therefore, the CRI and CQS were modified by CIECAM02 colour appearance model and the result showed that the new method was better in agreement with visual experiment than traditional CRI and CQS (Luo, Cui et al. 2006).

Mahler et al. studied the efficiency of colour discrimination by arranging 32 hue test samples in order under various LED and incandescent sources at the same colour temperature. The conclusion was that, if the colour discrimination efficiency was in relation to the CRI as well as CQS, then it was independent on chroma of sample when increased by a light source (Mahler, Ezarati et al. 2009).

The Gamut Area Index (GAI) was represented as a new indicator for estimating the quality of light source. It was defined by the polygon area of 8 CIE standard samples on chromaticity colour space when illuminated by a test light source. Rea et al. studied colour discrimination and observer's preference under various illuminants. Colour discrimination was tested by Farnworth-Munsell 100- hue test method under various light sources. They found that colour discrimination was not related to any CRI value, while increasing GAI value led to good colour discrimination. Moreover, GAI and CRI was a good indicator when samples were illuminated by warm white and cool white source respectively, but not when it happened vice versa. It might be concluded that using only CRI was not enough to express the light source quality. Both CRI and GAI have advantages in different aspect and should be used together for assessing the quality of the light sources (Rea and Freyssinier-Nova 2008).

Thompson et al. examined colour perception of 24 stimuli which were rendered by composite spectrum of 7 LED sources with various colour rendering index comparing with incandescent source while illumination and chromaticity were held constant at approximately 300 lux and 3000 K respectively. When incandescent source was set up as a reference, the observer rated the colour samples under blending LED sources in 4 categories; same, just noticeably different, different, or very

different. The result showed that the CRI of LED source was more effective on red and yellow stimuli than green and blue stimuli, and the green stimuli could be distinguishably seen easier than blue ones. When red and yellow samples had lower saturation, perception tolerance could be acceptable even though there is less CRI of LED source (Thompson and O'Reilly 2007).

3.3. Colour Quality Scale

The Colour Quality Scale (CQS) uses a new set of test colour samples that are more saturated than the CRI colour samples. The CQS method introduces, along with the new set of test colours, an important principle in light quality assessment by not penalizing the quality of a LED light source that shows increases in chromatic saturation of the test colours compared to the reference light. CQS uses the CIELAB trichromatic values for defining the colour points and better chromatic adaptation transforms than Von Kries. However, the CQS calculation methodology has not been adopted by CIE at the moment of writing this Thesis and will not be used in this work. But the set of colours proposed by NIST for the CQS will be used as a start-point in determining the colour wheel that has to fulfill the conditions imposed in the original contribution part of this work (Davis and Ohno 2009, Davis and Ohno 2010).

The colour samples proposed by NIST for CQS are shown in Figure 3.4.

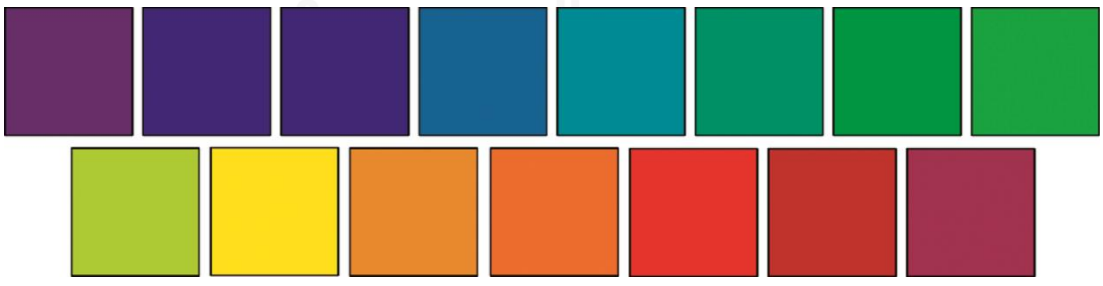

Figure 3.4 CQS test colours presented solely to give a general idea of the colours and range.

The CQS colours shown in Figure 3.3 have the following Munsell notation: 7.5P 4/10, 10PB 4/10, 5PB 4/12, 7.5B 5/10, 10BG 6/8, 2.5BG 6/10, 2.5G 6/12, 7.5GY

7/10, 2.5GY 8/10, 5Y 8.5/12, 10YR 7/12, 5YR 7/12, 10R 6/12, 5R 4/14, and 7.5RP 4/12. A comparison between the trichromatic colour points of the CQS and CRI test samples in CIELAB, is shown in Figure 3.5.

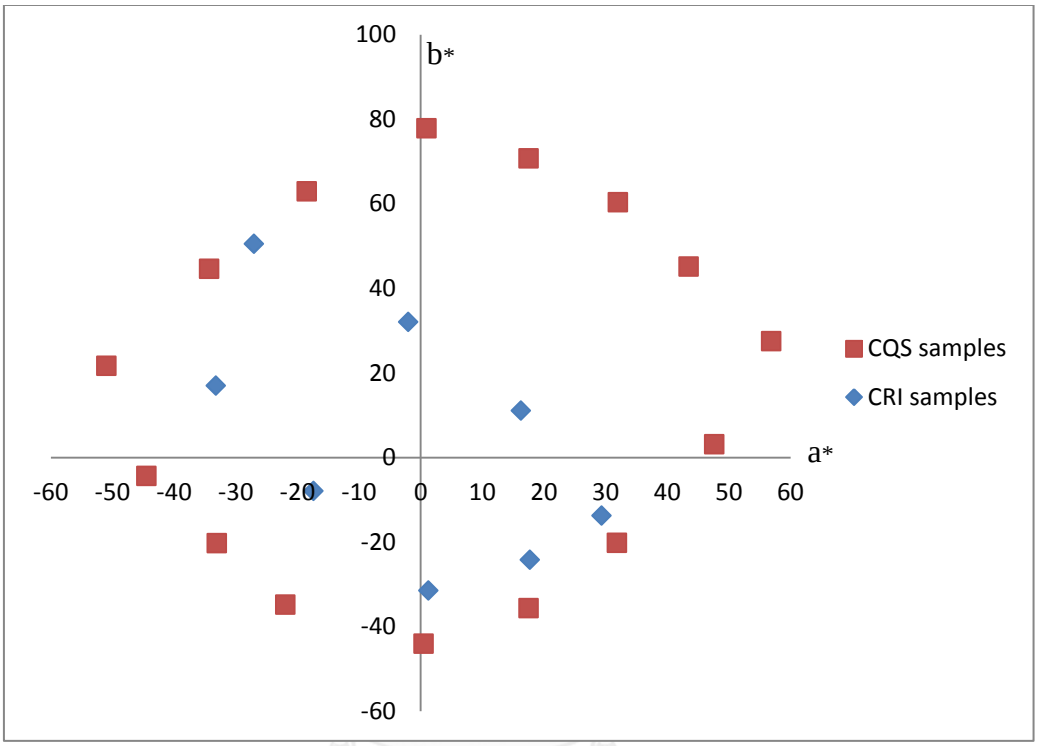

Figure 3.5 CQS vs. CRI colours in CIELAB space viewed perpendicular on the L*-axis.

There are several improvements in the CQS over the CRI but the most significant change is the inclusion of the saturation factor that can be clearly seen in Figure 3.5. While traditional light sources mostly do not enhance chroma, the saturation factor is generally effective on new light sources, such as LEDs, which enhance object chroma.

Below is a summary of the improvements and calculation processes proposed by NIST for CQS (Davis and Ohno 2010):

1. To solve number of pastel samples used in calculating the CRI, the CQS has been compensated with 15 samples that have higher saturation and cover all hue angles since CRI only contains a fewer samples with moderate saturation.

2. The 1964 W^* U^* V^* using in the CRI is outdated and not widely used. Therefore, a CIE recommended CIELAB which has a more uniform colour difference, is used instead of CIE W^* U^* V^* colour space for finding out colour differences between samples under test and reference source.
3. The CRI determines the changing of colour attribute of object in all direction including hue, chroma, and lightness. However, increasing in object saturation under the test source lead to an enhance brightness perception which is positive effects and usually preferred. In case of CQS, this equation determines only the hue and lightness shift where chroma is taken into consideration upon the increase and decrease value of the object under the test sources. Chroma will not be calculated toward the equation if object have more saturation under test source.

$$\Delta E_i = \Delta E^*_{ab,i} \quad \textit{if} \quad \Delta C^*_{ab,i} \ \textit{is negative} \qquad \text{Eqn. 3-12}$$

$$\Delta E_i = \Delta E^*_{ab,i} - \Delta C^*_{ab,i} \quad \textit{if} \quad \Delta C^*_{ab,i} \ \textit{is positive} \qquad \text{Eqn. 3-13}$$

4. According to the CRI method, the CCT of the reference sources should matched to that of the test source where CRI value remain the same whether value of CCT changes or not. For solving this problem, CQS establishes the multiple factors to determine sources in case of any changes in CCT.
5. In the CRI, the colour difference for all samples is averaged. It is possible for CRI light source to have high score over poor rendering of one or two colours. To ensure the influence of any shifting samples, CQS uses the root mean square (RMS) to replace the averaged method.

$$\Delta E_{RMS} = \sqrt{\frac{1}{15}\sum_{i=1}^{15}\Delta E_i^2} \qquad \text{Eqn. 3-14}$$

6. In some of the result of CRI, it may appear to have negative values. Therefore, in order to avoid confusion, CQS uses scale conversion to range the value between 0-100.

3.4. Chromatic Adaptation Transforms

A general structure for chromatic adaptation is presented in Figure 3.6. The flow starts with the CIE tristimulus values ($X_1Y_1Z_1$) for the first viewing conditions that are transformed to cone excitations ($L_1M_1S_1$). The chromatic adaptation model incorporates information about the first viewing conditions to predict adapted cone signals ($L_aM_aS_a$). Then the process is reversed for the second set of viewing conditions to determine the corresponding colour in terms of cone excitations ($L_2M_2S_2$) and finally the CIE tristimulus values ($X_2Y_2Z_2$).

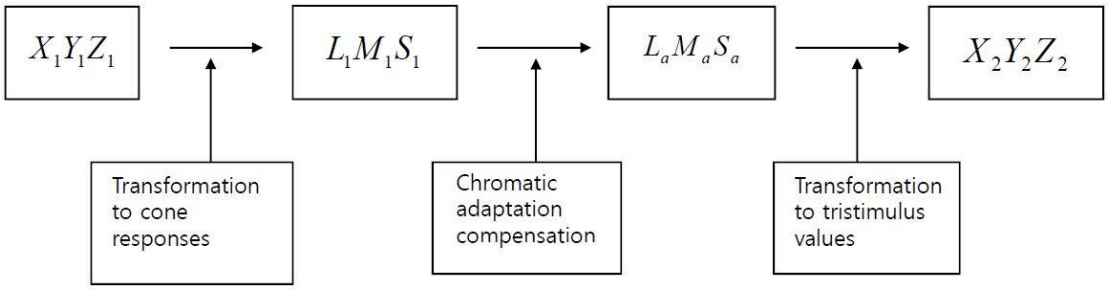

Figure 3. 6 General flow chart for a chromatic adaptation.

Mathematically, a destination colour characterized through its trichromatic $X_DY_DZ_D$ values can be calculated from a source colour having the trichromatic values $X_SY_SZ_S$, considering the linear transform noted with M, by the following equation:

$$\begin{bmatrix} X_D \\ Y_D \\ Z_D \end{bmatrix} = [M] \cdot \begin{bmatrix} X_S \\ Y_S \\ Z_S \end{bmatrix} \qquad \text{Eqn.3-15}$$

where [M] is dependent on the source reference white and the destination reference white. There are different types of transforms, resulting in different [M] matrices in equation 3-15. To enumerate a few: there are XYZ scaling, Von Kries, Bradford, CMCCAT2000, CIECAM02 (Hunt, Li et al. 2005).

XYZ Scaling is considered to be an inferior chromatic adaptation algorithm, being the method that would result from transforming the source $X_SY_SZ_S$ colour to

Lab using the white point of the reference source followed by conversion to $X_D Y_D Z_D$ using the white point of the destination light source.

The von Kries chromatic adaptation transform is based on the Young-Helmholtz theory, which assumes that, although the responses of the three cone types are affected differently by chromatic adaptation, the relative sensitivities of each of the three cone mechanisms remain unchanged (Kries 1970). CRI uses this model according to the mathematical model shown next:

$$\begin{aligned} L_a &= k_L L \\ M_a &= k_M M \\ S_a &= k_S S \end{aligned} \qquad \text{Eqn. 3-16}$$

where

$$k_L = \frac{1}{L_{MAX}} \qquad k_L = \frac{1}{L_{WHITE}}$$
$$k_M = \frac{1}{M_{MAX}} \qquad k_M = \frac{1}{M_{WHITE}}$$
$$k_S = \frac{1}{S_{MAX}} \quad \text{or} \quad k_S = \frac{1}{S_{WHITE}} \qquad \text{Eqn. 3-17}$$

$$\begin{aligned} L_2 &= \frac{L_1}{L_{MAX\,1}} \cdot L_{MAX\,2} \\ M_2 &= \frac{M_1}{M_{MAX\,1}} \cdot M_{MAX\,2} \\ S_2 &= \frac{S_1}{S_{MAX\,1}} \cdot S_{MAX\,2} \end{aligned} \qquad \text{Eqn. 3-18}$$

$$\begin{bmatrix} X_2 \\ Y_2 \\ Z_2 \end{bmatrix} = M^{-1} \begin{bmatrix} L_{MAX\,2} & 0 & 0 \\ 0 & M_{MAX\,2} & 0 \\ 0 & 0 & S_{MAX\,2} \end{bmatrix} \cdot \begin{bmatrix} \frac{1}{L_{MAX\,1}} & 0 & 0 \\ 0 & \frac{1}{M_{MAX\,1}} & 0 \\ 0 & 0 & \frac{1}{S_{MAX\,1}} \end{bmatrix} \cdot M \begin{bmatrix} X_1 \\ Y_1 \\ Z_1 \end{bmatrix} \qquad \text{Eqn.3-19}$$

Von Kries model is luminance-independent and does not account for incomplete adaptation.

CHAPTER 4

METHODOLOGY FOR USING SINGLE LENS REFLEX (SLR) DIGITAL CAMERAS TO EVALUATE LIGHT QUALITY OF LED LIGHT SOURCES.

4.1. Preamble

Latest studies have been searching for methods aimed to obtain colorimetric data from user grade digital cameras because, unlike colorimetric measurement devices, they have smaller size, lighter weight, less power requirement, lower cost and the potential of storing thousands of images. Despite some promising results, obtaining colorimetric outputs from digital cameras has had limited success, mostly because of signal aberrations that are due to the colour signal acquiring and to onboard image processing systems.

The parameters set up for correcting the colour output of one camera, could never be reproduced for obtaining similar results on different digital cameras. In other words, there is absolutely no way of applying a general method for turning multiple digital cameras into colorimeters and even when a method is particularly applied for one camera alone, it does not give satisfactory results.

However, quantitative colour data acquisition capabilities of consumer grade digital cameras prove to be better for some colours than for others in certain condition. This fact could form the basis for developing a method to establish a set of colour samples from 1300 Munsell matte sheets of colours that could be used for obtaining colorimetric values from their digital images, with the aim of creating a colour wheel that permits the replacement of spectroradiometer with a consumer grade digital camera in the process of light source quality comparisons. The colours in this wheel should fulfill two conditions: they must be part of a set for which multiple cameras give a good response when applying the same restraints for taking pictures and they must be properly selected for a meaningful evaluation of colour rendering of different light source types. This last condition can be fulfilled only if the selected

colours cover all hue angles. However, although this condition is necessary, it is not sufficient in some cases. For example, in case of light sources with highly discontinuous spectral power distribution, such as LED light sources, the selected colours must have a higher degree of saturation too.

Colour wheels have been created throughout the history starting with Robert Grosseteste (Huxtable. 2013), who introduced the notion of controlled experiment and related it to demonstrative science at the beginning of the 13th century. The colour wheels of the last century that defined some of the colour spaces we use today, such as the Munsell space. In chapter 2, many colour wheels have been presented, but not all of them resulted in colour spaces. For example, Chevreul's colour circle, shown in chapter 2 Figure 2.5, was an attempt to create colour harmonies. Newton's colour circle, mentioned in the same chapter and probably the most known colour wheel, was a direct result of experiments combined with his desire of associating colour with music. Unlike other colour wheels, the wheel resulted from this work has colours that meet digital camera's capability of having a good response in certain restraint conditions and simultaneously meet the necessary conditions for describing the faithfulness of colour rendering, in order to compare the quality of light for different light sources.

Although there is no general method that can be applied for obtaining output from multiple digital cameras, the methodology explained in this chapter will demonstrate that in certain conditions, colorimetric output can be obtained with different SLR digital cameras for a limited number of colours grouped in a colour wheel that can be used in evaluating the quality of LED light sources.

4.2. Defining the principles on which the method is developed

Developments in camera's sensor technologies have made consumer grade digital cameras one of the latest research objects for obtaining colorimetric data from digital images (Wu, Allebach et al. 2000).

Single Lens Reflex (SLR) digital cameras have Charge-Coupled Device (CCD) or Complementary Metal Oxide (CMOS) sensors and a red-green-blue (RGB) colour filter array (CFA) or a Bayer filter. The light that enters the camera is

controlled by means of the aperture, exposure time and International Organization for Standardization sensitivity value (ISO), then is handled by colour processing algorithms and stored as a colour number in the camera's memory. Obtaining colorimetric data from this colour number means to reverse the camera's process of producing it from the colour signal that entered initially through the camera's lens. There are several factors that make this difficult: 1) lens aberrations that vary across digital cameras, 2) factors related to camera settings, 3) environmental factors including but not limited to: the angle of incident light on colour object, type of light source, distance and angle of the camera towards the colour object, 4) factors related to the camera processing algorithms which are usually proprietary and 5) factors related to brightness fall on the image frame. Various spectral-recovery method as a way to achieve colorimetric characterization, proved to be not as good as trying to go from RGB to XYZ directly (Cheung, Westland et al. 2004).

The way SLR cameras with RGB CFA work, could be summarized in the following steps.

1. Image capture, when the button for taking a picture is pressed. The camera's lens diaphragm opens at an aperture fixed manually or decided automatically for a reasonable shutter time by the camera's central systems.
2. Image transmission to the sensors, guided by the system of lenses that direct the light reflected from the colour object(s) to focus on an array of photosensitive semiconductor cells (CCD or CMOS) through RGB filters, positioned next to each other in a definite pattern and in close proximity to the sensors. Only one of the primary RGB colours can pass through each filter.
3. Transmission of image information by the sensors. The photosensitive conductor cells respond to light and generate charges proportional to the intensity of the incoming light, which are conducted across the chip and converted to values that are transformed into an array of digital values by an analog-digital converter.
4. Recording of the Raw and generating the input for the computer, which is then processed in different ways.

5. After converting Raw to Tiff, image processing of the array of digital values, resulted from the sensors and the filter pattern was done. Because only one of the primary RGB colours can pass through each filter, the other two which are necessary for creating a pixel's colour are calculated through interpolation, based on proprietary algorithms, from the primaries that pass through neighboring filters on the array.

The proprietary algorithms used in image processing deal with brightness, gamma correction, geometric distortion, high and low pass filters, edge enhancement device and processing efficiencies, sensor characteristics and limitations, colour saturation, etc. Raw data, which should be in theory the output from each original red, green, blue sensitive pixels of the image sensor after being read out of the CFA matrix, seems to be preprocessed in some way (Hytti 2006).

CMOS and CCD technologies should confer system linearity to SLR cameras but in practice this linearity is limited. Lens aberrations combined with a 2/3 intensity loss of the signal through the colour filter array and with onboard processing algorithms that try to compensate signal loss and distortion, as well as to emulate the non-linear behavior of the human eye in different ways, depending on camera type and manufacturer, are several reasons why these systems cannot be considered to have a linear response.

Despite the above mentioned difficulties in obtaining colorimetric data from digital images, literature shows that digital cameras can be used as tristimulus colourimeters to some extent (Martinez-Verdu, Pujol et al. 2003, Haralabidis and Pilinis 2005, Solli, Anderson et al. 2005, Marguier, Bhatti et al. 2007) and camera response is better for some colours than for others (Cheung and Westland 2006).

The methodology presented in this work is developed from the assumption that the causes for non-linear response to colour signals in digital cameras produce acceptable errors for some digitized colours in certain conditions. In other words, it is assumed that when particular constrained conditions are applied for taking pictures, the digital cameras' behavior can be considered linear for a variable but determined number of colours within variable. This assumption will become the basis principle on which the presented methodology relies upon, once demonstrated through experiment.

4.3. Designing the experimental setup

4.3.1. Equipment and materials

The equipment consists of colorimetric devices, as defined in 1.8., and digital image acquisition devices, as defined in 1.9.

For this experiment the following imaging devices were chosen:

1) Canon EOS X4 SLR digital camera, with CMOS sensor, shown in Figure 4.1;

2) Nikon D40x SLR digital camera, with CCD sensor, shown in Figure 4.2,

3) Nikon D70 SLR digital camera, with CCD sensor,

4) Canon 60D SLR digital camera, with CMOS sensor,

5) Canon 600D SLR digital camera, with CMOS sensor,

all having red-green-blue colour filter arrays and powerful zoom lenses, not shown in the Figures. The selected digital cameras have different type of architectures, different type of sensors and are produced by different manufacturers in order to test if the experiment can be reproduced on a wider range of digital camera types, not just on one particular model. The last three digital cameras in the list were used to verify the results. One thousands three hundreds Munsell matte colour sheets produced by X-Rite were used for combining in colour wheels. The Canon and Nikon lenses of 135 focal length were used.

Figure 4.1 Canon EOS X4.

Figure 4.2 Nikon D40x.

Two boxes were built from light materials painted matte black, with light source holders. The ceilings have an adjustable mechanism for fixing the height so that light intensity at the bottom of the box can have values in the range of 600-650 lx on a determined surface. The selected light sources are two commercially available light sources:

1) Philips Ambience fluorescent D65 Tornado, 13 watts, E27/ES 650 lumen, shown in Figure 4.3;

2) Osram Parathom classic LED A40 cool white, 8 watts, E27/ES, 450 lumen, shown in Figure 4.4.

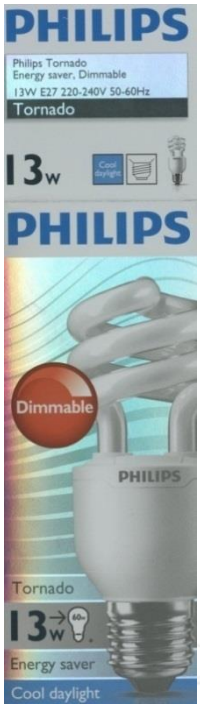

Figure 4.3 Philips fluorescent D65 Tornado.

Figure 4.4 Osram Parathom classic LED A40.

Each light source is placed in a separate box. Light sources are not connected directly to a plug but through a stabilizer, in order to avoid intensity variations during the experiment. Boxes and cameras were placed in a dark room.

The following equipment was prepared for colorimetric measurements:

1. X-Rite Spectrophotometer SP62, shown in Figure 4.5, used for measuring the CIELAB D65/2 values of the Munsell matte sheets used for combining in colour wheels.

Figure 4.5 SP62 X-Rite portable Spectrophotometer.

2. Konica Minolta CS1000 Spectroradiometer, shown in Figure 4.6, used for measuring the CIELAB values of the Munsell matte colours combined in colour wheel under the considered light sources.

Figure 4.6 Konica Minolta CS1000 Spectroradiometer.

3. Konica Minolta CL-500A illuminance spectrophotometer, shown in Figure 4.7, used for measuring the CRI of the considered light sources.

Figure 4.7 Konica Minolta CL-500 Illuminance spectrophotometer.

4. Konica Minolta CL200 Chroma meter, shown in Figure 4.8, used for measuring the light intensity of the considered light sources at the bottom of the designed boxes.

Figure 4.8 Konica Minolta CL200 Chroma meter.

4.3.2. Apparatus design

The apparatus consists of a box with adjustable ceiling, placeholder for colour samples and a light source holder. The design of the box is based on photometry (see 1.6).

Light intensity decreases with the square distance (*d*) measured from the source; reflected in a direct proportional decrease in the illuminance as shown in Eqn 4-1.

$$E = K\frac{I}{d^2} \qquad \text{Eqn.4-1}$$

The constant *K* depends on the shape and position of light source relative to the measuring point. To simplify the calculations, the light source is considered to be a point source. Point light sources emit light of equal intensity in all directions and the radiation around the source has the shape of a sphere. The intensity decreases towards

the edge of this sphere with the square distance measured from the sphere's center (where the source is placed). The illuminance, E (lumen/m^2), of any distance from the point source is obtained by dividing the emitted intensity to the entire sphere's surface which is $4\pi r^2$:

$$E = \frac{I}{4\pi r^2} \qquad \text{Eqn.4-2}$$

where I = Intensity of light source and r = Radius of sphere

If the light source is placed in the center of the box, the distance d from light source to the bottom of the box will be the radius of the sphere: with $d = r$. Therefore the above equation can be written as:

$$E = \frac{I}{4\pi d^2} \qquad \text{Eqn.4-3}$$

This way, equation 4, has been simplified by identifying the constant K with $\frac{1}{4\pi}$

Imposing E = 630 lux at the bottom of the box and knowing the intensity emitted by the lamp results d, which is half height of the box. This is the only dimension needed for building the box as a cube. To compensate the design errors that result in different intensity of light at the bottom of the box, the ceiling is provided with an adjustable mechanism.

The walls of the box will have to be black so that the light (outside of the considered sphere) should not be reflected by the walls and should not add to the light rays that fall on the sample placeholder. Figure 4.9 shows the schematic design of the box.

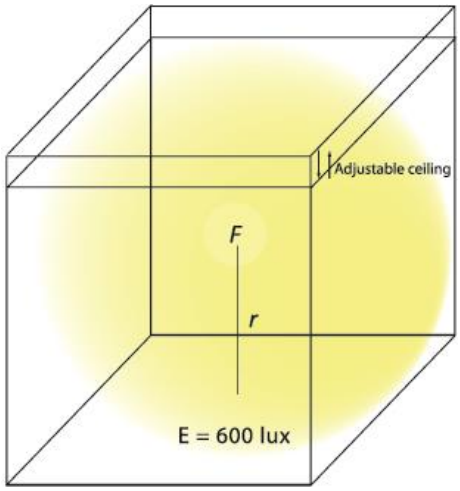

Figure 4.9 Box designed for the experiment.

4.3.3. Setup

The constrained conditions mentioned in 4.2. for taking pictures consist in the experimental setup described as follows.

Both boxes, designed as described before, are placed in a dark room. Each box has a different light source (one of the 2 mentioned in 4.3.1.) in its light source holder. The ceilings of the boxes are fixed through their adjustable mechanism, so that the light intensity at the bottom of each box has values in the range of 600-650 lx on a determined surface. Light sources are not connected directly to a plug but through a stabilizer, in order to avoid intensity variations during the experiment. On the bottom of each box was placed an achromatic wheel composed of the neutral Munsell sheets N2, N3.5, N5, N6.5, N8, N9.5, with the N9.5 (white) positioned in the middle.

The Canon camera was placed on a tripod and pictures were taken from different distances and angles to determine the best linear response of the two cameras. From each picture was cropped an area around the center that corresponds to a wheel-surface with a diameter of 12 cm on the wheel. The diameter was selected to reduce the vignetting effect by measuring the light intensity drop from the center of the wheel with Konica Minolta CL200 Chroma meter (Zheng, Lin et al. 2006). Light intensity on the considered area was between 600-650 lx for both light sources, according to the preliminary condition. This intensity interval was obtained by fixing the intensity in the center of both boxes around 630 lx through the adjustable

mechanism of the boxes' ceiling. From the cropped pictures, the average RGB values were calculated for each neutral colour depicted with the cameras' software, used to connect the cameras to computer (Digital Photo Professional for the Canon camera and Camera Control Pro 2 for the Nikon camera). Pictures were taken with 135 mm lens, ISO 100, minimum aperture and flashlight off, in sRGB mode, leaving all other settings in automatic mode.

Spectrophotometric curves measured for the neutral Munsell sheets have similar shape and are almost invariant to wavelength in the range of 430-700 nm interval. The reflection measured at 480 nm was considered for blue, the one measured at 530 nm was considered for green and the reflection measured at 640 nm was considered for red. Around these wavelengths, digital cameras have generally high sensitivity as shown in literature (Cheung, Westland et al. 2004). Assuming that the RGB data obtained from the digital images are the result of an encoding process that fits best an inverse power function, the picture for which the relations between the average RGB values and the selected spectrophotometric reflection values of the six neutrals are given by the best fit inverse power functions with the highest correlation coefficients, determines the best shooting position for which the camera system has a linear behavior with low error margin. The best shooting distance resulted to be 1 m and the best shooting angle 45^{o}. The final setup is shown in Figure 4.10.

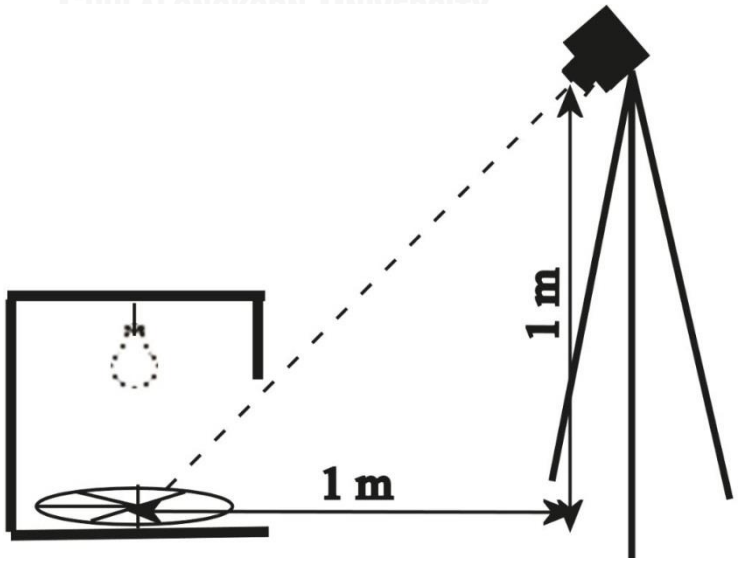

Figure 4.10 Experimental setup.

4.4. Describing the methodology

The processes mentioned and described in 4.1. and 4.2. can be schematically represented through the diagram shown in Figure 4.11. The diagram shows the path of the light reflected by the colour sheets, which carries the colour signal, through the system of lenses, through the colour filter array, into and out of the sensor until it is encoded and stored. The intensity of light that exits the lens system I_i is different from the intensity that enters I, but between the two, a linear relation is assumed. Aberrations in lens geometry can affect the assumed linearity. Mechanical defects and contamination of the imager or lens can result in random amplification of stray light artifacts by the sensors contributing to non-linearity of the system (Raizner and Fritsch 2010). Digital cameras have embedded software that tries to compensate for these problems. The described method assumes that for some colour clusters compensation is successful. The light of intensity I_i travels through the Colour Filter Array (CFA), which collects red, green and blue light in separate pixels. Only one third of the light is captured in each pixel, resulting in loss of colour accuracy and image resolution, which is compensated through complex signal processing algorithms, known as Colour Filter Array Interpolation or demosaicking algorithms (Bahadir, Glotzboch et al. 2005). This method assumes that compensation is successful in case of limited colour cluster volumes across the sRGB colour space. Raw data, which should be in theory the output from each original red, green and blue sensitive pixels of the image sensor after being read out of the Bayer matrix, seems to be preprocessed in some way (Hytti 2006). Through the described method is assumed that the preprocessing is not affecting the linear response of camera for all received colour signals.

CMOS and CCD technologies should confer system linearity to digital cameras. In practice, this linearity is limited. For example, if the number of received photons is small during image exposure, the output digital values are dominated by noise. The attempt to decrease the noise by modifying the ISO settings results in the opposite effect. On the other hand, if the number of received photons is too big then the physical saturation of the detector elements is overflown and the digital values exhibit strong non-linearity. Digital saturation is reached before physical saturation,

producing non-linearity as well. It is assumed that such non-linearities are not excessive in some colour space regions and therefore, they do not have an unreasonable negative impact on the colour output calculated with this method.

The assumptions mentioned before can be easily tested as follows. The encoding process of the colour and the decoding process for creating the image on monitor, which are shown in Figure 4.11 through rough graphic representations of the functions at the lower end of the diagram, are known to be inverse power and respectively power functions. Therefore, if the device dependent data obtained from digital images for a colour and the colour's colorimetric data are highly correlated with determined inverse power functions of variable parameters, then the assumed linearity exists for the considered colour. In fact, the experimental setup at 4.3.3. was established based on the construction of such inverse power function around the set of 6 achromatic colours and based on the comparison of the correlation coefficients obtained for pictures taken from different positions. The main question that arises after outlining this method is if the functions calculated for the selected neutrals are good enough to predict the colorimetric values of a colour described through its device dependent RGB data. The assumed answer, which must be sustained through the experiments carried out in this work, is that the predicted CIELAB values in certain regions of the sRGB colour space will not be unreasonable far from their colorimetric measured values.

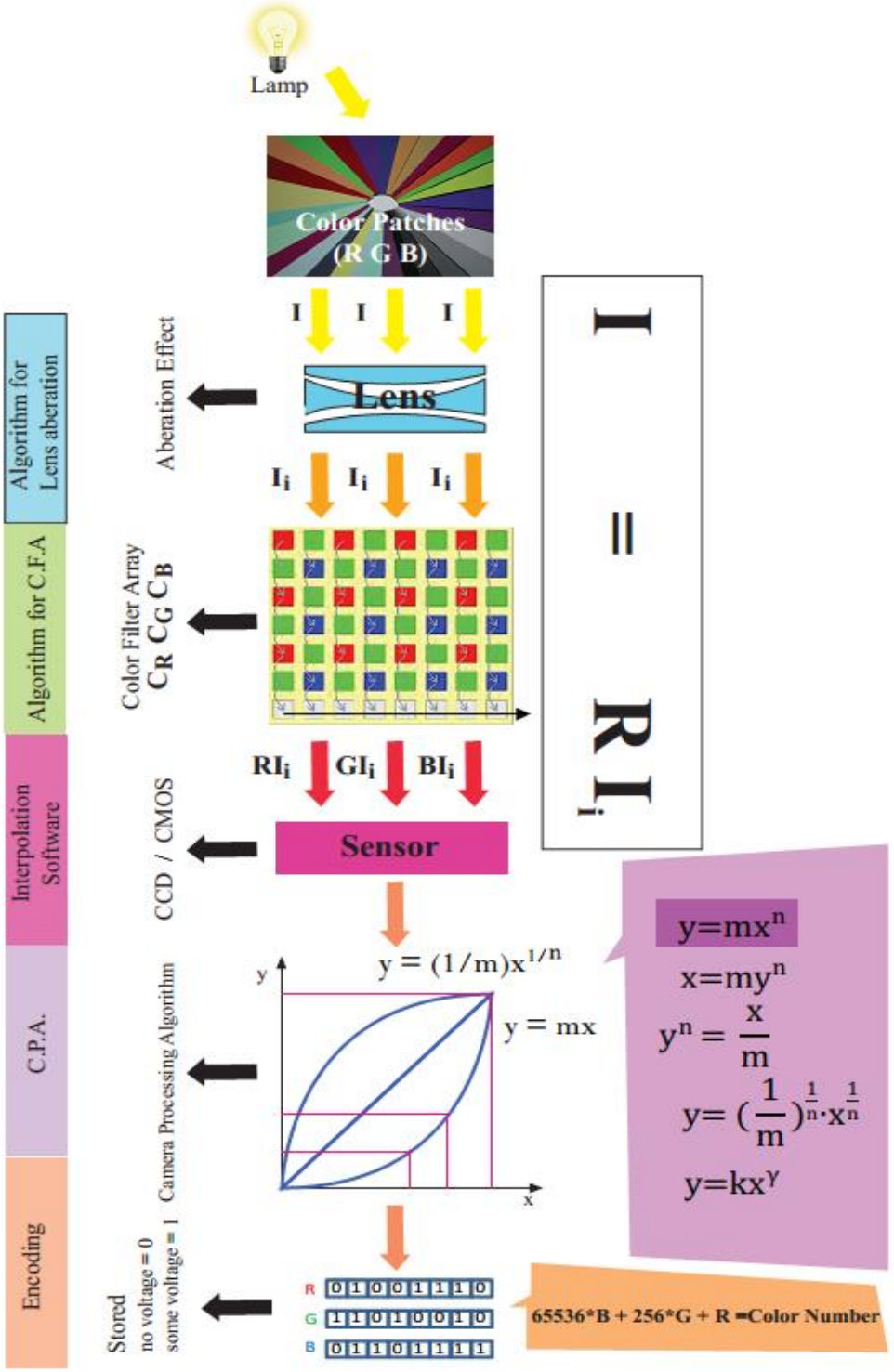

Figure 4.11 Light's path from the reflected colour sheet until being stored as digital number.

In this method, the 6 achromatic colours are permanently associated with different colours in the physical colour-wheel. Based on a trial and error process performed on 1300 Munsell matte colour sheets, it is verified which colour-codes revolve around the inverse power functions calculated for having a best fit of the colorimetric data predicted for the neutrals. The purpose is to collect these colours in a colour wheel that can be used for light quality assessments.

The working colour boundaries for this method are set through the sRGB colour space. Both digital cameras used as imaging systems in this method have menu options for setting these boundaries. sRGB is a standard RGB colour space as described in 2.2, but created specially for use on monitors, printers and the Internet (Stokes, Anderson et al. 1996). LCDs, digital cameras, printers, and scanners comply with the sRGB standard and devices which do not naturally follow sRGB, usually include compensating circuitry or software to obey this standard. This is why it can be generally assumed that in absence of embedded profiles or any other information, any 24 bit RGB image file (8 bit per channel) can be treated as being in the sRGB colour space. This does not mean, however, that colour is correctly displayed without performing colour corrections.

The sRGB Munsell colour-codes collected for the colour wheel must fulfill the conditions described in chapter 3 in order to be used in light quality assessments.

A colour set for assessing light quality is defined for the general Colour Rendering Index (CRI), recommended by the International Commission on Illumination (CIE 1995) and has the following Munsell notations: 7.5R 6/4, 5Y 6/4, 5GY 6/8, 2.5G 6/6, 10BG 6/4, 5PB 6/8, 2.5P 6/8, 10P 6/8. These 8 colour samples are evenly distributed over the complete range of hues but are characterized by low to medium chromatic saturation and do not adequately span the range of normal object colours. Due to this characteristic they are considered inappropriate to be used in evaluating some lights, particularly Light Emitting Diodes (LEDs) as the Osram Parathom classic LED cool white used in the present work (Davis and Ohno 2010). LEDs have high peaked spectral power distributions and the peaks can incidentally or intentionally match up with the 8 mentioned test colours (or the 14 colour samples of the special CRI) to result in high CRI values, while generally, the considered light source might render object colours poorly. Such misleading results can be avoided by

using the Colour Quality Scale (CQS) developed by the National Institute of Standards and Technology (NIST), which used the following 15 test colours: 7.5P 4/10, 10PB 4/10, 5PB 4/12, 7.5B 5/10, 10BG 6/8, 2.5BG 6/10, 2.5G 6/12, 7.5GY 7/10, 2.5GY 8/10, 5Y 8.5/12, 10YR 7/12, 5YR 7/12, 10R 6/12, 5R 4/14, 7.5RP 4/12. These Munsell sheets are high in colour saturation covering all hue angles across the visible spectrum. But some are too saturated to fit in the sRGB colour space. The matte Munsell sheets which do not fit in the sRGB gamut are: 5PB 4/12, 2.5BG 6/10, 5Y 8.5/12, 5YR 7/12 and 5R 4/14. They were replaced with others having the same hue and value but lower chroma. The new sheets are within the borders of the sRGB colour space and have the following Munsell notations: 5PB 4/10, 2.5BG 6/8, 5Y 8.5/8, 5YR 7/8, 5R 4/12.

With the 15 colours of CQS, having the 5 mentioned colours replaced, and with the 6 neutrals from the achromatic wheel, a colour-wheel was built and pictures of it were taken as shown in Figure 4.10, respecting the conditions described in 4.3.3. The first picture was marked "scene 1". The three best fit functions were calculated for the achromatic colours of scene 1 same way as they have been calculated for the achromatic wheel before, then the resulted parameters were used for the inverse power functions to correct the 15 colours from scene 1. CIE $L^*a^*b^*$ values were calculated for each digitized colour and compared with the spectrophotometric measured CIE $L^*a^*b^*$ ($D65/2^o$) values of the corresponding colours on the wheel, by means of ΔE_{00}. Colours for which the colour difference was greater than 6 ΔE_{00} units were replaced, keeping in mind that the colours of this wheel must cover all hue angles in order to offer meaningful colorimetric data for light quality assessment. After each replacement, a new picture was taken. The RGB data of each colour was read in close proximity to the wheel's center. The CIE L*a*b* values and the colour differences were recalculated towards the spectrophotometric measurements.

Although intensity of light was maintained constant throughout the experiment, each colour replacement modified the camera responses to the achromatic patches because of the camera's automatic colour correction (Wyszecki and Stiles 2000). Figure 4.12, 4.13 and 4.14 show the best fit functions obtained for the achromatic colours of the first 3 scenes. It results that colour-correction has to be performed based on the dynamic changes of the parameters describing the best fit inverse power

functions calculated for each scene. These dynamic changes, that reflect modifications in camera response, do not represent a deviation from linearity as long as the best fit power functions, with newly calculated parameters, continue to have high correlation coefficients and low standard deviation of error estimation toward the experimental data. The CIELAB values calculated for each Munsell colour code in different illuminations define a colour region. If the predicted CIELAB values are close to their colorimetric measurements under several lights and for more than one camera, it can be considered that the colour region is generally favorized by DSLR cameras under the established shooting conditions.

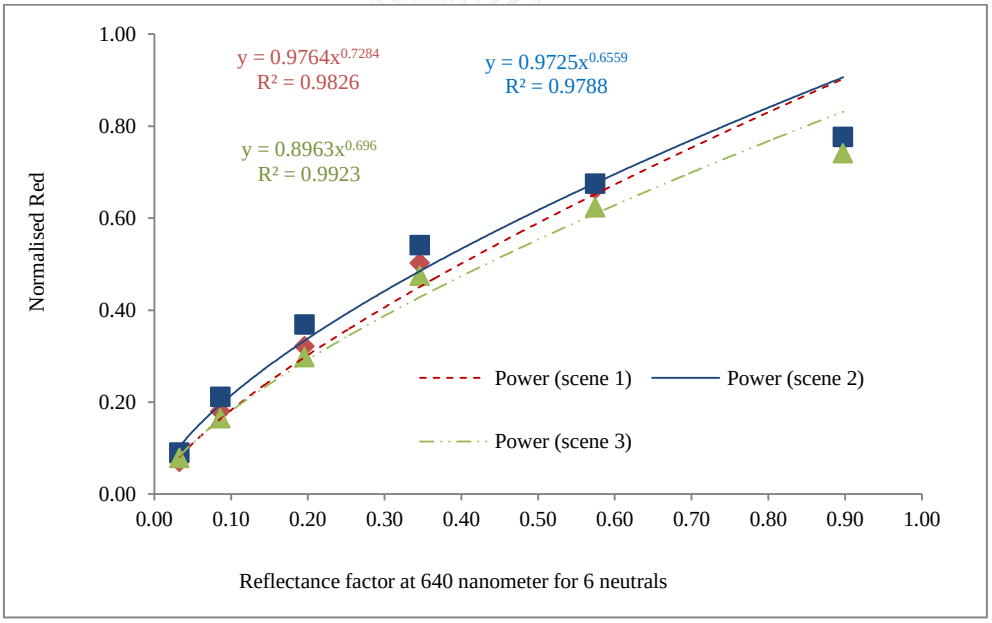

Figure 4.12 Correlation of the digital red values obtained for the 6 neutrals versus the 6 neutrals' reflection values at 640 nm, under the fluorescent D65 light source.

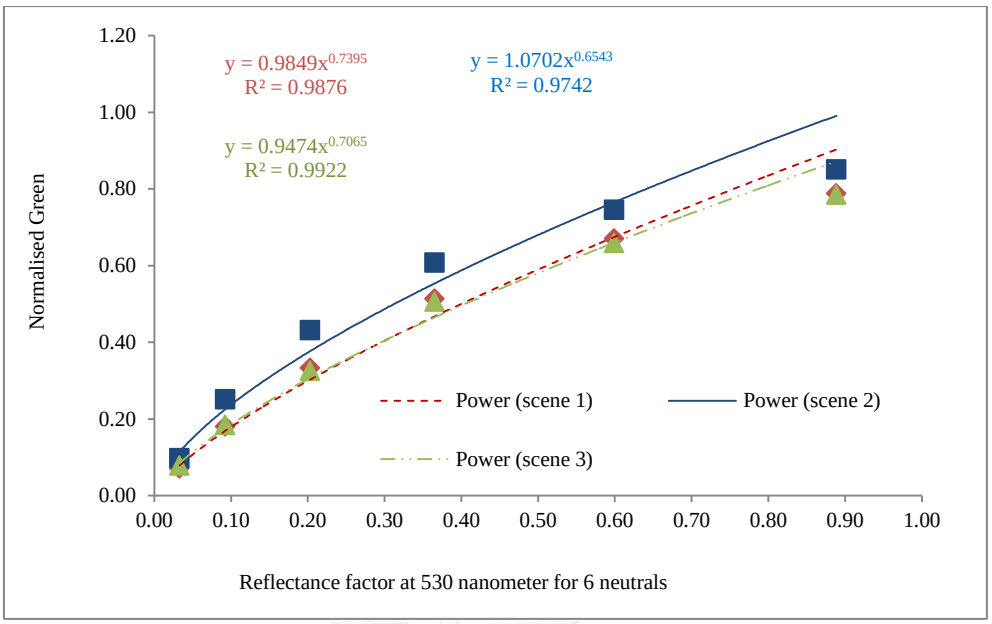

Figure 4.13 Correlation of the digital green values obtained for the 6 neutrals versus the 6 neutrals' reflection value at 530 nm, under the fluorescent D65 light source.

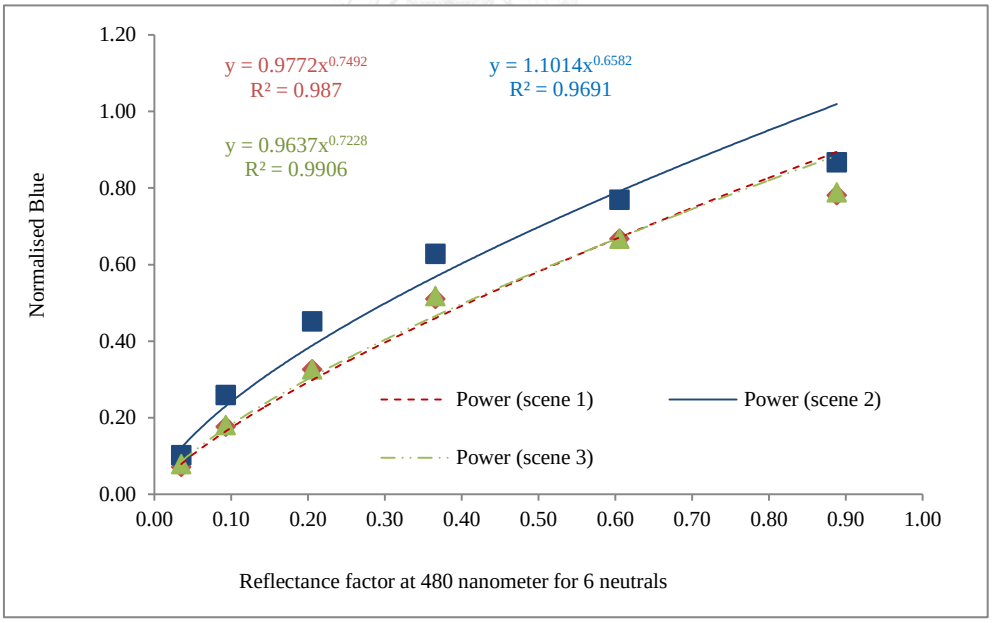

Figure 4.14 Correlation of the digital blue values obtained for the 6 neutrals versus the 6 neutrals' reflection value at 480 nm, under the fluorescent D65 light source.

The colour selection process is schematically described in the diagram presented in Figure 4.15.

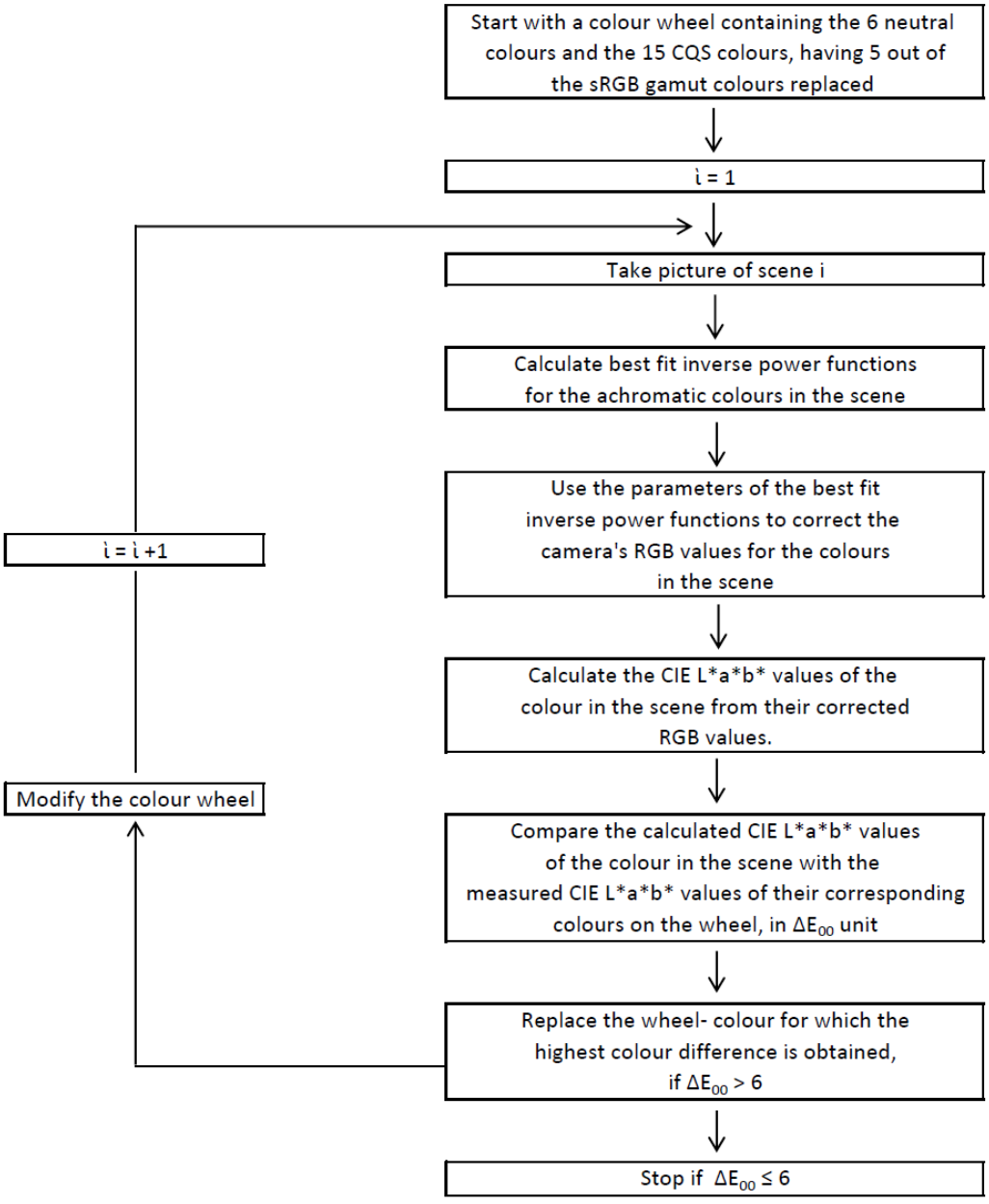

Figure 4.15 Schematic diagram of the colour selection process.

Each step mentioned in the diagram has been described previously. Similar functions to those shown in Figures 4.12, 4.13, 4.14 with different parameters are calculated for the other scenes. The parameters result from linear regression. Each

scene has its own set of parameters, used to correct the camera's RGB values for the colours in that scene and for calculating the CIE $L^*a^*b^*$ values, according to the algorithm described in Figure 4.16. The notations in the flowchart have the following meaning:

Rd, Gd, Bd = device dependent RGB data read from the digital image for one colour of the colour wheel as integer numbers between 0 and 255;

Rn, Gn, Bn = device dependent RGB data normalized to the [0,1] interval;

K1, K2, K3 = coefficients of the best fit inverse power functions calculated for each scene from the neutrals of the colour wheel;

gamma1, gamma2, gamma3 = powers of the best fit inverse power functions calculated for each scene from the neutrals of the colour wheel;

Rl, Gl, Bl = RGB data in linear RGB colour space;

X, Y, Z = trichromatic colour coordinates in CIEXYZ colour space;

L^*, a^*, b^* = calculated CIELAB values of the considered colour from the considered colour wheel.

The algorithm uses the CIE transformations from the calculated linear RGB values to the CIELAB values. Because we use the sRGB colour space, the following matrix is used in this transformation:

$$\begin{bmatrix} \mathbf{0.4124564} & \mathbf{0.3575761} & \mathbf{0.1804375} \\ \mathbf{0.2126729} & \mathbf{0.7151522} & \mathbf{0.0721750} \\ \mathbf{0.0193339} & \mathbf{0.1191920} & \mathbf{0.9503041} \end{bmatrix}$$

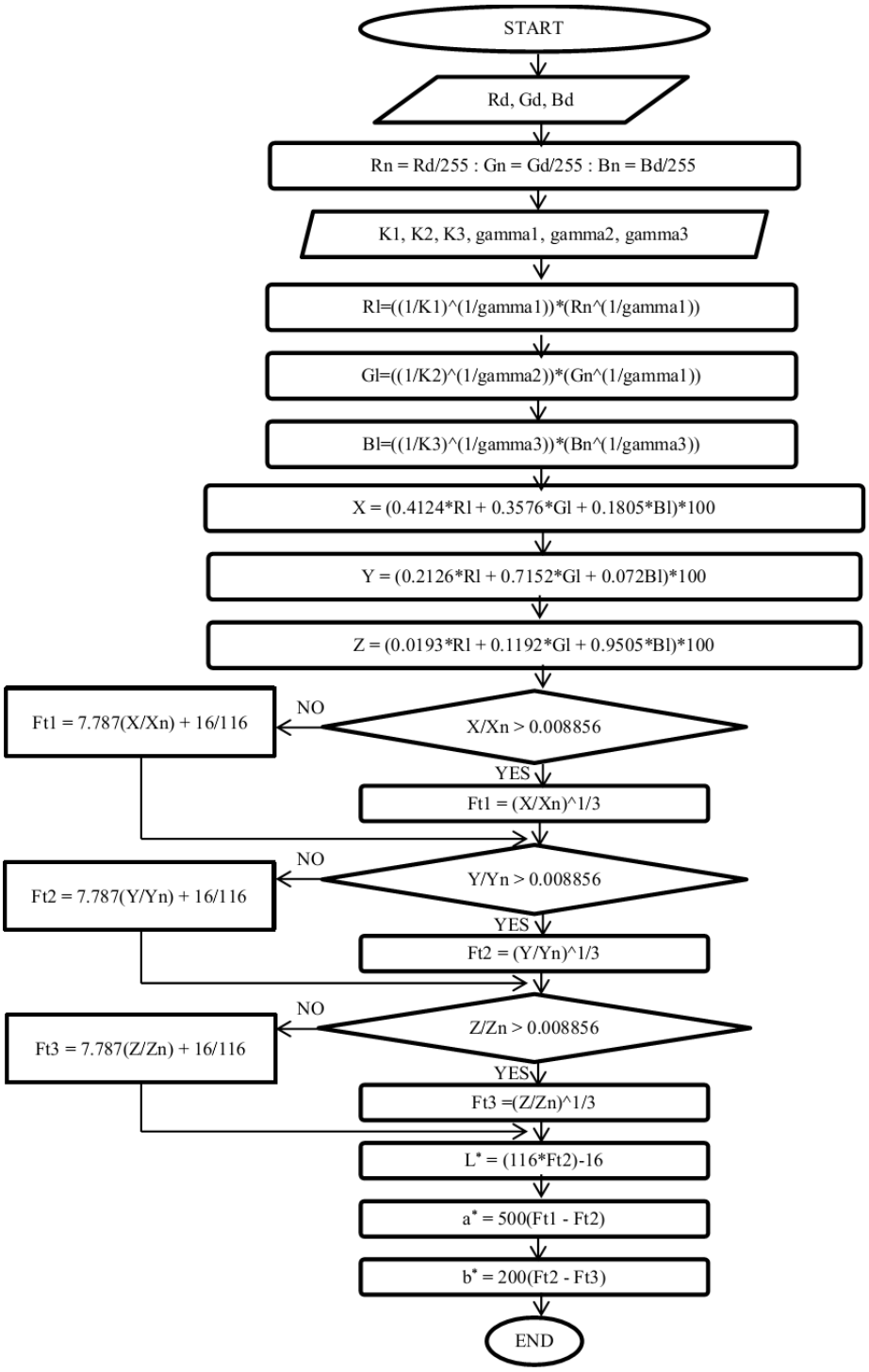

Figure 4.16 Algorithm for calculating the CIE $L^*a^*b^*$ values.

The aim of this experiment is to obtain a colour difference between calculated and measured CIE $L^*a^*b^*$ that has a maximum value of 6 ΔE_{00} units for any of the considered colours and an average value of 3 ΔE_{00} units for all 15 colours of the colour-wheel. After achieving this aim, the number of colours was increased in the wheel following the experimental cycle described before but modifying the scenes by adding colours, not by replacing them, until reaching 24 colours in the wheel. The resulted colour-wheel was used for taking pictures in the second box under the Osram Parathom LED A40 cool white light source. The same experimental cycle was followed with the difference that if the data was improving compared to the previous scene, the colour differences were checked to remain under 6 ΔE_{00} units when taking pictures in the first box. In the stage of colour sample selecting, ΔE_{00} was calculated between spectrophotometer and calculated values. After the final colour samples were selected according to criteria mentioned above, ΔE_{00} was calculated between spectroradiometric and calculated values.

The Munsell sheets used in the final colour-wheel are: N2, N3.5, N5, N6.5, N8, N9.5, 7.5P 4/10, 10PB 4/6, 2.5GY 8/8, 7.5GY 7/10, 10R 6/8, 7.5RP 4/12, 10YR 7/4, 7.5B 8/4, 7.5PB 4/6, 5P 4/10, 5R 4/10, 10GY 7/8, 5YR 7/6, 7.5R 4/10, 5Y 8/4, 2.5BG 7/4, 2.5G 8/2, 5RP 4/12, 10BG 8/2, 5PB 4/2, 10Y 8/4, 2.5B 8/2, 7.5G 8/4 and 10P 6/4 as shown in Figure 4.17.

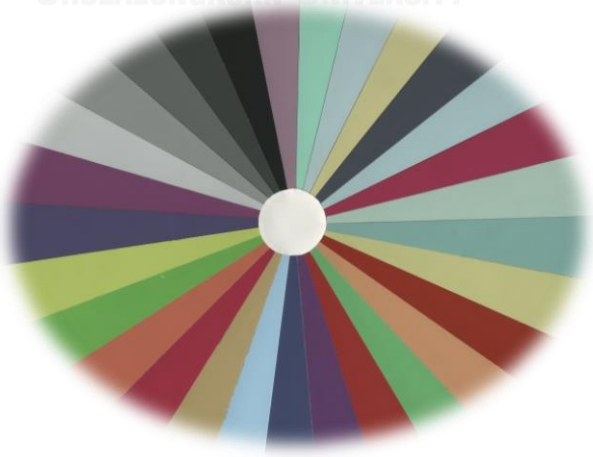

Figure 4.17 Colour-wheel.

This colour-wheel was obtained using only the Canon EOS X4 with CMOS sensor. After taking pictures of this wheel with the Nikon D40x with CCD sensor, in the same conditions, the maximum and average colour differences resulted in smaller values, an expected outcome due to the superior performance in colour output of the CCD sensors versus the CMOS sensor (Blanksby and Loinaz 2000, Hain, Kahler et al. 2007). However, after testing the colour-wheel with three more cameras it was concluded that camera manufacturing quality overseeds the performance of sensor type.

Both light sources used in this experiment were assessed with an illuminance spectrophotometer (Konica Minolta illuminance spectrophotometer CL-500A), by means of CRI and the resulted CRI values were compared with those calculated using the digital images with the ones calculated by using the spectroradiometric measurements and with those specified by the manufacturer. The CRI values were calculated from CIE $L^*a^*b^*$ values obtained by applying the Bradford transform (Hunt 1995) to the CIE $L^*a^*b^*$ values resulted from pictures, as described before. Von Krise transform, originally used in CRI determinations, is proven to be less accurate (Süsstrunka, Holmb et al. 2006, Đorđević, Hladnik. et al. 2009). The CIEXYZ tristimulus values of N9.5 in the scene were calculated under the considered light source and the values were used as white point coordinates to calculate the new CIE L*a*b* values with the Bradford transform.

4.5. Software development within the described methodology

The methodology is quite laborious; therefore software was written to perform the following tasks:

a.) Calculate the parameters of the best fit inverse power functions for the achromatic colours in each scene;

b.) Calculate the CIE $L^*a^*b^*$ values from the averaged RGB values (depicted as described in 4.4) according to the algorithm shown there;

c.) Apply a Bradford transform to the calculated CIE $L^*a^*b^*$ values, instead of Von Kries transform proposed in CRI;

d.) Compare the CIE $L^*a^*b^*$ values calculated from the digital images with the spectrophotometric and spectroradiometric measured CIE $L^*a^*b^*$ values, by means of ΔE_{00};

e.) Calculate the CRI according to the classic formulation but applied on the colours established in the experiment, not on the CRI colour-set, and using CIE $L^*a^*b^*$ values instead of CIEUVW.

CRI values are usually determined using the 1976 colour difference formula, but in the software was also added the option of using the 2000 colour difference formula implemented as specified in literature (CIE 2005).

The best fit inverse power functions for scene 1 are shown in Figures 4.12, 4.13, 4.14. The software calculates these parameters using the constant spectrophotometric CIE $L^*a^*b^*$ values measured on the achromatic Munsell sheets and the average RGBs calculated from the RGB triplets depicted with the camera software from the achromatic Munsell colours shot in the first scene. Optional spectroradiometric measurements can be added to the input screen for testing the colour differences. Trichromaticity coordinates of the considered light source can also be introduced as measured X, Y, Z values or as RGB values of the N9.5 Munsell sheet that appears in the picture taken under the considered light source. Figure 4.18 shows a copy of the input screen.

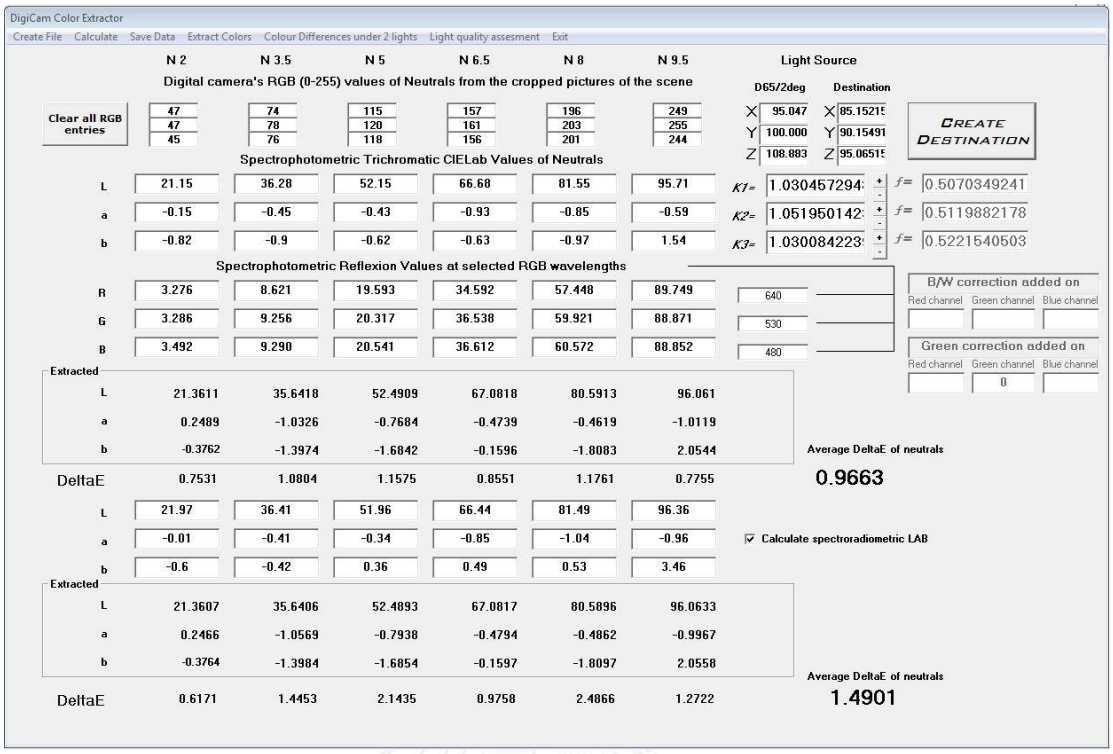

Figure 4.18 Copy of the input screen.

In the next step, averaged RGB values resulted from the picture are introduced as input data for each of the colours used in scene 1. Their spectroradiometric measured CIE $L^*a^*b^*$ values can be added to the input. The option for introducing spectroradiometric measurements is for evaluating the calculation process by means of maximum and average colour differences between calculated and measured data for the scene, as well as by means of CRI, calculated from digital image, versus CRI calculated from colorimetric measured data. The calculated CIE $L^*a^*b^*$ values and colour differences towards their spectroradiometric measurement (if they are introduced) are shown immediately after inputting each RGB value, as shown in Figure 4.19.

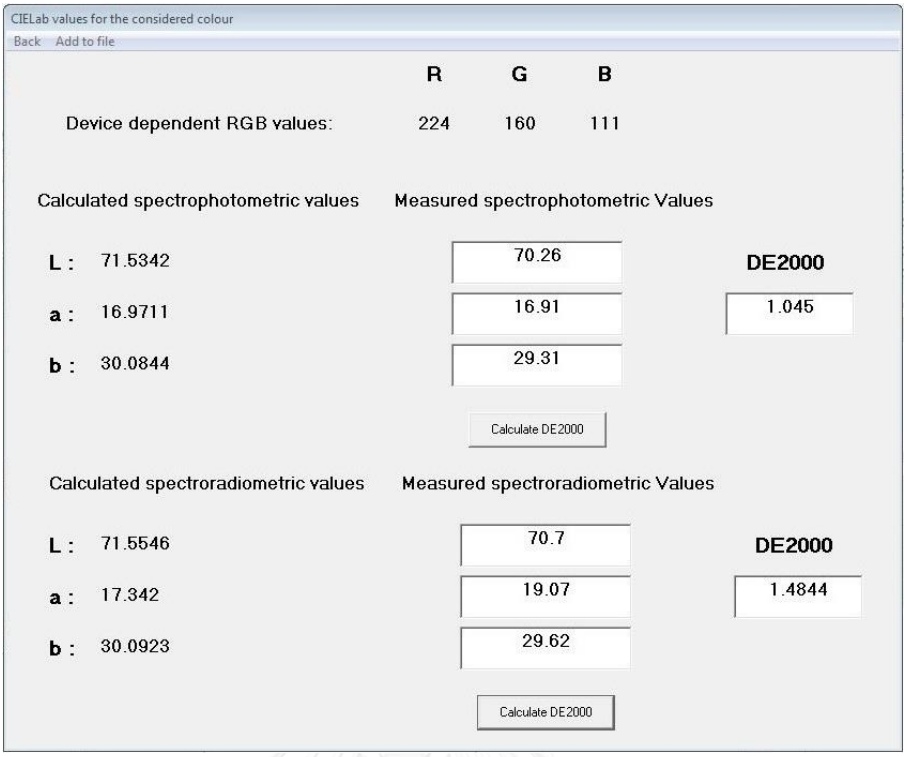

Figure 4.19 Copy of screen for calculating colour differences between obtained CIE $L^*a^*b^*$ values and measured CIE $L^*a^*b^*$ values (spectrophotometric and spectroradiometric).

4.6. Experimental results sustaining the applied methodology

Table 4.1 presents the data obtained for scene 1.

The Munsell sheets with colour differences above 6 ΔE_{00} units between CIE $L^*a^*b^*$ values calculated from digital picture and spectrophotometric measured CIE $L^*a^*b^*$ values, are 7.5B 5/10 (ΔE_{00} = 11.01), 5PB 4/10 (ΔE_{00} = 9.07), 10YR 7/12 (ΔE_{00} = 8.32), 10BG 6/8 (ΔE_{00} = 8.22), 2.5BG 6/8 (ΔE_{00} = 7.44), 2.5G 6/12 (ΔE_{00} = 7.25), 5Y 8.5/8 (ΔE_{00} = 6.11). They are enumerated in descending order of the colour differences because during the experiment they were replaced in this order.

Table 4.1 Calculated CIELAB from Canon EOS X4's digital image scene 1 under Fluorescent D65 and ΔE_{00} toward spectrophotometric measured CIELAB, D65/2°.

Table 1. Calculated CIELAB from Canon's digital image scene 1 under Fluorescent D65 and DE00 toward measured CIELAB, D65/2

Munsell Patches	Spectrophotometer			R	G	B	Calculated L*	Calculated a*	Calculated b*	ΔE_{00}
	L*	a*	b*							
N2	21.15	-0.15	-0.82	18	18	18	19.3	-0.1	-1.11	1.31
N3.5	36.28	-0.45	-0.9	46	46	45	37.9	-0.27	-0.42	1.46
N5	52.15	-0.43	-0.62	82	85	83	54.88	-1.33	-0.41	2.94
N6.5	66.68	-0.93	-0.63	128	131	130	70.32	-0.7	-0.8	2.89
N8	81.55	-0.85	-0.97	169	171	170	81.48	-0.18	-0.58	1.03
N9.5	95.71	-0.59	1.54	196	201	199	88.71	-0.85	-0.39	4.70
7.5P4/10	42.23	34.78	-23.65	92	43	109	44.78	34.37	-29.71	3.97
10PB4/10	41.59	23.16	-37	70	53	136	46.52	26.06	-40.24	4.79
2.5GY8/10	81.54	-22.1	70.22	159	186	26	81.56	-25.15	68.13	1.84
7.5GY7/10	71.18	-39.34	53.3	95	168	34	74.63	-39.18	55.09	2.65
10R6/12	62.25	44.21	46.53	196	58	25	57.56	42.89	45.02	4.17
7.5RP4/12	41.9	53.46	1.07	124	20	57	40.42	51.84	-4.63	3.11
10YR7/12	71.74	15.86	75.28	205	101	21	67.58	22.6	58.78	8.32
2.5G6/12	61.72	-62.73	30.64	27	159	66	70.02	-53.46	29.79	7.25
10BG6/8	62.11	-34.32	-16.73	43	155	164	71.73	-28	-13.4	8.22
7.5B5/10	50.42	-19.67	-37.39	28	113	171	61.4	-12.74	-32.02	11.01
5R4/12	41.59	52.54	27.9	131	17	27	39.66	52.14	19.84	4.53
2.5BG6/8	61.62	-41.41	-0.06	40	153	128	70.37	-35.42	-0.42	7.44
5YR7/8	71.96	22	42.34	190	115	55	69.82	14.78	37.94	4.45
5PB4/10	40.82	4.06	-40.81	41	71	146	49.82	7.54	-39.66	9.07
5Y8.5/8	86.06	-2.57	56.97	195	185	57	83.71	-11.47	53.61	6.11

After modifying the first scene 5 times (i=6 in the diagram shown in Figure 4.15) the results shown in Table 4.2 were obtained.

Table 4.2 Calculated CIELAB from Canon EOS X4's digital image scene 6 under Fluorescent D65 and ΔE_{00} toward spectrophotometric measured CIELAB, D65/2°.

Table 2 Calculated CIELAB from Canon's digital image scene 6 under Fluorescent D65 and ΔE_{00} toward measured CIELAB, D65/2										
Munsell Patches	Spectrophotometer CIELAB			R	G	B	Calculated CIELAB of scene 6			ΔE_{00}
	L*	a*	b*				L*	a*	b*	
N2	21.15	-0.15	-0.82	21	22	21	19.98	-0.02	-0.01	1.16
N3.5	36.28	-0.45	-0.9	45	50	51	37.41	-0.78	-1.63	1.26
N5	52.15	-0.43	-0.62	76	84	89	52.84	-0.35	-2.77	2.11
N6.5	66.68	-0.93	-0.63	122	134	139	70.36	-0.84	-1.06	2.93
N8	81.55	-0.85	-0.97	160	173	178	81.89	-0.54	0.25	1.29
N9.5	95.71	-0.59	1.54	190	205	208	90.28	-0.89	1.74	3.34
7.5P4/10	42.23	34.78	-23.65	89	45	117	43.91	35.92	-31.1	3.88
10PB4/10	41.59	23.16	-37	67	54	144	45.09	27.83	-42.36	3.88
2.5GY8/10	81.54	-22.1	70.22	149	191	30	82.69	-27.49	69.17	2.86
7.5GY7/10	71.18	-39.34	53.3	83	174	42	75.38	-44.23	53.83	3.59
10R6/10	61.56	37.79	38.58	184	68	38	59.07	41.28	39.89	2.58
7.5RP4/12	41.9	53.46	1.07	115	21	57	38.97	51.59	-2.54	3.19
10YR7/10	72.17	14.04	61.92	171	121	16	69.27	7.92	65.13	4.79
7.5YR7/8	71.7	16.85	45.85	174	119	40	69.37	11.69	50.06	4.71
7.5PB4/8	41.17	11.07	-33.45	48	59	133	44.23	15.46	-38.74	3.36
5P4/10	40.38	32.56	-28.57	77	40	119	40.98	36.28	-36.83	3.54
5R4/12	41.59	52.54	27.9	122	19	25	38.69	51.41	24.24	3.09
10GY7/8	71.45	-38.29	32.69	84	178	95	77.07	-37.91	28.2	4.55
5YR7/6	71.12	17	30.11	173	125	89	71.35	13.37	24.54	2.80
7.5R4/10	41.55	43.6	30.73	129	30	28	42.59	46.56	26.46	3.33
5Y8/8	81.48	-2.98	57.75	173	177	49	80.36	-10.33	57.06	4.71

Munsell sheets were added afterwards to the colour-wheel until completing it with 30 sheets (24 colours + 6 neutrals) as described in 4.4. Colours were added until scene 15, when satisfactory data was obtained. Table 4.3 shows the results obtained for scene 15.

Table 4.3 Calculated CIELAB from Canon EOS X4's digital image scene 15 under Fluorescent D65 and ΔE_{00} toward spectrophotometric measured CIELAB, D65/2°.

Calculated CIELAB from Canon's digital image scene 15 under Fluorescent D65 and DE00 toward measured CIELAB, D65/2										
Munsell Patches	Spectrophotometer			R	G	B	Calculated CIELAB of scene 15			ΔE_{00}
	L*	a*	b*				L*	a*	b*	
N2	21.15	-0.15	-0.82	17	22	21	20.26	-1.41	-0.63	1.91
N3.5	36.28	-0.45	-0.9	43	45	46	36.14	2.05	-0.98	3.61
N5	52.15	-0.43	-0.62	78	85	87	54.31	-0.26	-1.15	2.18
N6.5	66.68	-0.93	-0.63	123	130	135	70.38	-0.36	-1.26	3.09
N8	81.55	-0.85	-0.97	160	167	172	81.42	-1.06	-0.34	0.70
N9.5	95.71	-0.59	1.54	191	201	204	90.28	-2.69	0.81	4.43
7.5P4/10	42.23	34.78	-23.65	89	43	113	44.02	37.06	-30.85	3.66
10PB4/10	41.59	23.16	-37	66	51	140	44.96	29.71	-42.87	4.14
2.5GY8/10	81.54	-22.1	70.22	152	185	29	82.55	-27.08	68.97	2.69
7.5GY7/10	71.18	-39.34	53.3	88	170	41	75.97	-41.76	54.28	3.64
10R6/10	61.56	37.79	38.58	185	69	38	59.21	38.11	38.85	2.06
7.5RP4/12	41.9	53.46	1.07	124	24	62	41.6	52.42	-3.58	2.29
10YR7/4	71.62	4.82	27.72	154	130	84	71.47	1.85	25.45	2.68
7.5YR7/6	71.22	12.54	34.09	168	122	71	70.44	8.37	31.41	2.97
7.5PB4/6	41.49	7.24	-24.49	51	59	114	44.83	12.71	-30.41	4.22
5P4/10	40.38	32.56	-28.57	80	41	121	42.69	37.49	-37.13	4.11
5R4/12	41.59	52.54	27.9	136	19	28	41.18	54.94	23.87	2.66
10GY7/8	71.45	-38.29	32.69	86	170	86	76.51	-36.22	30.39	3.86
5YR7/6	71.12	17	30.11	178	121	86	71.22	13.49	24.35	2.83
7.5R4/10	41.55	43.6	30.73	129	27	24	41.91	47.5	28.47	2.56
5Y8/4	81.15	-3.75	30.09	167	170	110	81.34	-8.41	26.02	4.51
2.5BG7/4	72.45	-21.21	1.02	103	165	155	77.52	-18.22	0.43	4.14
2.5G8/4	81.38	-22.31	13.49	135	187	158	83.89	-17.51	8.64	3.96
5RP4/12	42.3	52.65	-7.02	122	30	79	43.43	50.08	-12.09	2.80
10BG8/2	81.76	-9.28	-3.85	148	180	185	83.64	-7.6	-2.18	2.36
5PB4/2	41.22	0.2	-8.86	54	64	78	45.38	1.37	-9.33	4.16
10Y8.5/6	86.51	-11.29	44.7	178	190	100	85.84	-14.24	36.75	4.11
2.5B8/2	80.85	-8.22	-3.72	151	181	186	84.02	-7.09	-1.98	2.75
7.5G8/4	81.9	-23.95	6.15	130	196	172	85.71	-20.17	5.7	3.28
10P4/6	41.22	25.07	-13.45	85	47	87	43.66	27.84	-17.03	3.04

Beginning with scene 16 the colour-wheel started to be improved under the second light source, Osram Parathom classic LED A40 cool white. The scene was modified 8 times by replacing the colours in order to obtain good data under both light sources as described in 4.4. The results for scene 23 are shown for both light sources in Table 4.4. Optimizing the colour-wheel this way improved slightly the data for the first light source, this scene having now the maximum colour difference resulted for an individual colour of 4.34 ΔE_{00} units (versus 4.51 ΔE_{00} units in scene 15) and the average ΔE_{00} of 2.91 (versus 3.18 ΔE_{00} units in scene 15).

The results obtained for scene 23 were considered good for the purpose of this work. Therefore pictures of the colour-wheel used in this scene were taken with the Nikon D40x digital camera. The data obtained under both considered light sources, are presented in Table 4.5. The results are better compared with the ones obtained with Canon EOS X4 camera. The maximum colour difference is of 3.81 ΔE_{00} units (versus 4.34 ΔE_{00} units for Canon), the average of 1.94 ΔE_{00} units (versus 2.91 ΔE_{00} units for Canon).

Table 4.4 Calculated CIELAB from Canon EOS X4's digital image scene 23 under Fluorescent D65 and ΔE_{00} toward spectrophotometric measured CIELAB, D65/2°.

Munsell	Fluorescent D65							LED D65						
Patches	R	G	B	L*	a*	b*	ΔE00	R	G	B	L*	a*	b*	ΔE00
N2	20	20	20	20.09	-0.22	-0.66	0.76	21	21	21	20.05	0.12	-0.56	0.90
N3.5	43	44	44	35.96	-0.45	-0.97	0.27	43	46	46	35.90	-1.04	-1.10	0.91
N5	86	88	88	55.73	-0.15	-1.14	3.50	86	91	92	55.79	-0.47	-1.60	3.62
N6.5	125	130	129	69.84	-0.63	-1.02	2.56	128	135	134	70.50	-0.53	-0.63	3.06
N8	161	169	167	80.88	-0.96	-0.93	0.49	161	171	169	80.66	-0.80	-0.39	0.83
N9.5	198	206	198	90.21	-1.13	1.09	3.46	196	207	202	89.82	-0.74	0.66	3.70
7.5P4/10	87	43	101	43.37	32.18	-27.15	3.24	91	46	109	44.29	33.28	-28.25	3.94
10PB4/6	61	51	98	42.78	16.54	-26.61	2.11	65	58	108	44.94	15.69	-26.92	3.75
2.5GY8/8	158	179	54	80.76	-19.91	52.36	1.99	158	182	58	80.79	-19.66	51.46	2.11
7.5GY7/10	92	163	36	73.45	-38.62	53.63	4.34	93	169	40	74.15	-39.25	53.05	4.84
10R6/8	177	79	58	61.06	30.97	25.84	2.60	179	82	61	61.44	31.55	25.98	2.67
7.5RP4/12	117	24	56	40.18	47.86	-2.98	2.48	124	27	61	41.70	48.86	-2.54	1.95
10YR7/4	153	132	82	71.24	0.34	24.77	4.01	157	137	84	71.96	0.65	26.26	3.79
7.5B8/4	136	185	196	83.11	-9.30	-9.00	3.55	136	187	199	82.88	-9.20	-8.82	3.61
7.5PB4/6	53	59	105	44.88	9.57	-27.27	3.80	54	62	112	45.29	9.97	-28.58	4.31
5P4/10	75	40	107	41.27	31.96	-33.85	3.46	82	44	115	42.89	33.15	-33.70	4.03
5R4/10	122	23	32	39.84	46.95	16.66	2.42	131	28	35	42.17	47.06	18.73	1.63
10GY7/8	87	169	80	75.15	-36.02	30.33	3.88	87	174	85	75.57	-36.63	29.78	4.22
5YR7/6	175	122	80	70.69	11.38	25.41	3.63	176	123	80	70.37	12.40	26.56	2.78
7.5R4/10	121	22	22	39.12	46.30	25.76	2.54	131	24	25	40.91	48.76	26.49	2.94
5Y8/4	165	165	102	79.15	-6.99	25.30	3.89	166	170	107	79.65	-7.14	25.18	4.03
2.5BG7/4	102	162	145	75.68	-18.09	0.22	3.84	106	169	152	76.76	-18.11	0.50	4.55
2.5G8/2	148	176	160	81.34	-8.13	2.48	3.54	151	182	166	82.12	-8.14	2.87	3.50
5RP4/12	115	29	67	41.65	45.23	-8.64	2.32	121	31	72	42.68	46.77	-8.61	2.06
10BG8/2	145	177	174	81.63	-7.27	-2.71	2.46	147	178	176	81.32	-6.30	-2.30	3.19
5PB4/2	49	58	68	42.69	-1.23	-8.58	2.70	57	65	75	45.11	-0.26	-7.69	4.12
10Y8/4	163	171	110	80.33	-8.85	23.07	3.72	164	173	113	80.21	-8.14	23.10	3.43
2.5B8/2	148	175	173	81.40	-5.86	-2.64	2.83	150	179	177	81.70	-5.73	-2.11	3.18
7.5G8/4	124	185	159	81.76	-18.12	3.35	3.51	129	192	167	82.86	-17.68	3.39	4.06
10P6/4	129	105	127	64.45	12.16	-8.01	3.55	133	109	134	65.10	13.21	-8.55	3.97
						Mean	2.91						Mean	3.19
						Max	4.34						Max	4.84
						Min	0.27						Min	0.83
						STD	1.03						STD	1.11

Due to the chosen light sources, that have a colour temperature of 6500K, CRI has an appropriate formulation for assessing their light quality. Using CRI gives also the possibility to compare the results with the measurements made with an illuminance spectrophotometer and with the manufacturer's published CRI. However, the described methodology uses CIE $L^*a^*b^*$ values in the CRI calculation because CIEUVW is an obsolete and non-uniform colour space. Also, instead of the Von Kries transform, the Bradford transform was used in the calculation process because it was proven to be much more accurate. The Bradford transform was preferred over CMCCAT2000 or CIECAT02 because the latter do not bring much improvement, if at all, according to literature (Süsstrunka, Holmb et al. 2006, Đorđević, Hladnik. et al. 2009).

Three more cameras: Nikon D70, Canon 6D and Canon 600D were used for verifying the results under both Fluorescent D65 and LED D65. The verifying results were shown in Table D1, D2, D3 for Nikon D70, Canon 6D and Canon 600D respectively.

Table 4.5 Calculated CIELAB from Nikon D40 x's digital image scene 23 under Fluorescent D65 and ΔE_{00} toward spectrophotometric measured CIELAB, D65/2°.

Munsell	Fluorescent D65							LED D65						
Patches	R	G	B	L*	a*	b*	ΔE00	R	G	B	L*	a*	b*	ΔE00
N2	47	47	45	21.36	0.25	-0.38	0.75	44	44	48	21.05	0.11	-1.16	0.50
N3.5	74	78	76	35.64	-1.03	-1.40	1.08	74	76	79	36.03	-0.95	-0.50	0.85
N5	115	120	118	52.49	-0.77	-1.68	1.16	118	118	120	52.87	-0.05	0.15	1.18
N6.5	157	161	156	67.08	-0.47	-0.16	0.86	156	161	164	67.47	-1.06	-1.30	0.91
N8	196	203	201	80.59	-0.46	-1.81	1.18	195	201	203	80.01	-0.99	-1.38	1.14
N9.5	249	255	244	96.06	-1.01	2.05	0.78	251	255	251	95.67	-0.60	0.51	0.98
7.5P4/10	124	78	130	42.93	29.19	-22.82	1.93	118	75	137	42.42	28.23	-25.14	3.28
10PB4/6	86	82	127	39.92	13.75	-26.09	1.87	87	79	134	40.21	15.36	-27.12	1.81
2.5GY8/8	203	218	85	82.54	-19.20	56.09	2.38	204	218	80	82.37	-20.14	59.75	2.65
7.5GY7/10	124	189	60	70.42	-37.88	52.91	2.11	130	188	49	70.63	-36.58	59.37	3.72
10R6/8	223	121	97	62.97	34.51	26.36	3.81	216	128	96	63.80	26.18	29.92	3.19
7.5RP4/12	160	61	94	42.71	44.39	-1.31	3.03	156	60	94	42.31	41.73	0.41	3.59
10YR7/4	195	171	116	71.55	1.99	27.05	2.58	194	169	116	71.14	0.89	28.61	3.48
7.5B8/4	161	216	230	82.12	-11.09	-12.97	1.17	164	212	232	81.29	-9.22	-12.93	2.08
7.5PB4/6	72	85	130	39.76	8.34	-28.15	1.86	73	80	133	39.26	10.16	-28.13	2.51
5P4/10	112	64	133	38.31	34.59	-31.86	2.02	106	63	139	38.23	32.46	-32.93	2.77
5R4/10	169	66	62	44.20	41.41	21.58	3.55	156	65	63	42.58	35.77	20.47	4.10
10GY7/8	118	193	102	71.66	-36.47	33.44	1.42	123	190	95	71.24	-35.18	38.45	3.21
5YR7/6	224	160	111	71.53	16.97	30.08	1.08	218	163	121	71.86	12.40	27.36	3.00
7.5R4/10	167	60	46	42.45	42.62	30.07	2.33	158	63	46	42.14	36.25	31.09	4.73
5Y8/4	209	207	136	81.12	-7.26	29.98	3.22	212	208	142	81.47	-7.36	29.71	3.40
2.5BG7/4	131	187	171	72.16	-18.05	-0.38	1.89	132	186	172	72.14	-18.27	1.40	1.83
2.5G8/2	185	213	194	81.98	-9.39	3.37	2.55	188	212	193	81.75	-9.40	5.74	1.79
5RP4/12	157	64	103	43.14	43.06	-6.25	2.92	152	63	116	43.08	41.83	-11.73	4.52
10BG8/2	179	207	205	80.49	-6.65	-3.93	2.90	176	207	209	80.30	-8.03	-3.87	1.62
5PB4/2	81	91	104	41.16	0.47	-10.70	1.35	80	89	106	41.37	-0.28	-9.18	1.02
10Y8/4	210	209	143	81.75	-6.96	27.45	1.51	212	214	141	82.75	-10.00	31.89	2.41
2.5B8/2	179	206	204	80.24	-6.38	-3.83	1.98	178	205	210	80.00	-6.43	-4.75	2.20
7.5G8/4	154	213	184	79.97	-20.28	4.91	1.69	158	218	189	81.33	-21.20	6.77	1.69
10P6/4	163	137	156	61.82	13.70	-7.86	1.20	163	136	164	62.16	13.54	-9.09	1.94
						Mean	1.94						Mean	2.40
						Max	3.81						Max	4.73
						Min	0.75						Min	0.50
						STD	0.84						STD	1.15

Table 4.6 shows the CRI values calculated for the Philips Ambience fluorescent D65 Tornado light source and for the Osram Parathom Classic LED cool white A40 light source from the digital images, using the colour-wheel established in scene 23. The CRI values are listed as obtained from the digital pictures taken with the Canon camera (CMOS sensor) and the Nikon camera (CCD sensor), using both 1976 and 2000 formulations for the colour differences. These values are compared to the CRI calculated with spectroradiometric data of the Munsell sheets. Only the CRI calculated with the 1976 colour difference formula should be compared with the CRI measured directly with the Konica Minolta illuminance spectrophotometer CL-500A, because the CRI formulation does not provide the 2000 colour difference formula.

Table 4.6 Comparison of CRI obtained from using the digital image of scene 23, from using spectroradiometric measurements and determined with Konica Minolta illuminance spectrophotometer.

Light Sources	Colour Rendering Index (CRI)				
	Digicam Canon	Digicam Nikon	SPD fromspectroradiometer	illuminance spectrophotometer	Manufacturer Specification
Philips Ambience fluorescent D65 Tornado	79.20 (ΔE^*_{ab}) 86.63 (ΔE_{00})	86.10 (ΔE^*_{ab}) 91.16 (ΔE_{00})	83.20 (ΔE^*_{ab}) 90.95 (ΔE_{00})	86	80-89
Osram Parathom Classic LED cool white A40	77.75 (ΔE^*_{ab}) 85.36 (ΔE_{00})	80.56 (ΔE^*_{ab}) 89.04 (ΔE_{00})	76.40 (ΔE^*_{ab}) 87.07 (ΔE_{00})	73	80

A CRI of 86 was obtained for the Philips fluorescent light source from digital image with Nikon SLR camera, the same as the CRI measured with the Konica Minolta illuminance spectrophotometer. The result is within the interval specified by the manufacturer: 80-89. For the Osram Parathom LED light source, the CRI obtained with the Nikon SLR camera from digital image was exactly the same CRI as the one specified by the manufacturer: 80. But this CRI is different from the one measured with the illuminance spectrophotometer, which is 73. The lower CRI measured with the Konica Minolta CL-500A could be explained by the fact that the illuminance spectrophotometers work with built in spectra of the CRI colour samples, which are less saturated than the ones resulted from applying this methodology (see Figure 4.20). The CRI calculated from spectroradiometric data is 76.40, exactly in-between the value of 80 (obtained from digital image and also listed in the manufacturer's technical data) and the value of 73 (measured with the Konica Minolta illuminance spectrophotometer).

The CRI obtained for both light sources from the pictures taken with the Canon camera are not very far from the CRI values determined with spectroradiometer and illuminance spectrophotometer but considering the better linear response of the Nikon CCD camera to the selected set of colours, it is probably better

to use a camera with CCD sensor if a method for light quality assessment is to be developed.

The CRI obtained from three testing cameras used for verifying results are shown in Table D4 of appendix D.

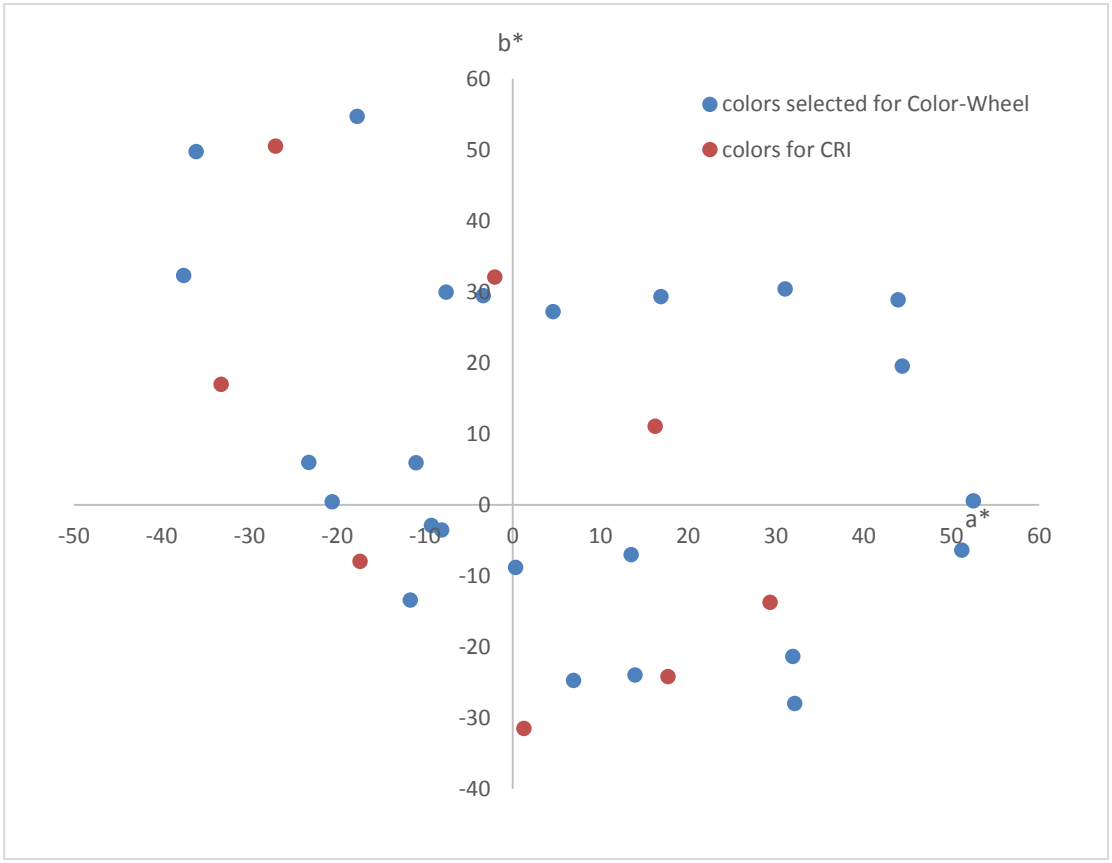

Figure 4.20 CIELAB coordinates of the CRI colour samples and of the samples ccontained in the final colour wheel.

CHAPTER 5

DETAILED DESCRIPTION OF CALCULATION PROCESSES, ALGORITHMS AND SOFTWARE CODE

5.1. Primary colour wheel selection

For establishing the primary colour wheel, the CQS colour set (Figure. 3.4) was considered as explained in 4.4. The colours were tested to fit the selected working space, sRGB colour space, using Babel Colour software. Figure 5.1 shows the CQS colours plotted on the CIE chromaticity diagram.

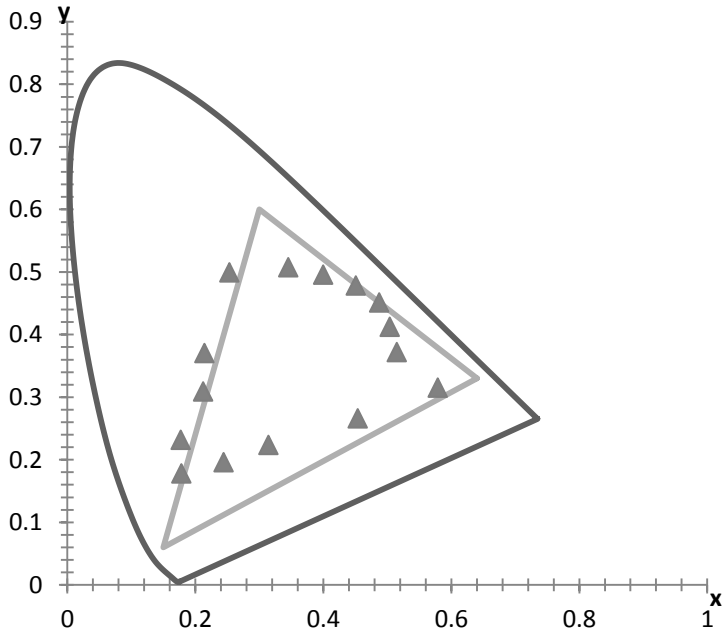

Figure 5.1 CIE x,y diagram of the CQS colour set.

The triangle in the diagram delimits the sRGB colour space. In this diagram can be seen the 5 colours that are out of the sRGB gamut and need to be replaced. The colours were verified in 3D representation of the sRGB colour space to eliminate the possibility of misinterpretation due to the fact that the chromaticity diagram shows merely the 2D projections of the considered colours. Table 5.1 shows the Munsell notations of the replaced colours and of the colours selected as replacements.

Table 5.1 Munsell notations of the replaced colours and of the colours selected as replacement.

Five CQS colour patches placed outside sRGB space	New colour patches selected for replacement
5 PB 4/12	5 PB 4/10
2.5 BG 6/10	2.5 BG 6/8
10 BG 6/8	10 BG 6/6
2.5 G 6/12	2.5 G 6/10
7.5 B 5/10	7.5 B 5/8

Figure 5.2 shows the colours used in scene 1, as described in 4.4., plotted on the CIE chromaticity diagram.

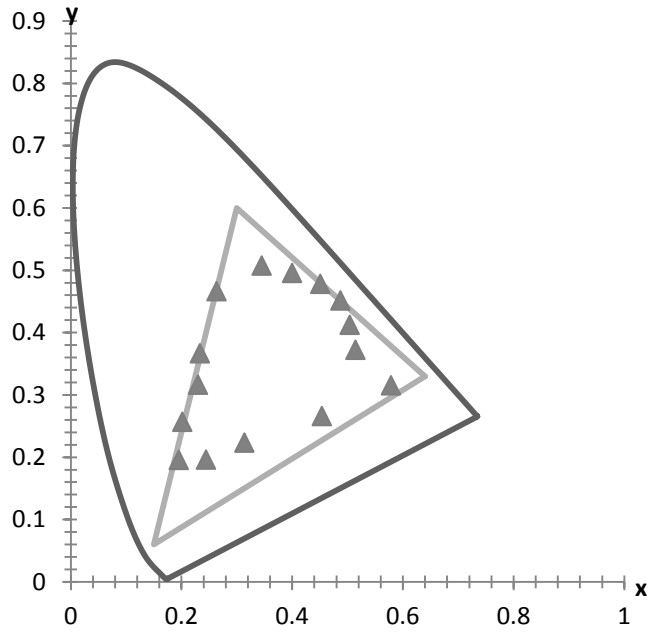

Figure 5.2 CIE x,y diagram of the selected colour set for scene 1.

To the 15 selected colours, 6 neutrals are added in the wheel, as explained in 4.4. The reflection curves of these neutrals are flattening above 430 nm. Some are presented in Figure 5.3.

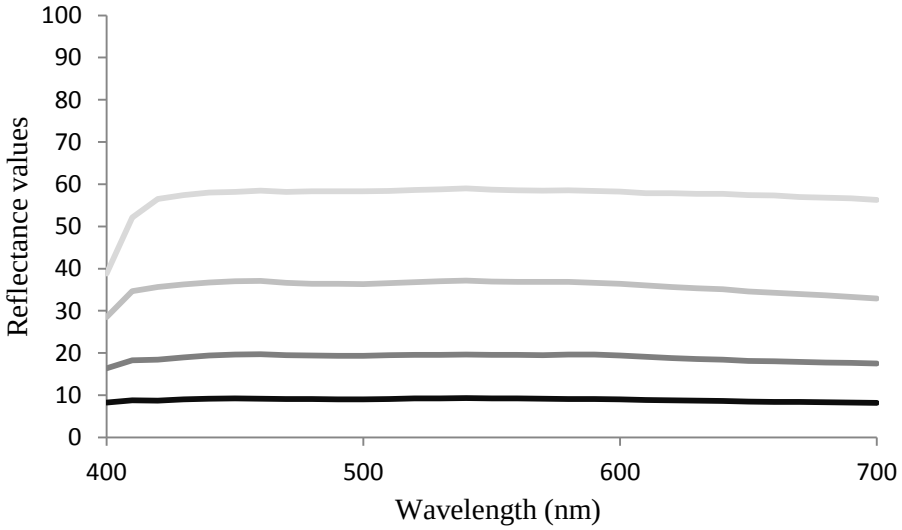

Figure 5.3 Reflection curves of N3.5, N5, N6.5, N8.

5.2. Colour correction in the scene

In this section, the colour correction is described for the first scene. In each following scene, until scene 23, the parameters of the calculated best fit functions change due to the variation of the neutral's RGB values, determined by the white balance of the camera, as explained in 4.4. The pictures are taken as shown in Figure 4.9 and as described in 4.3.3. Both cameras' settings were left in automatic mode; except for ISO that was fixed at 100 and aperture that was set at minimum, but the minimum aperture of the 2 cameras have different values. The sRGB option was chosen from the menu of both cameras. The RGB values (0-255) of the neutrals and of the colours in "scene 1" are read with the help of camera software directly from the RAW files on computer screen (the cameras' software offers this possibility).

For the calculation sequence presented next, the data entries are the RGB values, read for the neutrals from scene 1, and their spectral measured reflection values at the wavelengths where digital cameras usually have maximum sensitivity, as shown in Figure 5.4.

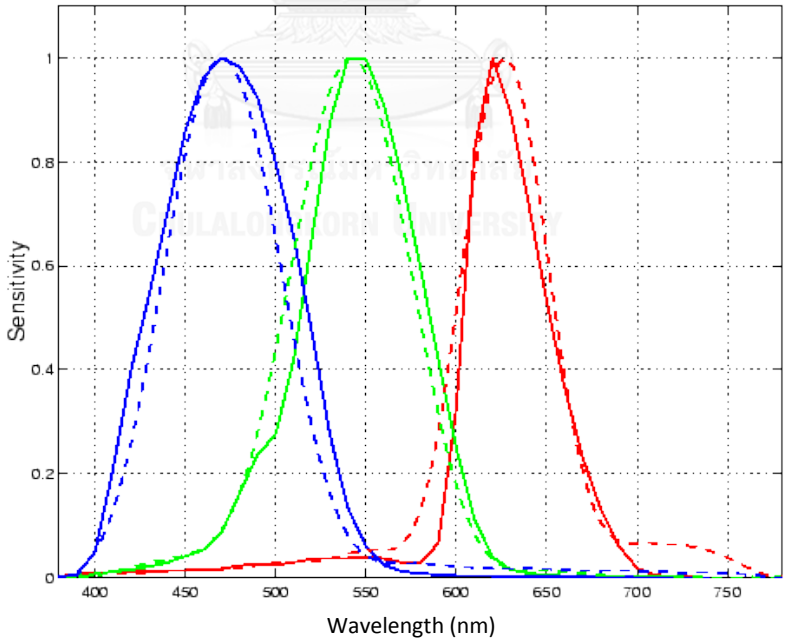

Figure 5.4 Spectral sensitivities of a typical digital camera (dotted lines) and the estimated sensitivities (solid line) which minimize error in a least-squares sense subject to the constraints specified in:

For each neutral in the scene there is a RGB triplet and there are also 3 reflection measurements, at 640 nm for red, at 530 nm for green and at 480 nm for blue. The digital values of red and the reflections at 640 nm of the 6 neutrals are used as input data for correcting the red channel. The digital values of green and the reflections at 530 nm of the 6 neutrals are used as input data for correcting the green channel. The digital values of blue and the reflections at 480 nm of the 6 neutrals are used as input data for correcting the blue channel.

All RGB triplets are normalized from [0, 255] to [0, 1] as shown in equation 5-1:

$$NormalizedRGB = \frac{ExtractedRGB}{255} \quad \text{Eqn.5-1}$$

All reflection values measured at the 3 specified wavelengths are in the interval [0,1]. Linear response can be assumed only if equations 5-2 to 5-4, describing an inverse power function, are satisfied simultaneously:

$$NR = K_1 \cdot R(\lambda)^{\gamma_1} \quad \text{Eqn.5-2}$$

$$NG = K_2 \cdot R(\lambda)^{\gamma_2} \quad \text{Eqn.5-3}$$

$$NB = K_3 \cdot R(\lambda)^{\gamma_3} \quad \text{Eqn.5-4}$$

To verify if the above equations are satisfied within an acceptable error margin, the best fit power function is calculated for each colour channel, using linear regression, as specified in 4.4. For this purpose, the power functions described through equations 5-2 to 5-4, are linearized, as shown in equations 5-5 to 5-10:

$$ln(NR) = ln(K_1 \cdot R(\lambda)^{\gamma_1}) \quad \text{Eqn.5-5}$$

$$ln(NG) = ln(K_2 \cdot R(\lambda)^{\gamma_2}) \quad \text{Eqn.5-6}$$

$$ln(NB) = ln(K_3 \cdot R(\lambda)^{\gamma_3}) \quad \text{Eqn.5-7}$$

$$ln(NR) = ln K_1 + \gamma_1 ln(R(\lambda)) \quad \text{Eqn.5-8}$$

$$ln(NG) = ln K_2 + \gamma_2 ln(R(\lambda)) \quad \text{Eqn.5-9}$$

$$ln(NB) = ln K_3 + \gamma_3 ln(R(\lambda)) \quad \text{Eqn.5-10}$$

After marking for the red channel (Eqn.5-8):*ln(Normalized R)*with y_i and *ln(R(λ))*with x_i, where *i* takes values from 1 to 6 (*i* = neutral sheet number). The graph of the plotted pairs x_i, y_i looks like the one in Figure 5.5. The equation of the linear regression is given by:

$$y_{a_i} = a + bx_{a_i} \qquad \text{Eqn.5-11}$$

where a is the notation for $ln(K_1)$ and b is γ_1.

The parameters *a* and *b* of equation 5-11 are calculated with the input data mentioned beforeby applying the least square method (see Figure 5.5 and equations 5-12 to 5-17). The area of each square is calculated as follows:

$$Area_i = (y_i - y_{ai})^2 \qquad \text{Eqn.5-12}$$

By substituting y_{ai} in Eqn.5-12 with its expression from Eqn.5-11, each area can be expressed as:

$$Area_i = (y_i - (a + bx_{a_i}))^2 \qquad \text{Eqn.5-13}$$

Because each predicted value of y_{ai} has the same coordinate as y_i, results that $x_i = x_{a_i}$ and Eqn.5-13 can be written as follows:

$$Area_i = (y_i - (a + bx_i))^2 \qquad \text{Eqn.5-14}$$

The summation of the six areas is:

$$\sum_{i=1}^{6} Area_i = Area_1 + Area_2 + \ldots + Area_6 \qquad \text{Eqn.5-15}$$

where each area can be substituted according to Eqn.5-14:

$$\sum_{i=1}^{6} Area_i = (y_1 - (a + bx_1))^2 + (y_2 - (a + bx_2))^2 + \ldots + (y_6 - (a + bx_6))^2 \qquad \text{Eqn.5-16}$$

Resulting an equation that is a function of *a*, and *b* ($f_{(a,b)}$). A good correlation between the experimental data and the predicted data is determined by a minimal value of the squares' area summation which is obtained by imposing the following simultaneous conditions for the $f_{(a,b)}$ function to be minimum:

$$\textit{Minimum}\ \ f(a,b) \Leftrightarrow \begin{matrix} \dfrac{\partial f(a,b)}{\partial a} = 0 \\ \dfrac{\partial f(a,b)}{\partial b} = 0 \end{matrix} \qquad \text{Eqn.5-17}$$

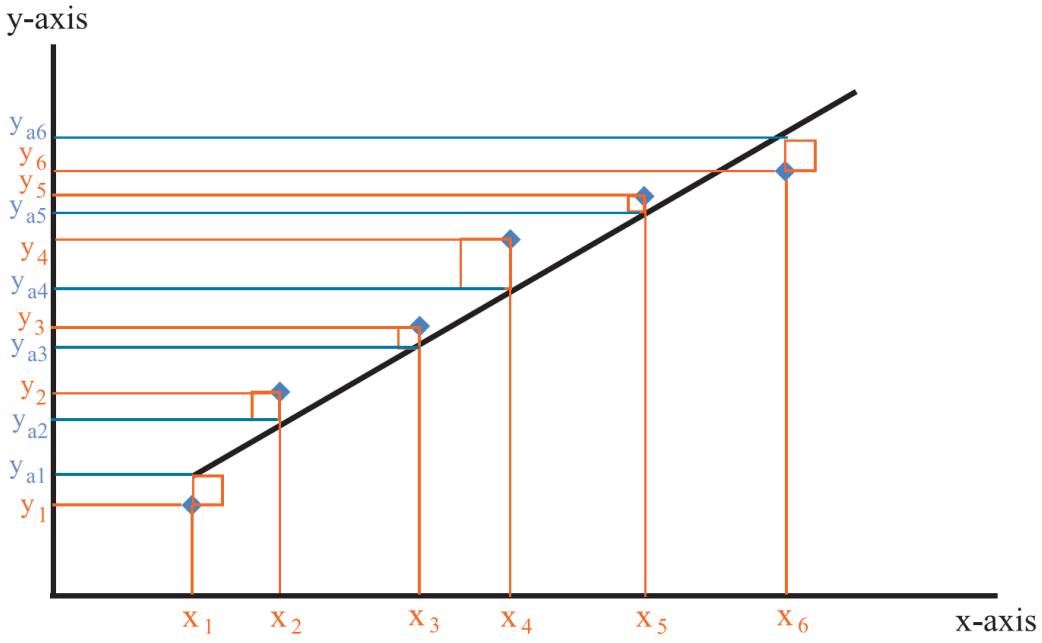

Figure 5.5 Least square diagram for the red channel colour correction.

Finding the solutions for the unknown variables "*a*" and "*b*" of equation system 5-17 means finding the parameters of equation 5-11 that was obtained by linearizing equation 5-5. The *a* and *b* parameters are calculated as follows:

$$\textit{Minimum}\ \ f(a,b) \Leftrightarrow \begin{matrix} \dfrac{\partial f \sum_{i=1}^{6} (y_i - a - b x_i)^2}{\partial a} = 0 \\ \dfrac{\partial f \sum_{i=1}^{6} (y_i - a - b x_i)^2}{\partial b} = 0 \end{matrix} \qquad \text{Eqn.5-18}$$

$$\textit{Minimum } f(a,b) \Leftrightarrow \begin{matrix} -2\left[\sum_{i=1}^{6} y_i - 6a - b\sum_{i=1}^{6} x_i\right] = 0 \\ -2\left[\sum_{i=1}^{6} x_i y_i - a\sum_{i=1}^{6} x_i - b\sum_{i=1}^{6} x_i^2\right] = 0 \end{matrix} \quad \text{Eqn.5-19}$$

The solutions for this system are:

$$a = \frac{\sum_{i=1}^{6} x_i \sum_{i=1}^{6} (x_i y_i) - \sum_{i=1}^{6} y_i \sum_{i=1}^{6} x_i^2}{\left[\left(\sum_{i=1}^{6} x_i\right)^2 - 6\left(\sum_{i=1}^{6} x_i^2\right)\right]} \quad \text{Eqn.5-20}$$

$$\textit{Minimum } f(a,b) \Leftrightarrow \quad b = \frac{\sum_{i=1}^{6} y_i - 6a}{\sum_{i=1}^{6} x_i} \quad \text{Eqn.5-21}$$

Extracting K_1 from the initial notation $a = ln(K_1)$, the coefficient of the power function represented by equation 5-5 is obtained:

$$K_1 = e^a \quad \text{Eqn.5-22}$$

$\gamma_1$power is b, according to the initial notation while K_1 preserves its notation as coefficient. The other coefficients: K_2, K_3 and the powers:γ_2, γ_3 are obtained by applying the calculation process shown for the red channel (starting with equation 5-8) on the green and blue channels (equations 5-9 and 5-10) and by introducing the resulted regression parameters a and b obtained in each case, in equations 5-3 and 5-4.

The colour correcting functions are the inverse functions of the considered power functions, because the best fits are calculated from the decoded colours while the correction must be applied on the encoded colours. The algorithm for calculating the CIELAB values using these corrections was presented in 4.4. and shown in Figure 4.16. Keeping the same notations as presented in 4.4, the equations 5-23 to 5-25 describing the colour correcting functions which result in linear RGB triplets for each colour are:

$$R_l = \left(\frac{R_d}{255} \cdot \frac{1}{K_1}\right)^{\frac{1}{\gamma_1}} \quad \text{Eqn.5-23}$$

$$G_l = \left(\frac{G_d}{255} \cdot \frac{1}{K_2} \right)^{\frac{1}{\gamma_2}} \qquad \text{Eqn.5-24}$$

$$B_l = \left(\frac{B_d}{255} \cdot \frac{1}{K_3} \right)^{\frac{1}{\gamma_3}} \qquad \text{Eqn.5-25}$$

In the software, the colour correction is calculated in 2 steps: 1.) colour corrections are performed for the achromatic colours, establishing the average colour difference of the calculated CIELAB values toward their spectrophotometric measured values, as shown by Figure 4.18 in 4.5., 2.) colour corections are calculated for each colour, immediately after its device dependent RGB triplet is introduced in the program, as shown in Figure 4.19.

Next is presented the code written for colour correction and CIELAB calculation of the neutrals. This code runs when the "Calculate" menu-option is pressed in the input-interface shown in Figure 4.18. The code is written extensively for each colour channel correction for a better understanding but the code for the 3 linear RGB calculation processes could be rewritten condensed in one loop that repeats 3 times. The code is stripped off declarations and user interface specific programming

'red channel correction

```
Rn(1) = R1 / 255: Rn(2) = R2 / 255: Rn(3) = R3 / 255: Rn(4) = R4 / 255
Rn(5) = R5 / 255: Rn(6) = R6 / 255
Gn(1) = G1 / 255: Gn(2) = G2 / 255: Gn(3) = G3 / 255: Gn(4) = G4 / 255
Gn(5) = G5 / 255: Gn(6) = G6 / 255
Bn(1) = B1 / 255: Bn(2) = B2 / 255: Bn(3) = B3 / 255: Bn(4) = B4 / 255
Bn(5) = B5 / 255: Bn(6) = B6 / 255
lnR1 = Log(Rn(1)): lnR2 = Log(Rn(2)): lnR3 = Log(Rn(3)): lnR4 = Log(Rn(4))
lnR5 = Log(Rn(5)): lnR6 = Log(Rn(6))
lnRR1 = Log(RR1): lnRR2 = Log(RR2): lnRR3 = Log(RR3)
lnRR4 = Log(RR4): lnRR5 = Log(RR5): lnRR6 = Log(RR6)
Sum_lnR = lnR1 + lnR2 + lnR3 + lnR4 + lnR5 + lnR6
Sum_sq_lnP_R = lnRR1 ^ 2 + lnRR2 ^ 2 + lnRR3 ^ 2 + lnRR4 ^ 2 + lnRR5 ^ 2 + lnRR6 ^ 2
Sum_lnP_R = lnRR1 + lnRR2 + lnRR3 + lnRR4 + lnRR5 + lnRR6
Sum_lnRlnP = (lnR1 * lnRR1) + (lnR2 * lnRR2) + (lnR3 * lnRR3) + (lnR4 * lnRR4) + (lnR5 *
lnRR5) + (lnR6 * lnRR6)
```

*A1 = ((Sum_lnP_R * Sum_lnRlnP) - (Sum_lnR * (Sum_sq_lnP_R))) / ((Sum_lnP_R ^ 2) - (6 * Sum_sq_lnP_R))*

*b_1 = (Sum_lnR - (6 * A1)) / Sum_lnP_R*

gamma1 = b_1

K1 = 2.718282 ^ (A1)

' linearized Red values for the neutral patches

*Rl(1) = ((1 / K1) ^ (1 / gamma1)) * (Rn(1) ^ (1 / gamma1))*

*Rl(2) = ((1 / K1) ^ (1 / gamma1)) * (Rn(2) ^ (1 / gamma1))*

*Rl(3) = ((1 / K1) ^ (1 / gamma1)) * (Rn(3) ^ (1 / gamma1))*

*Rl(4) = ((1 / K1) ^ (1 / gamma1)) * (Rn(4) ^ (1 / gamma1))*

*Rl(5) = ((1 / K1) ^ (1 / gamma1)) * (Rn(5) ^ (1 / gamma1))*

*Rl(6) = ((1 / K1) ^ (1 / gamma1)) * (Rn(6) ^ (1 / gamma1))*

‘green channel correction

lnG1 = Log(Gn(1)): lnG2 = Log(Gn(2)): lnG3 = Log(Gn(3))

lnG4 = Log(Gn(4)): lnG5 = Log(Gn(5)): lnG6 = Log(Gn(6))

lnRG1 = Log(RG1): lnRG2 = Log(RG2): lnRG3 = Log(RG3)

lnRG4 = Log(RG4): lnRG5 = Log(RG5): lnRG6 = Log(RG6)

Sum_lnG = lnG1 + lnG2 + lnG3 + lnG4 + lnG5 + lnG6

Sum_sq_lnG = (lnG1 ^ 2) + (lnG2 ^ 2) + (lnG3 ^ 2) + (lnG4 ^ 2) + (lnG5 ^ 2) + (lnG6 ^ 2)

Sum_sq_lnP_G = lnRG1 ^ 2 + lnRG2 ^ 2 + lnRG3 ^ 2 + lnRG4 ^ 2 + lnRG5 ^ 2 + lnRG6 ^ 2

Sum_lnP_G = lnRG1 + lnRG2 + lnRG3 + lnRG4 + lnRG5 + lnRG6

*Sum_lnGlnP = (lnG1 * lnRG1) + (lnG2 * lnRG2) + (lnG3 * lnRG3) + (lnG4 * lnRG4) + (lnG5 * lnRG5) + (lnG6 * lnRG6)*

*A2 = ((Sum_lnP_G * Sum_lnGlnP) - (Sum_lnG * (Sum_sq_lnP_G))) / ((Sum_lnP_G ^ 2) - (6 * Sum_sq_lnP_G))*

*b_2 = (Sum_lnG - (6 * A2)) / Sum_lnP_G*

gamma2 = b_2

K2 = 2.718282 ^ (A2)

' linearized Green values for the neutral patches

*Gl(1) = ((1 / K2) ^ (1 / gamma2)) * (Gn(1) ^ (1 / gamma2))*

*Gl(2) = ((1 / K2) ^ (1 / gamma2)) * (Gn(2) ^ (1 / gamma2))*

*Gl(3) = ((1 / K2) ^ (1 / gamma2)) * (Gn(3) ^ (1 / gamma2))*

*Gl(4) = ((1 / K2) ^ (1 / gamma2)) * (Gn(4) ^ (1 / gamma2))*

*Gl(5) = ((1 / K2) ^ (1 / gamma2)) * (Gn(5) ^ (1 / gamma2))*

*Gl(6) = ((1 / K2) ^ (1 / gamma2)) * (Gn(6) ^ (1 / gamma2))*

‘blue channel correction

lnB1 = Log(Bn(1)): lnB2 = Log(Bn(2)): lnB3 = Log(Bn(3)): lnB4 = Log(Bn(4))lnB5 = Log(Bn(5)): lnB6 = Log(Bn(6))

lnRB1 = Log(RB1): lnRB2 = Log(RB2): lnRB3 = Log(RB3): lnRB4 = Log(RB4): lnRB5 = Log(RB5): lnRB6 = Log(RB6)

Sum_lnB = lnB1 + lnB2 + lnB3 + lnB4 + lnB5 + lnB6

Sum_sq_lnB = (lnB1 ^ 2) + (lnB2 ^ 2) + (lnB3 ^ 2) + (lnB4 ^ 2) + (lnB5 ^ 2) + (lnB6 ^ 2)

Sum_sq_lnP_B = lnRB1 ^ 2 + lnRB2 ^ 2 + lnRB3 ^ 2 + lnRB4 ^ 2 + lnRB5 ^ 2 + lnRB6 ^ 2

Sum_lnP_B = lnRB1 + lnRB2 + lnRB3 + lnRB4 + lnRB5 + lnRB6

*Sum_lnBlnP = (lnB1 * lnRB1) + (lnB2 * lnRB2) + (lnB3 * lnRB3) + (lnB4 * lnRB4) + (lnB5 * lnRB5) + (lnB6 * lnRB6)*

*a3 = ((Sum_lnP_B * Sum_lnBlnP) - (Sum_lnB * (Sum_sq_lnP_B))) / ((Sum_lnP_B ^ 2) - (6 * Sum_sq_lnP_B))*

*b_3 = (Sum_lnB - (6 * a3)) / Sum_lnP_B*

gamma3 = b_3

K3 = 2.718282 ^ (a3)

' linearized Blue values for the neutral patches

*Bl(1) = ((1 / K3) ^ (1 / gamma3)) * (Bn(1) ^ (1 / gamma3))*

*Bl(2) = ((1 / K3) ^ (1 / gamma3)) * (Bn(2) ^ (1 / gamma3))*

*Bl(3) = ((1 / K3) ^ (1 / gamma3)) * (Bn(3) ^ (1 / gamma3))*

*Bl(4) = ((1 / K3) ^ (1 / gamma3)) * (Bn(4) ^ (1 / gamma3))*

*Bl(5) = ((1 / K3) ^ (1 / gamma3)) * (Bn(5) ^ (1 / gamma3))*

*Bl(6) = ((1 / K3) ^ (1 / gamma3)) * (Bn(6) ^ (1 / gamma3))*

‘CIELAB calculation sequence

For I = 1 To 6

*X(I) = ((0.4124 * (Rl(I) + R_added)) + (0.3576 * (Gl(I) + G_added)) + (0.1805 * (Bl(I) + B_added))) * 100*

*Y(I) = ((0.2126 * (Rl(I) + R_added)) + (0.7152 * (Gl(I) + G_added)) + (0.072 * (Bl(I) + B_added))) * 100*

*Z(I) = ((0.0193 * (Rl(I) + R_added)) + (0.1192 * (Gl(I) + G_added)) + (0.9505 * (Bl(I) + B_added))) * 100*

If (X(I) / 95.047) > 0.008856 Then

Ft1 = (X(I) / 95.047) ^ (1 / 3)

Else

*Ft1 = (7.787 * (X(I) / 95.047)) + (16 / 116)*

End If

If (Y(I) / 100) > 0.008856 Then

Ft2 = (Y(I) / 100) ^ (1 / 3)

```
    Else
       Ft2 = (7.787 * (Y(I) / 100)) + (16 / 116)
    End If
    If (Z(I) / 108.883) > 0.008856 Then
       Ft3 = (Z(I) / 108.883) ^ (1 / 3)
    Else
       Ft3 = (7.787 * (Z(I) / 108.883)) + (16 / 116)
    End If
    a(I) = 500 * (Ft1 - Ft2)
    B(I) = 200 * (Ft2 - Ft3)
    If (Y(I) / 100) > 0.008856 Then
       L(I) = (116 * Ft2) - 16
    Else
       L(I) = 903.3 * (Y(I) / 100)
    End If
Next I
```

Next is presented the code written for colour correction and CIELAB calculation of the colours. This code runs when the “Extract Colours” menu-option is pressed in the input-interface shown in Figure 4.19. Declarations and user interface specific code are omitted in the program listing that follows.

```
R_norm = RC / 255: G_norm = GC / 255: B_norm = BC / 255
R_lin = ((1 / K1) ^ (1 / gamma1)) * (R_norm ^ (1 / gamma1))
G_lin = ((1 / K2) ^ (1 / gamma2)) * (G_norm ^ (1 / gamma2))
B_lin = ((1 / K3) ^ (1 / gamma3)) * (B_norm ^ (1 / gamma3))
    XC = ((0.4124 * (R_lin + R_added)) + (0.3576 * (G_lin + G_added)) + (0.1805 * (B_lin +
B_added))) * 100
    YC = ((0.2126 * (R_lin + R_added)) + (0.7152 * (G_lin + G_added)) + (0.072 * (B_lin +
B_added))) * 100
    ZC = ((0.0193 * (R_lin + R_added)) + (0.1192 * (G_lin + G_added)) + (0.9505 * (B_lin +
B_added))) * 100
    If (XC / 95.047) > 0.008856 Then
       Ft1 = (XC / 95.047) ^ (1 / 3)
    Else
       Ft1 = (7.787 * (XC / 95.047)) + (16 / 116)
    End If
    If (YC / 100) > 0.008856 Then
       Ft2 = (YC / 100) ^ (1 / 3)
```

```
Else
   Ft2 = (7.787 * (YC / 100)) + (16 / 116)
End If
If (ZC / 108.883) > 0.008856 Then
   Ft3 = (ZC / 108.883) ^ (1 / 3)
Else
   Ft3 = (7.787 * (ZC / 108.883)) + (16 / 116)
End If
ac = 500 * (Ft1 - Ft2)
bbc = 200 * (Ft2 - Ft3)
If (YC / 100) > 0.008856 Then
   LC = (116 * Ft2) - 16
Else
   LC = 903.3 * (YC / 100)
End If
```

5.3. Bradford Chromatic Adaptation Transform

The software performs Bradford Transform, as shown in 4.5., which was preferred over other chromatic adaptation transformsform the reasons explained in 4.4 and 4.6. The general flowchart for a chromatic adaptation transform is shown in Figure 3.6 and explained in 3.4. The trichromatic CIEXYZ values for the destination light source are calculated from the CIEXYZ values of the source light with equation 3-12.

The calculation process for determining matrix M in equation 3-12 has following steps, keeping the same notations as in :

1. Calculation of the parameters ρ_d(ro), γ_d(gama), β_d(beta) for the destination light, using M_A matrix and the CIEXYZ trichromatic values of the destination light X_{WD}, Y_{WD}, Z_{WD};
2. Calculation of the parameters ρ_s (ro), γ_s(gama), β_s(beta) for the source light, using M_A^{-1}matrix and the CIEXYZ trichromatic values of the source light X_{WS}, Y_{WS}, Z_{WS};
3. Calculation of the Matrix M using ρ_d, γ_d, β_d, ρ_s, γ_s, β_s

The mathematical formulation is shown next:

$$\begin{bmatrix}\rho_D\\ \gamma_D\\ \beta_D\end{bmatrix}=[M_A]\cdot\begin{bmatrix}X_{WD}\\ Y_{WD}\\ Z_{WD}\end{bmatrix}\qquad [M_A]=\begin{bmatrix}0.8951000 & 0.2664000 & -0.1614000\\ -0.7502000 & 1.7135000 & 0.0367000\\ 0.0389000 & -0.0685000 & 1.0296000\end{bmatrix}$$

$$\begin{bmatrix}\rho_S\\ \gamma_S\\ \beta_S\end{bmatrix}=[M_A]\cdot\begin{bmatrix}X_{WS}\\ Y_{WS}\\ Z_{WS}\end{bmatrix}\qquad [M_A]^{-1}=\begin{bmatrix}0.9869929 & -0.1470543 & 0.1599627\\ 0.4323053 & 0.5183603 & 0.0492912\\ -0.0085287 & 0.0400428 & 0.9684867\end{bmatrix}$$

$$[M]=[M_A]^{-1}\begin{bmatrix}\frac{\rho_D}{\rho_S} & 0 & 0\\ 0 & \frac{\gamma_D}{\gamma_S} & 0\\ 0 & 0 & \frac{\beta_D}{\beta_S}\end{bmatrix}\cdot[M_A]$$

The program-sequence written for calculating the Bradford transform is listed below, with all declarations, user-interface code, error trapping code etc. stripped off. The programming sequence uses as input the RGB triplet (RC, GC, BC) of the N9.5 in the scene.

```
R_norm = RC / 255: G_norm = GC / 255: B_norm = BC / 255
R_lin = ((1 / K1) ^ (1 / gamma1)) * (R_norm ^ (1 / gamma1))
G_lin = ((1 / K2) ^ (1 / gamma2)) * (G_norm ^ (1 / gamma2))
B_lin = ((1 / K3) ^ (1 / gamma3)) * (B_norm ^ (1 / gamma3))
XC = ((0.4124 * R_lin) + (0.3576 * G_lin) + (0.1805 * B_lin)) * 100
YC = ((0.2126 * R_lin) + (0.7152 * G_lin) + (0.072 * B_lin)) * 100
ZC = ((0.0193 * R_lin) + (0.1192 * G_lin) + (0.9505 * B_lin)) * 100
'ro(1), gama(1), beta(1) are for the source and ro(2), gama(2), beta(2) for destination
  For I = 1 To 2
    ro(I) = 0.8951 * XC + 0.2664 * YC - 0.1614 * ZC
    gama(I) = -0.7502 * XC + 1.7135 * YC + 0.0367 * ZC
    beta(I) = 0.0389 * XC - 0.0685 * YC + 1.0296 * ZC
  Next I
```

```
For I = 1 To 6
XD(I) = (0.9869929 * 0.8951 * (ro(2) / ro(1)) + 0.1470543 * 0.7502 * (gama(2) / gama(1)) + 0.1599627 * 0.0389 * (beta(2) / beta(1))) * X(I) + (0.9869929 * 0.2664 * (ro(2) / ro(1)) - 0.1470543 * 1.7135 * (gama(2) / gama(1)) - 0.1599627 * 0.0685 * (beta(2) / beta(1))) * Y(I) + (-0.9869929 * 0.1614 * (ro(2) / ro(1)) - 0.1470543 * 0.0367 * (gama(2) / gama(1)) + 0.1599627 * 1.0296 * (beta(2) / beta(1))) * Z(I)
YD(I) = (0.4323053 * 0.8951 * (ro(2) / ro(1)) - 0.5183605 * 0.7502 * (gama(2) / gama(1)) + 0.0492912 * 0.0389 * (beta(2) / beta(1))) * X(I) + (0.4323053 * 0.2664 * (ro(2) / ro(1)) + 0.5183605 * 1.7135 * (gama(2) / gama(1)) - 0.0492912 * 0.0685 * (beta(2) / beta(1))) * Y(I) + (-0.4323053 * 0.1614 * (ro(2) / ro(1)) + 0.5183605 * 0.0367 * (gama(2) / gama(1)) + 0.0492912 * 1.0296 * (beta(2) / beta(1))) * Z(I)
ZD(I) = (-0.0085287 * 0.8951 * (ro(2) / ro(1)) - 0.0400428 * 0.7502 * (gama(2) / gama(1)) + 0.9684867 * 0.0389 * (beta(2) / beta(1))) * X(I) + (-0.0085287 * 0.2664 * (ro(2) / ro(1)) + 0.0400428 * 1.7135 * (gama(2) / gama(1)) - 0.9684867 * 0.0685 * (beta(2) / beta(1))) * Y(I) + (0.0085287 * 0.1614 * (ro(2) / ro(1)) + 0.0400428 * 0.0367 * (gama(2) / gama(1)) + 0.9684867 * 1.0296 * (beta(2) / beta(1))) * Z(I)
```

5.4. CIE ΔE_{00} calculation

The 2000 colour difference is calculated in different stages, as explained in 4.4. and 4.5. and as can be seen in Figures 4.18 and 4.19. The implementation of the 2000 colour difference formula has been done following the suggestions given in literature (CIE 2005). The code written for the calculation subroutine is listed next.

```
Pi = 4 * Atn(1)
kL = 1: kC = 1: kH = 1
Radians = Pi / 180
degrees = 1 / Radians
'calculate c1,c2,h1,h2
'*********************************************
C1 = Sqr(A1 ^ 2 + B1 ^ 2)
```

```
C2 = Sqr(A2 ^ 2 + B2 ^ 2)
Cab = (C1 + C2) / 2
G = 0.5 * (1 - Sqr(Cab ^ 7 / (Cab ^ 7 + 25 ^ 7)))
aP1 = (1 + G) * A1
aP2 = (1 + G) * A2
CP1 = Sqr(aP1 ^ 2 + B1 ^ 2)
CP2 = Sqr(aP2 ^ 2 + B2 ^ 2)
If (B1 = 0 And aP1 = 0) Then
   hP1 = 0
Else
   hP1 = degrees * Atan2(B1, aP1)
   If hP1 < 0 Then
      hP1 = hP1 + 360
   End If
End If
If (B2 = 0 And aP2 = 0) Then
   hP2 = 0
Else
 hP2 = degrees * Atan2(B2, aP2)
   If hP2 < 0 Then
      hP2 = hP2 + 360
   End If
End If
'calculate Delta L',Delta C',Delta h',Delta H'
'*****************************************
DLP = L2 - L1
DCP = CP2 - CP1
If CP1 * CP2 = 0 Then
   DhP = 0
ElseIf (CP1 * CP2 <> 0 And Abs(hP2 - hP1) <= 180) Then
      DhP = hP2 - hP1
ElseIf (CP1 * CP2 <> 0 And (hP2 - hP1) > 180) Then
      DhP = hP2 - hP1 - 360
ElseIf (CP1 * CP2 <> 0 And (hP2 - hP1) < -180) Then
   DhP = hP2 - hP1 + 360
End If
DelHp = 2 * Sqr(CP1 * CP2) * Sin(Radians * (DhP / 2))
```

```
'calculate DE 2000'
'*****************************************
 Lbar = (L1 + L2) / 2
 Cbar = (CP1 + CP2) / 2
 If (CP1 * CP2 = 0) Then
    hbar = (hP1 + hP2)
ElseIf (Abs(hP1 - hP2) <= 180) Then
    hbar = (hP1 + hP2) / 2
ElseIf (Abs(hP1 - hP2) > 180 And (hP1 + hP2) < 360) Then
    hbar = (hP1 + hP2 + 360) / 2
ElseIf (Abs(hP1 - hP2) > 180 And (hP1 + hP2) >= 360) Then
    hbar = (hP1 + hP2 - 360) / 2
End If
t = 1 - 0.17 * Cos(Radians * (hbar - 30)) + 0.24 * Cos(Radians * (2 * hbar)) + 0.32 * Cos(Radians *
(3 * hbar + 6)) - 0.2 * Cos(Radians * (4 * hbar - 63))
DelTheta = 30 * Exp(-((hbar - 275) / 25) ^ 2)
RC = 2 * Sqr(Cbar ^ 7 / (Cbar ^ 7 + 25 ^ 7))
SL = 1 + (0.015 * (Lbar - 50) ^ 2) / Sqr(20 + (Lbar - 50) ^ 2)
Sc = 1 + 0.045 * Cbar
Sh = 1 + 0.015 * Cbar * t
RT = -Sin(Radians * 2 * DelTheta) * RC
DE00 = Sqr((DLP / (kL * SL)) ^ 2 + (DCP / (kC * Sc)) ^ 2 + (DelHp / (kH * Sh)) ^ 2 + RT * (DCP /
(kC * Sc)) * (DelHp / (kH * Sh)))
```


The calculation of the CRI is shown schematically in Figure 3.2 and explained in detail in 3.1. The procedures for calculating the data needed in the CRI formulas have been described in the section 3.1. The formulas are given in equations 3-10 and 3-11. The colour difference used in CRI calculation is calculated based on the 1976 formula but the software has the option of replacing the 1976 formula with the 2000 colour difference formula, using the subroutine listed in 5.3.

CHAPTER 6

RESULTS AND DISCUSSIONS

6.1. Preliminary discussions

Pictures of the achromatic wheel (described in 4.3.3) were taken for finding the right distance and right angle in order to position the SLR digital camera on the bottom and in center of the boxes (design described in 4.3.2). The resulted distance from applying the procedure presented in 4.3.3 is 1 meter and the resulted angle is 45 degrees as shown in Figure 4.10. The setup was left unchanged for all scenes. Twenty three scenes were recorded.

Most settings of both cameras were left in automatic mode, except for ISO that was fixed at 100 and aperture that was set at minimum but the minimum aperture of the 2 cameras, shown in 4.3.1., has different values. The sRGB option was selected from the set up menu of both cameras. The main objective of colour selection, described in 4.4 and schematically shown in Figure 4.15, was to compare how different cameras behave in constrained conditions toward sets of Munsell colour sheets under different light sources, without doing anything special about one camera or the other. The colour correction is not a result of "properly calibrating" one specific camera and is supposed to work satisfactory across SLR digital cameras. This is an original approach and there is no evidence in literature that it has been tried before. The aim is not to transform one single camera in a colorimeter for a range of colours but to determine a way for obtaining colorimetric values with different cameras under different light sources for a set of colour-code. If these colours cover all hue angles then the colour set could be used in light quality assessments.

The 15 CQS samples proposed by NIST (see 3.3.) were added to the achromatic wheel but 5 were out of the sRGB gamut and were replaced as described in 4.4. The colour wheel with 15 colours and 6 neutrals was recorded as 'scene 1' with camera connected to computer. The RGB values (0-255) of the neutrals and of the colours in "scene 1" were read with the help of camera software directly from the RAW files on

computer screen (the camera software offers this possibility). With the RGB values of the 6 neutrals in the picture and the 3 reflectance values measured for each neutral with a spectrophotometer at 480, 530 and 640 nm, the best fit power functions were calculated. Using these functions, the RGB of the 15 colours from the picture were transformed in linear RGB and then the linear RGB in CIELAB values, as shown in the flowchart from Figure 4.16.The results obtained for this scene is shown in Table 4.1 in 4.6, while the best fit power functions are shown in Figures 4.12, 4.13 and 4.14 in 4.4.

The obtained CIELAB values of the 15 colours were compared with their CIELAB spectrophotometric measured values using the 2000 colour difference formula imposing a limit of 6 units for keeping the colour in the wheel. The other colours were replaced as shown in the schematic diagram of the colour selection process from Figure 4.15, but replacing more than one colour in a step. After the first replacements, another picture was taken: ‘scene 2’. After the replacement of colours, the RGB values of the neutrals changed. The 3 spectral reflectance values of each neutral remained the same as before because they were determined with a spectrophotometer. However, because the RGB values of the neutrals have changed, the pairs of values from which the best fit functions were calculated for red, green and blue are different than in the first picture. So the parameters of the best fit power functions for red, green and blue used for calculating the CIELAB values of the colours in the second picture (scene 2) are different from the ones used for the first picture (scene 1), as can be seen in Figures 4.12, 4.13, 4.14 in 4.4. The colour differences were calculated again and the process was repeated 5 times, then no colours were replaced in the wheel any more but colours were added until scene 15. After that, the colour-wheel was improved under the LED D65 light source until scene 23. CIELAB values of selected colour codes change under different illumination. Using more light sources in the colour selection process, insures a good selection of the colour regions where the colour correction method can be applied successfully across digital cameras. Light sources were changed and scene 23 was recalculated under the other light sources mentioned in 4. Further, the Nikon D40x camera was used under all 4 considered light sources.

The results for scene 1, 6 and 15 are already presented in Tables 4.1, 4.2 and 4.3 in 4.6, therefore they will not be shown again in this chapter. The results of scene 23 calculated for the Canon camera under the considered fluorescent and LED D65 light sources are presented in Table 4.4 in 4.6, therefore they will not be listed here again. Table 6.1 to 6.11 show the calculated CIELAB values from Canon's digital images corresponding to scenes 2, 3, 5 and 7 to 14 under Fluorescent D65 light source and the ΔE_{00} toward measured CIELAB D65/2. Similar tables the scenes 1, 3, 6 and 15 have been presented in section 4, 6, therefore they are not added anymore in this chapter. The hue chroma chart of scene 15 was shown in chapter 4, therefore is not repeated here. Results that are not critical for the discussions in this chapter were added to the Appendices, not to this chapter. Appendices contain also results obtained with a third SLR digital camera having white Balance (WB) preset, in order to prove that automatic WB does not have a negative impact on the results compared with the case of using a preset WB. The results show that automatic WB sometime leads to better CIELAB predictions. CRI results calculated for the two considered D65 light sources were presented in sustenance of the applied methodology in 4.6 but they will appear again accompanying the CRI results obtained with this method for the other 2 light sources, because they are part of the final results that constitute the aim of this work.

The cameras used are cheap, old, entry levels in their series at the time they were produced. When taking pictures, the scene in the picture contains only the wheel's colours, without including any environment.

The wheel was preferred over a square chart due to the light intensity drop from the center of the box toward margins. As can be seen in the experiment and 4.3.3, the drop is significant. If a square chart would have been selected, then on each colour of that chart the incident light would be of different intensity, while on a wheel, an area can be defined around the center where all colours are equally distanced and therefore are illuminated in a narrow intensity interval. Simple commercial lamps were used to make sure that results would only improve by using better ones.

6.2. Intermediary results during the colour selection process obtained with Canon EOS X4

The results are divided in 3 parts: a). scene 1 to 6, when the colour wheel had 15 colours that were changed across the scenes and 6 fixed neutrals, b). scene 7 to 14, when Munsell colour patches were added to the wheel until it contained 24 patchs that respected the imposed conditions, c). scene 15 to 23. Tables and graphs that are already presented in previous chapters will be only referenced, as explained in section 6.1.

6.2.1. Results obtained for the 15 colour wheel.

The best fits used to calculate scene 1 are shown in Figures 4.12, 4.13, 4.14 in 4.4. Calculation results are listed in Table 4.1 in 4.6. The best fit functions for scenes 2 and 3 are shown on the same graphs with those of scene 1 in Figures 4.12, 4.13 and 4.14. Calculation results for scene 3 are presented in Table 4.2 in 4.6 and results obtained for scene 2 are listed in Table 6.1.

Table 6.1 Calculated CIELAB from Canon EOS X4's digital image scene 2 under Fluorescent D65 and ΔE_{00} toward measured CIELAB, D65/2°.

Munsell Patches	Measured spectrophotometric			R	G	B	Calculated	CIELAB	of scene 2	ΔE_{00}
	L*	a*	b*				L*	a*	b*	
N2	21.15	-0.15	-0.82	23	25	26	18.42	0.53	-0.50	2.16
N3.5	36.28	-0.45	-0.9	54	64	66	39.03	-1.67	-1.06	2.89
N5	52.15	-0.43	-0.62	94	110	115	56.62	-1.61	-1.81	4.70
N6.5	66.68	-0.93	-0.63	138	155	160	70.79	-0.63	-0.68	3.26
N8	81.55	-0.85	-0.97	172	190	196	80.44	0.01	-0.37	1.56
N9.5	95.71	-0.59	1.54	198	217	221	87.23	0.03	0.72	5.37
7.5 P 4/10	42.23	34.78	-23.65	113	62	150	47.77	37.21	-31.44	6.33
10 PB 4/8	41.4	18.53	-30.93	85	79	168	49.75	22.22	-36.39	8.30
2.5 GY 8/10	81.54	-22.1	70.22	165	211	41	81.88	-25.78	67.36	2.30
7.5 GY 7/10	71.18	-39.34	53.3	102	195	55	75.38	-40.49	52.87	3.17
10 R 6/10	61.56	37.79	38.58	207	88	52	61.12	39.29	40.07	0.72
7.5 RP 4/12	41.9	53.46	1.07	150	31	84	43.66	55.92	-3.80	2.89
10 YR 7/10	72.17	14.04	61.92	190	145	22	70.54	6.17	66.13	5.58
2.5 G 5/10	51.58	-54.71	25.46	15	151	67	61.71	-52.72	29.27	9.55
10 BG 4/8	40.35	-31.99	-20.14	14	106	143	51.50	-18.27	-23.08	13.05
7.5 B 5/8	50.78	-17.35	-28.26	37	136	190	61.49	-15.51	-27.30	10.03
5 R 4/12	41.59	52.54	27.9	155	23	33	41.68	56.77	28.37	1.36
2.5 BG 4/8	41.46	-42.02	-2.54	14	108	100	50.82	-30.73	-3.41	10.04
5 YR 7/6	71.12	17	30.11	189	143	104	71.06	13.16	24.89	2.78

The best fit power functions for scenes 4 to 6 and the calculation sheets for scenes 4 and 5 follow next. Calculations for scene 6 are presented in Table 4.2 in 4.6.

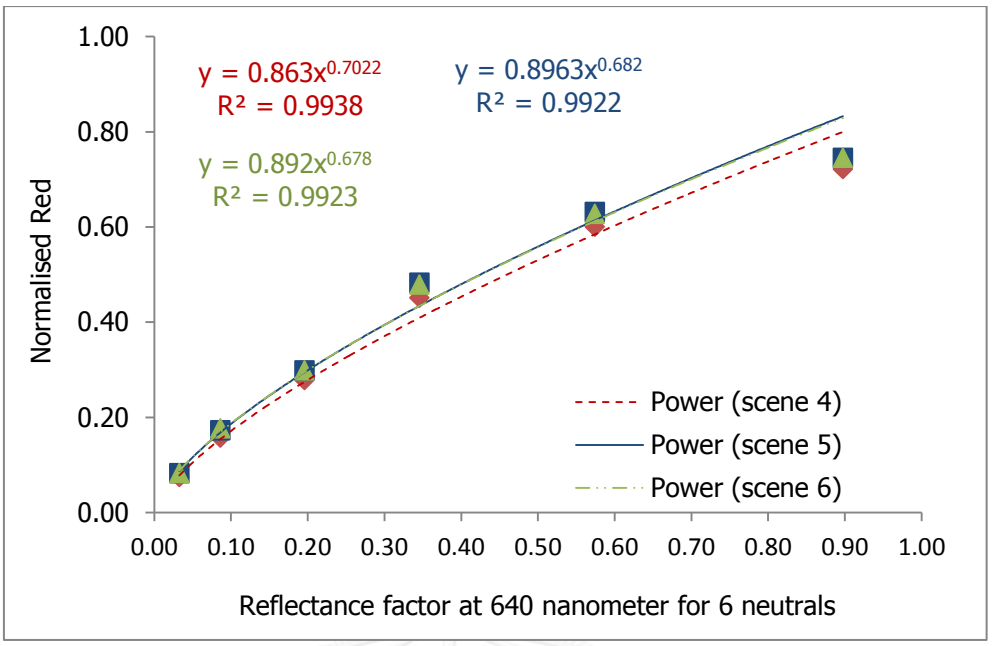

Figure 6.1 Best fit power functions (Red) for scene 4 to 6.

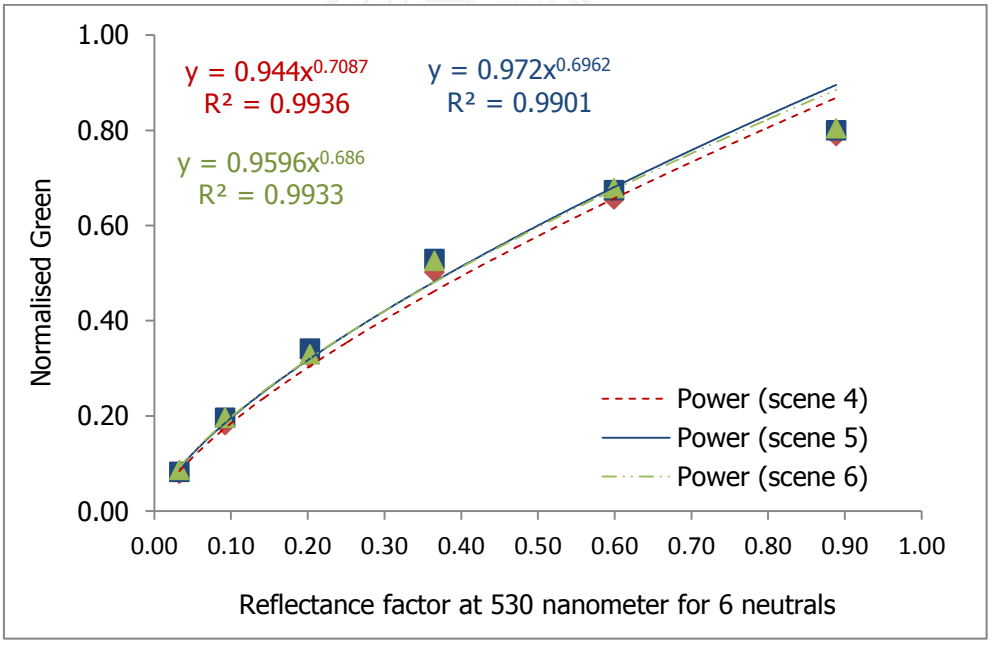

Figure 6.2 Best fit functions (Green) for scenes 4 to 6.

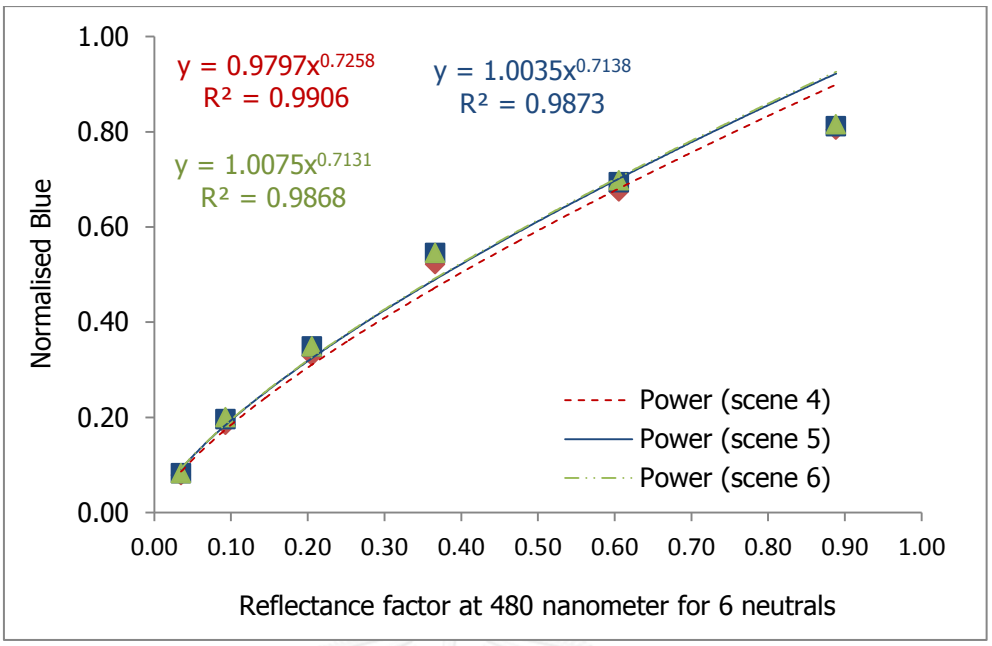

Figure 6.3 Best fit functions (Blue) for scenes 4 to 6.

Table 6.2 Calculated CIELAB from Canon EOS X4's digital image scene 4 under Fluorescent D65 and ΔE_{00} toward measured CIELAB, D65/2°.

Munsell Patches	Measured spectrophotometric			R	G	B	Calculated	CIELAB	of scene 4	ΔE_{00}
	L*	a*	b*				L*	a*	b*	
N2	21.15	-0.15	-0.82	19	20	20	20.08	0.46	-0.44	1.23
N3.5	36.28	-0.45	-0.9	40	46	47	36.97	-1.20	-1.36	1.27
N5	52.15	-0.43	-0.62	71	82	84	53.49	-1.74	-1.27	2.32
N6.5	66.68	-0.93	-0.63	115	128	133	70.03	-0.53	-1.23	2.77
N8	81.55	-0.85	-0.97	153	167	172	81.66	0.00	-0.11	1.49
N9.5	95.71	-0.59	1.54	184	201	205	90.51	-0.30	0.86	3.25
7.5 P 4/10	42.23	34.78	-23.65	80	43	109	43.69	33.35	-29.81	3.78
10 PB 4/10	41.59	23.16	-37	62	51	135	45.07	26.66	-40.71	3.58
2.5 GY 8/10	81.54	-22.1	70.22	141	182	29	81.76	-26.24	67.73	2.43
7.5 GY 7/10	71.18	-39.34	53.3	79	166	40	74.73	-42.53	52.87	2.96
10 R 6/10	61.56	37.79	38.58	174	64	38	58.78	40.72	37.75	3.00
7.5 RP 4/12	41.9	53.46	1.07	110	22	57	40.09	50.29	-3.11	2.79
10 YR 7/10	72.17	14.04	61.92	166	118	18	69.88	8.12	63.66	4.32
2.5 G 6/8	61.25	-42.29	21.76	39	144	82	68.02	-43.01	20.13	5.67
10 BG 6/6	61.36	-27.37	-12.65	42	144	155	69.74	-26.99	-11.64	6.87
7.5 B 5/6	51.12	-14	-21.5	39	101	137	58.00	-12.43	-21.62	6.64
5 R 4/12	41.59	52.54	27.9	116	18	25	39.05	51.17	22.96	3.28
2.5 BG 6/6	61.04	-30.57	0.51	46	142	125	68.77	-31.22	0.02	6.38
5 YR 7/6	71.12	17	30.11	165	119	85	71.01	13.74	24.05	2.88
5 PB 4/8	41.13	1.9	-33.59	36	65	128	46.65	5.75	-35.04	5.66
5 Y 8/8	81.48	-2.98	57.75	165	169	47	80.88	-11.58	57.20	5.41

Table 6.3 Calculated CIELAB from Canon EOS X4's digital image scene 5 under Fluorescent D65 and ΔE_{00} toward measured CIELAB, D65/2°.

Munsell Patches	Measured spectrophotometric			R	G	B	Calculated	CIELAB	of scene 5	ΔE_{00}
	L*	a*	b*				L*	a*	b*	
N2	21.15	-0.15	-0.82	21	21	21	19.73	0.79	-0.53	1.73
N3.5	36.28	-0.45	-0.9	44	50	50	37.49	-1.79	-0.98	2.13
N5	52.15	-0.43	-0.62	76	87	89	53.78	-2.06	-1.63	2.90
N6.5	66.68	-0.93	-0.63	123	135	139	70.53	-0.68	-1.07	3.08
N8	81.55	-0.85	-0.97	161	172	177	81.47	0.51	-0.28	2.13
N9.5	95.71	-0.59	1.54	190	204	207	89.69	0.02	0.92	3.83
7.5 P 4/10	42.23	34.78	-23.65	87	45	115	43.76	34.64	-30.62	3.86
10 PB 4/10	41.59	23.16	-37	67	54	143	45.24	27.43	-41.95	3.92
2.5 GY 8/10	81.54	-22.1	70.22	150	189	30	81.99	-25.96	68.40	2.19
7.5 GY 7/10	71.18	-39.34	53.3	86	175	43	75.48	-42.84	53.29	3.47
10 R 6/10	61.56	37.79	38.58	185	69	40	59.45	40.78	38.75	2.32
7.5 RP 4/12	41.9	53.26	1.07	119	23	61	40.38	51.55	-3.46	2.65
10 YR 7/10	72.17	14.04	61.92	175	125	17	70.38	7.49	65.53	4.76
2.5 G 5/8	51.12	-42.78	20.02	26	116	59	57.88	-42.19	21.28	6.49
10 BG 5/8	51.67	-32.95	-17.85	22	121	142	61.11	-25.34	-17.09	9.40
7.5 B 4/6	40.81	-12.19	-23.6	26	73	112	46.31	-7.34	-25.56	6.26
5 R 4/12	41.59	52.54	27.9	127	21	27	40.17	51.41	24.14	2.20
2.5 BG 5/6	51.23	-30.15	-0.49	33	117	103	59.51	-29.97	-0.99	7.81
5 YR 7/6	71.12	17	30.11	174	124	89	71.10	14.19	23.99	2.83
5 PB 3/8	31.52	4.39	-34.85	30	42	102	35.31	13.86	-37.55	6.51
5 Y 8/8	81.48	-2.98	57.75	174	176	48	81.12	-11.65	58.29	5.36

In the process of colour replacement between scene 1 and 6 the average colour differences between calculated and measured CIELAB values improve for the wheel's colours but the green, bluish-green and blue regions of the colour space are not covered anymore after the final replacements. The evolution of the colour positioning in the Hue-Chroma chart from scene 1 to 6 is represented in Figures 6.4 to 6.9.

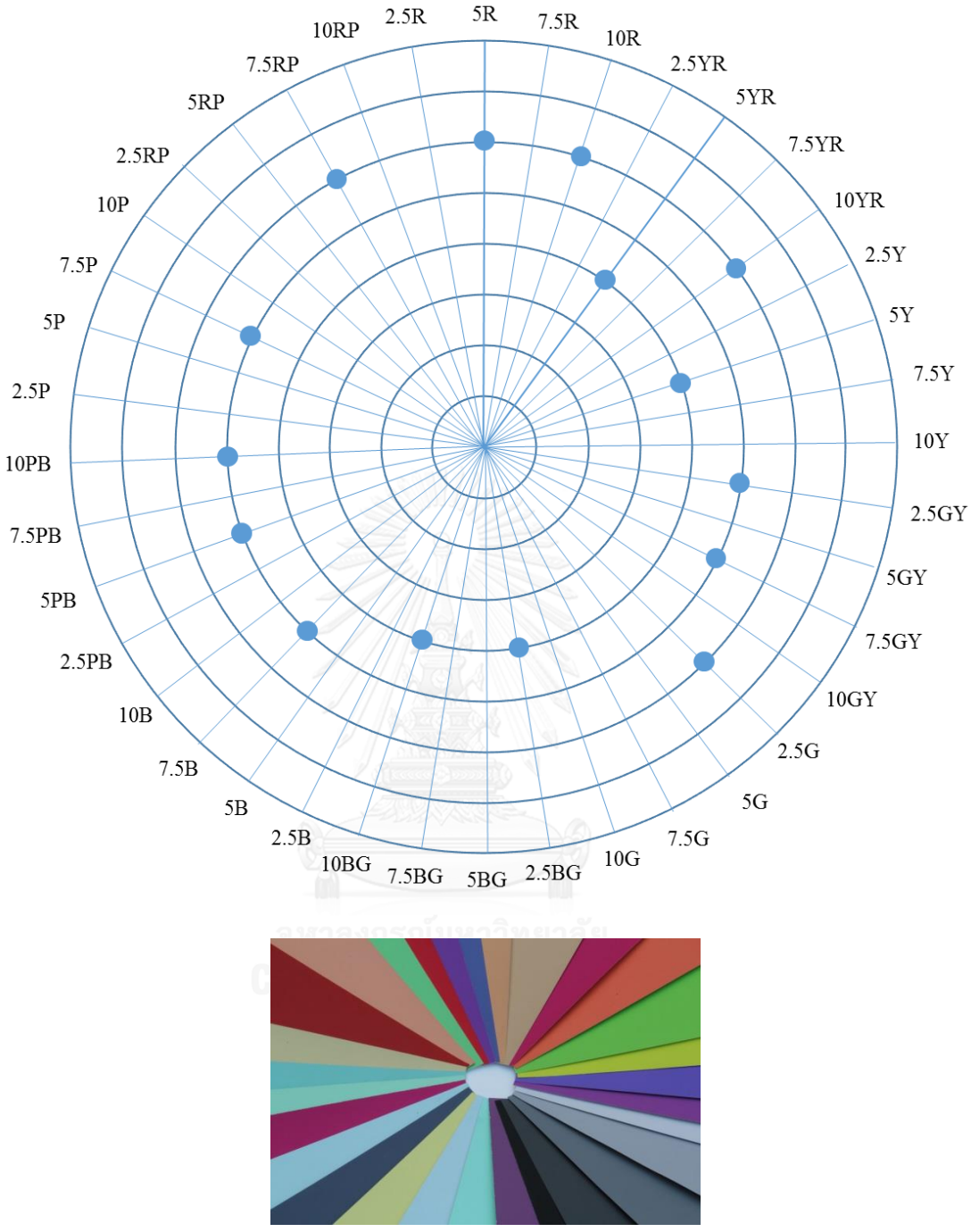

Figure 6.4 Hue-Chroma chart of the colours used in scene 1.

As can be seen in Figure 6.4, the 5 colours that replace the out of sRGB gamut colours of the CQS set cover well the green, bluish-green and blue regions of the colour space, in the lower left part of the chart. However, 7 colours of the wheel have

the colour differences between calculated and measured values over the imposed threshold of 6 ΔE_{00} units, as shown in Table 4.1, and must be replaced. 4.82. 5.28

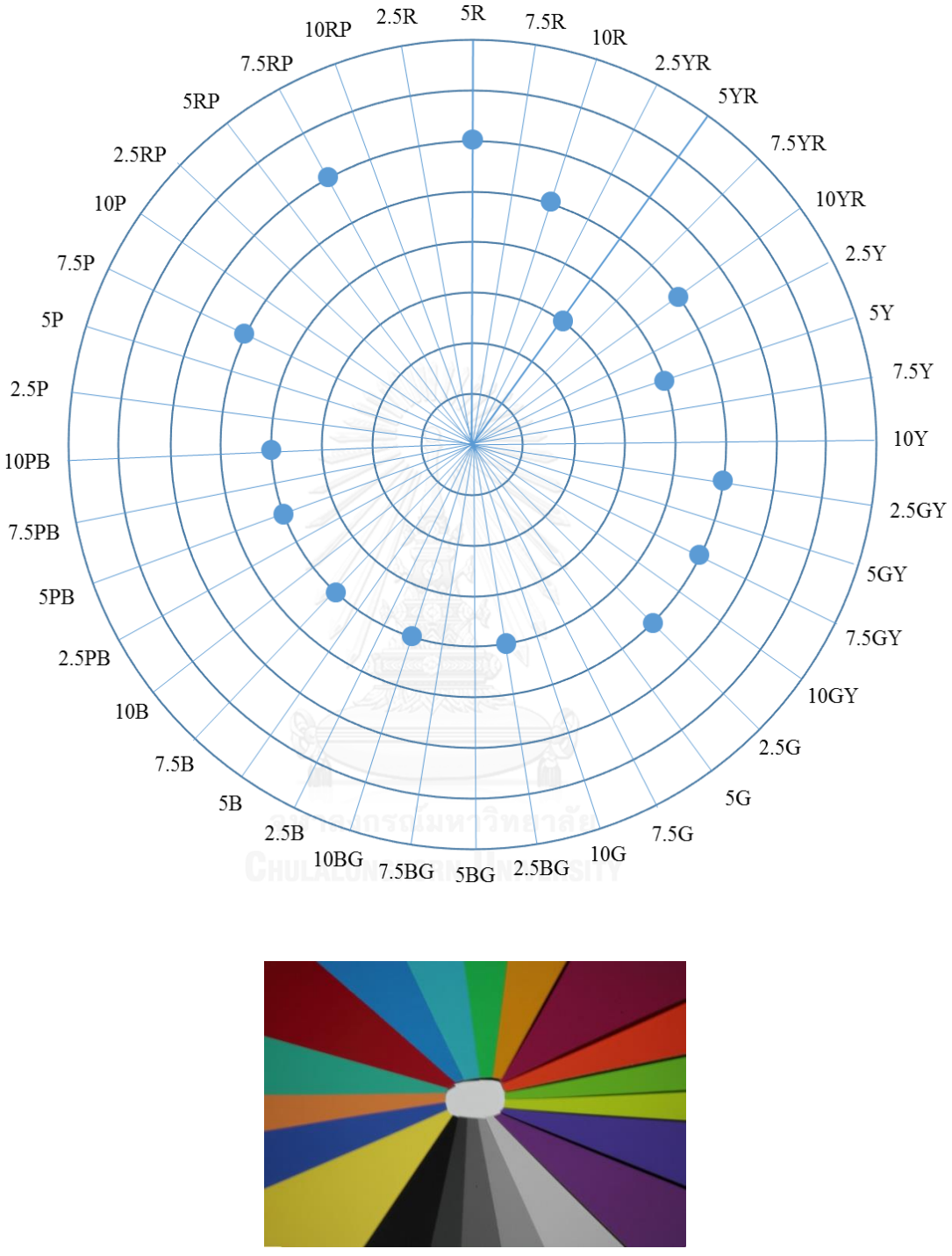

Figure 6.5 Hue-Chroma chart of the colours used in scene 2.

In scene 2 the selected colours still cover well all regions of the colour space.

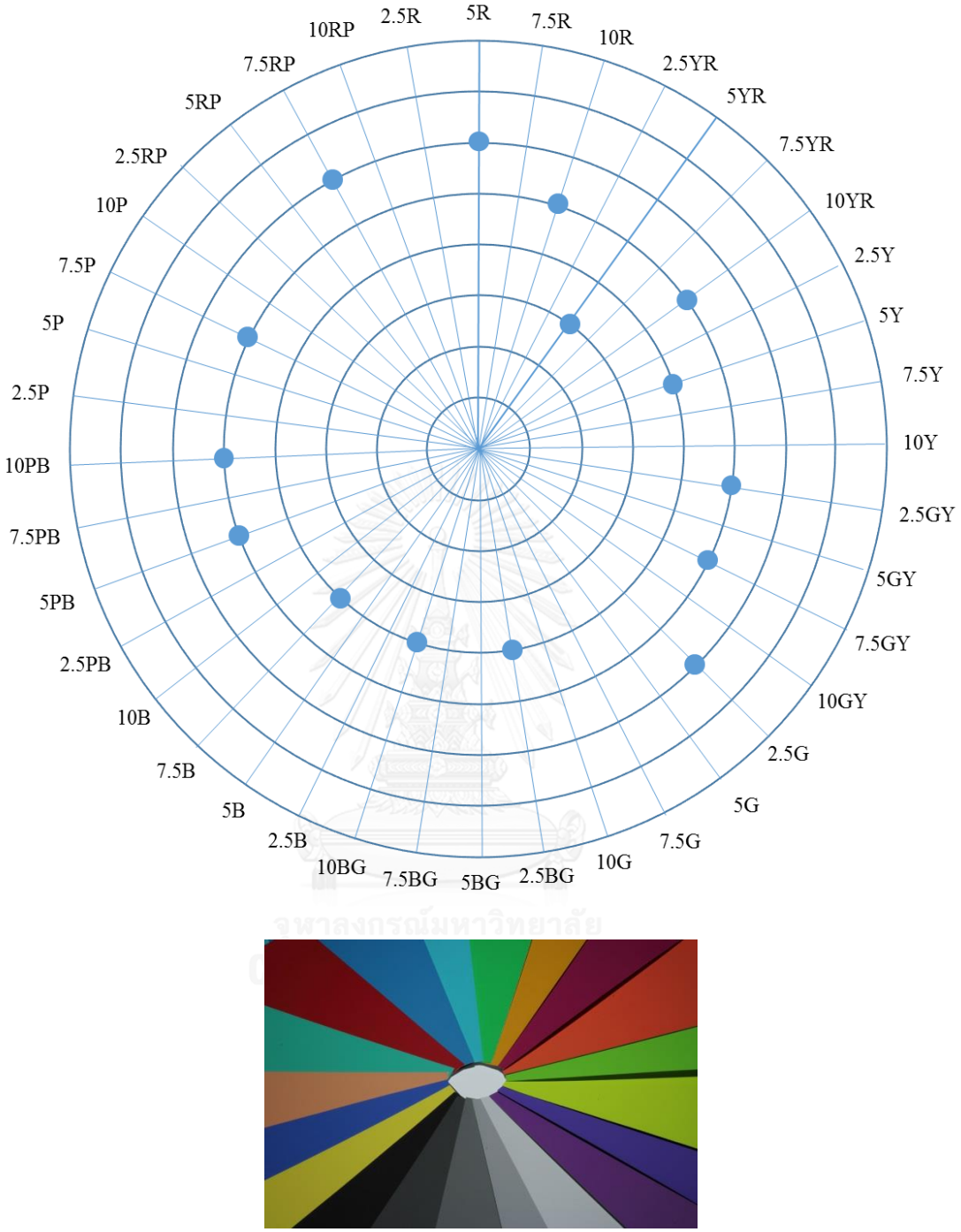

Figure 6.6 Hue-Chroma chart of the colours used in scene 3.

In scene 3, the average colour difference between calculated and measured CIELAB values of the selected colours drops significantly and the colours cover the green, bluish-green and blue regions of the colour space but the chroma values in those regions are quite low.

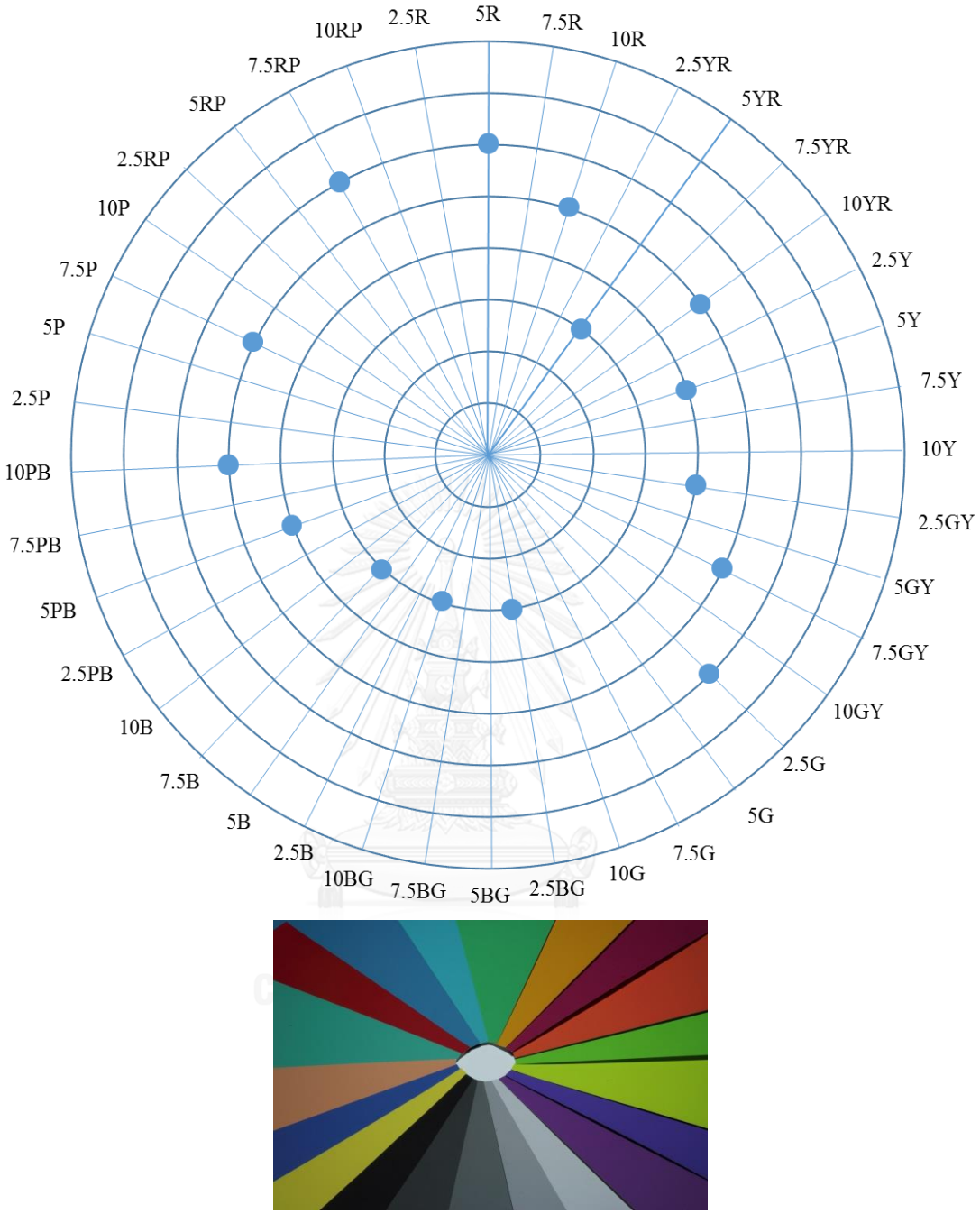

Figure 6.7 Hue-Chroma chart of the colours used in scene 4.

In scene 4, the average colour difference between calculated and measured CIELAB values of the colour-wheel's colours continues to drop but the colours that cover the green, bluish-green and blue regions of the colour space have the chroma values too low for being representative in an LED light quality assessment.

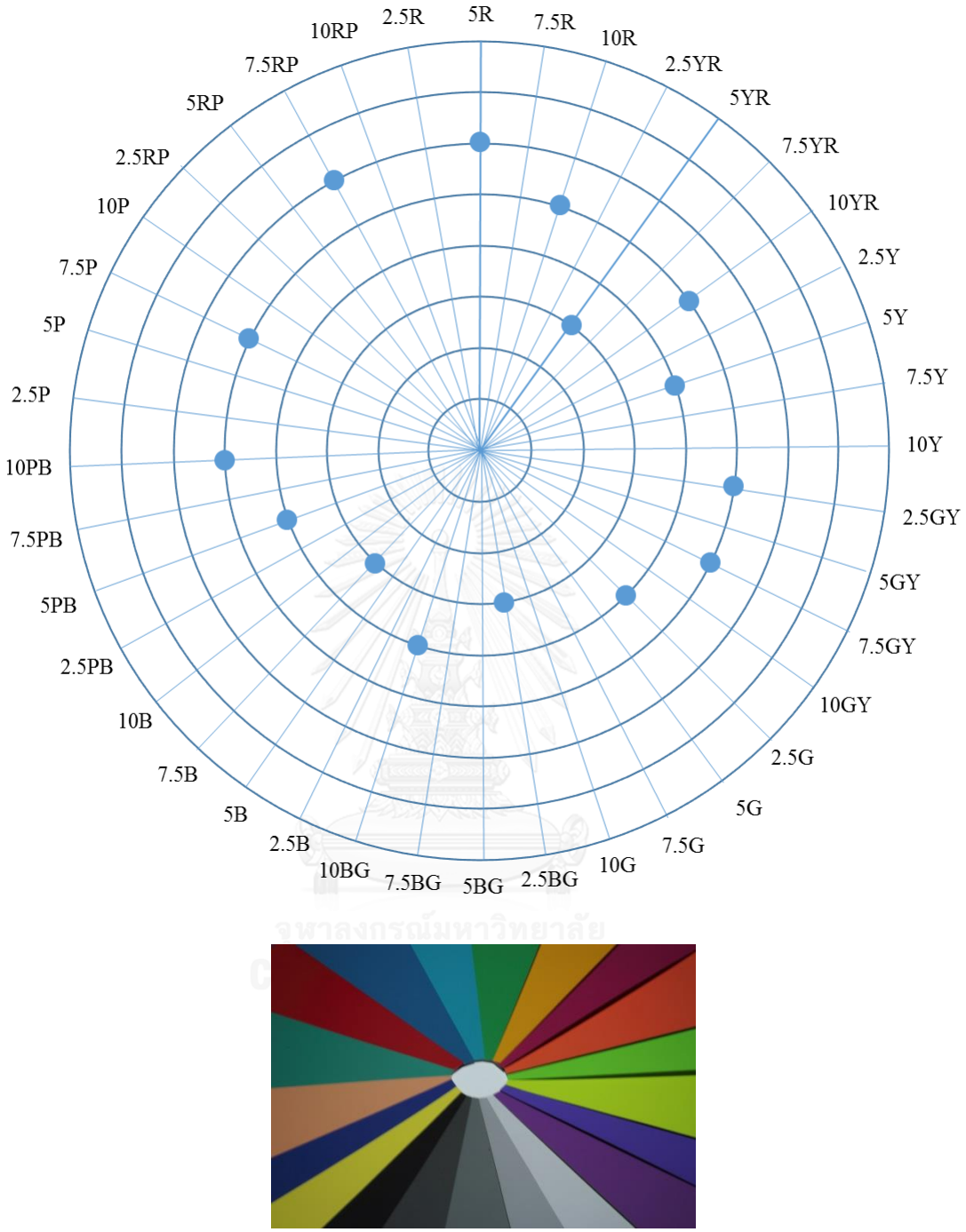

Figure 6.8 Hue-Chroma chart of the colours used in scene 5.

In scene 5, the chroma of the replacing colours for the green, bluish-green and blue regions of the colour space has been increased but this resulted in an incease of the average colour difference between calculated and measured CIELAB values of the colour-wheel's colours. Therefore, in the next scene, the colours of this region have been totally ignored in the replacement process, in order to observe the effect on the

colour difference evolution of the average colour differences between calculated and measured CIELAB.

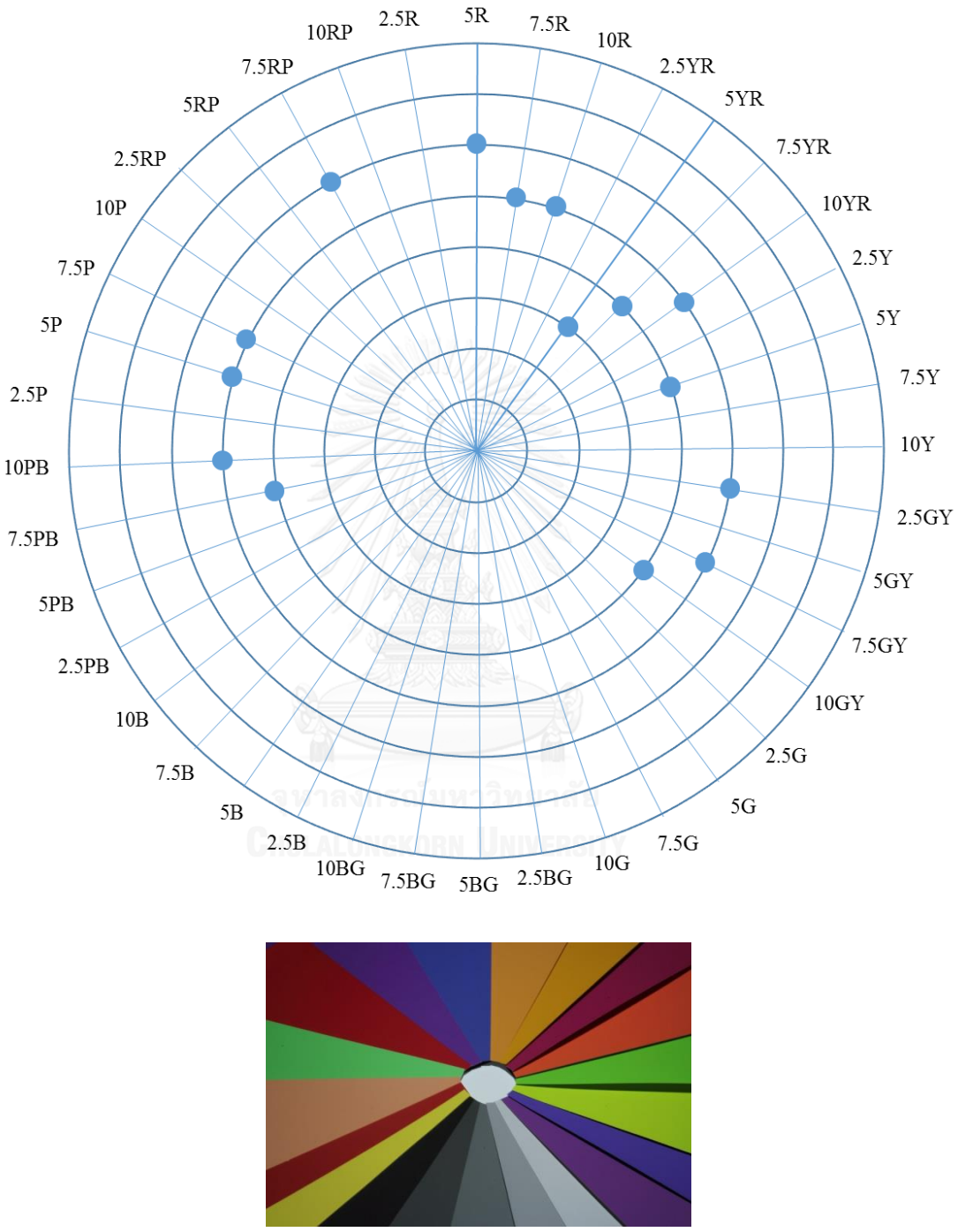

Figure 6.9 Hue-Chroma chart of the colours used in scene 6.

In scene 6, there are no colours in the green, bluish-green and blue regions of the colour space. As can be seen in the Hue-Chroma chart in Figure 6.9, the lower

part of the chart is empty. This selection leads to an average colour difference between calculated and measured CIELAB values of the colour-wheel's colours that is slightly over 3 ΔE_{00} units, with no individual colour differences over the imposed threshold of 6 units. However, this colour-wheel cannot be used in light quality assessments because its colours do not cover all hue angles. But it fulfills the requirement of producing the desired colourimetric output within imposed error margins. For this reason, this colour wheel was used as the base for adding colours that fill up the green, bluish-green and blue empty regions, while controlling the colourimetric output and while using colours with decent chroma values for the LED light assessment requirement.

6.2.2. Results obtained in the process of adding colours to the wheel.

The detailed steps of the methodology described in 4.4 emerged during a trial-error experimentation of the generally outlined method presented in chapter 4. Removing all colours in the green, bluish-green and blue regions for testing the effects on the average colour difference drop between calculated and measured CIELAB data is part of the trial-error experimentation, not part of the final established methodology itself. This removal determined the need of a minimum coverage of the mentioned regions with 4 colours in one step (2.5BG7/4, 2.5G6/4, 5RP4/12, 10B6/4) and subsequent corrections that will be discussed further. Figure 6.10 shows the Hue-Chroma chart of the colours in the colour-wheel used for scene 7.

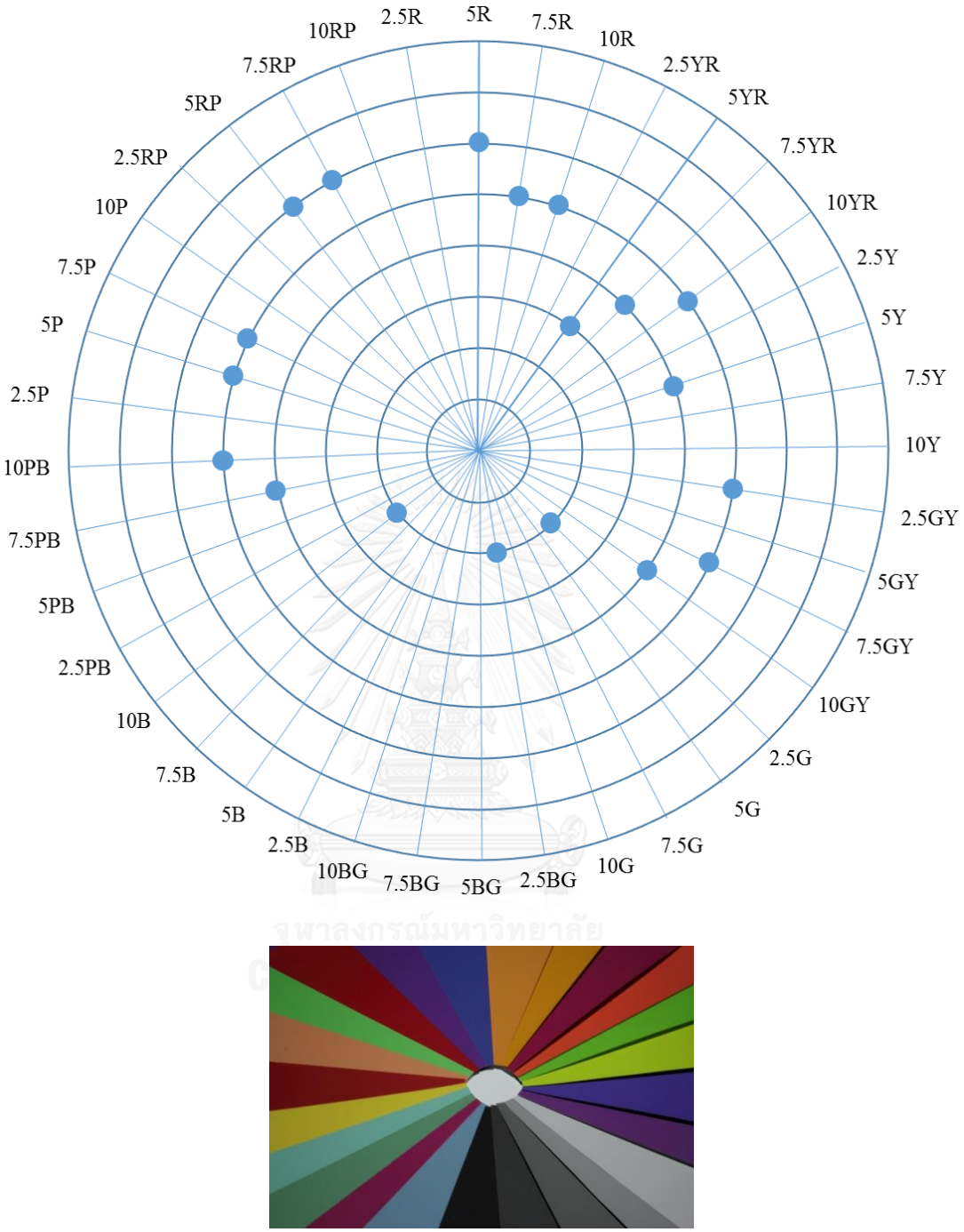

Figure 6.10 Hue-Chroma chart of the colours used in scene 7.

The best fit functions determined for the colour corrections in this scene are shown in Figures 6.11 to 6.13 and the calculation sheet is presented in Table 6.4.

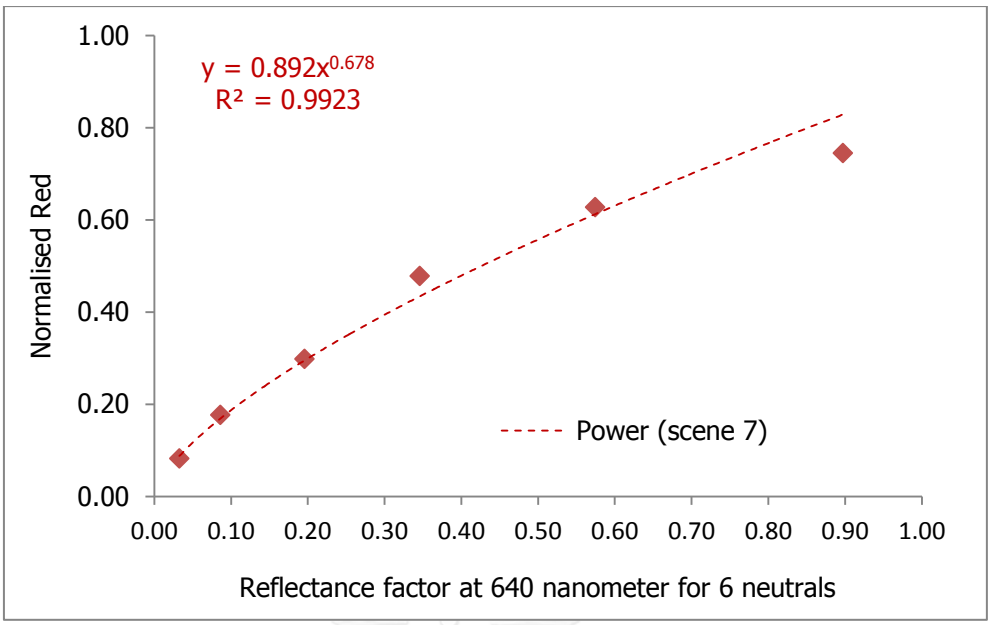

Figure 6.11 Best fit power function for the red channel correction in scene 7.

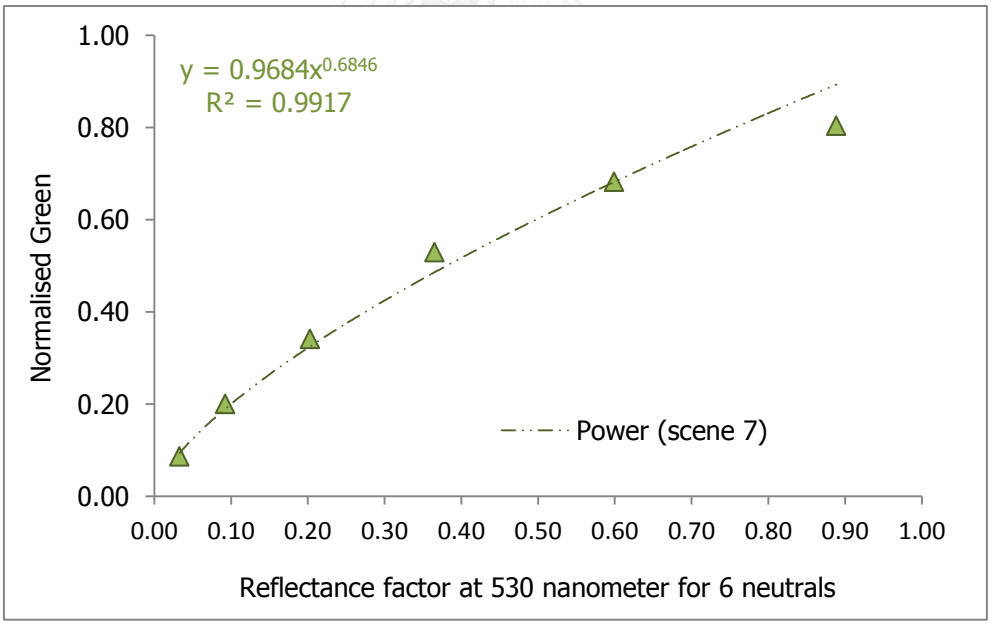

Figure 6.12 Best fit power function for the green channel correction in scene 7.

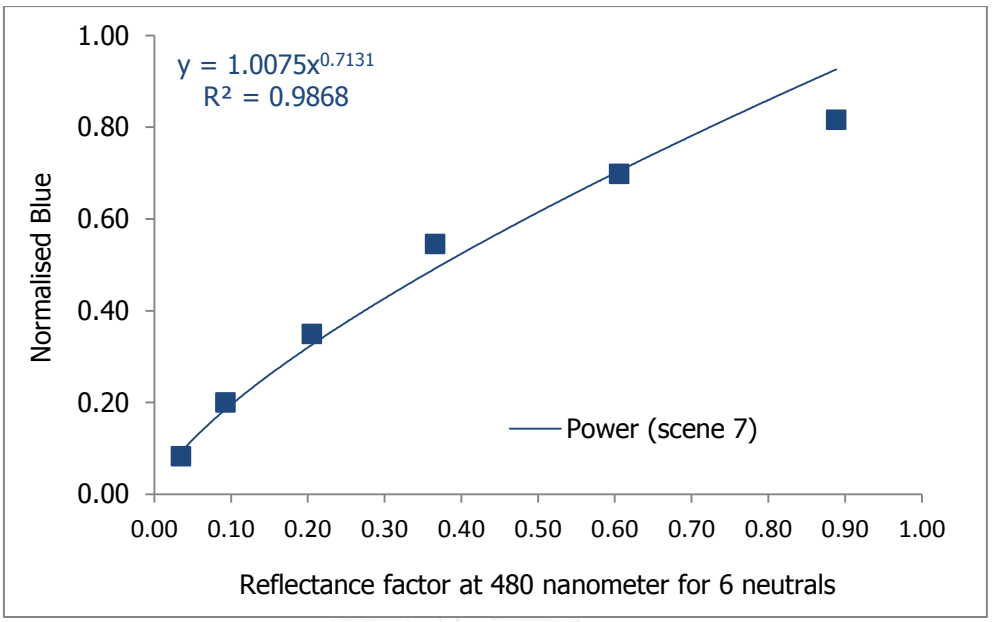

Figure 6.13 Best fit power function for the blue channel correction in scene 7.

Table 6.4 Calculated CIELAB from Canon EOS X4's digital image scene 7 under Fluorescent D65 and ΔE_{00} toward measured CIELAB, D65/2°.

Munsell Patches	Measured Spectrophotometer			R	G	B	Calculated CIELAB of scene 7			ΔE_{00}
	L*	a*	b*				L*	a*	b*	
N2	21.15	-0.15	-0.82	21	22	21	19.80	0.35	-0.27	1.32
N3.5	36.28	-0.45	-0.90	45	51	51	37.54	-1.06	-1.42	1.45
N5	52.15	-0.43	-0.62	76	87	89	53.42	-1.52	-1.92	2.29
N6.5	66.68	-0.93	-0.63	122	135	139	70.26	-0.66	-1.20	2.90
N8	81.55	-0.85	-0.97	160	174	178	81.75	-0.25	0.04	1.31
N9.5	95.71	-0.59	1.54	190	205	208	89.93	-0.17	1.23	3.59
7.5 P 4/10	42.23	34.78	-23.65	89	45	117	43.75	36.34	-31.35	3.87
10 PB 4/10	41.59	23.16	-37.00	67	54	144	44.89	28.31	-42.67	3.82
2.5 GY 8/10	81.54	-22.10	70.22	149	191	30	82.32	-26.84	68.80	2.57
7.5 GY 7/10	71.18	-39.34	53.30	83	174	42	74.99	-43.67	53.39	3.28
10 R 6/10	61.56	37.79	38.58	184	68	38	58.90	41.72	39.68	2.84
7.5 RP 4/12	41.90	53.46	1.07	115	21	57	38.90	51.79	-2.65	3.26
10 YR 7/10	72.17	14.04	61.92	171	123	16	69.43	7.59	65.27	4.93
7.5YR7/8	71.70	16.85	45.85	174	119	40	69.09	12.30	49.75	4.39
7.5PB4/8	41.17	11.07	-33.45	48	59	133	44.00	15.98	-39.10	3.30
5P4/10	40.38	32.56	-28.57	77	40	119	40.83	36.68	-37.08	3.59
5 R 4/12	41.59	52.54	27.90	122	19	25	38.63	51.59	24.16	3.18
10GY7/8	71.45	-38.29	32.69	84	178	95	76.68	-37.31	27.68	4.37
5 YR 7/6	71.12	17.00	30.11	173	125	89	71.06	13.99	24.16	2.79
7.5 R 4/10	41.55	43.60	30.73	129	30	28	42.49	46.83	26.34	3.45
5 Y 8/8	81.48	-2.98	57.75	173	177	49	81.22	-11.98	58.01	5.57
2.5BG7/4	72.45	-21.21	1.02	101	160	144	74.54	-17.35	2.73	3.16
2.5G6/4	62.00	-22.12	10.71	77	126	95	64.04	-19.59	10.21	2.23
5RP4/12	42.30	52.65	-7.02	114	26	68	40.35	49.60	-8.13	2.08
10B6/4	62.07	-7.16	-14.64	88	122	143	64.91	-5.08	-11.14	3.61

Two of the colours removed from scene 5, that were not having very high colour differences between calculated and measured CIELAB values were reintroduced at much lower saturation, due to the observation that the digital camera has a better response toward low saturated colours. These colours are 2.5BG7/4 for the blue-green region and 2.5G6/4 for the green region. A new colour was introduced in the wheel to represent the blue region: 10B6/4 and a highly saturated colour was added to increase the average saturation of the colour-wheel. However, for assessing LED light, more saturated colours are needed in the green, bluish-green and blue regions too. However a lightness decrease and a chroma increase in these regions, while keeping the rest of the wheel unmodified, would negatively affect the colour differences between calculated and measured CIELAB values, as proven through the selection process performed from scene 1 to 6. Therefore, the saturation increase of the colours in these regions had to be done in parallel with modifications in lightness and chroma for the already selected colours and in rare cases with a hue modification but without a shift to another region of the colour space. In scene 7, the average colour difference between calculated and measured CIELAB values for the entire wheel had a slight drop compared to scene 6. In scene 6 there is a large empty region in the Hue-Chroma chart. The colour difference had a quite significant drop in scene 6 compared with scene 5 where all regions of the colour space were covered.

In scene 8, the colour with the Munsell notation 10BG5/4 was added to fill the gap in the lower left part of the Hue-Chroma chart, as can be seen in Figure 6.14, comparative with Figure 6.10. The saturation of the 10YR colour was decreased from 7/10 to 7/6 and the saturation of 5Y was decreased from 8/8 to 8.5/6. Only one colour hue was changed, 10B6/4 to 7.5B5/4. These modifications raised the average colour difference between calculated and measured CIELAB values of the colours in the wheel, as was expected to happen by adding new colours.

The best fit functions determined for the colour corrections on each channel (red, green and blue) in this scene are shown in Figures 6.15 to 6.17 and the results of calculations are presented in Table 6.5.

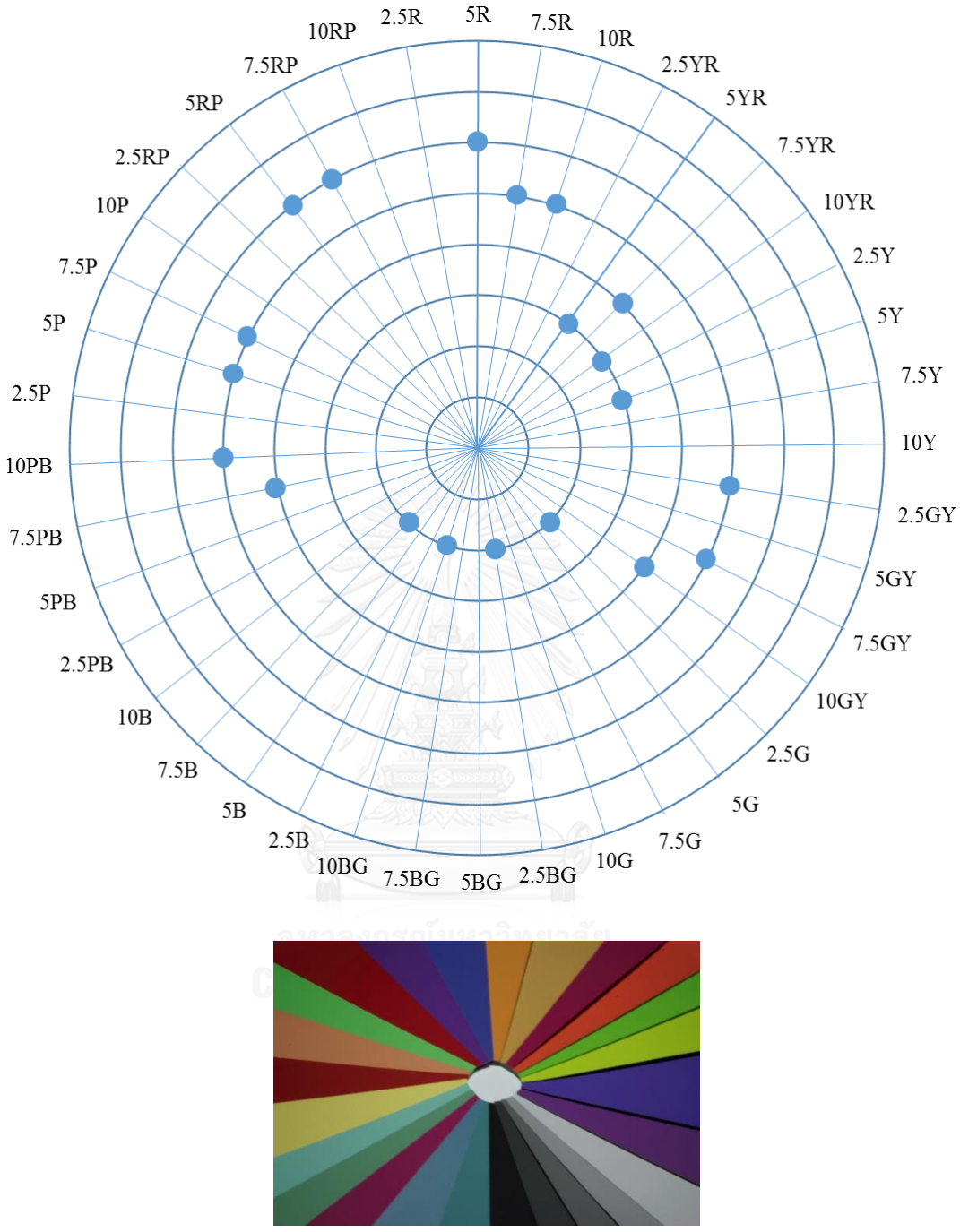

Figure 6.14 Hue-Chroma chart of the colours used in scene 8.

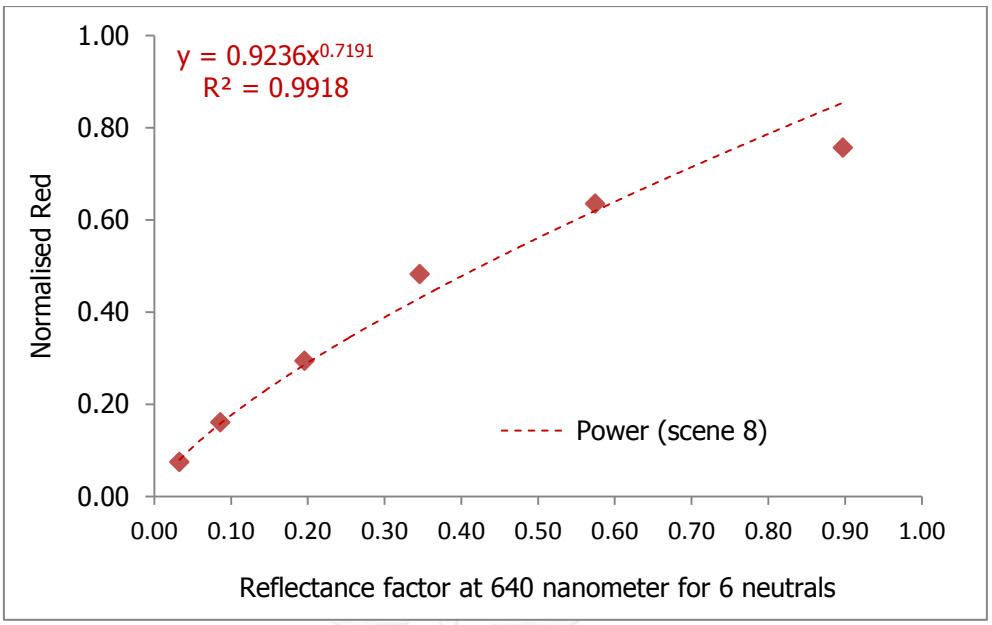

Figure 6.15 Best fit power function for the red channel correction in scene 8.

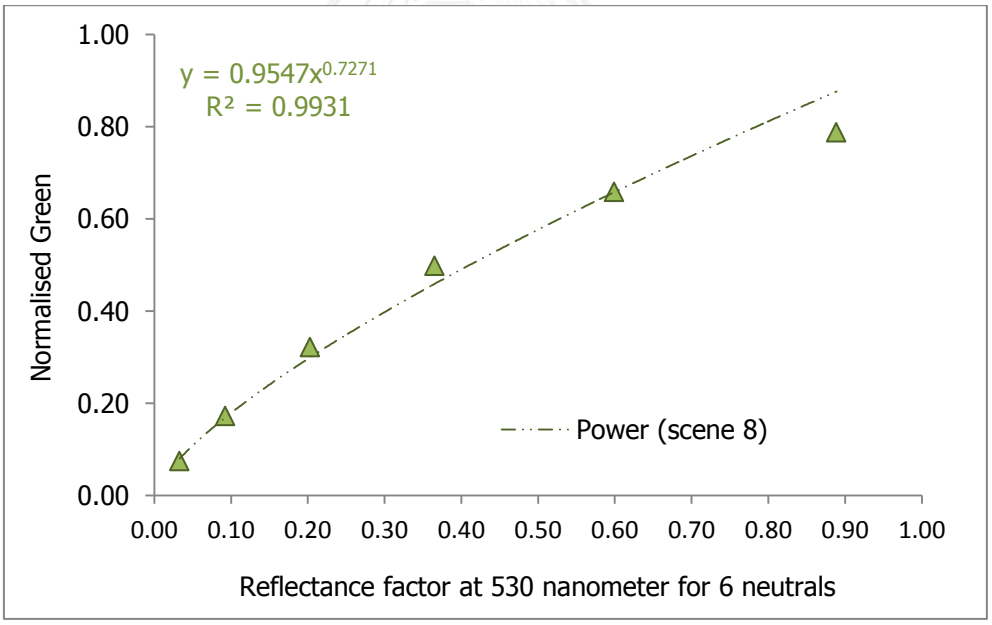

Figure 6.16 Best fit power function for the green channel correction in scene 8.

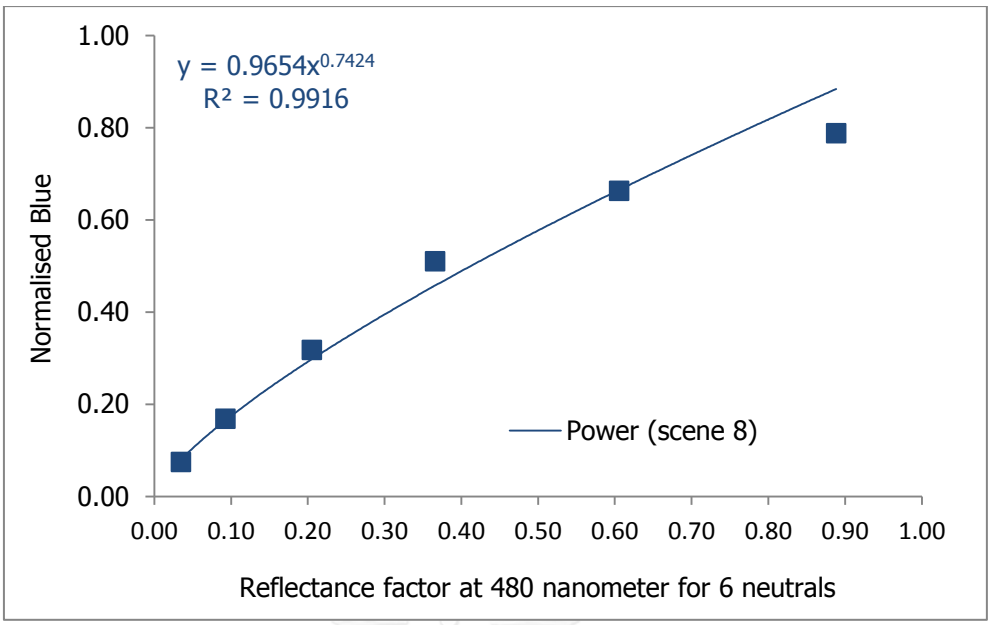

Figure 6.17 Best fit power function for the blue channel correction in scene 8.

Table 6.5 Calculated CIELAB from Canon's digital image scene 8 under Fluorescent D65 and ΔE_{00} toward measured CIELAB, D65/2°.

Munsell Patches	Measured Spectrophotometer			R	G	B	Calculated CIELAB of scene 8			ΔE_{00}
	L*	a*	b*				L*	a*	b*	
N2	21.15	-0.15	-0.82	19	19	19	20.10	0.45	-0.94	1.16
N3.5	36.28	-0.45	-0.90	41	44	43	36.66	-1.25	-0.52	1.24
N5	52.15	-0.43	-0.62	75	82	81	53.98	-2.05	-0.71	2.86
N6.5	66.68	-0.93	-0.63	123	127	130	70.10	0.32	-1.49	3.35
N8	81.55	-0.85	-0.97	162	168	169	81.79	-0.23	-0.29	1.12
N9.5	95.71	-0.59	1.54	193	201	201	90.11	-0.59	0.29	3.62
7.5 P 4/10	42.23	34.78	-23.65	85	40	106	43.41	35.15	-30.56	3.61
10 PB 4/10	41.59	23.16	-37.00	63	48	132	44.48	27.60	-42.05	3.35
2.5 GY 8/10	81.54	-22.10	70.22	151	185	28	82.31	-26.39	67.85	2.53
7.5 GY 7/10	71.18	-39.34	53.30	88	166	36	74.94	-40.70	54.28	2.85
10 R 6/10	61.56	37.79	38.58	182	63	35	58.53	39.50	38.04	2.87
7.5 RP 4/12	41.90	53.46	1.07	118	20	57	40.30	51.90	-4.75	3.20
10 YR 7/6	71.91	7.46	37.72	165	133	59	72.99	1.28	39.29	4.84
7.5YR7/8	71.70	16.85	45.85	176	114	38	69.43	11.24	48.42	4.63
7.5PB4/8	41.17	11.07	-33.45	47	54	122	44.34	15.46	-37.56	3.42
5P4/10	40.38	32.56	-28.57	75	36	110	41.09	36.05	-36.40	3.39
5 R 4/12	41.59	52.54	27.90	126	15	25	39.22	53.74	21.58	4.12
10GY7/8	71.45	-38.29	32.69	87	171	83	76.67	-36.02	29.94	4.02
5 YR 7/6	71.12	17.00	30.11	174	119	80	71.05	12.74	25.01	2.93
7.5R4/10	41.55	43.60	30.73	124	26	24	41.73	45.24	25.72	3.19
5Y8.5/6	86.09	-3.33	42.52	185	183	94	84.72	-8.68	36.12	4.94
2.5BG7/4	72.45	-21.21	1.02	103	163	148	77.01	-17.83	0.73	3.93
2.5G6/4	62.00	-22.12	10.71	79	130	99	67.23	-20.59	8.74	4.53
5RP4/12	42.30	52.65	-7.02	118	20	57	40.30	51.90	-4.75	2.09
7.5B5/4	51.98	-10.11	-14.95	61	103	123	59.88	-9.51	-13.92	7.41
10BG5/4	52.78	-17.91	-9.03	50	105	110	59.34	-17.15	-8.52	6.13

In scene 9 the colour wheel was filled with another colour of medium saturation in the purple-blue region, 5PB4/6. The lightness and chroma of 5 existing colours were modified, testing the effects of a slight saturation increase in the blue region, without changing the hue of any colour from the previous scene. The Hue-Chroma chart of the colours is presented in Figure 6.18, the best fit functions used for colour corrections in this scene are shown in Figures 6.19 to 6.21 and the results are listed in Table 6.6.

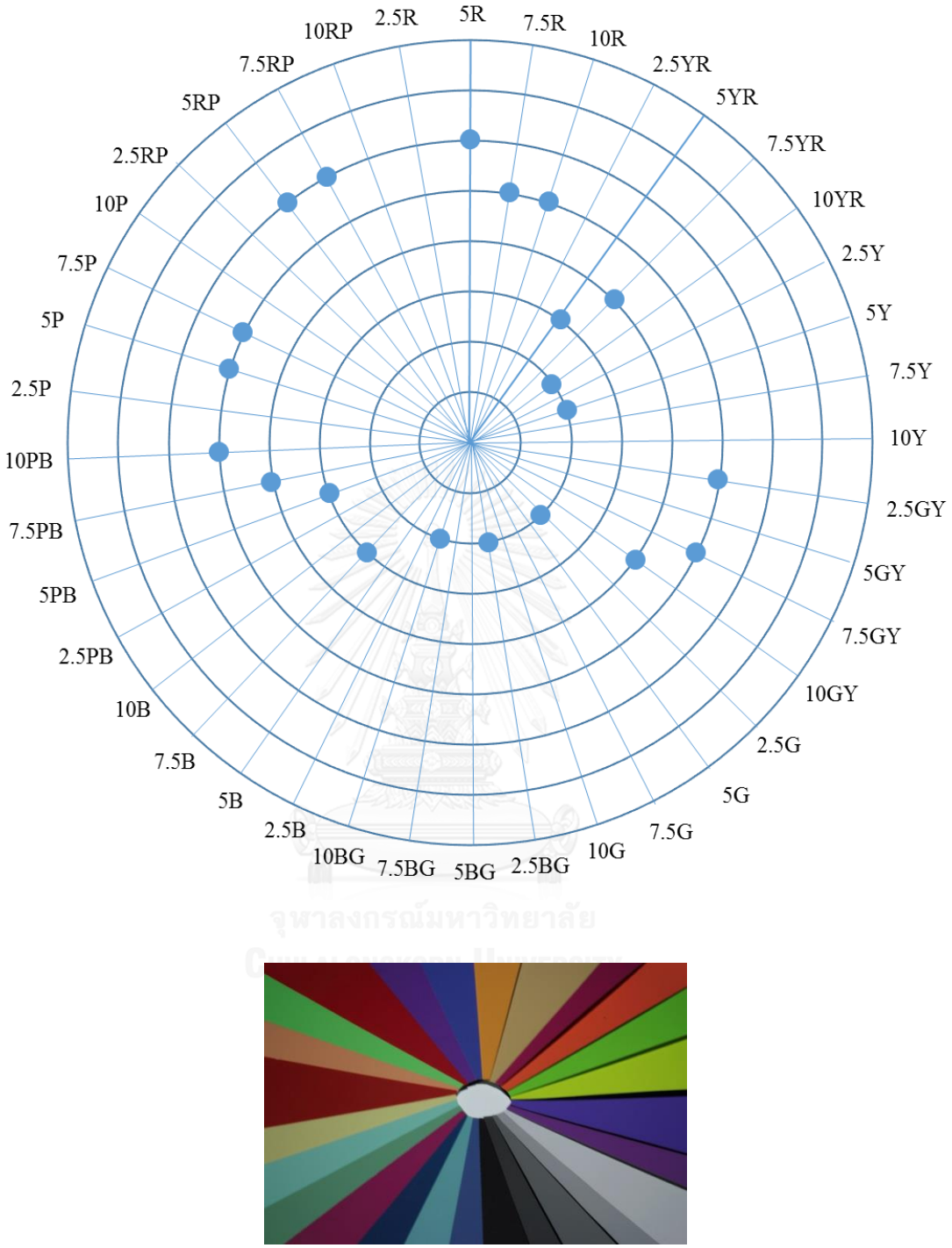

Figure 6.18 Hue-Chroma chart of the colours used in scene 9.

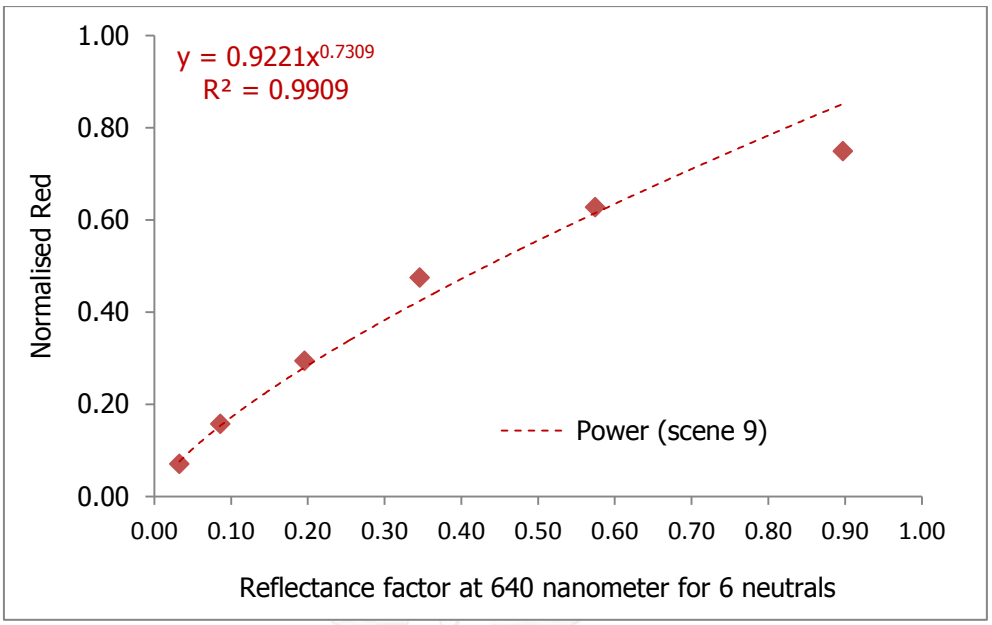

Figure 6.19 Best fit power function for the red channel correction in scene 9.

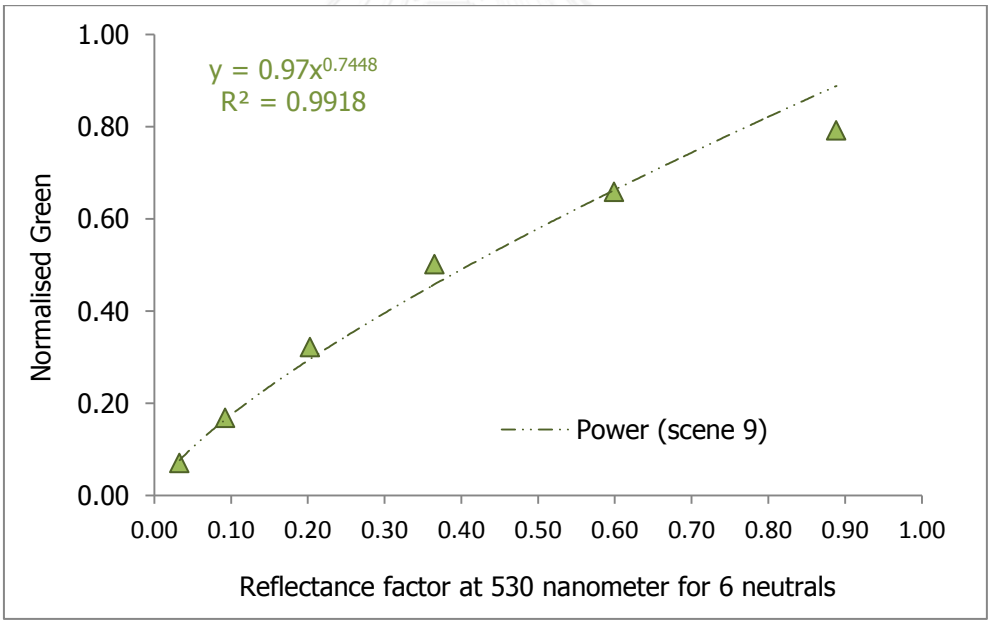

Figure 6.20 Best fit power function for the green channel correction in scene 9.

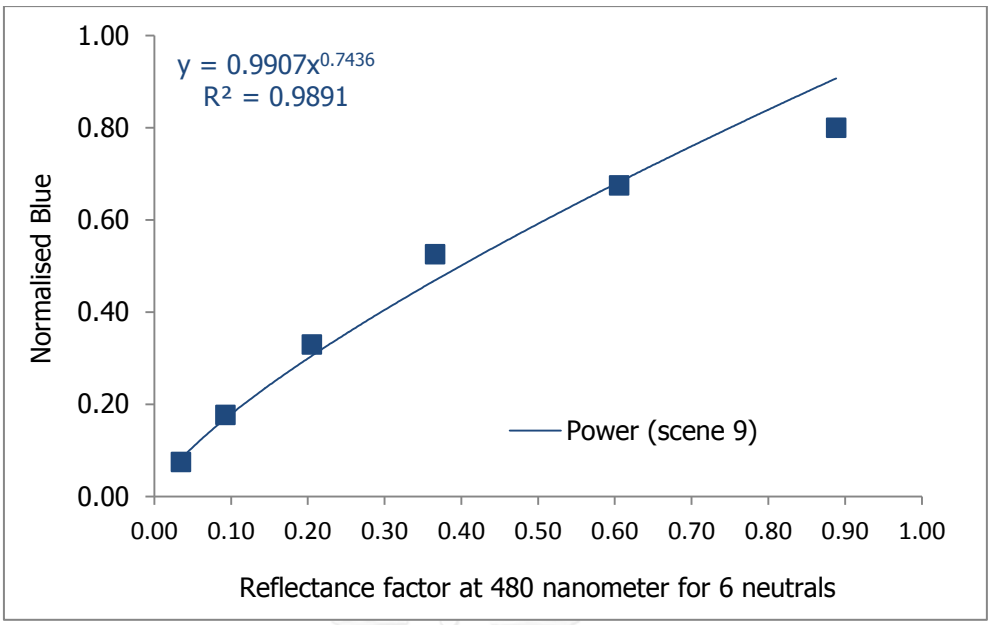

Figure 6.21 Best fit power function for the blue channel correction in scene 9.

Table 6.6 Calculated CIELAB from Canon EOS X4's digital image scene 9 under Fluorescent D65 and ΔE_{00} toward measured CIELAB, D65/2°.

Munsell Patches	Measured Spectrophotometer			R	G	B	Calculated CIELAB of scene 9			ΔE_{00}
	L*	a*	b*				L*	a*	b*	
N2	21.15	-0.15	-0.82	18	18	19	19.94	0.28	-0.64	1.07
N3.5	36.28	-0.45	-0.90	40	43	45	36.78	-0.94	-1.15	0.84
N5	52.15	-0.43	-0.62	75	82	84	54.38	-1.74	-0.69	2.83
N6.5	66.68	-0.93	-0.63	121	128	134	70.29	-0.16	-1.52	3.17
N8	81.55	-0.85	-0.97	160	168	172	81.51	-0.15	-0.21	1.24
N9.5	95.71	-0.59	1.54	191	202	204	89.81	-0.66	0.59	3.72
7.5 P 4/10	42.23	34.78	-23.65	84	40	110	43.87	34.72	-30.54	3.84
10 PB 4/10	41.59	23.16	-37.00	64	48	136	45.12	27.65	-41.33	3.79
2.5 GY 8/10	81.54	-22.10	70.22	149	184	29	81.76	-25.68	67.08	2.30
7.5 GY 7/10	71.18	-39.34	53.30	85	167	39	74.87	-40.92	52.88	2.84
10 R 6/10	61.56	37.79	38.58	183	65	38	59.47	38.54	37.57	2.00
7.5 RP 4/12	41.90	53.46	1.07	117	21	58	40.87	50.61	-3.65	2.64
10 YR 7/4	71.62	4.82	27.72	151	131	83	72.01	0.79	25.47	3.61
7.5YR7/8	71.70	16.85	45.85	175	115	40	69.73	10.79	48.03	4.76
7.5PB4/8	41.17	11.07	-33.45	46	55	125	45.05	13.98	-36.40	3.77
5P4/10	40.38	32.56	-28.57	75	37	114	42.00	35.07	-35.60	3.40
5 R 4/12	41.59	52.54	27.90	125	16	25	39.73	52.57	22.82	3.15
10GY7/8	71.45	-38.29	32.69	86	171	88	76.48	-34.98	28.22	4.15
5 YR 7/6	71.12	17.00	30.11	173	119	84	71.14	12.94	24.04	3.11
7.5R4/10	41.55	43.60	30.73	123	24	24	41.51	46.08	26.01	3.28
5Y8/4	81.15	-3.75	30.09	166	171	113	81.41	-6.99	23.90	4.34
2.5BG7/4	72.45	-21.21	1.02	101	165	153	77.21	-18.13	0.52	3.96
2.5G6/4	62.00	-22.12	10.71	78	131	103	67.51	-20.51	8.38	4.80
5RP4/12	42.30	52.65	-7.02	113	27	73	42.48	47.10	-11.37	2.90
7.5B3/6	30.93	-10.32	-26.11	18	44	82	36.48	-0.68	-27.17	8.66
10BG6/4	61.69	-17.41	-8.03	73	134	140	68.71	-16.65	-6.78	5.84
5PB4/6	41.32	0.79	-25.69	43	64	111	47.11	3.05	-26.31	5.71

The increase in saturation in the blue region, for 7.5B from 5/4 to 3/6 produced a slight deterioration of the average colorimetric response, with an individual colour difference of 8.66 ΔE_{00} units between calculated and measured CIELAB values for this specific colour. Therefore, in scene 10, the saturation of this colour was lowered to 4/4, so that overall change between scenes 7 to 10 for this colour was 5/4 to 4/4. In the same time, the saturation of 10BG was lowered from 6/4 to 6/2 and the saturation of 5PB was lowered from 4/6 to 4/4, because these 2 colours presented the highest colour differences between calculated and measured CIELAB values. Scene 10 had a corrective purpose, no colours were added. The Hue-Chroma chart, the best fit functions for colour corrections and the table of results are shown next.

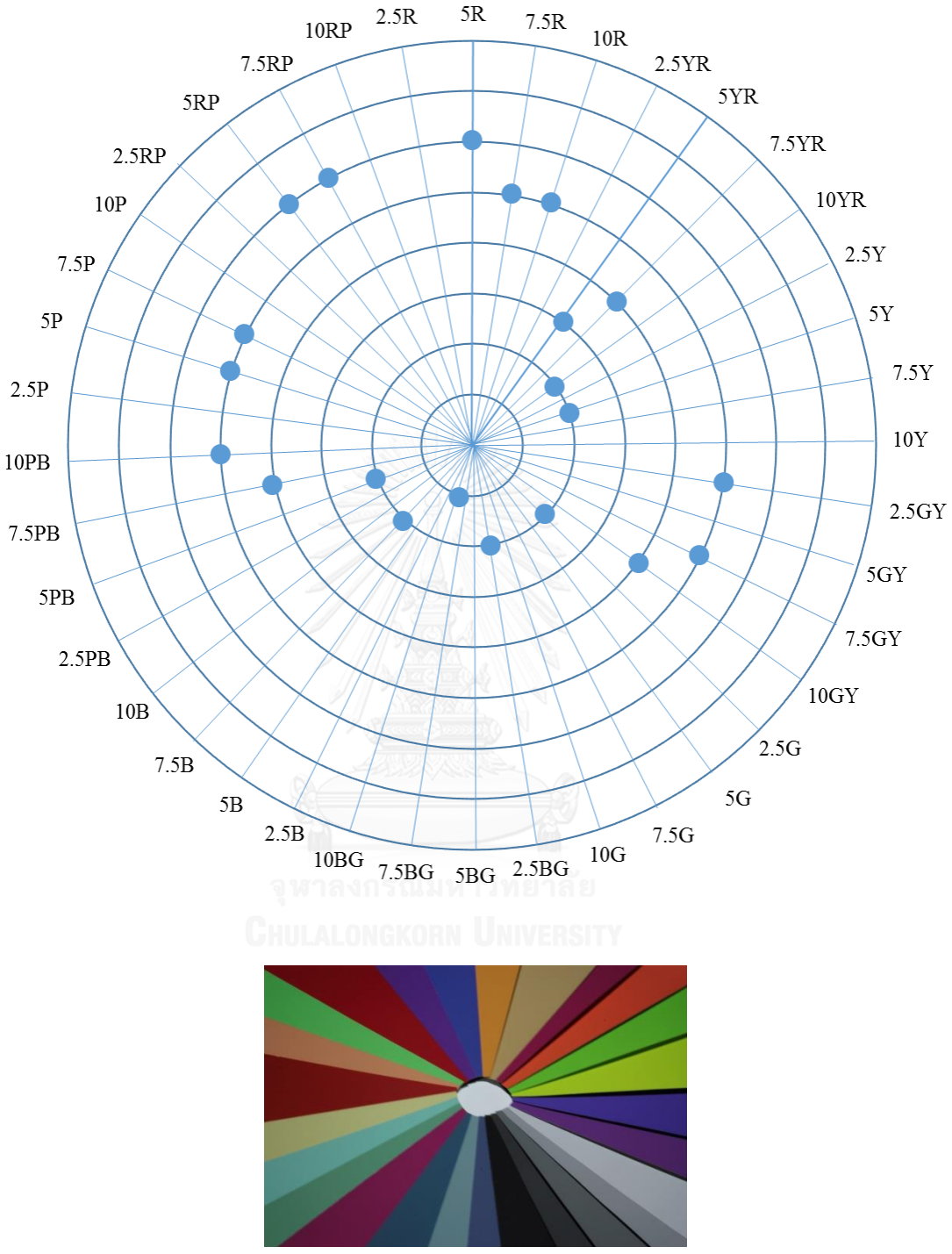

Figure 6.22 Hue-Chroma chart of the colours used in scene 10.

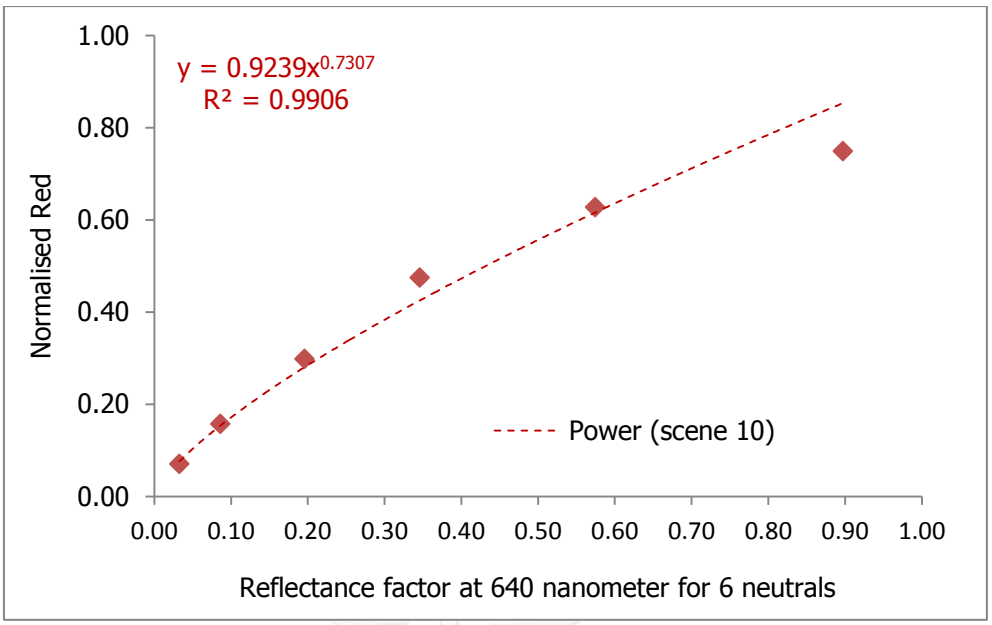

Figure 6.23 Best fit power function for the red channel correction in scene 10.

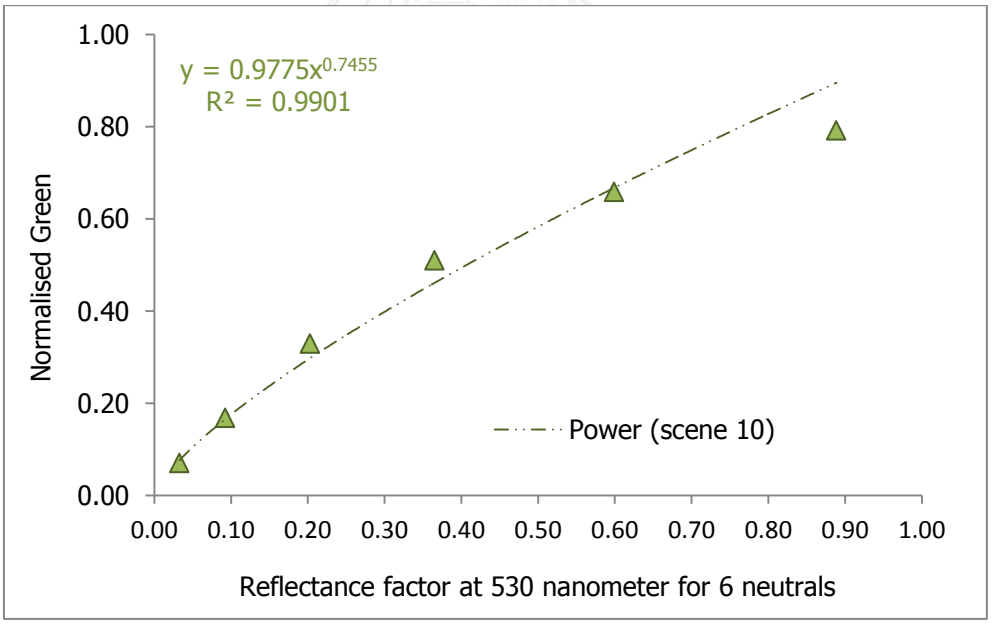

Figure 6.24 Best fit power function for the green channel correction in scene 10.

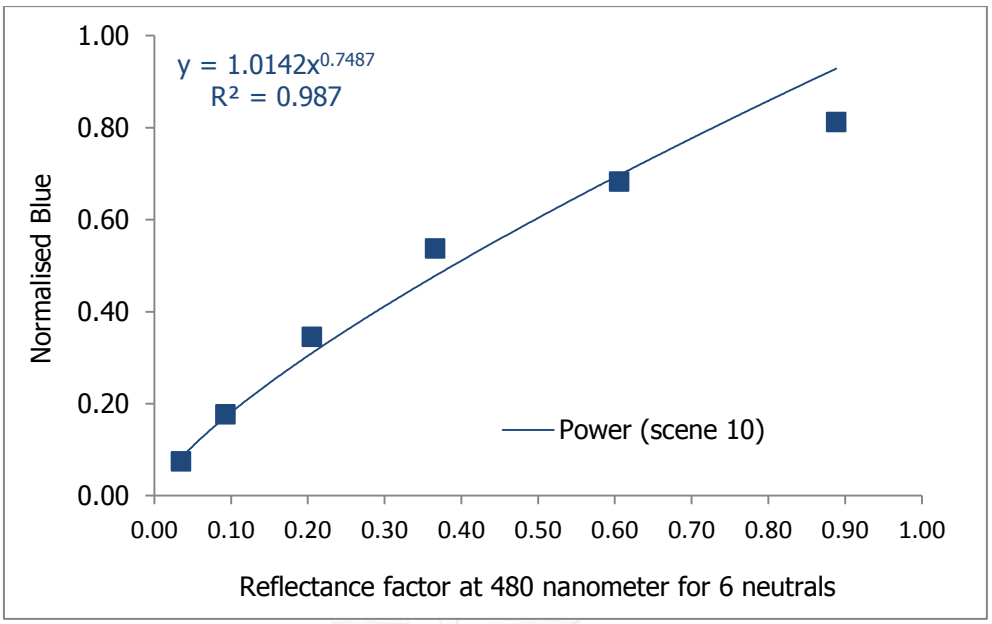

Figure 6.25 Best fit power function for the blue channel correction in scene 10

Table 6.7 Calculated CIELAB from Canon EOS X4's digital image scene 10 under Fluorescent D65 and ΔE_{00} toward measured CIELAB, D65/2°.

Munsell Patches	Measured Spectrophotometer			R	G	B	Calculated CIELAB of scene 10			ΔE_{00}
	L*	a*	b*				L*	a*	b*	
N2	21.15	-0.15	-0.82	18	18	19	19.86	0.31	-0.62	1.15
N3.5	36.28	-0.45	-0.90	40	43	45	36.64	-0.93	-0.94	0.75
N5	52.15	-0.43	-0.62	76	84	88	54.92	-1.71	-1.33	3.28
N6.5	66.68	-0.93	-0.63	121	130	137	70.52	-0.66	-1.37	3.13
N8	81.55	-0.85	-0.97	160	168	174	81.23	0.02	-0.02	1.58
N9.5	95.71	-0.59	1.54	191	202	207	89.51	-0.41	0.66	3.89
7.5 P 4/10	42.23	34.78	-23.65	85	41	113	44.24	34.58	-30.47	3.99
10 PB 4/10	41.59	23.16	-37.00	64	49	140	45.38	27.37	-41.53	3.98
2.5 GY 8/10	81.54	-22.10	70.22	149	186	31	81.88	-25.83	66.22	2.57
7.5 GY 7/10	71.18	-39.34	53.30	85	169	42	75.06	-40.91	51.58	3.07
10 R 6/10	61.56	37.79	38.58	183	67	39	59.80	37.60	37.51	1.61
7.5 RP 4/12	41.90	53.46	1.07	118	23	60	41.53	49.58	-3.50	2.57
10 YR 7/4	71.62	4.82	27.72	151	132	86	72.03	0.86	24.63	3.66
7.5YR7/8	71.70	16.85	45.85	175	117	42	69.98	10.27	47.31	4.91
7.5PB4/8	41.17	11.07	-33.45	47	56	130	45.45	14.45	-36.99	4.19
5P4/10	40.38	32.56	-28.57	76	38	117	42.39	34.89	-35.44	3.52
5 R 4/12	41.59	52.54	27.90	128	17	26	40.43	52.73	22.99	2.82
10GY7/8	71.45	-38.29	32.69	87	173	92	76.72	-34.58	27.31	4.47
5 YR 7/6	71.12	17.00	30.11	174	121	87	71.45	12.79	23.63	3.30
7.5R4/10	41.55	43.60	30.73	125	26	26	42.33	45.41	25.29	3.54
5Y8/4	81.15	-3.75	30.09	167	172	118	81.44	-6.37	22.68	4.50
2.5BG7/4	72.45	-21.21	1.02	100	166	156	77.10	-18.42	0.38	3.82
2.5G6/4	62.00	-22.12	10.71	77	133	106	67.71	-21.13	8.08	4.98
5RP4/12	42.30	52.65	-7.02	115	28	75	42.99	47.09	-11.12	2.87
7.5B4/4	40.79	-9.85	-15.62	39	68	93	47.20	-5.96	-15.90	6.92
10BG6/2	61.56	-9.52	-4.24	91	123	131	66.84	-7.92	-4.44	4.66
5PB4/4	42.03	0.45	-18.02	49	64	100	47.04	2.37	-19.80	5.11

The saturation decrease for 7.5B improved the colour difference between its calculated and measured CIELAB values from 8.66 to 6.92 ΔE_{00} units, but the difference is still too big compared with the imposed limit. The hue of this colour was changed from 7.5B to 2.5 B in scene 12, after temporary removing it in scene 11 and replacing it with 10BG8/2 for testing the effect. Because all the other colours except for the 3 colours corrected in scene 10 have the difference between calculated and measured CIELAB values lower than 5 ΔE_{00} units, the saturation was further decreased for 10BG6/2 and 5PB4/4 to 7/2 and respectively 4/2. The Hue-Chroma chart for scene 11 is shown in Figure 6.26, the colour corrective functions are shown in Figures 6.27 to 6.29 and the results are listed in Table 6.8.

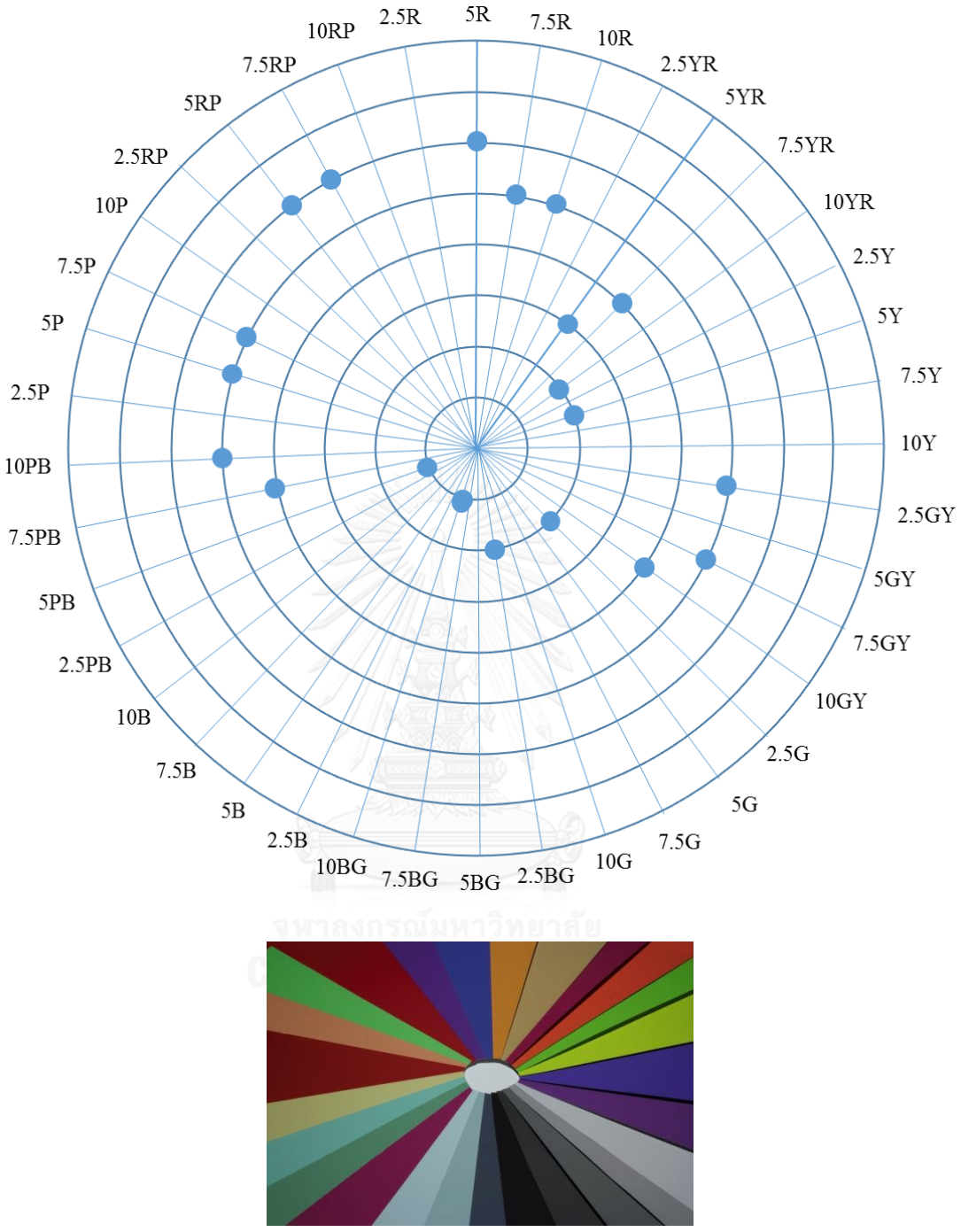

Figure 6.26 Hue-Chroma chart of the colours used in scene 11.

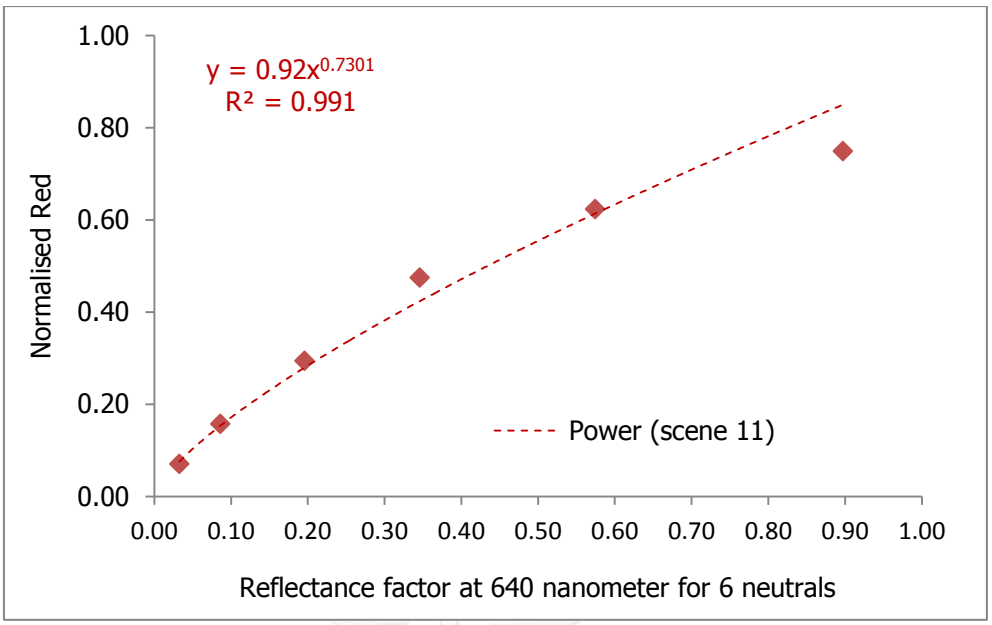

Figure 6.27 Best fit power function for the red channel correction in scene 11.

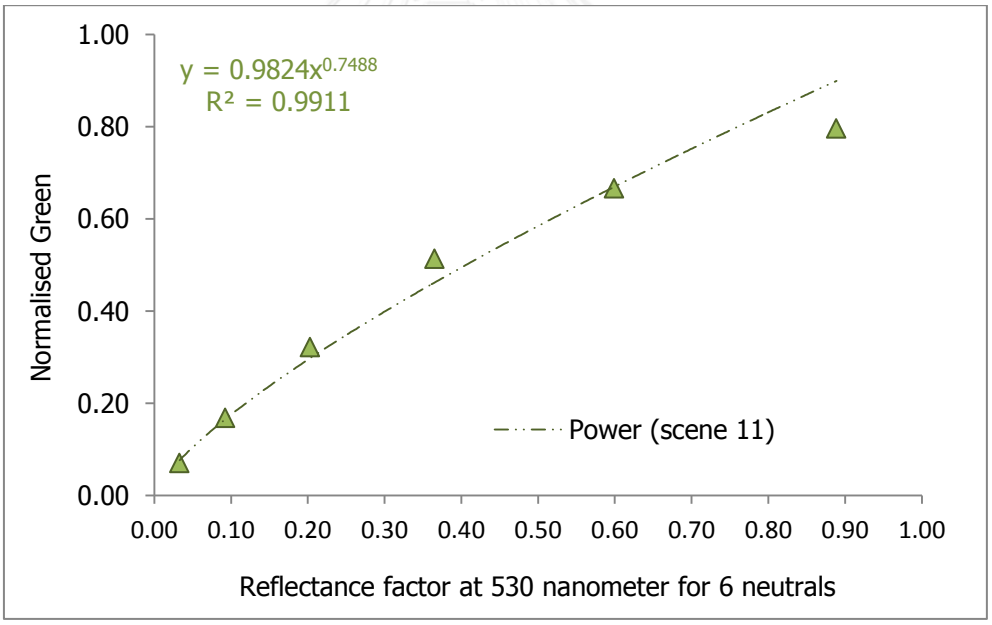

Figure 6.28 Best fit power function for the green channel correction in scene 11.

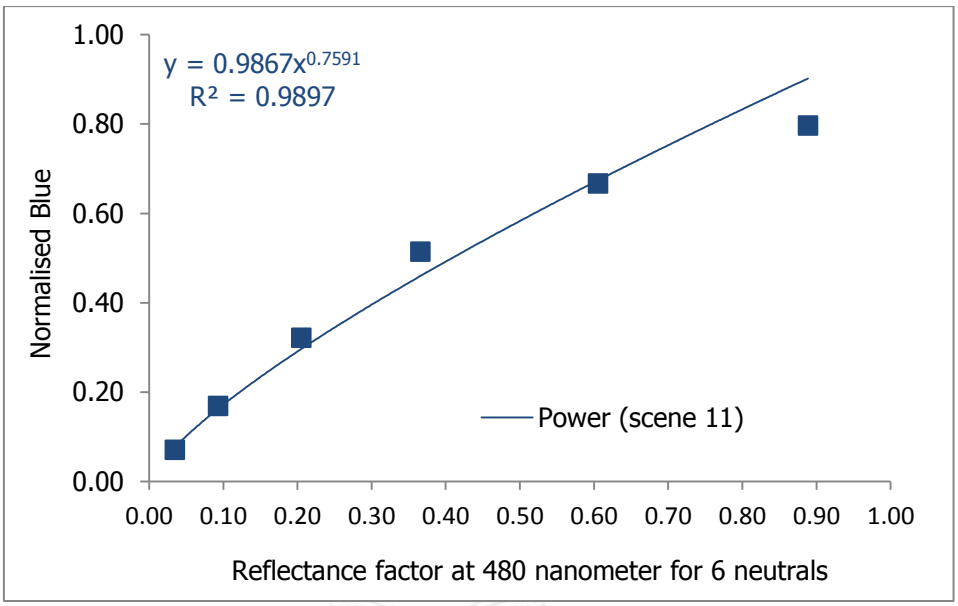

Figure 6.29 Best fit power function for the blue channel correction in scene 11.

Table 6.8 Calculated CIELAB from Canon EOS X4's digital image scene 11 under Fluorescent D65 and ΔE_{00} toward measured CIELAB, D65/2°.

Munsell Patches	Measured Spectrophotometer			R	G	B	Calculated CIELAB of scene 11			ΔE_{00}
	L*	a*	b*				L*	a*	b*	
N2	21.15	-0.15	-0.82	18	17	18	19.71	0.77	-1.07	1.70
N3.5	36.28	-0.45	-0.90	40	43	43	37.24	-1.95	-0.28	2.33
N5	52.15	-0.43	-0.62	75	81	82	54.58	-2.05	-0.52	3.26
N6.5	66.68	-0.93	-0.63	121	125	131	70.08	0.21	-1.52	3.27
N8	81.55	-0.85	-0.97	159	165	170	81.32	-0.03	-0.51	1.27
N9.5	95.71	-0.59	1.54	191	199	203	89.72	-0.23	0.21	3.91
7.5 P 4/10	42.23	34.78	-23.65	83	40	108	44.12	33.63	-30.33	4.10
10 PB 4/10	41.59	23.16	-37.00	64	47	134	45.22	27.54	-41.30	3.85
2.5 GY 8/10	81.54	-22.10	70.22	148	183	28	81.96	-26.29	67.04	2.60
7.5 GY 7/10	71.18	-39.34	53.30	87	165	38	75.04	-40.15	52.71	2.91
10 R 6/10	61.56	37.79	38.58	182	63	37	59.30	38.70	36.88	2.31
7.5 RP 4/12	41.90	53.46	1.07	117	21	58	41.17	50.37	-4.61	3.02
10 YR 7/4	71.62	4.82	27.72	151	129	81	72.05	0.88	25.40	3.54
7.5YR7/8	71.70	16.85	45.85	174	113	39	69.68	10.66	47.52	4.77
7.5PB4/8	41.17	11.07	-33.45	48	55	124	45.74	13.99	-35.93	4.41
5P4/10	40.38	32.56	-28.57	74	39	113	42.92	32.56	-34.82	3.96
5 R 4/12	41.59	52.54	27.90	124	21	27	41.20	48.54	21.33	3.04
10GY7/8	71.45	-38.29	32.69	86	169	86	76.54	-34.98	28.16	4.20
5 YR 7/6	71.12	17.00	30.11	173	118	84	71.41	12.84	23.24	3.42
7.5R4/10	41.55	43.60	30.73	123	25	25	42.11	45.02	24.46	3.84
5Y8/4	81.15	-3.75	30.09	166	169	111	81.47	-6.94	23.85	4.33
2.5BG7/4	72.45	-21.21	1.02	100	163	151	77.21	-18.42	0.43	3.88
2.5G6/4	62.00	-22.12	10.71	76	128	100	67.16	-20.90	8.19	4.55
5RP4/12	42.30	52.65	-7.02	113	28	72	43.07	45.89	-11.20	3.22
10BG8/2	81.76	-9.28	-3.85	148	177	181	83.12	-5.97	-2.01	3.57
10BG7/2	71.91	-9.46	-4.04	122	154	157	76.75	-7.74	-2.47	4.06
5PB4/2	41.22	0.2	-8.86	48	57	72	44.38	-0.58	-10.00	3.19

Except for the corrected hue, mentioned before, 2 other colours were desaturated in scene 12: 7.5YR from 7/8 to 7/6 and 7.5PB from 4/8 to 4/6. In this scene, the following colours were added for covering more hue angles: 10P4/10 (saturated colour), 7.5G6/4 (low saturated) and 10Y8.5/6 (medium saturated). The Hue-Chroma chart, the corrective functions for each colour channel and the table of results are presented next.

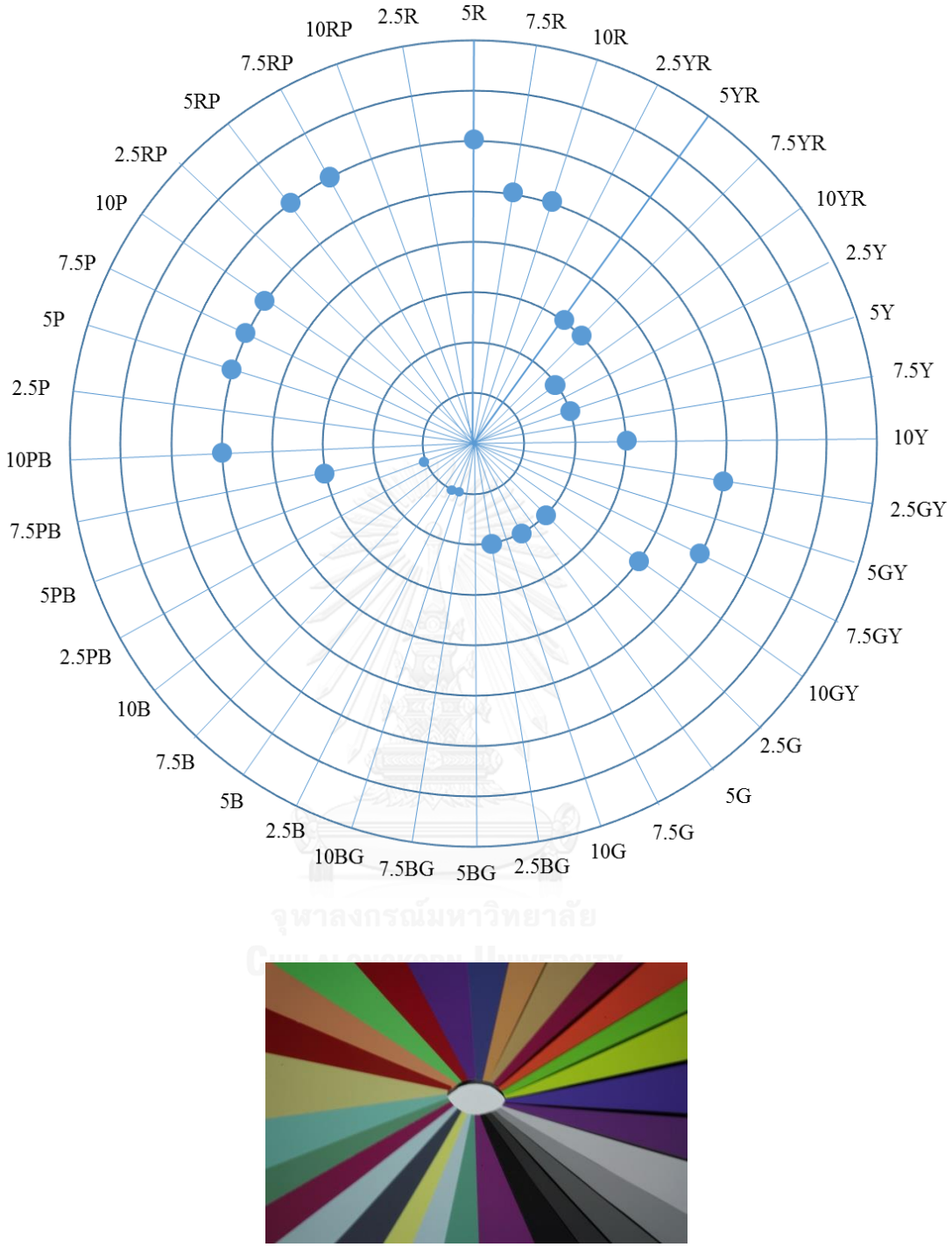

Figure 6.30 Hue-Chroma chart of the colours used in scene 12.

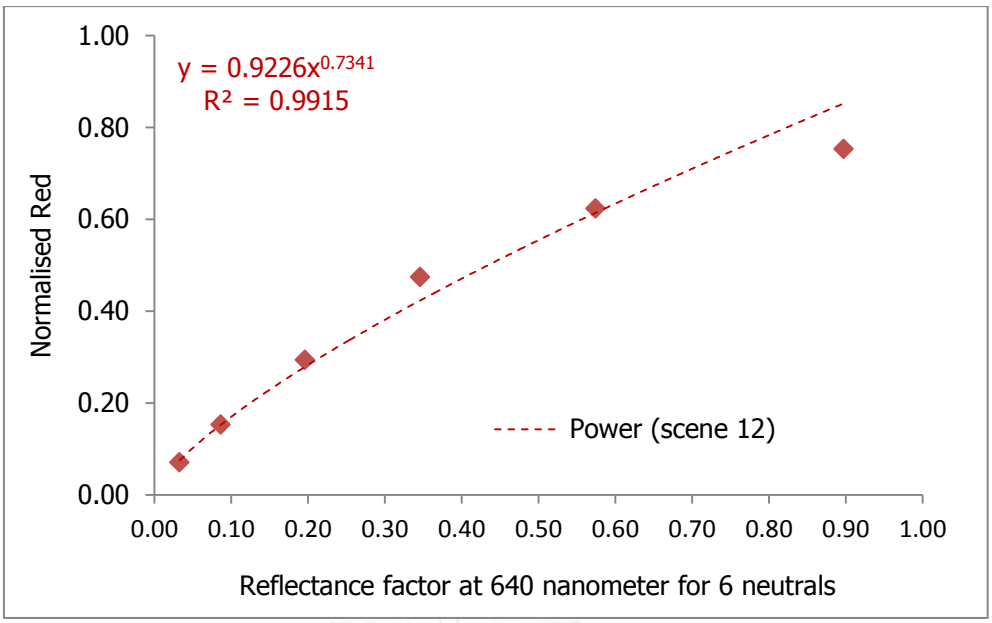

Figure 6.31 Best fit power function for the red channel correction in scene 12.

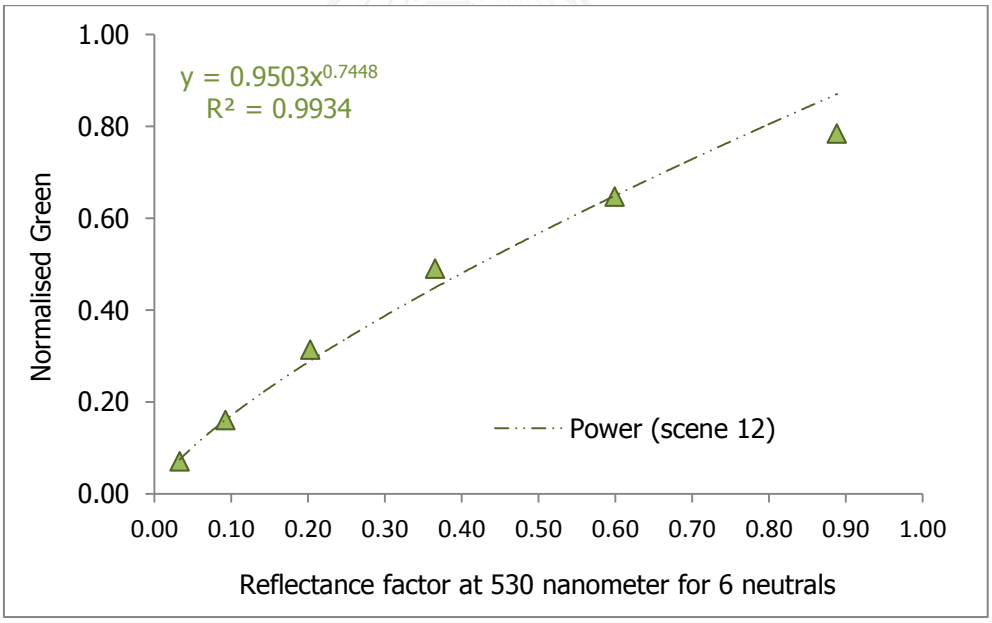

Figure 6.32 Best fit power function for the green channel correction in scene 12.

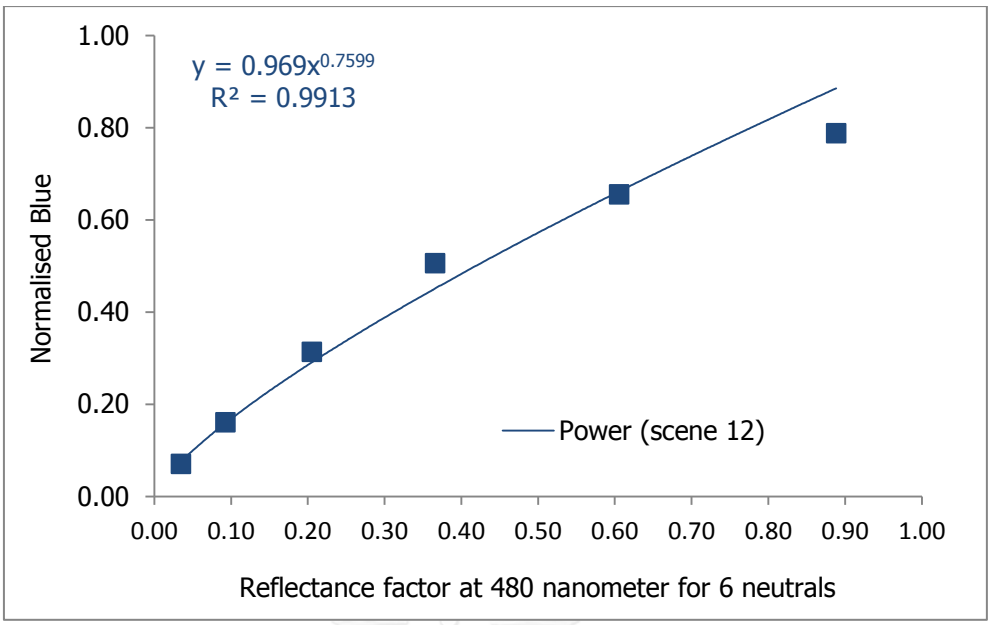

Figure 6.33 Best fit power function for the blue channel correction in scene 12.

Table 6.9 Calculated CIELAB from Canon EOS X4's digital image scene 12 under Fluorescent D65 and ΔE_{00} toward measured CIELAB, D65/2°.

Munsell Patches	Measured Spectrophotometer			R	G	B	Calculated CIELAB of scene 12			ΔE_{00}
	L*	a*	b*				L*	a*	b*	
N2	21.15	-0.15	-0.82	18	18	18	20.25	0.16	-0.78	0.78
N3.5	36.28	-0.45	-0.90	39	41	41	36.17	-0.81	-0.89	0.53
N5	52.15	-0.43	-0.62	75	80	80	54.31	-1.46	-0.67	2.55
N6.5	66.68	-0.93	-0.63	121	125	129	70.22	0.06	-1.51	3.25
N8	81.55	-0.85	-0.97	159	165	167	81.54	-0.51	-0.23	0.86
N9.5	95.71	-0.59	1.54	192	200	201	90.27	-0.86	0.44	3.50
7.5 P 4/10	42.23	34.78	-23.65	81	40	103	43.68	32.72	-29.46	3.79
10 PB 4/10	41.59	23.16	-37.00	62	47	130	44.88	26.88	-41.14	3.48
2.5 GY 8/10	81.54	-22.10	70.22	149	182	27	82.11	-26.20	67.47	2.49
7.5 GY 7/10	71.18	-39.34	53.30	87	163	37	74.87	-39.85	52.68	2.78
10 R 6/10	61.56	37.79	38.58	181	62	35	58.88	38.90	37.32	2.59
7.5 RP 4/12	41.90	53.46	1.07	114	20	55	40.30	50.33	-4.59	3.27
10 YR 7/4	71.62	4.82	27.72	149	127	78	71.58	0.66	25.52	3.71
7.5YR7/6	71.22	12.54	34.09	165	120	67	71.04	7.46	31.14	3.59
7.5PB4/6	41.49	7.24	-24.49	50	53	104	44.49	12.03	-28.98	3.77
5P4/10	40.38	32.56	-28.57	72	35	108	41.19	34.95	-36.08	3.40
5 R 4/12	41.59	52.54	27.90	123	16	24	39.55	51.95	21.73	3.64
10GY7/8	71.45	-38.29	32.69	83	167	80	76.17	-36.32	29.87	3.67
5 YR 7/6	71.12	17.00	30.11	174	118	80	71.52	12.59	24.68	3.09
7.5R4/10	41.55	43.60	30.73	119	22	21	40.47	45.98	26.00	3.39
5Y8/4	81.15	-3.75	30.09	165	169	107	81.62	-7.98	24.91	4.61
2.5BG7/4	72.45	-21.10	1.02	101	162	149	77.32	-18.02	0.28	4.06
2.5G6/4	62.00	-22.12	10.71	77	128	99	67.40	-20.56	8.10	4.77
5RP4/12	42.30	52.65	-7.02	112	26	69	42.23	47.18	-11.43	2.90
10BG8/2	81.76	-9.28	-3.85	146	176	178	83.09	-6.62	-2.17	2.93
5PB4/2	41.22	0.2	-8.86	49	57	70	44.41	-0.02	-9.55	2.98
10Y8.5/6	86.51	-11.29	44.7	175	186	95	85.20	-12.69	35.34	4.08
2.5B8/2	80.85	-8.22	-3.72	149	175	179	83.09	-5.33	-2.53	3.39
7.5G6/4	61.24	-22.46	5.30	77	128	99	67.40	-20.56	8.10	5.62
10P4/10	41.83	39.20	-19.04	62	47	130	44.88	26.88	-41.14	15.27

The colour difference between calculated and measured CIELAB values for 10P4/10 colour code that was added in scene 12 is 15.27 ΔE_{00} units because of its high chroma.Therefore it was desaturated to 4/6 in the next step. Also the lightness of Munsell colours 7.5G6/4 and 2.5G6/4 were raised to 7. Next are shown the Hue-Chroma diagram, the colour corrective functions and the result sheet for scene 13.

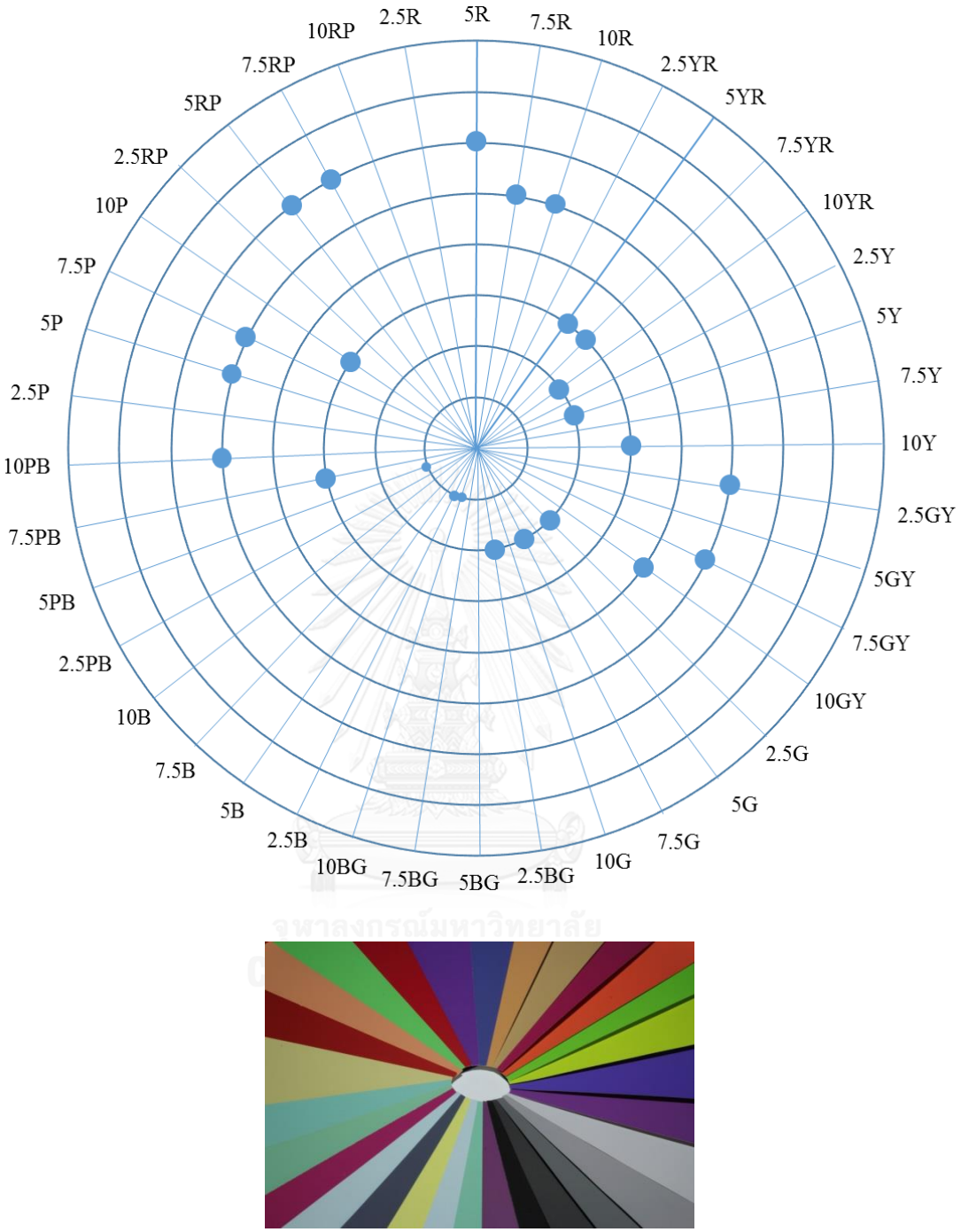

Figure 6.34 Hue-Chroma chart of the colours used in scene 13.

The Hue-Chroma chart in Figure 94 shows the very low saturation that had to be selected for 5PB, 2.5B and 10BG in order to have the left lower region of the chart covered.

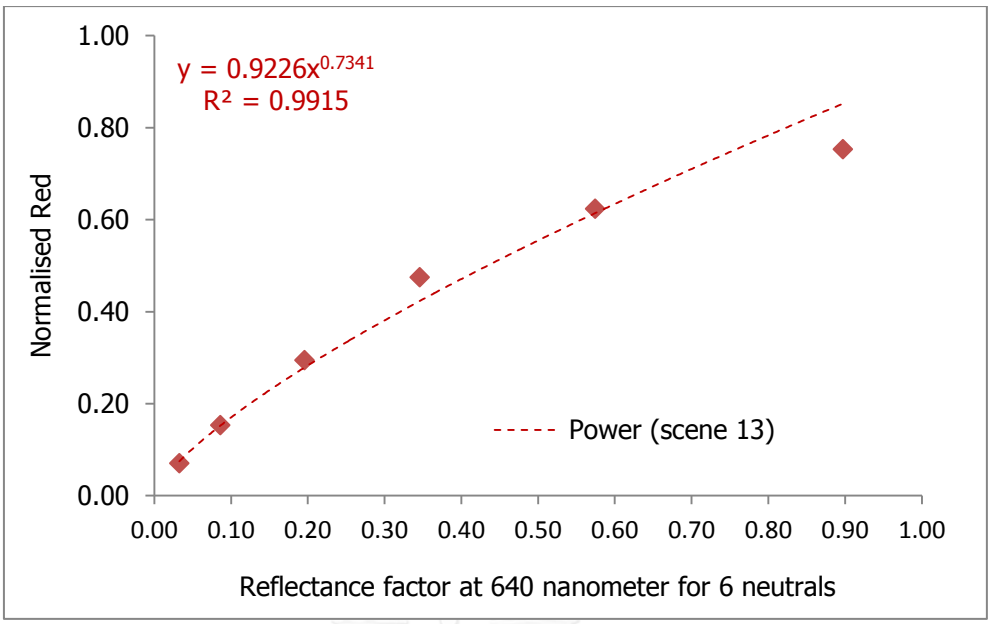

Figure 6.35 Best fit power function for the red channel correction in scene 13.

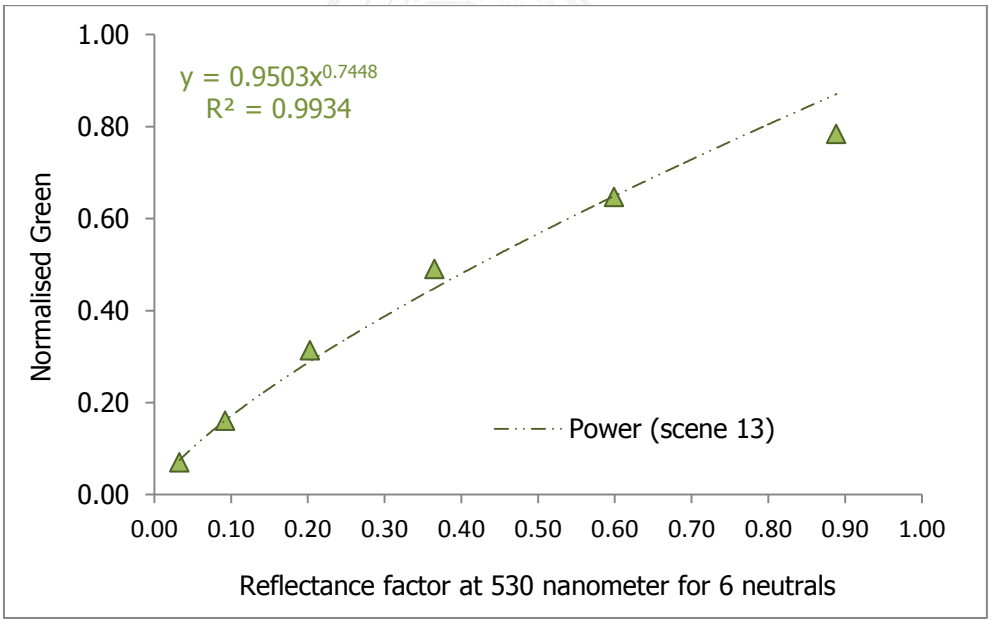

Figure 6.36 Best fit power function for the green channel correction in scene 13.

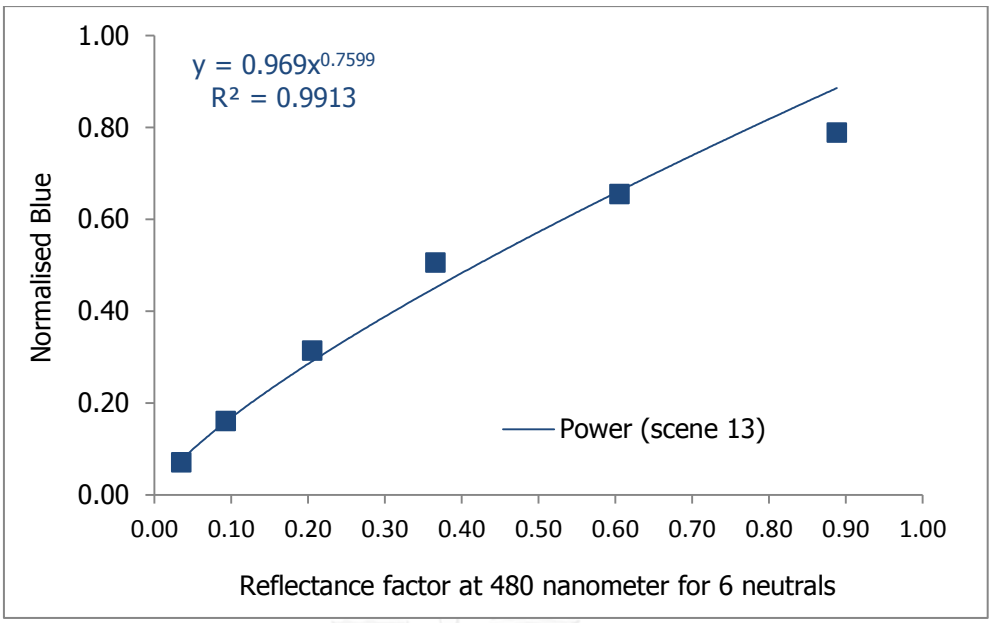

Figure 6.37 Best fit power function for the blue channel correction in scene 13.

Table 6.10 Calculated CIELAB from Canon EOS X4's digital image scene 13 under Fluorescent D65 and ΔE_{00} toward measured CIELAB, D65/2°.

Munsell Patches	Measured Spectrophotometer			R	G	B	Calculated CIELAB of scene 13			ΔE_{00}
	L*	a*	b*				L*	a*	b*	
N2	21.15	-0.15	-0.82	20	20	20	19.55	0.28	-0.67	1.29
N3.5	36.28	-0.45	-0.90	45	48	48	37.14	-1.08	-0.80	1.16
N5	52.15	-0.43	-0.62	83	90	92	55.18	-1.56	-1.54	3.43
N6.5	66.68	-0.93	-0.63	131	136	140	70.68	-0.09	-1.12	3.40
N8	81.55	-0.85	-0.97	168	174	176	81.19	-0.38	0.24	1.38
N9.5	95.71	-0.59	1.54	197	205	208	88.88	-0.55	0.25	4.37
7.5 P 4/10	42.23	34.78	-23.65	97	46	118	45.25	35.73	-29.82	4.08
10 PB 4/10	41.59	23.16	-37.00	70	54	147	45.79	27.78	-42.63	4.48
2.5 GY 8/10	81.54	-22.10	70.22	158	191	31	81.75	-25.64	67.07	2.29
7.5 GY 7/10	71.18	-39.34	53.30	93	176	41	75.34	-41.18	53.69	3.17
10 R 6/10	61.56	37.79	38.58	194	72	40	59.96	37.95	38.49	1.39
7.5 RP 4/12	41.90	53.46	1.07	133	25	66	42.51	52.36	-4.26	2.66
10 YR 7/4	71.62	4.82	27.72	160	138	88	72.06	0.82	25.11	3.63
7.5YR7/6	71.22	12.54	34.09	177	131	74	71.58	7.42	31.98	3.66
7.5PB4/6	41.49	7.24	-24.49	56	63	120	46.07	11.08	-29.83	4.83
5P4/10	40.38	32.56	-28.57	85	43	124	43.26	35.51	-35.97	4.12
5 R 4/12	41.59	52.54	27.90	144	23	29	42.53	52.49	24.60	1.92
10GY7/8	71.45	-38.29	32.69	92	179	90	76.60	-35.90	29.48	4.02
5 YR 7/6	71.12	17.00	30.11	186	129	90	72.10	12.67	24.47	3.18
7.5R4/10	41.55	43.60	30.73	138	29	26	43.01	46.68	27.82	2.88
5Y8/4	81.15	-3.75	30.09	177	178	118	81.49	-6.52	24.06	3.98
2.5BG7/4	72.45	-21.21	1.02	112	175	162	78.04	-17.78	0.60	4.58
2.5G7/4	71.75	-23.56	11.28	113	173	140	77.29	-20.08	8.33	4.69
5RP4/12	42.30	52.65	-7.02	133	24	66	42.27	53.02	-4.62	1.15
10BG8/2	81.76	-9.28	-3.85	158	187	190	83.30	-5.98	-1.87	3.64
5PB4/2	41.22	0.2	-8.86	60	68	83	46.65	0.57	-9.44	5.10
10Y8.5/6	86.51	-11.29	44.7	185	196	105	85.07	-12.15	34.64	4.20
2.5B8/2	80.85	-8.22	-3.72	160	186	191	83.24	-4.98	-2.30	3.81
7.5G7/4	72.14	-23.45	6.17	110	175	151	77.74	-20.01	4.48	4.59
10P4/6	41.22	25.07	-13.45	92	49	91	44.50	27.16	-16.90	3.58

In scene 12, the number of colours in the colour-wheel reached already 24, which together with the 6 neutrals give a total of 30 Munsell sheets in the colour wheel. This results in an angle of approximately 12.5 for each Munsel patch in the wheel. Adding more colours to the wheel would decrease the surface of each colour in the considered 12 cm diameter around the wheel's center, reducing each colour to a narrow stripe that would be difficult to crop from the scene's picture. For this reason, no other colours were added in scenes 13, 14 and 15. In scene 14 only the lightness of 2.5G and 7.5G are modified by reducing them from 7 to 4. Hue-Chroma chart, best fit functions and result sheet are shown next.

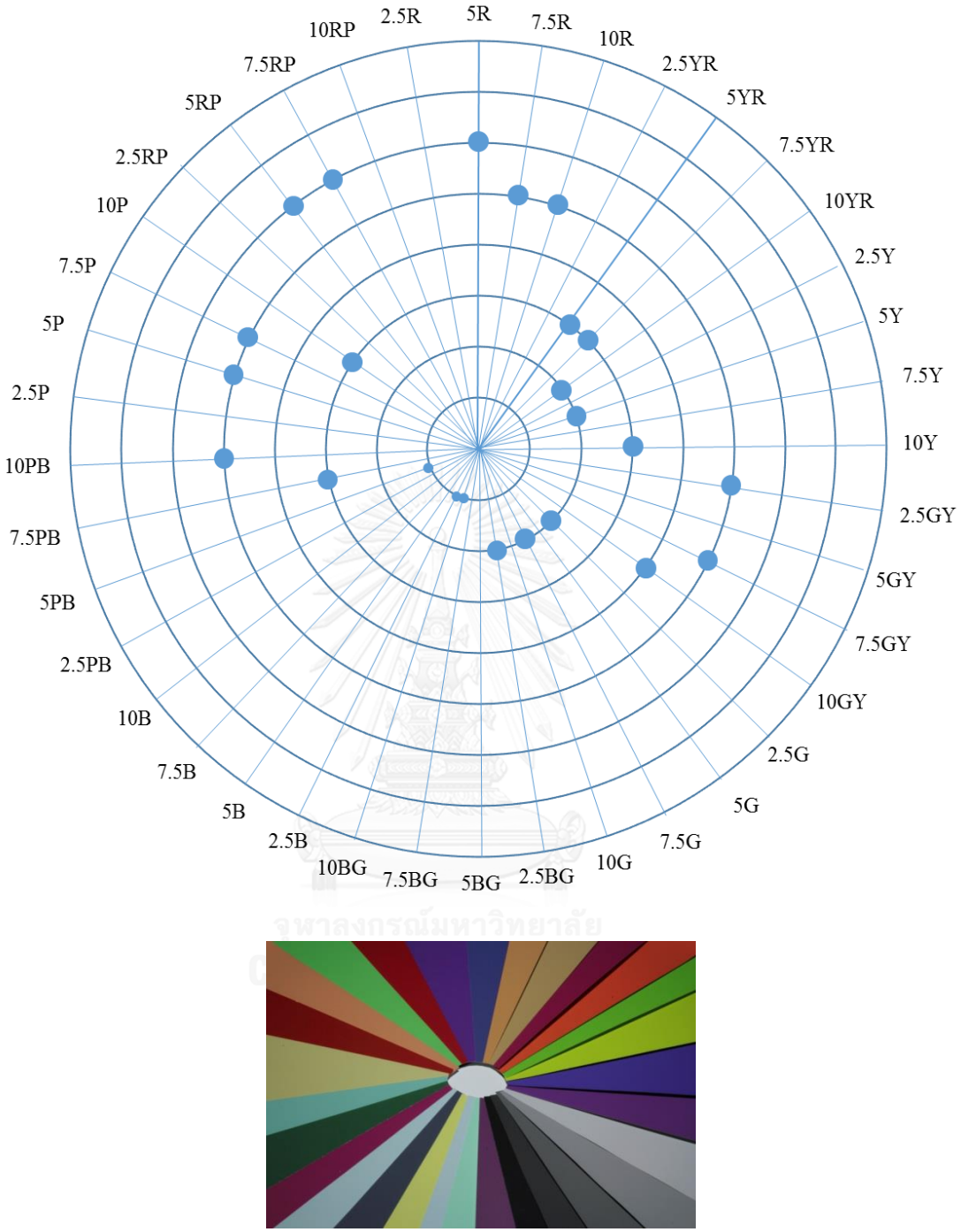

Figure 6.38 Hue-Chroma chart of the colours used in scene 14.

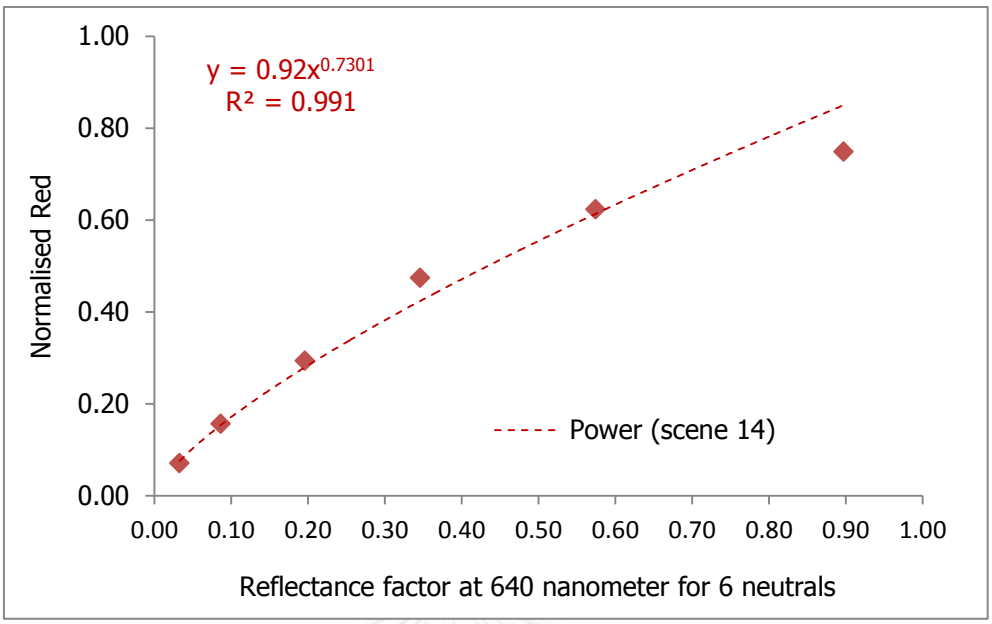

Figure 6.39 Best fit power function for the red channel correction in scene 14.

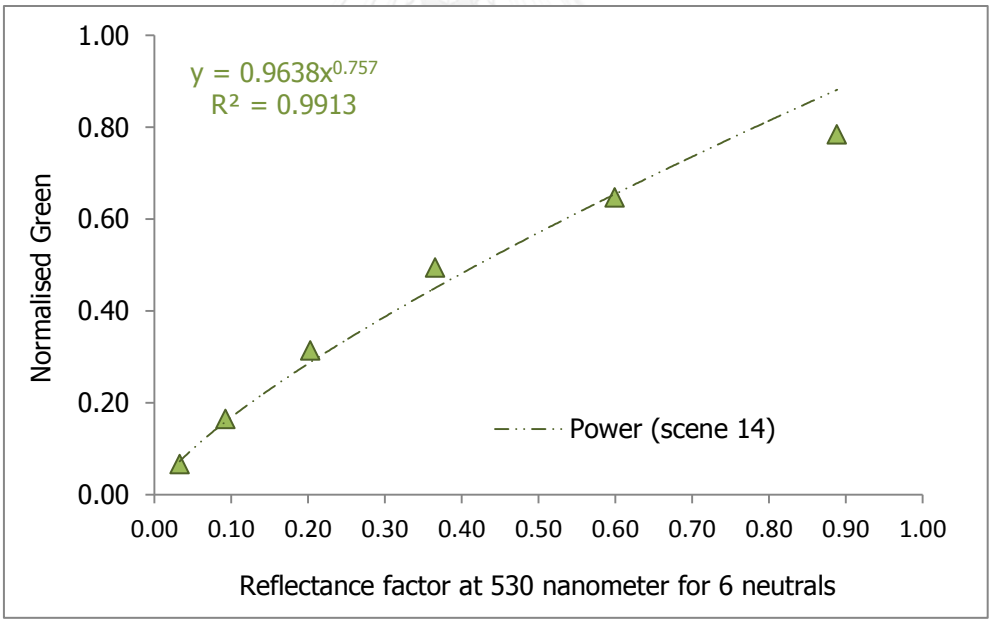

Figure 6.40 Best fit power function for the green channel correction in scene 14.

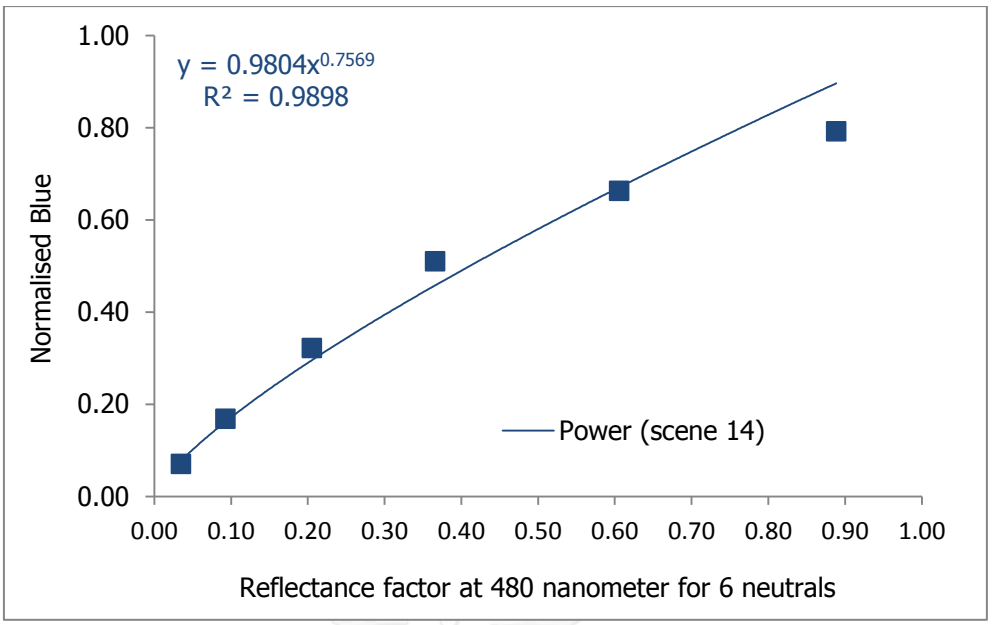

Figure 6.41 Best fit power function for the blue channel correction in scene 14.

Table 6.11 Calculated CIELAB from Canon EOS X4's digital image scene 14 under Fluorescent D65 and ΔE_{00} toward measured CIELAB, D65/2°.

Munsell Patches	Measured Spectrophotometer			R	G	B	Calculated CIELAB of scene 14			ΔE_{00}
	L*	a*	b*				L*	a*	b*	
N2	21.15	-0.15	-0.82	18	17	18	19.85	0.47	-0.83	1.29
N3.5	36.28	-0.45	-0.90	40	42	43	36.97	-1.38	-0.72	1.45
N5	52.15	-0.43	-0.62	75	80	82	54.39	-1.60	-0.94	2.74
N6.5	66.68	-0.93	-0.63	121	126	130	70.32	-0.36	-0.99	3.00
N8	81.55	-0.85	-0.97	159	165	169	81.30	-0.02	-0.49	1.29
N9.5	95.71	-0.59	1.54	191	200	202	89.84	-0.45	0.33	3.77
7.5 P 4/10	42.23	34.78	-23.65	84	40	108	44.35	33.78	-30.17	4.09
10 PB 4/10	41.59	23.16	-37.00	64	49	134	45.97	25.90	-40.39	4.29
2.5 GY 8/10	81.54	-22.10	70.22	149	182	29	81.80	-25.49	66.32	2.39
7.5 GY 7/10	71.18	-39.34	53.30	87	164	38	74.81	-39.81	52.43	2.74
10 R 6/10	61.56	37.79	38.58	183	64	38	59.72	38.32	36.64	1.98
7.5 RP 4/12	41.90	53.46	1.07	117	21	58	41.24	50.20	-4.59	3.02
10 YR 7/4	71.62	4.82	27.72	151	129	81	72.08	0.85	25.31	3.58
7.5YR7/6	71.22	12.54	34.09	166	121	70	71.30	7.72	30.45	3.41
7.5PB4/6	41.49	7.24	-24.49	52	55	108	45.60	11.38	-28.48	4.42
5P4/10	40.38	32.56	-28.57	74	36	111	41.99	34.44	-35.50	3.45
5 R 4/12	41.59	52.54	27.90	126	17	26	40.47	51.80	21.46	3.43
10GY7/8	71.45	-38.29	32.69	85	169	82	76.41	-35.85	29.85	3.86
5 YR 7/6	71.12	17.00	30.11	175	119	83	71.79	12.81	24.16	3.16
7.5R4/10	41.55	43.60	30.73	122	23	23	41.40	45.83	25.61	3.41
5Y8/4	81.15	-3.75	30.09	166	168	111	81.28	-6.49	23.38	4.25
2.5BG7/4	72.45	-21.21	1.02	101	163	151	77.27	-18.00	0.22	4.06
2.5G4/4	41.82	-22.37	10.49	33	72	48	47.48	-23.41	10.40	5.37
5RP4/12	42.30	52.65	-7.20	114	27	72	43.02	46.76	-11.39	3.00
10BG8/2	81.76	-9.28	-3.85	148	177	182	83.13	-5.66	-2.72	3.75
5PB4/2	41.22	0.2	-8.86	50	59	72	45.37	-1.24	-8.62	4.29
10Y8.5/6	86.51	-11.29	44.7	174	187	97	85.01	-12.57	34.85	4.26
2.5B8/2	80.85	-8.22	-3.72	151	177	182	83.29	-4.87	-2.45	3.90
7.5G8/4	81.90	-23.95	6.15	128	191	168	84.38	-17.80	4.14	3.98
10P4/6	41.22	25.07	-13.45	82	42	81	43.65	26.32	-16.37	2.73

The last 3 scenes of this session are of corrective nature, having the aim of reducing the individual colour differences between calculated and measured CIELAB values to under 5 ΔE_{00} units for each colour in the colour wheel. As can be seen in the result sheet of scene 14, only 2.5G4/4 has a colour difference greater than 5 ΔE_{00} units between calculated and measured CIELAB values. Due to the observation that lower chroma and higher lightness improve the colorimetric results and because the chroma of this colour is already quite low in scene 15 only the lightness of this colour was modified by increasing it from 4 to 8, considering the aim of having higher saturated colours for LED light quality assessments. The change in lightness cannot be seen on the Hue-Chroma chart, therefore this chart will not be presented for scene 15. For this scene, the chart is identical to the one presented for scene 14. Figures 6.42-6.44 show

the colour correction functions for scene 15. The table of results for this scene has been already presented in 4.6 (Table 4.3).

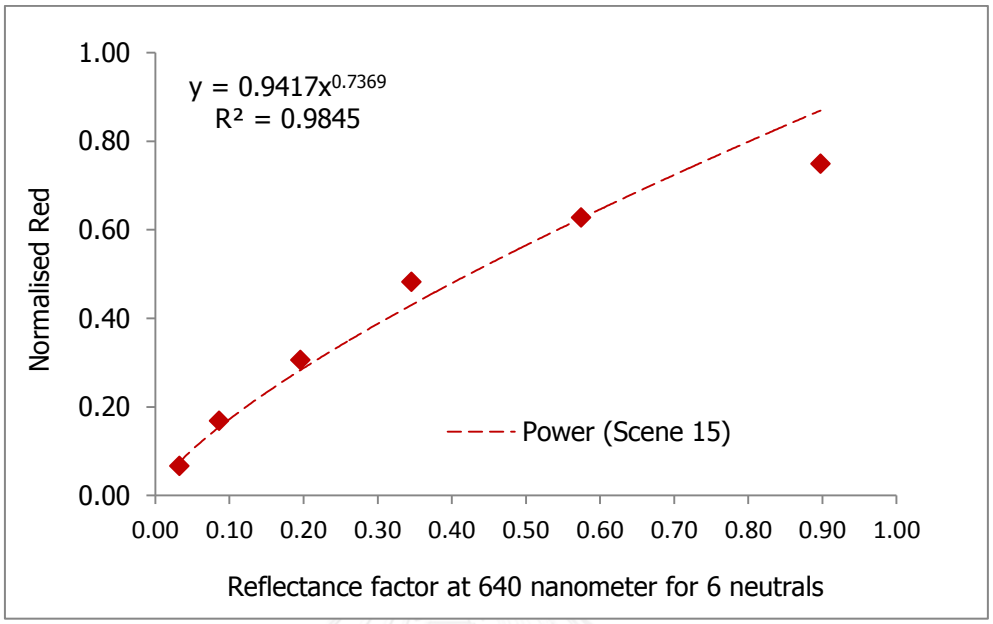

Figure 6.42 Best fit power function for the red channel correction in scene 15.

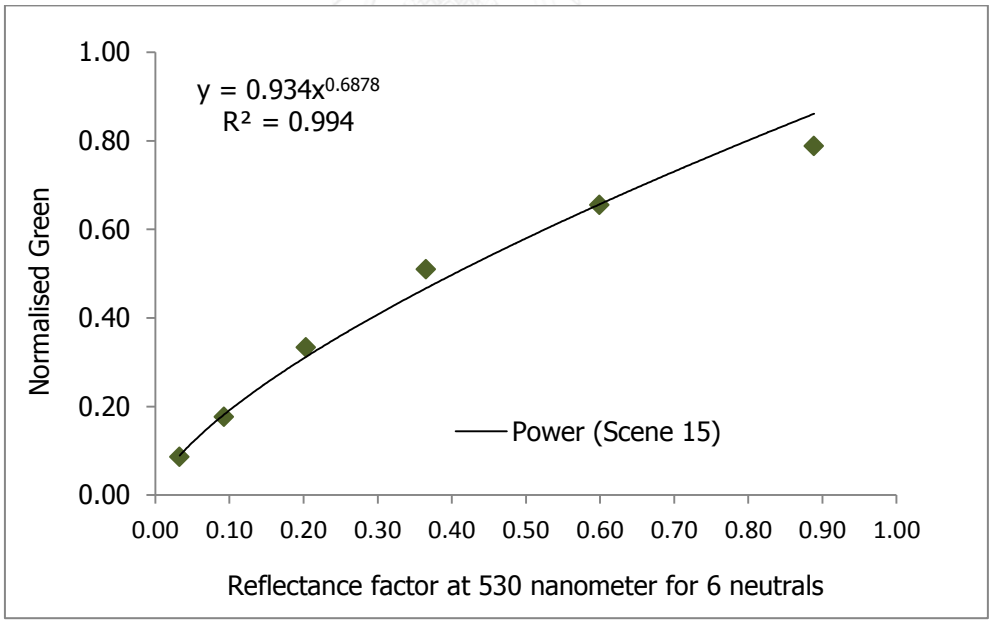

Figure 6.43 Best fit power function for the green channel correction in scene 15.

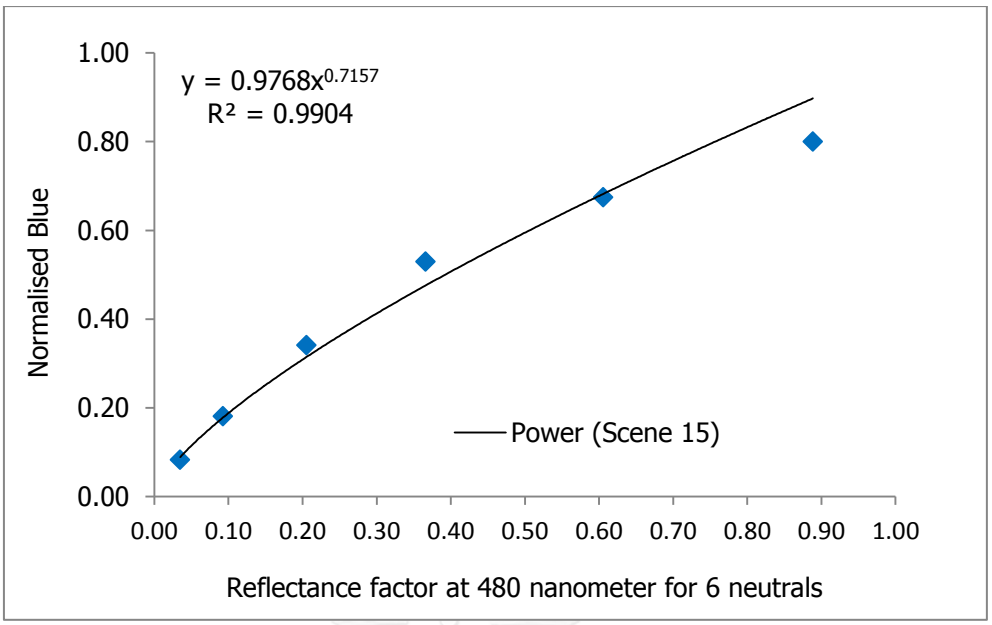

Figure 6.44 Best fit power function for the blue channel correction in scene 15.

6.2.3. Results obtained during improving the 24 colour wheel under 2 light sources.

In scenes 16 to 23 the colour wheel was optimized mainly by lowering the saturation of some colours. In scene 16, 10PB4/10 was replaced with 10PB4/8 and 10R6/10 was replaced with 10R6/8. In scene 17, 2.5GY8/10 was replaced with 2.5GY8/8. In scene 18, the chroma of 4 hues were decreased: 10PB from 4/8 to 4/6, 10P from 4/6 to 4/4, 10Y from 8.5/6 to 8.5/4, 2.5G from 8/4 to 8/2 and chroma of one hue was increased: 2.5GY from 8/8 to 8/10. This last change was however reversed in scene 20. In scene 19 the chroma of 5R was decreased from 4/12 to 4/10 and the chroma of 10 PB was increased from 4/6 to 4/8. Once more the increase in chroma had to be reversed in scene 20. Other two colours that were modified by means of chroma from scene 17 to 18 had their lightness modified now as follows: 10P4/4 to 10P6/4 and 10Y8.5/4 to 10Y8/4. The only hue change of a colour was performed in scene 21 when 7.5YR7/6 was replaced with 7.5B7/8, because response of the camera under the LED D65 light source was very bad for this hue. The next 2 scenes, 22 and 23 were of corrective nature for the newly introduced hue. In scene 22 its chroma was reduced from 8 to 6 and in scene 23 its lightness was increased from 7 to 8.

The optimization described above will be shown by tracing the evolution of each of the 24 colour hues that are not changed in the optimization process, by means of ΔE_{00}

between calculated and measured CIELAB values, across scenes 15 to 23. The chroma and luminance of the considered hues are marked above the plotted points on the graph. CIELAB coordinates of the colour samples contained in the final colour wheel were shown in Figure 4.20 of chapter 4.

The calculates CIELAB from Canon EOS X4, best fit functions and hue-chroma charts for scenes 15 to 23 are presented in the Appendix B, A and C respectively.

Next are presented 24 graphs tracing each of the 24 colour hues of the wheel from scene 15 to 23.

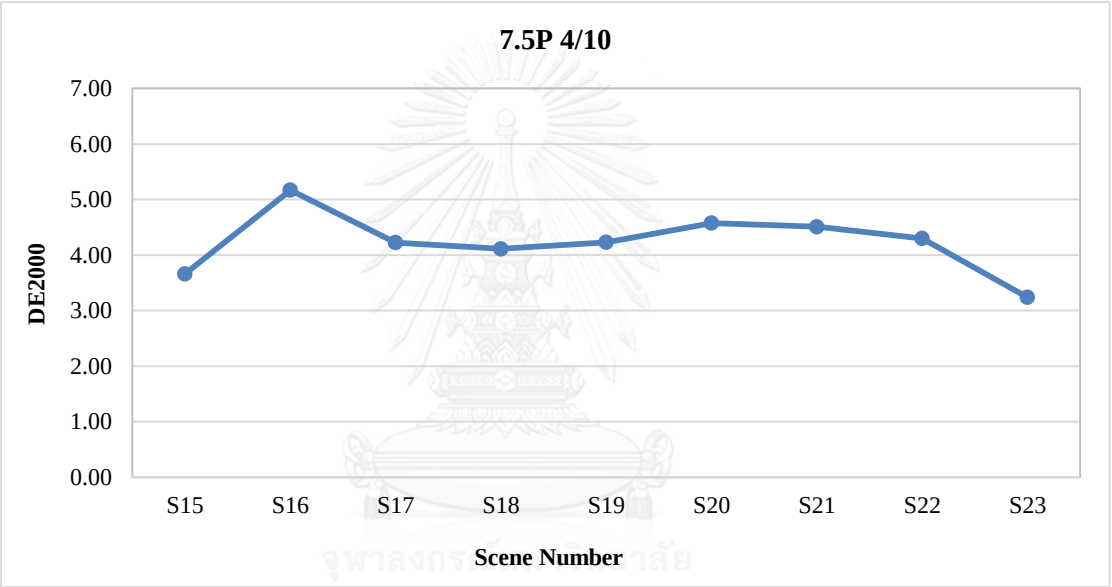

Figure 6.45 Colour differences between calculated and measured CIELAB values across scenes 15 to 23 for the wheel's Munsell Hue 7.5P, keeping chroma/lightness at 4/10.

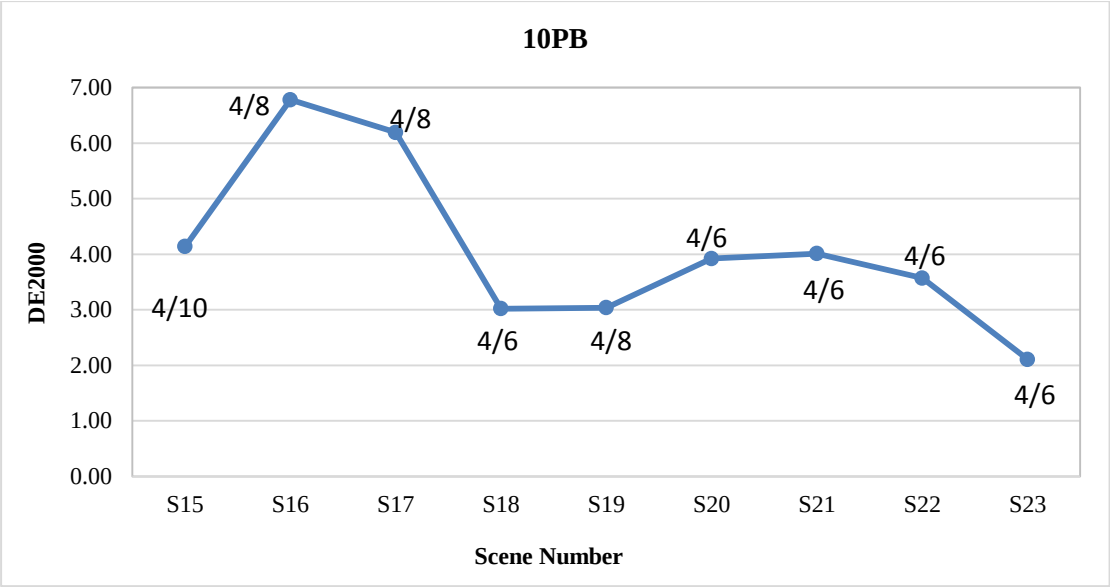

Figure 6.46 Colour differences between calculated and measured CIELAB values across scenes 15 to 23 for the wheel's Munsell Hue 10PB.

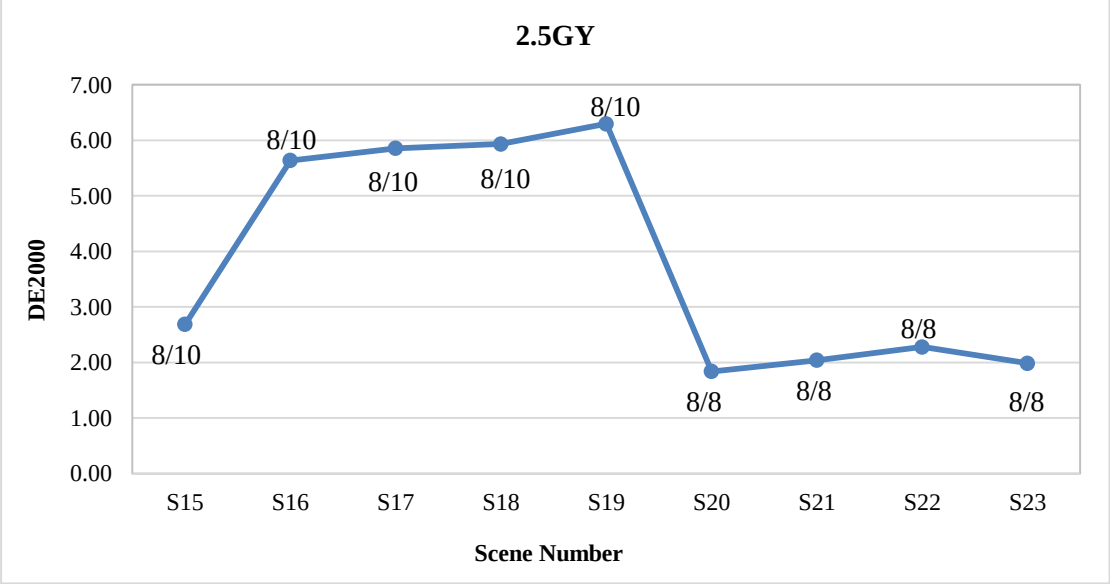

Figure 6.47 Colour differences between calculated and measured CIELAB values across scenes 15 to 23 for the wheel's Munsell Hue 2.5GY.

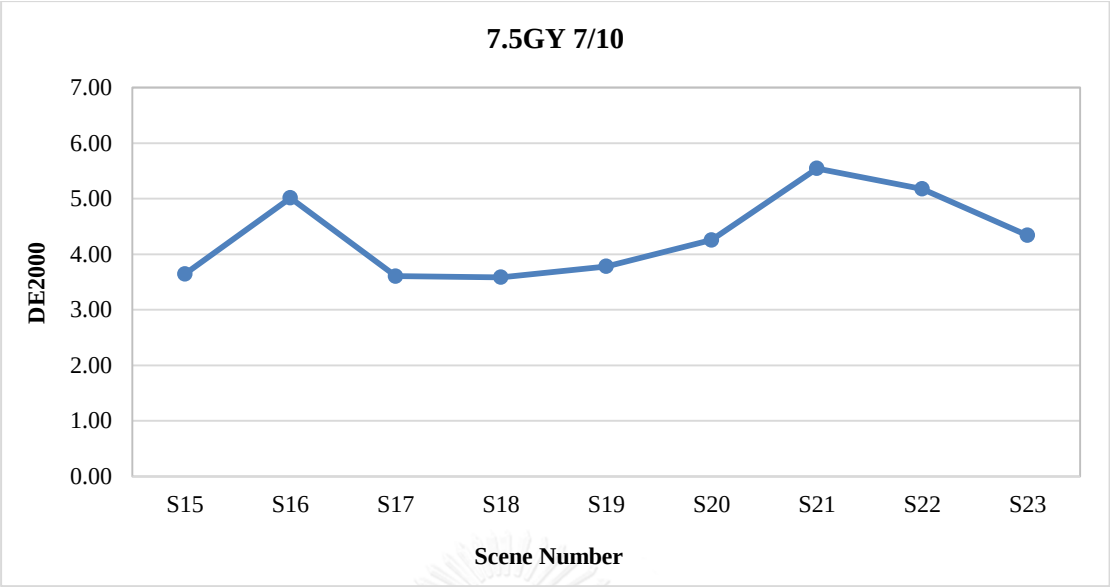

Figure 6.48 Colour differences between calculated and measured CIELAB values across scenes 15 to 23 for the wheel's Munsell Hue 7.5GY, keeping chroma/lightness at 7/10.

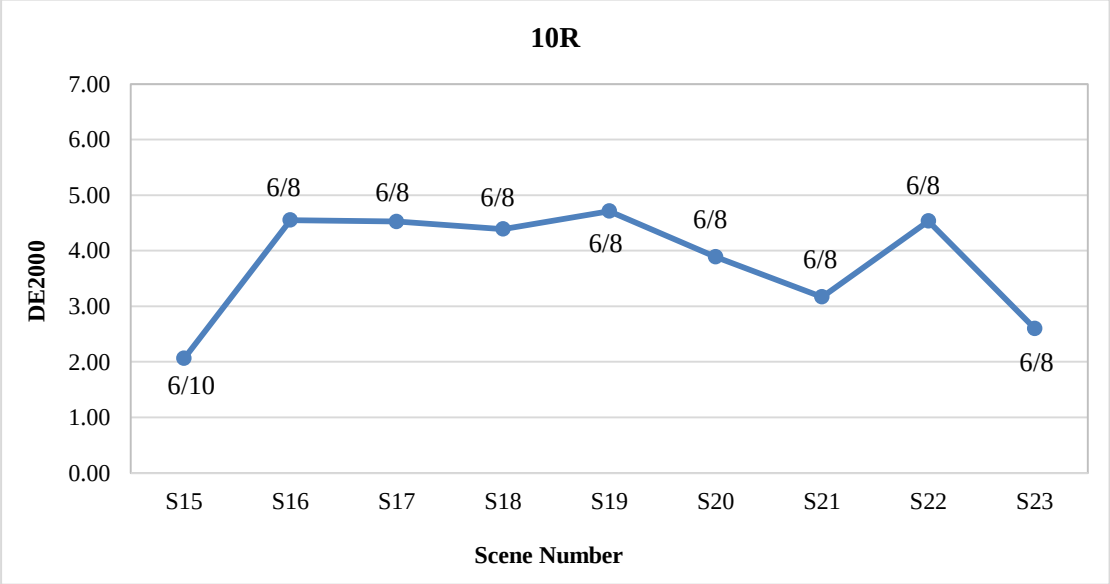

Figure 6.49 Colour differences between calculated and measured CIELAB values across scenes 15 to 23 for the wheel's Munsell Hue 10R.

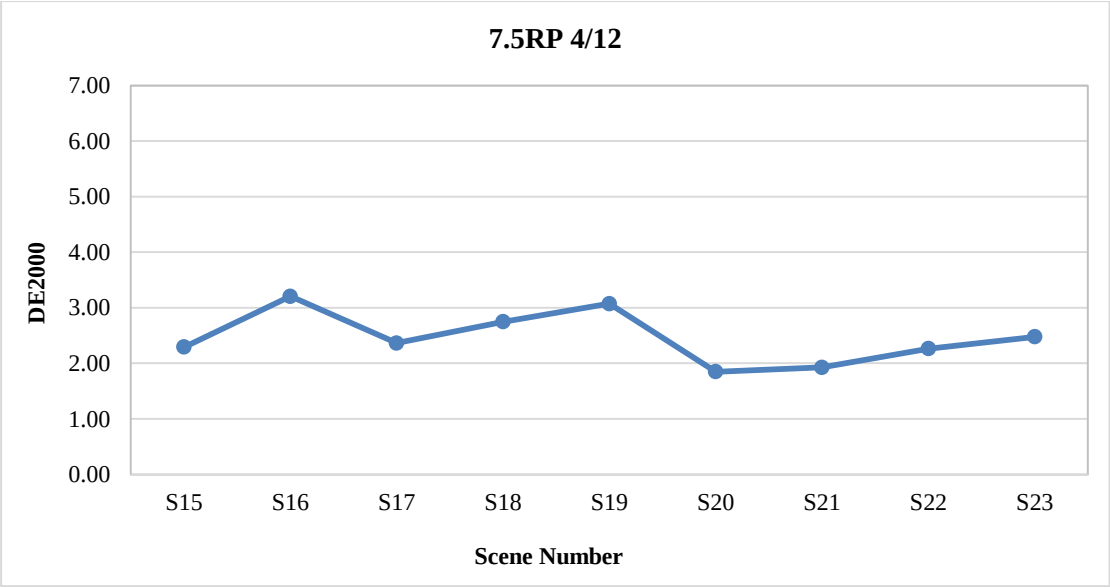

Figure 6.50 Colour differences between calculated and measured CIELAB values across scenes 15 to 23 for the wheel's Munsell Hue 7.5RP, keeping chroma/lightness at 4/12.

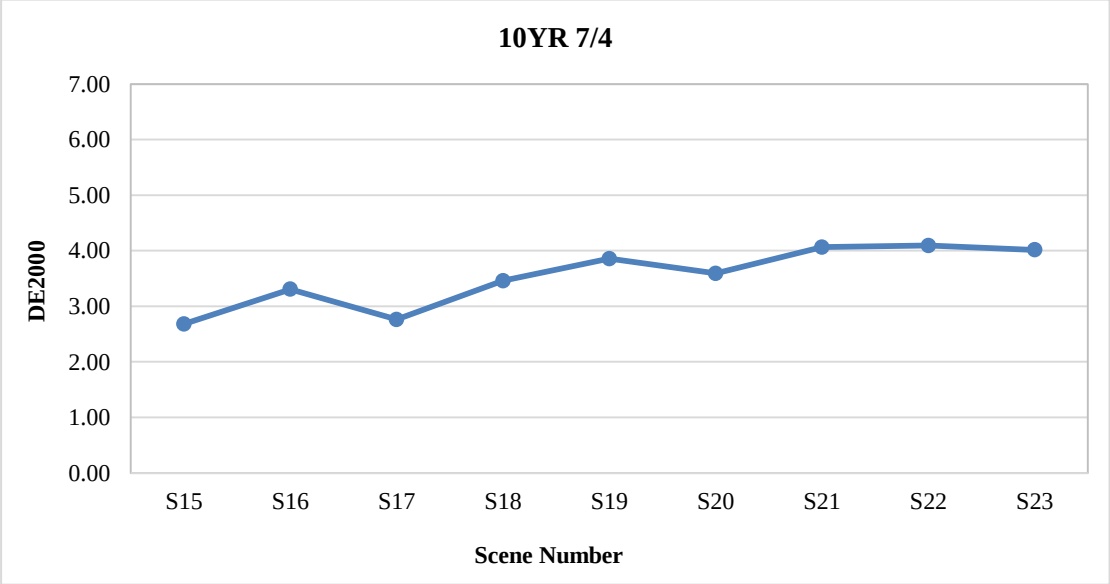

Figure 6.51 Colour differences between calculated and measured CIELAB values across scenes 15 to 23 for the wheel's Munsell Hue 10YR, keeping chroma/lightness at 7/4.

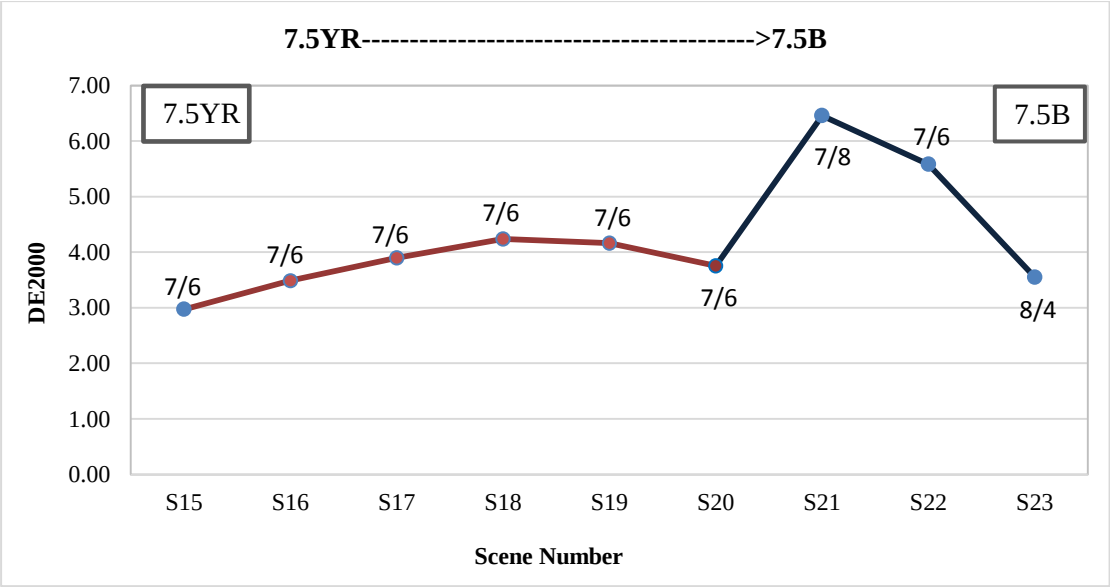

Figure 6.52 Colour differences between calculated and measured CIELAB values across scenes 15 to 23 for the wheel's Munsell Hue 7.5YR until scene 20 and for Munsell Hue 7.5B from scene 20.

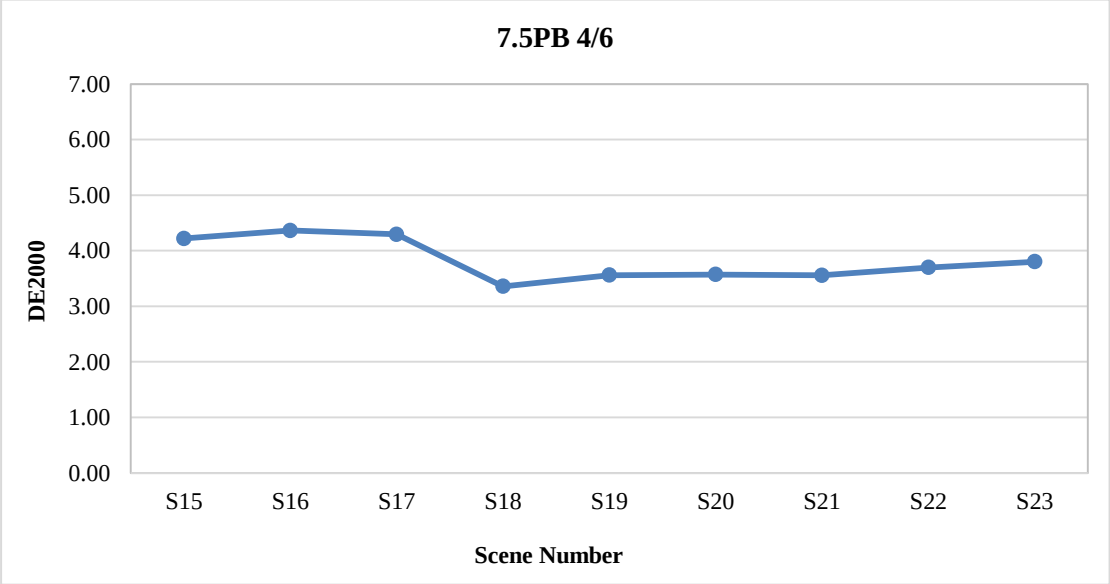

Figure 6.53 Colour differences between calculated and measured CIELAB values across scenes 15 to 23 for the wheel's Munsell Hue 7.5PB, keeping chroma/lightness at 4/6.

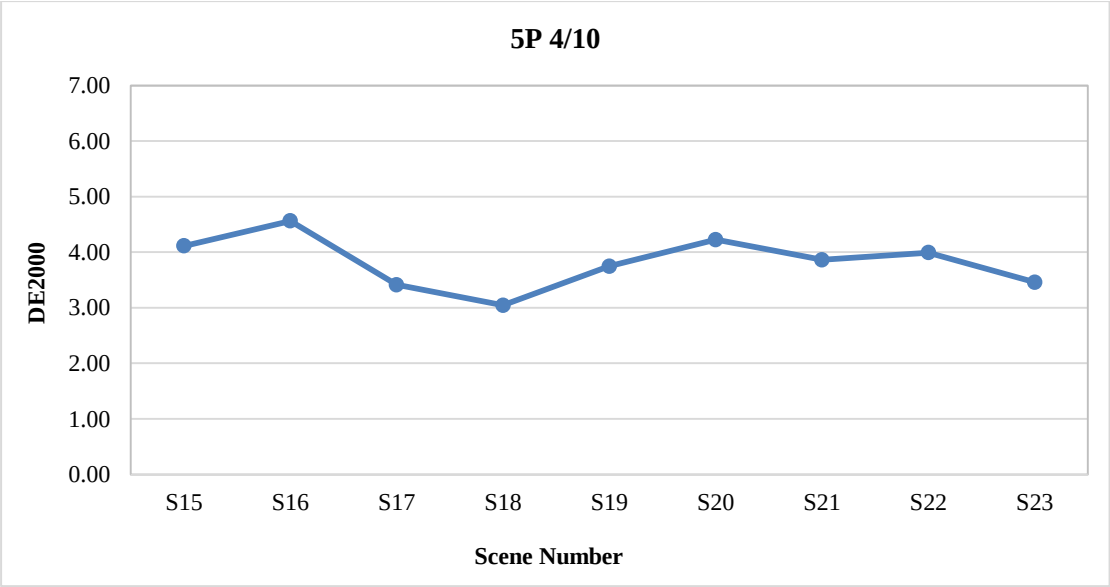

Figure 6.54 Colour differences between calculated and measured CIELAB values across scenes 15 to 23 for the wheel's Munsell Hue 5P, keeping chroma/lightness at 4/10.

Figure 6.55 Colour differences between calculated and measured CIELAB values across scenes 15 to 23 for the wheel's Munsell Hue 5R.

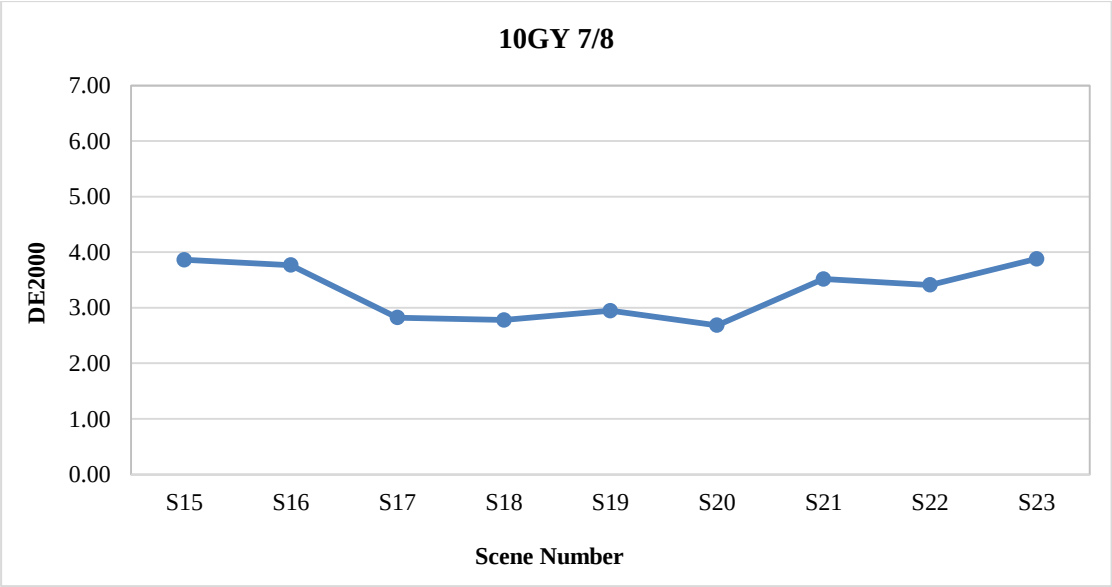

Figure 6.56 Colour differences between calculated and measured CIELAB values across scenes 15 to 23 for the wheel's Munsell Hue 10GY, keeping chroma/lightness at 7/8.

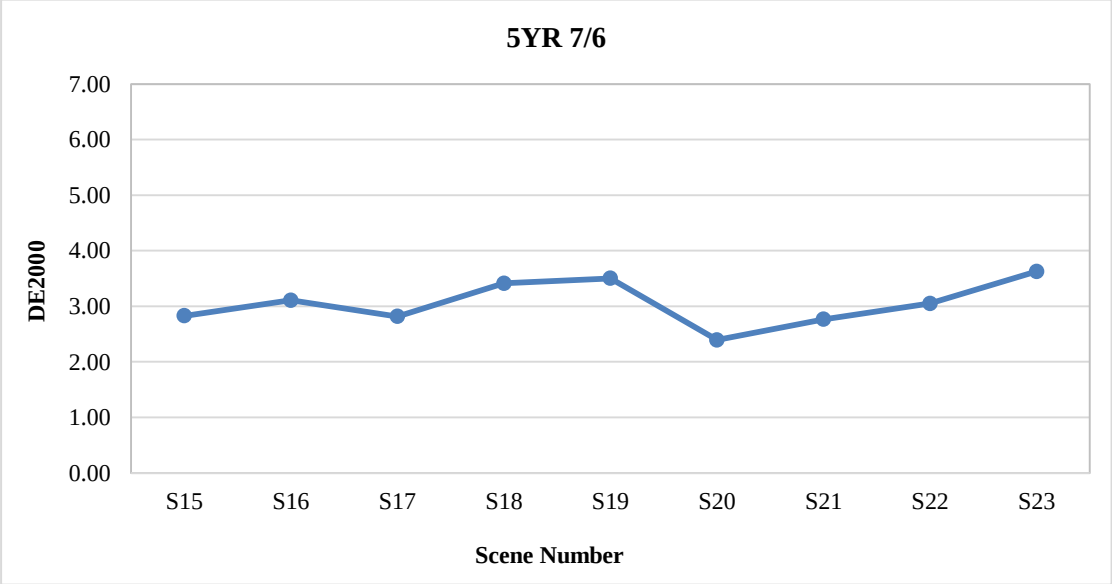

Figure 6.57 Colour differences between calculated and measured CIELAB values across scenes 15 to 23 for the wheel's Munsell Hue 5YR, keeping chroma/lightness at 7/6.

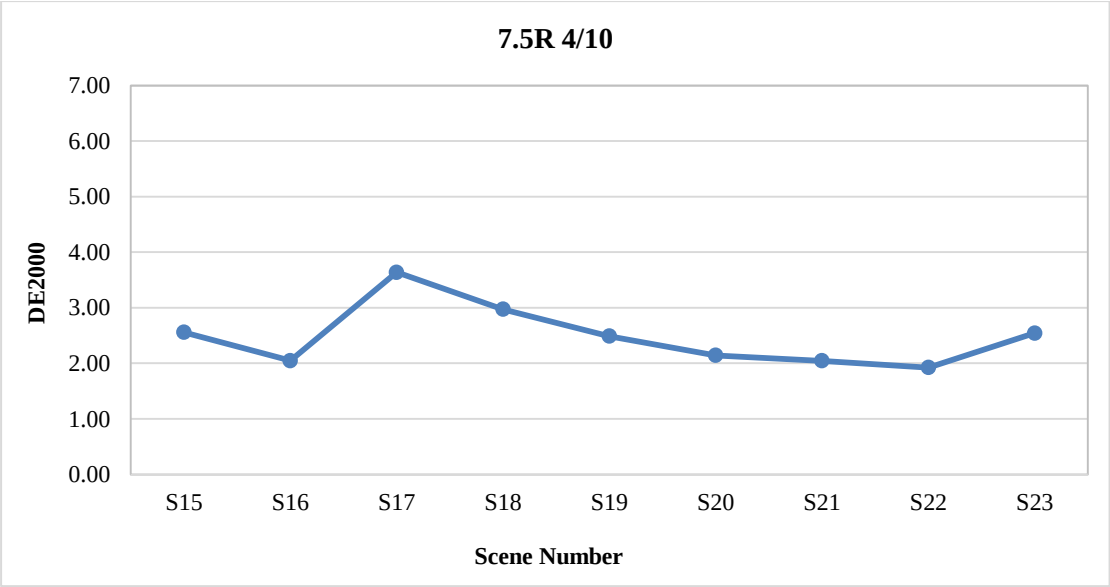

Figure 6.58 Colour differences between calculated and measured CIELAB values across scenes 15 to 23 for the wheel's Munsell Hue 7.5R, keeping chroma/lightness at 4/10.

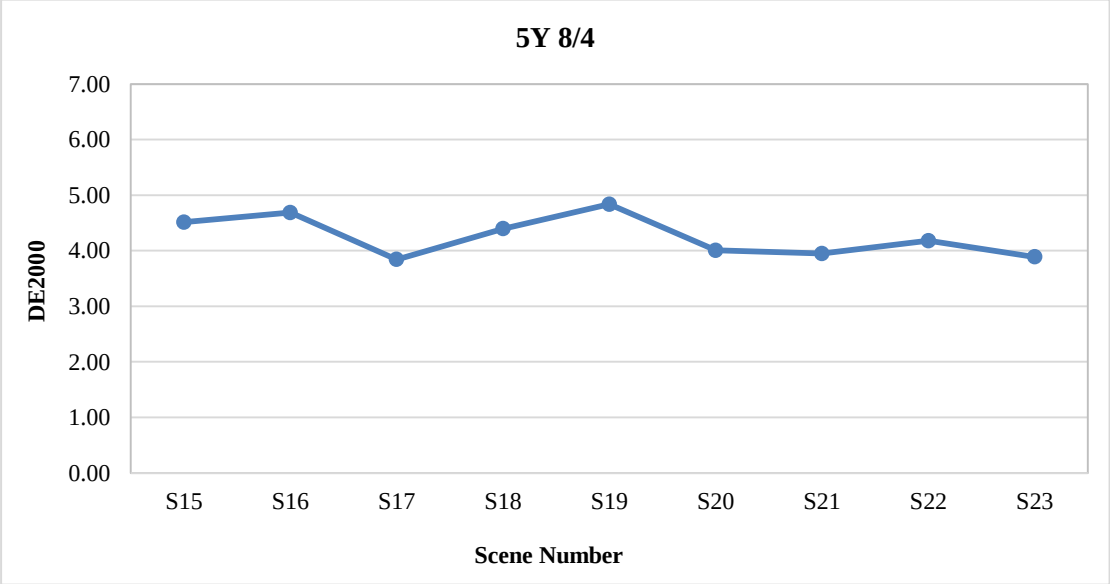

Figure 6.59 Colour differences between calculated and measured CIELAB values across scenes 15 to 23 for the wheel's Munsell Hue 5Y, keeping chroma/lightness at 8/4.

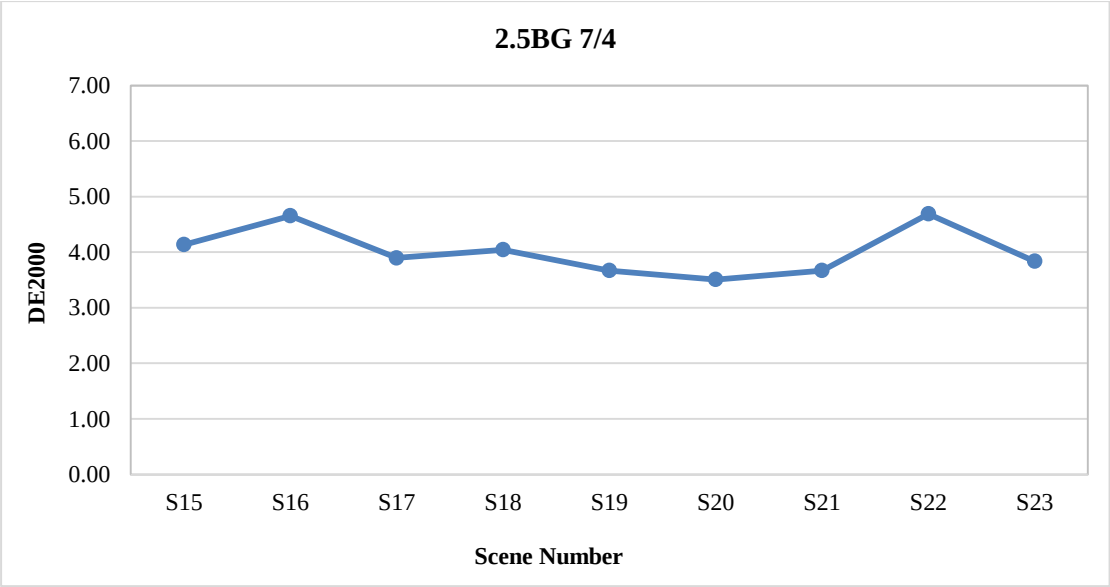

Figure 6.60 Colour differences between calculated and measured CIELAB values across scenes 15 to 23 for the wheel's Munsell Hue 2.5BG, keeping chroma/lightness at 7/4.

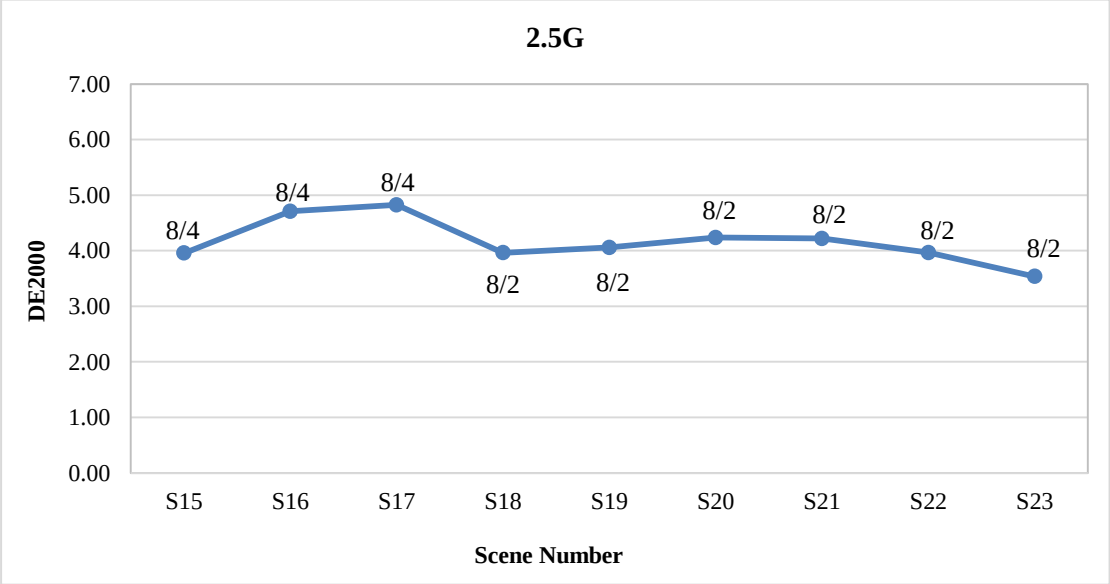

Figure 6.61 Colour differences between calculated and measured CIELAB values across scenes 15 to 23 for the wheel's Munsell Hue 2.5G.

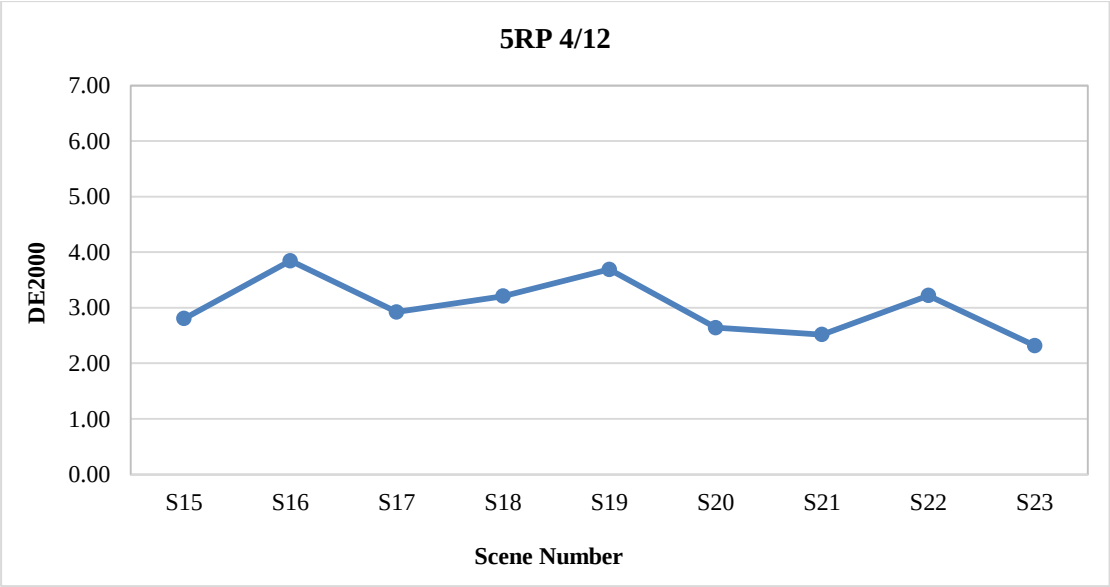

Figure 6.62 Colour differences between calculated and measured CIELAB values across scenes 15 to 23 for the wheel's Munsell Hue 5RP, keeping chroma/lightness at 4/12.

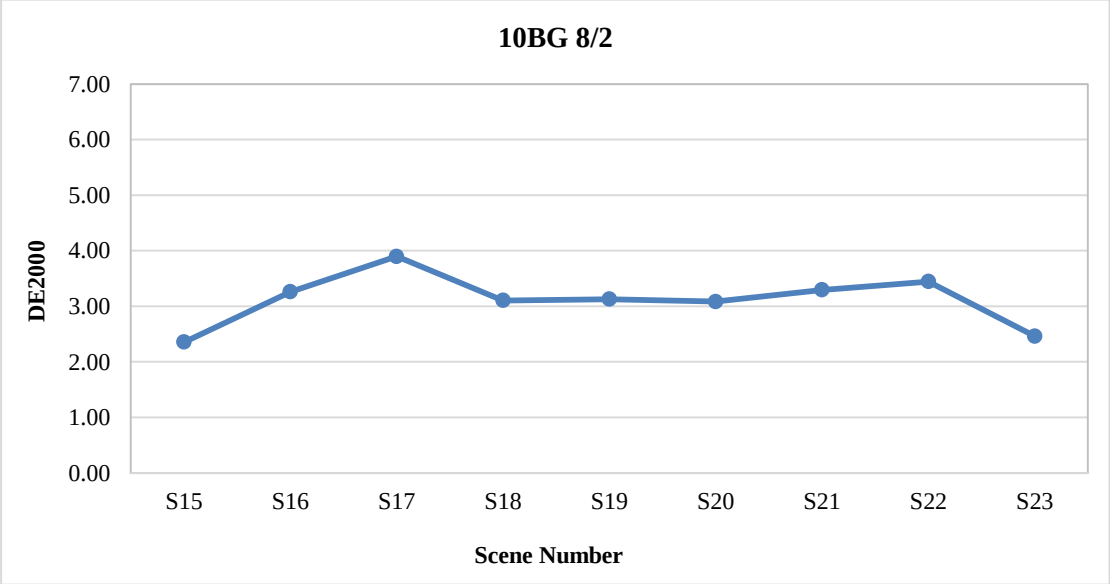

Figure 6.63 Colour differences between calculated and measured CIELAB values across scenes 15 to 23 for the wheel's Munsell Hue 10BG, keeping chroma/lightness at 8/2.

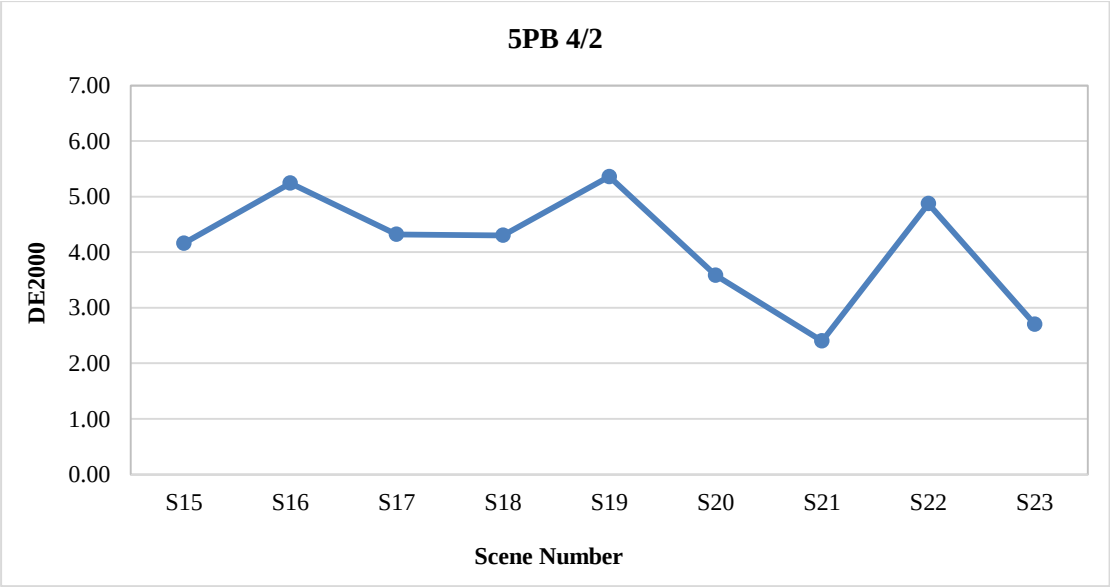

Figure 6.64 Colour differences between calculated and measured CIELAB values across scenes 15 to 23 for the wheel's Munsell Hue 5PB, keeping chroma/lightness at 4/2.

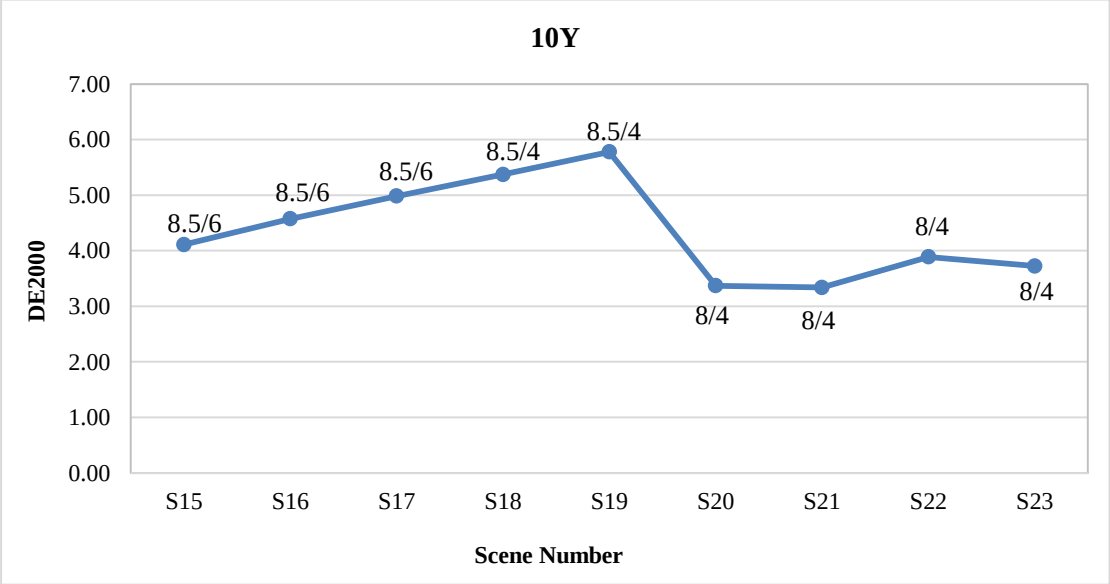

Figure 6.65 Colour differences between calculated and measured CIELAB values across scenes 15 to 23 for the wheel's Munsell Hue 10Y.

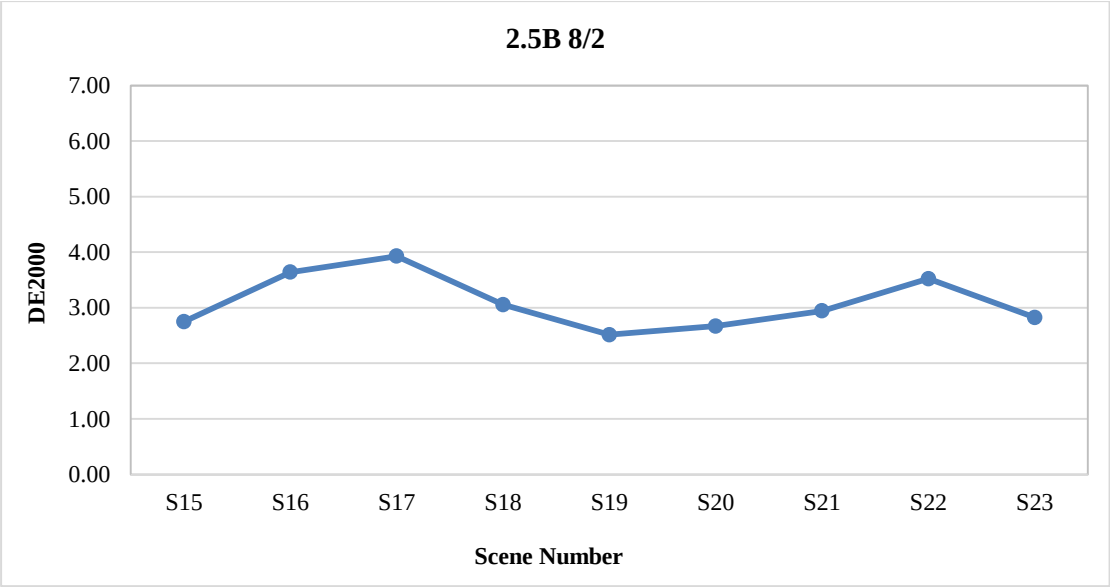

Figure 6.66 Colour differences between calculated and measured CIELAB values across scenes 15 to 23 for the wheel's Munsell Hue 2.5B, keeping chroma/lightness at 8/2.

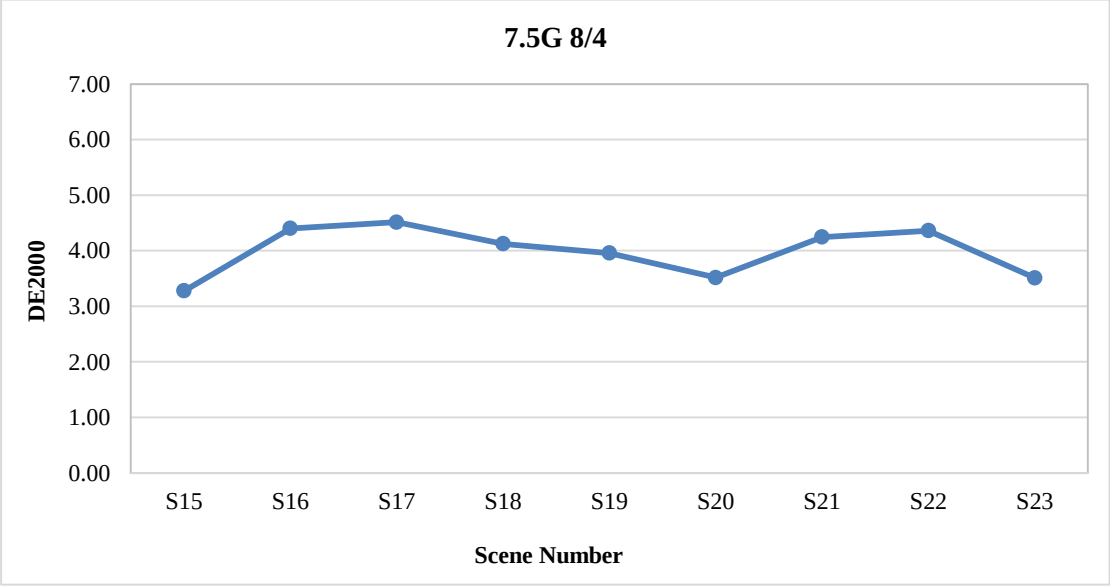

Figure 6.67 Colour differences between calculated and measured CIELAB values across scenes 15 to 23 for the wheel's Munsell Hue 7.5G, keeping chroma/lightness at 8/4.

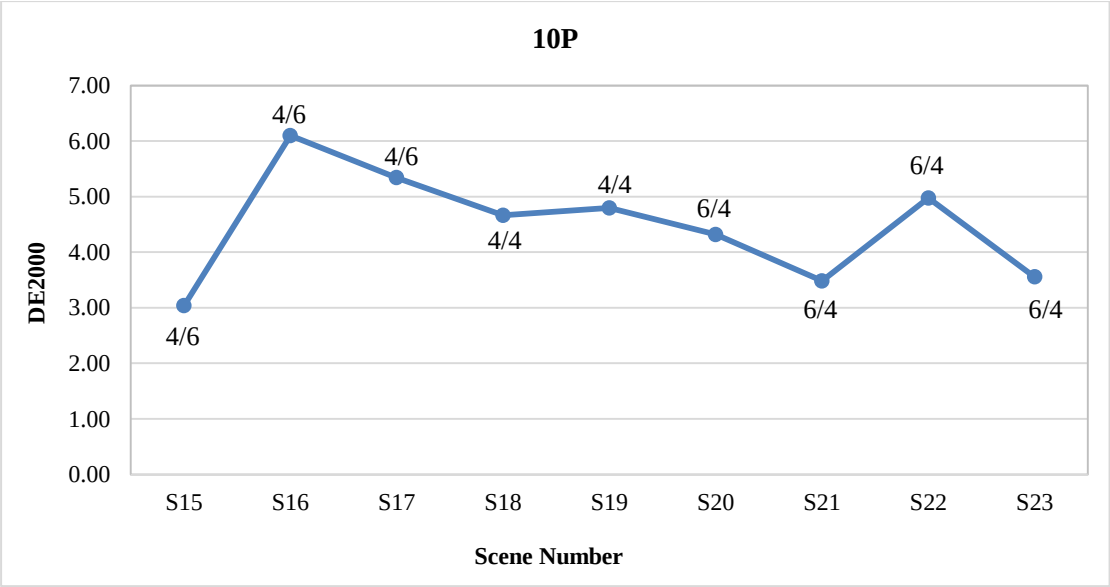

Figure 6.68 Colour differences between calculated and measured CIELAB values across scenes 15 to 23 for the wheel's Munsell Hue 10P.

The final aim is to show that the colour differences of the colour wheel between the reference light source and tested light source that are calculated from pictures are close to the ones measured with colorimetric devices. If these differences are very close to each other, then the colour shifts of the wheel's colours, when changing the light source, are described accurately by the calculated values. This will be reflected in good results obtained for the light quality assessments performed with digital cameras using the method described in this work because all light quality assessment methods (existing or proposed) rely basically on calculations that take into account these colour shifts.

The colour differences between calculated CIELAB data and colorimetric measured CIELAB values under each light source were important in the colour selection process for determining Munsell colour codes that are representing best the colour space regions were SLR cameras have a good response but are not important any more in this final stage. However the difference of their differences across reference and test light source, are important. The question is if the differences of the colour shifts between reference light source and test light source, calculated from the digital pictures, are close enough to the colorimetric measured ones, in order to allow the

replacement of colorimetric devices with digital cameras in the light quality assessment process.

Tables 6.12 to 6.15 show the sprectroradiometric CIELAB values calculated from pictures taken with the Canon CMOS and the Nikon CCD digital camera under the 4 considered light sources, compared with the CIELAB values measured with the colorimetric devices described in 4.3. The reference light sources are the fluorescent ones while the test light sources are the LED ones. The results for the D65 light sources are grouped in 2 tables: Table 6.12 shows the spectroradiometric calculations from pictures taken with Canon CMOS camera under fluorescent D65 and LED D65 and Table 6.14 shows the same type of results for the A light sources. Tables 6.13 and 6.15 lists the results obtained with the Nikon CCD camera in the same order as those presented in Tables 6.12 and 6.14. The spectrophotometric results of the colours under the D65 light sources obtained with both cameras have been presented in Tables 4.4 and 4.5, section 4.6 and have been discussed there.

Table 6.12 Canon EOS X4's spectroradiometric calculated values under the fluorescent D65 reference and LED D65 test light source, showing the ΔE_{00} between calculated and colourimetric measured CIELAB values.

Munsell	Fluorescent D65							LED D65						
Patches	R	G	B	L*	a*	b*	ΔE00	R	G	B	L*	a*	b*	ΔE00
N2	20	20	20	20.09	-0.23	-0.66	1.35	21	21	21	20.05	0.12	-0.56	0.75
N3.5	43	44	44	35.96	-0.46	-0.97	0.65	43	46	46	35.90	-1.05	-1.10	1.41
N5	86	88	88	55.73	-0.16	-1.14	3.93	86	91	92	55.79	-0.48	-1.60	4.34
N6.5	125	130	129	69.84	-0.64	-1.02	3.08	128	135	134	70.50	-0.53	-0.63	3.53
N8	161	169	167	80.88	-0.98	-0.93	1.49	161	171	169	80.66	-0.80	-0.39	0.40
N9.5	198	206	198	90.21	-1.13	1.09	5.28	196	207	202	89.82	-0.74	0.66	3.81
7.5P4/10	87	43	101	43.33	32.28	-27.20	2.10	91	46	109	44.26	33.36	-28.28	3.93
10PB4/6	61	51	98	42.76	16.51	-26.64	1.75	65	58	108	44.93	15.67	-26.93	4.86
2.5GY8/8	158	179	54	80.79	-19.82	52.34	2.99	158	182	58	80.81	-19.62	51.45	3.72
7.5GY7/10	92	163	36	73.48	-38.65	53.60	2.00	93	169	40	74.17	-39.29	53.04	3.17
10R6/8	177	79	58	61.05	31.29	25.81	2.86	179	82	61	61.42	31.76	25.95	5.02
7.5RP4/12	117	24	56	40.14	48.21	-3.03	0.86	124	27	61	41.67	49.09	-2.58	4.41
10YR7/4	153	132	82	71.25	0.46	24.76	3.54	157	137	84	71.96	0.73	26.26	1.71
7.5B8/4	136	185	196	83.11	-9.43	-9.00	2.88	136	187	199	82.89	-9.28	-8.82	3.46
7.5PB4/6	53	59	105	44.86	9.46	-27.29	3.36	54	62	112	45.27	9.90	-28.59	5.51
5P4/10	75	40	107	41.23	32.01	-33.90	2.94	82	44	115	42.86	33.21	-33.73	4.61
5R4/10	122	23	32	39.81	47.35	16.61	3.45	131	28	35	42.15	47.33	18.70	4.90
10GY7/8	87	169	80	75.18	-36.13	30.34	3.60	87	174	85	75.59	-36.71	29.79	5.50
5YR7/6	175	122	80	70.70	11.58	25.39	4.75	176	123	80	70.37	12.53	26.54	2.49
7.5R4/10	121	22	22	39.09	46.72	25.71	3.61	131	24	25	40.88	49.04	26.45	6.48
5Y8/4	165	165	102	79.16	-6.92	25.30	4.04	166	170	107	79.66	-7.10	25.18	3.20
2.5BG7/4	102	162	145	75.69	-18.22	0.23	4.26	106	169	152	76.76	-18.20	0.51	5.00
2.5G8/2	148	176	160	81.34	-8.17	2.49	4.41	151	182	166	82.12	-8.17	2.87	4.03
5RP4/12	115	29	67	41.61	45.54	-8.69	1.53	121	31	72	42.65	46.98	-8.65	5.33
10BG8/2	145	177	174	81.64	-7.34	-2.70	2.12	147	178	176	81.32	-6.34	-2.29	1.10
5PB4/2	49	58	68	42.68	-1.29	-8.58	2.48	57	65	75	45.11	-0.29	-7.69	5.63
10Y8/4	163	171	110	80.35	-8.80	23.07	5.01	164	173	113	80.22	-8.11	23.10	4.74
2.5B8/2	148	175	173	81.40	-5.93	-2.64	2.82	150	179	177	81.70	-5.76	-2.10	2.27
7.5G8/4	124	185	159	81.78	-18.24	3.37	5.27	129	192	167	82.86	-17.76	3.40	4.28
10P6/4	129	105	127	64.44	12.21	-8.02	4.27	133	109	134	65.09	13.25	-8.56	4.88

Mean	3.09	Mean	3.82
Max	5.28	Max	6.48
Min	0.65	Min	0.40
STD	1.28	STD	1.56

The mean colour difference between calculated and colorimetric measured CIELAB values in the fluorescent D65 light source is 3.09 ΔE_{00} units and the same type of difference in LED D65 light source is 3.82. The difference between these differences (3.82-3.09) is very small, 0.73 ΔE_{00} units, which is in the imperceptible interval of [0;1] ΔE_{00} units.

Table 6.13 Nikon D40x spectroradiometric calculated values under the fluorescent D65 reference and LED D65 test light source, showing the ΔE_{00} between calculated and colourimetric measured CIELAB values.

Munsell	Fluorescent D65							LED D65						
Patches	R	G	B	L*	a*	b*	ΔE00	R	G	B	L*	a*	b*	ΔE00
N2	47	47	45	21.36	0.25	-0.38	0.49	44	44	48	21.05	0.10	-1.16	0.29
N3.5	74	78	76	35.64	-1.06	-1.40	1.47	74	76	79	36.03	-0.96	-0.50	1.38
N5	115	120	118	52.49	-0.79	-1.69	1.90	118	118	120	52.87	-0.05	0.15	1.43
N6.5	157	161	156	67.08	-0.48	-0.16	0.89	156	161	164	67.47	-1.07	-1.30	1.67
N8	196	203	201	80.59	-0.49	-1.81	1.29	195	201	203	80.01	-1.00	-1.38	1.21
N9.5	249	255	244	96.06	-1.00	2.06	0.48	251	255	251	95.67	-0.61	0.51	1.77
7.5P4/10	124	78	130	42.90	29.17	-22.85	2.71	118	75	137	42.40	28.28	-25.16	3.40
10PB4/6	86	82	127	39.88	13.52	-26.13	1.95	87	79	134	40.20	15.35	-27.13	1.42
2.5GY8/8	203	218	85	82.59	-18.85	56.06	1.85	204	218	80	82.39	-20.11	59.73	1.77
7.5GY7/10	124	189	60	70.47	-37.66	52.86	2.75	130	188	49	70.65	-36.60	59.35	1.51
10R6/8	223	121	97	62.99	34.94	26.37	2.83	216	128	96	63.80	26.33	29.90	2.40
7.5RP4/12	160	61	94	42.69	44.69	-1.31	2.50	156	60	94	42.30	41.89	0.38	5.66
10YR7/4	195	171	116	71.57	2.26	27.05	1.65	194	169	116	71.15	0.95	28.61	0.87
7.5B8/4	161	216	230	82.11	-11.35	-12.98	2.15	164	212	232	81.29	-9.29	-12.93	1.17
7.5PB4/6	72	85	130	39.72	8.02	-28.19	2.53	73	80	133	39.25	10.11	-28.14	1.92
5P4/10	112	64	133	38.26	34.51	-31.91	1.16	106	63	139	38.21	32.50	-32.95	0.85
5R4/10	169	66	62	44.21	41.83	21.60	2.76	156	65	63	42.57	35.93	20.45	4.42
10GY7/8	118	193	102	71.70	-36.39	33.43	2.10	123	190	95	71.25	-35.22	38.45	0.95
5YR7/6	224	160	111	71.55	17.34	30.09	1.48	218	163	121	71.85	12.50	27.35	2.37
7.5R4/10	167	60	46	42.45	43.07	30.09	1.37	158	63	46	42.13	36.42	31.07	3.90
5Y8/4	209	207	136	81.15	-7.02	29.98	1.51	212	208	142	81.48	-7.32	29.70	1.33
2.5BG7/4	131	187	171	72.17	-18.20	-0.38	3.98	132	186	172	72.15	-18.34	1.41	1.97
2.5G8/2	185	213	194	81.98	-9.42	3.37	3.26	188	212	193	81.76	-9.42	5.74	1.70
5RP4/12	157	64	103	43.12	43.31	-6.26	3.24	152	63	116	43.06	41.96	-11.76	4.93
10BG8/2	179	207	205	80.49	-6.75	-3.93	3.30	176	207	209	80.30	-8.08	-3.86	1.34
5PB4/2	81	91	104	41.15	0.34	-10.71	1.76	80	89	106	41.37	-0.30	-9.18	2.97
10Y8/4	210	209	143	81.77	-6.74	27.45	2.55	212	214	141	82.76	-9.97	31.89	1.55
2.5B8/2	179	206	204	80.24	-6.47	-3.84	2.69	178	205	210	80.00	-6.47	-4.75	0.54
7.5G8/4	154	213	184	79.98	-20.38	4.91	4.04	158	218	189	81.34	-21.27	6.78	1.61
10P6/4	163	137	156	61.81	13.71	-7.87	2.01	163	136	164	62.16	13.57	-9.10	2.42
						Mean	2.16						Mean	2.02
						Max	4.04						Max	5.66
						Min	0.48						Min	0.29
						STD	0.92						STD	1.28

The difference of the differences resulted from table 19 is 0.13 ΔE_{00} units versus 0.73 in the precedent one. Both values are in the [0;1] ΔE_{00} interval where any colour differences are considered imperceptible. This shows that both cameras perform quite similar despite the proven superiority of the CCD sensors over the CMOS sensors.

Table 6.14 Canon EOS X4 spectroradiometric calculated values under the fluorescent A reference and LED A test light source, showing the ΔE_{00} between calculated and colorimetric measured CIELAB values.

Munsell	Fluorescent A							LED A						
Patches	R	G	B	L*	a*	b*	ΔE00	R	G	B	L*	a*	b*	ΔE00
N2	29	21	17	19.44	-0.64	-1.99	2.45	28	20	19	19.06	-0.34	-1.46	2.37
N3.5	62	47	36	36.52	-0.56	-0.55	0.57	61	48	43	37.22	-1.34	-0.85	1.19
N5	120	92	67	57.19	0.69	2.61	4.77	119	92	79	57.42	0.53	1.54	5.80
N6.5	158	130	97	70.13	-0.83	1.03	2.36	159	129	113	70.19	-0.12	-0.02	3.37
N8	193	163	127	80.14	-0.96	-1.67	2.93	192	162	144	79.95	-0.97	-1.63	1.17
N9.5	225	196	156	88.99	-1.67	-3.61	9.50	224	194	171	88.49	-1.68	-1.64	6.32
7.5P4/10	135	47	76	46.63	27.90	-18.29	5.28	149	47	89	48.71	31.70	-16.12	5.15
10PB4/6	93	55	76	43.99	10.36	-23.20	4.08	92	57	87	44.87	8.92	-21.88	5.66
2.5GY8/8	191	178	51	82.09	-9.50	45.32	5.21	188	176	61	81.59	-9.61	43.39	4.67
7.5GY7/10	122	163	39	74.57	-24.03	43.26	4.91	117	164	52	74.73	-25.15	39.11	5.79
10R6/8	218	97	40	67.00	25.18	39.05	6.70	219	101	48	68.11	23.56	38.91	6.60
7.5RP4/12	173	31	48	47.10	44.86	6.71	0.40	199	30	61	50.83	50.83	8.30	2.86
10YR7/4	192	142	57	74.71	2.19	33.49	5.01	194	139	70	74.40	3.78	30.51	3.83
7.5B8/4	168	172	154	80.83	-8.18	-14.89	4.85	168	171	168	80.62	-8.22	-12.10	5.12
7.5PB4/6	71	54	74	41.25	3.06	-26.24	2.20	72	57	87	42.80	2.02	-25.34	3.55
5P4/10	116	36	75	41.01	28.74	-26.31	3.41	119	38	86	42.32	28.35	-24.32	3.96
5R4/10	176	36	28	48.24	42.42	28.39	2.53	190	35	36	50.20	45.99	28.14	2.71
10GY7/8	115	161	61	73.97	-24.22	27.60	4.48	110	165	77	74.84	-26.03	24.56	5.87
5YR7/6	212	130	52	73.65	11.42	36.60	7.79	214	132	64	74.39	11.14	34.88	6.82
7.5R4/10	174	35	21	47.62	42.28	35.70	3.55	183	34	24	48.85	44.67	38.11	1.83
5Y8/4	196	168	71	80.59	-4.48	31.17	4.11	198	165	88	80.27	-2.86	27.23	3.40
2.5BG7/4	135	151	112	73.61	-12.87	-3.46	6.30	136	156	129	74.96	-13.93	-2.22	4.83
2.5G8/2	177	168	120	80.02	-6.82	1.60	4.51	177	171	138	80.75	-7.62	1.98	4.04
5RP4/12	164	32	54	46.17	42.49	-0.30	1.47	190	33	69	50.36	47.80	1.28	2.66
10BG8/2	174	166	133	79.62	-6.22	-5.88	4.23	174	168	151	80.13	-6.81	-4.99	3.79
5PB4/2	73	57	54	41.87	0.02	-9.44	2.18	76	62	64	44.28	-1.23	-7.36	3.93
10Y8/4	199	168	82	80.93	-3.24	24.90	5.47	199	169	97	81.24	-3.47	23.61	4.81
2.5B8/2	176	164	134	79.35	-5.06	-6.74	4.44	176	166	149	79.82	-5.83	-4.46	3.46
7.5G8/4	156	176	122	80.45	-14.22	0.71	6.61	152	177	139	80.52	-15.37	0.75	6.13
10P6/4	171	102	95	64.67	13.14	-4.84	2.17	173	105	110	65.77	12.41	-4.08	3.32
						Mean	4.15						Mean	4.17
						Max	9.50						Max	6.82
						Min	0.40						Min	1.17
						STD	2.06						STD	1.56

Table 6.14 and 6.15 show colour differences between calculated and colorimetric measured CIELAB values that are greater than the ones listed in Tables 6.12 and 6.13 for the D65 light sources. This is normal, considering the great SPD differences and the fact that the colours were mainly optimized under the D65 light sources for the reasons explained in chapter 4. The difference of differences is low: 0.5 ΔE_{00} units for

the Canon camera and 0.75 ΔE_{00} units for the Nikon D40x camera, both values being in the imperceptible colour difference interval of [0;1], so the performances of the two cameras keep staying close even when changing the light source type by means of correlated colour temperature.

Table 6.15 Nikon D40x spectroradiometric calculated values under the fluorescent A reference and LED A test light source, showing the ΔE_{00} between calculated and colouimetrically measured CIELAB values.

Munsell	Fluorescent A							LED A						
Patches	R	G	B	L*	a*	b*	ΔE00	R	G	B	L*	a*	b*	ΔE00
N2	46	32	11	20.73	-0.25	1.09	2.17	46	30	13	20.64	0.12	1.01	2.15
N3.5	78	58	27	36.43	-0.48	-3.71	2.96	77	56	31	36.65	-1.15	-3.25	2.34
N5	120	93	47	53.46	-1.08	-2.91	3.73	119	89	54	53.37	-1.06	-3.64	3.41
N6.5	159	124	67	66.72	-0.56	-2.55	3.03	158	120	75	66.86	-0.97	-2.12	1.45
N8	201	160	88	80.26	-1.04	0.21	2.12	200	154	98	80.10	-0.92	0.07	1.12
N9.5	254	203	113	95.18	-0.60	4.33	2.48	255	196	125	95.15	0.11	4.40	2.01
7.5P4/10	125	61	59	44.43	19.04	-27.80	5.18	132	60	63	45.81	20.15	-22.35	5.75
10PB4/6	96	65	58	42.29	6.77	-30.63	4.04	93	62	62	41.86	5.47	-28.18	2.77
2.5GY8/8	202	172	7	82.21	-9.84	70.67	2.43	200	162	26	81.12	-8.05	56.52	1.82
7.5GY7/10	127	148	0	70.24	-24.53	62.71	5.84	124	139	11	68.98	-23.62	55.19	5.99
10R6/8	215	99	34	64.98	26.30	29.38	5.11	212	99	39	65.73	23.67	30.04	4.66
7.5RP4/12	156	50	39	44.90	33.34	-4.55	7.71	172	49	42	47.75	37.35	2.80	6.52
10YR7/4	195	139	38	73.33	2.28	33.51	5.03	195	131	48	72.65	4.04	28.74	3.51
7.5B8/4	172	165	108	79.89	-9.54	-14.99	3.67	173	160	117	80.09	-9.52	-12.94	3.92
7.5PB4/6	80	62	58	39.61	3.02	-34.96	2.49	79	61	62	40.09	1.20	-31.09	1.24
5P4/10	113	52	61	40.25	20.60	-36.33	6.01	113	50	64	40.26	19.95	-32.01	4.56
5R4/10	164	53	20	46.28	33.06	23.31	5.91	172	51	25	47.79	35.48	23.32	5.00
10GY7/8	119	147	26	69.73	-25.24	38.68	4.55	119	141	39	69.65	-24.16	30.52	4.51
5YR7/6	216	129	41	72.74	13.29	30.86	5.86	218	125	49	73.24	13.90	29.55	4.23
7.5R4/10	165	52	12	45.99	33.54	36.28	5.36	168	50	15	46.71	34.42	36.02	4.53
5Y8/4	208	165	44	81.30	-3.77	37.27	2.85	209	156	59	80.66	-1.44	29.50	1.82
2.5BG7/4	137	142	75	70.40	-13.81	-4.62	6.00	140	139	83	71.23	-13.66	-2.66	5.24
2.5G8/2	186	163	84	79.83	-6.84	2.23	4.12	186	160	93	80.53	-7.67	3.74	3.36
5RP4/12	151	50	45	44.37	32.26	-12.45	7.64	167	51	49	47.70	35.20	-4.93	6.60
10BG8/2	181	160	93	78.86	-6.41	-5.78	4.15	181	157	102	79.54	-7.29	-3.80	3.23
5PB4/2	85	66	40	40.69	-0.41	-13.99	3.29	86	65	45	41.56	-1.08	-12.06	2.27
10Y8/4	211	163	53	81.17	-1.59	29.39	3.10	213	160	65	82.11	-1.50	26.73	2.68
2.5B8/2	182	159	93	78.67	-5.74	-6.02	3.61	184	156	103	79.51	-5.97	-4.45	3.33
7.5G8/4	161	166	81	78.84	-15.31	2.61	5.41	159	162	91	79.20	-16.23	2.75	5.20
10P6/4	166	104	69	61.80	10.92	-10.88	5.66	165	103	76	62.62	9.18	-8.57	4.82
						Mean	4.38						Mean	3.67
						Max	7.71						Max	6.60
						Min	2.12						Min	1.12
						STD	1.56						STD	1.59

In Table 6.16 are listed the colour differences between the individual measured colours of the colour wheel under the D65 light sources (reference and test) and between their calculated values from Canon pictures taken under the 2 light sources in the specified conditions, as well as the difference of these differences.

Table 6. 16 Colour differences between the individual measured colours of the colour wheel under the D65 light sources (reference and test) and between their calculated values from Canon EOS X4 pictures taken under the 2 light sources.

	Konica Minolta Spectroradiometric measurement (D65/2)							Canon Digital Camera							
	Fluorescent D65			LED D65				Fluorescent D65			LED D65				
Samples	L*	a*	b*	L*	a*	b*	DE00	L*	a*	b*	L*	a*	b*	DE00	$\Delta(\Delta E_{00})$
N2	21.97	-0.01	-0.60	21.04	0.15	-0.86	0.74	20.09	-0.23	-0.66	20.05	0.12	-0.56	0.52	0.22
N3.5	36.41	-0.41	-0.42	35.87	-0.07	-1.00	0.88	35.96	-0.46	-0.97	35.90	-1.05	-1.10	0.84	0.04
N5	51.96	-0.37	0.36	51.51	-0.08	-0.34	0.93	55.73	-0.16	-1.14	55.79	-0.48	-1.60	0.63	0.30
N6.5	66.44	-0.85	0.49	66.04	-0.42	-0.45	1.16	69.84	-0.64	-1.02	70.50	-0.53	-0.63	0.65	0.51
N8	81.49	-1.04	0.53	80.86	-0.55	-0.47	1.28	80.88	-0.98	-0.93	80.66	-0.80	-0.39	0.59	0.69
N9.5	96.36	0.96	3.46	95.48	-0.88	2.36	2.89	90.21	-1.13	1.09	89.82	-0.74	0.66	0.72	2.18
7.5P4/10	41.40	34.51	-26.72	40.05	34.00	-30.27	2.29	43.33	32.28	-27.20	44.26	33.36	-28.28	1.01	1.28
10PB4/6	41.17	14.84	-24.89	39.71	17.37	-27.20	1.92	42.76	16.51	-26.64	44.93	15.67	-26.93	2.14	0.22
2.5GY8/8	82.40	-21.89	62.22	81.86	-23.67	64.59	0.92	80.79	-19.82	52.34	80.81	-19.62	51.45	0.27	0.65
7.5GY7/10	72.61	-43.71	59.55	71.89	-40.08	61.78	1.92	73.48	-38.65	53.60	74.17	-39.29	53.04	0.64	1.29
10R6/8	59.97	37.83	27.91	61.01	25.61	29.72	7.21	61.05	31.29	25.81	61.42	31.76	25.95	0.39	6.83
7.5RP4/12	40.61	49.80	-1.95	37.79	44.88	-7.24	4.03	40.14	48.21	-3.03	41.67	49.09	-2.58	1.42	2.61
10YR7/4	71.67	3.92	29.42	71.16	0.06	29.59	3.27	71.25	0.46	24.76	71.96	0.73	26.26	0.91	2.35
7.5B8/4	81.75	-12.69	-10.61	80.24	-8.25	-12.64	4.49	83.11	-9.43	-9.00	82.89	-9.28	-8.82	0.23	4.27
7.5PB4/6	41.31	8.67	-25.49	39.76	12.27	-27.66	2.47	44.86	9.46	-27.29	45.27	9.90	-28.59	0.71	1.76
5P4/10	39.39	34.12	-30.55	37.68	34.20	-33.32	2.03	41.23	32.01	-33.90	42.86	33.21	-33.73	1.61	0.41
5R4/10	42.05	46.69	21.48	38.51	36.76	16.52	4.79	39.81	47.35	16.61	42.15	47.33	18.70	2.38	2.41
10GY7/8	72.55	-40.83	38.44	70.88	-37.56	40.40	2.18	75.18	-36.13	30.34	75.59	-36.71	29.79	0.50	1.67
5YR7/6	70.70	19.07	29.62	70.39	11.29	30.41	5.83	70.70	11.58	25.39	70.37	12.53	26.54	0.76	5.07
7.5R4/10	41.75	46.27	30.58	38.26	35.50	27.25	5.03	39.09	46.72	25.71	40.88	49.04	26.45	1.74	3.29
5Y8/4	81.95	-6.96	33.23	80.46	-8.09	32.36	1.42	79.16	-6.92	25.30	79.66	-7.10	25.18	0.39	1.03
2.5BG7/4	72.61	-22.37	4.21	70.80	-18.87	3.76	2.45	75.69	-18.22	0.23	76.76	-18.20	0.51	0.80	1.65
2.5G8/2	82.11	-11.33	7.51	80.99	-9.94	8.00	1.54	81.34	-8.17	2.49	82.12	-8.17	2.87	0.62	0.92
5RP4/12	40.89	49.77	-9.82	37.82	45.13	-14.89	4.10	41.61	45.54	-8.69	42.65	46.98	-8.65	1.06	3.04
10BG8/2	81.73	-9.44	-2.13	80.13	-6.99	-2.73	2.71	81.64	-7.34	-2.70	81.32	-6.34	-2.29	1.07	1.63
5PB4/2	40.98	0.16	-8.22	39.72	1.59	-9.31	2.34	42.68	-1.29	-8.58	45.11	-0.29	-7.69	2.68	0.34
10Y8/4	82.48	-8.50	33.18	81.00	-11.36	33.64	2.17	80.35	-8.80	23.07	80.22	-8.11	23.10	0.58	1.59
2.5B8/2	81.59	-8.73	-2.80	79.66	-6.39	-4.15	3.05	81.40	-5.93	-2.64	81.70	-5.76	-2.10	0.52	2.53
7.5G8/4	82.37	-25.70	9.46	80.78	-21.07	9.13	2.66	81.78	-18.24	3.37	82.86	-17.76	3.40	0.80	1.86
10P6/4	60.93	16.12	-7.30	59.38	13.58	-8.85	2.67	64.44	12.21	-8.02	65.09	13.25	-8.56	0.99	1.68
						Average:	2.71					Average:		0.94	Max: 6.83

The average measured colourimetric differences for all wheel's colours between the D65 light sources is 2.71 ΔE_{00} units and the average of the differences between the calculated CIELAB values in the 2 lights is 0.94. The difference of these differences is 1.77, which means that the difference in colour shifts from reference to test light source determined with the digital camera method is close to the difference in colour

shifts measured colorimetric. There are however 3 individual colours for that the difference of the differences exceed 4 ΔE_{00} units. They are marked with red in Table 6.16. Although they should not affect the general CRI, they might affect the special CRI. Usually, the special CRI for 4.5R4/13 is checked, but the CRI sample had to be replaced with 10R5/8.

Table 6.17 shows the colour differences between the individual measured colours of the colour wheel under the reference light source fluorescent D65 and test light source LED D65 and between their calculated values from Nikon D40x pictures taken under the 2 light sources in the specified conditions, as well as the difference of these differences.

Table 6.17 Colour differences between the individual measured colours of the colour wheel under the D65 light sources (reference and test) and between their calculated values from Nikon D40x pictures taken under the 2 light sources

	Konica Minolta Spectroradiometric measurement (D65/2)							Nikon Digital Camera							
	Fluorescent D65			LED D65				Fluorescent D65			LED D65				
Samples	L*	a*	b*	L*	a*	b*	DE00	L*	a*	b*	L*	a*	b*	DE00	$\Delta(\Delta E_{00})$
N2	21.97	-0.01	-0.60	21.04	0.15	-0.86	0.74	21.36	0.25	-0.38	21.05	0.10	-1.16	0.82	0.08
N3.5	36.41	-0.41	-0.42	35.87	-0.07	-1.00	0.88	35.64	-1.06	-1.40	36.03	-0.96	-0.50	0.92	0.04
N5	51.96	-0.37	0.36	51.51	-0.08	-0.34	0.93	52.49	-0.79	-1.69	52.87	-0.05	0.15	2.09	1.16
N6.5	66.44	-0.85	0.49	66.04	-0.42	-0.45	1.16	67.08	-0.48	-0.16	67.47	-1.07	-1.30	1.39	0.24
N8	81.49	-1.04	0.53	80.86	-0.55	-0.47	1.28	80.59	-0.49	-1.81	80.01	-1.00	-1.38	0.93	0.35
N9.5	96.36	0.96	3.46	95.48	-0.88	2.36	2.89	96.06	-1.00	2.06	95.67	-0.61	0.51	1.56	1.34
7.5P4/10	41.40	34.51	-26.72	40.05	34.00	-30.27	2.29	42.90	29.17	-22.85	42.40	28.28	-25.16	1.60	0.69
10PB4/6	41.17	14.84	-24.89	39.71	17.37	-27.20	1.92	39.88	13.52	-26.13	40.20	15.35	-27.13	1.05	0.87
2.5GY8/8	82.40	-21.89	62.22	81.86	-23.67	64.59	0.92	82.59	-18.85	56.06	82.39	-20.11	59.73	1.05	0.13
7.5GY7/10	72.61	-43.71	59.55	71.89	-40.08	61.78	1.92	70.47	-37.66	52.86	70.65	-36.60	59.35	2.38	0.46
10R6/8	59.97	37.83	27.91	61.01	25.61	29.72	7.21	62.99	34.94	26.37	63.80	26.33	29.90	6.09	1.12
7.5RP4/12	40.61	49.80	-1.95	37.79	44.88	-7.24	4.03	42.69	44.69	-1.31	42.30	41.89	0.38	1.36	2.67
10YR7/4	71.67	3.92	29.42	71.16	0.06	29.59	3.27	71.57	2.26	27.05	71.15	0.95	28.61	1.41	1.85
7.5B8/4	81.75	-12.69	-10.61	80.24	-8.25	-12.64	4.49	82.11	-11.35	-12.98	81.29	-9.29	-12.93	1.84	2.65
7.5PB4/6	41.31	8.67	-25.49	39.76	12.27	-27.66	2.47	39.72	8.02	-28.19	39.25	10.11	-28.14	1.72	0.76
5P4/10	39.39	34.12	-30.55	37.68	34.20	-33.32	2.03	38.26	34.51	-31.91	38.21	32.50	-32.95	1.33	0.69
5R4/10	42.05	46.69	21.48	38.51	36.76	16.52	4.79	44.21	41.83	21.60	42.57	35.93	20.45	2.71	2.08
10GY7/8	72.55	-40.83	38.44	70.88	-37.56	40.40	2.18	71.70	-36.39	33.43	71.25	-35.22	38.45	2.35	0.17
5YR7/6	70.70	19.07	29.62	70.39	11.29	30.41	5.83	71.55	17.34	30.09	71.85	12.50	27.35	3.10	2.73
7.5R4/10	41.75	46.27	30.58	38.26	35.50	27.25	5.03	42.45	43.07	30.09	42.13	36.42	31.07	3.45	1.59
5Y8/4	81.95	-6.96	33.23	80.46	-8.09	32.36	1.42	81.15	-7.02	29.98	81.48	-7.32	29.70	0.37	1.05
2.5BG7/4	72.61	-22.37	4.21	70.80	-18.87	3.76	2.45	72.17	-18.20	-0.38	72.15	-18.34	1.41	1.31	1.14
2.5G8/2	82.11	-11.33	7.51	80.99	-9.94	8.00	1.54	81.98	-9.42	3.37	81.76	-9.42	5.74	1.84	0.30
5RP4/12	40.89	49.77	-9.82	37.82	45.13	-14.89	4.10	43.12	43.31	-6.26	43.06	41.96	-11.76	2.91	1.19
10BG8/2	81.73	-9.44	-2.13	80.13	-6.99	-2.73	2.71	80.49	-6.75	-3.93	80.30	-8.08	-3.86	1.35	1.35
5PB4/2	40.98	0.16	-8.22	39.72	1.59	-9.31	2.34	41.15	0.34	-10.71	41.37	-0.30	-9.18	1.35	0.99
10Y8/4	82.48	-8.50	33.18	81.00	-11.36	33.64	2.17	81.77	-6.74	27.45	82.76	-9.97	31.89	2.70	0.53
2.5B8/2	81.59	-8.73	-2.80	79.66	-6.39	-4.15	3.05	80.24	-6.47	-3.84	80.00	-6.47	-4.75	0.77	2.28
7.5G8/4	82.37	-25.70	9.46	80.78	-21.07	9.13	2.66	79.98	-20.38	4.91	81.34	-21.27	6.78	1.58	1.08
10P6/4	60.93	16.12	-7.30	59.38	13.58	-8.85	2.67	61.81	13.71	-7.87	62.16	13.57	-9.10	0.91	1.76
						Average:	2.71						Average:	1.81	Max 2.73

The difference in colour shifts from reference to test light source determined with the Nikon D40x CCD digital camera is even closer to the difference in colour shifts measured colorimetric than in case of the Canon EOS X4 CMOS camera, as can be seen by comparing Table 6.17 with 6.16. For the Nikon camera, no difference of the differences is above 3 ΔE_{00} units, the maximum being 2.73 ΔE_{00} units. The average colour differences under the 2 lights for colorimetric measured CIELAB values are very close to the average colour differences determined from calculated CIELAB values: 2.71-1.81=0.9. General CRI and special CRI must therefore result very accurately when using Nikon D40x camera with the described method.

Table 6.18 uses the same template as Table 6.16 for presenting the results obtained with Canon camera for the fluorescent A and LED A light sources.

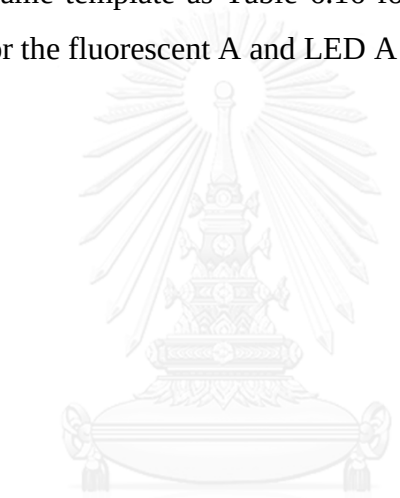

Table 6.18 Colour differences between the individual measured colours of the colour wheel under the illuminant A sources (reference and test) and between their calculated values from Canon EOS X4 pictures taken under the 2 light sources.

	Konica Minolta Spectroradiometric measurement (D65/2)							Canon Digital Camera							
	Fluorescent A			LED A				Fluorescent A			LED A				
Samples	L*	a*	b*	L*	a*	b*	DE00	L*	a*	b*	L*	a*	b*	DE00	$\Delta(\Delta E_{00})$
N2	22.22	0.04	-0.79	22.31	-0.11	-0.79	0.23	19.44	-0.64	-1.99	19.06	-0.34	-1.46	0.69	0.46
N3.5	36.86	-0.22	-0.51	36.29	-0.72	-1.04	1.00	36.52	-0.56	-0.55	37.22	-1.34	-0.85	1.28	0.28
N5	52.68	0.22	0.43	51.85	-0.43	-0.40	1.51	57.19	0.69	2.61	57.42	0.53	1.54	1.02	0.49
N6.5	67.53	-0.10	0.47	66.30	-0.97	-0.66	1.94	70.13	-0.83	1.03	70.19	-0.12	-0.02	1.45	0.49
N8	82.65	-0.12	0.45	81.16	-1.05	-0.78	2.06	80.14	-0.96	-1.67	79.95	-0.97	-1.63	0.13	1.93
N9.5	97.57	0.81	4.18	96.04	-0.06	2.19	2.30	88.99	-1.67	-3.61	88.49	-1.68	-1.64	1.79	0.51
7.5P4/10	43.94	26.74	-26.00	44.69	30.54	-21.86	3.65	46.63	27.90	-18.29	48.71	31.70	-16.12	3.18	0.47
10PB4/6	41.13	8.07	-25.56	40.39	6.82	-25.70	1.30	43.99	10.36	-23.20	44.87	8.92	-21.88	1.27	0.03
2.5GY8/8	83.68	-10.04	62.29	81.96	-10.99	58.58	1.76	82.09	-9.50	45.32	81.59	-9.61	43.39	0.78	0.98
7.5GY7/10	71.41	-33.40	54.87	69.83	-34.64	50.96	2.06	74.57	-24.03	43.26	74.73	-25.15	39.11	1.97	0.09
10R6/8	66.70	37.43	39.61	66.16	33.99	37.78	1.45	67.00	25.18	39.05	68.11	23.56	38.91	1.31	0.14
7.5RP4/12	46.87	45.62	6.38	48.44	53.37	11.28	3.55	47.10	44.86	6.71	50.83	50.83	8.30	4.21	0.65
10YR7/4	74.59	8.56	33.35	73.11	8.48	31.31	1.40	74.71	2.19	33.49	74.40	3.78	30.51	1.91	0.51
7.5B8/4	79.92	-13.97	-14.17	79.11	-14.59	-15.40	0.93	80.83	-8.18	-14.89	80.62	-8.22	-12.10	1.75	0.82
7.5PB4/6	40.01	1.61	-27.81	39.72	0.48	-27.56	0.91	41.25	3.06	-26.24	42.80	2.02	-25.34	1.56	0.65
5P4/10	41.43	25.04	-29.67	40.50	24.23	-27.75	1.23	41.01	28.74	-26.31	42.32	28.35	-24.32	1.56	0.33
5R4/10	49.24	45.41	33.78	48.37	48.68	32.78	1.94	48.24	42.42	28.39	50.20	45.99	28.14	2.51	0.57
10GY7/8	70.66	-32.40	34.24	68.99	-34.32	31.75	2.07	73.97	-24.22	27.60	74.84	-26.03	24.56	2.12	0.05
5YR7/6	75.80	22.58	36.74	74.20	21.00	35.19	1.44	73.65	11.42	36.60	74.39	11.14	34.88	0.86	0.58
7.5R4/10	49.30	45.04	43.46	47.62	46.31	41.65	2.13	47.62	42.28	35.70	48.85	44.67	38.11	1.56	0.58
5Y8/4	84.58	-1.43	35.57	81.94	-0.30	32.55	2.29	80.59	-4.48	31.17	80.27	-2.86	27.23	2.01	0.28
2.5BG7/4	70.69	-19.61	1.03	69.84	-20.74	-0.32	1.36	73.61	-12.87	-3.46	74.96	-13.93	-2.22	1.67	0.31
2.5G8/2	81.86	-9.27	6.60	80.90	-11.22	5.59	2.12	80.02	-6.82	1.60	80.75	-7.62	1.98	0.99	1.13
5RP4/12	46.72	44.04	-2.71	47.89	50.80	2.08	3.48	46.17	42.49	-0.30	50.36	47.80	1.28	4.58	1.10
10BG8/2	80.86	-9.30	-3.06	80.09	-10.74	-4.76	1.81	79.62	-6.22	-5.88	80.13	-6.81	-4.99	1.09	0.72
5PB4/2	40.60	-1.39	-9.33	40.33	-1.74	-9.44	0.50	41.87	0.02	-9.44	44.28	-1.23	-7.36	3.18	2.68
10Y8/4	83.85	0.05	34.52	82.97	-1.24	32.78	1.37	80.93	-3.24	24.90	81.24	-3.47	23.61	0.73	0.64
2.5B8/2	80.59	-8.58	-4.50	79.99	-9.30	-5.76	1.17	79.35	-5.06	-6.74	79.82	-5.83	-4.46	2.15	0.98
7.5G8/4	80.52	-23.50	6.16	79.61	-25.13	4.22	1.77	80.45	-14.22	0.71	80.52	-15.37	0.75	0.84	0.93
10P6/4	62.65	14.96	-5.00	62.10	13.75	-5.40	1.08	64.67	13.14	-4.84	65.77	12.41	-4.08	1.16	0.08
						Average:	1.73					Average:		1.71	Max 2.68

Unlike the results presented in Table 6.16, where 3 colours had to be marked with red, in this case no difference of the differences is above 3 ΔE_{00} units, the maximum being 2.68 ΔE_{00} units. For the incandescent type of light sources, the average colour differences under the 2 lights for colorimetric measured CIELAB values are very close to the average colour differences determined from calculated CIELAB values: 1.73-1.71=0.02, therefore general CRI and special CRI must be very accurate for the A type light sources when using Canon camera with the described method.

Table 6.19 uses the same template as Table 6.17 for presenting the results obtained with Nikon camera for the fluorescent A and LED A light sources.

Table 6.19 Colour differences between the individual measured colours of the colour wheel under the illuminant A sources (reference and test) and between their calculated values from Nikon D40x pictures taken under the 2 light sources.

	Fluorescent A			LED A				Fluorescent A			LED A				
Samples	L*	a*	b*	L*	a*	b*	DE00	L*	a*	b*	L*	a*	b*	DE00	$\Delta(\Delta E_{00})$
N2	22.22	0.04	-0.79	22.31	-0.11	-0.79	0.23	20.73	-0.25	1.09	20.64	0.12	1.01	0.23	0.56
N3.5	36.86	-0.22	-0.51	36.29	-0.72	-1.04	1.00	36.43	-0.48	-3.71	36.65	-1.15	-3.25	1.00	1.03
N5	52.68	0.22	0.43	51.85	-0.43	-0.40	1.51	53.46	-1.08	-2.91	53.37	-1.06	-3.64	1.51	0.64
N6.5	67.53	-0.10	0.47	66.30	-0.97	-0.66	1.94	66.72	-0.56	-2.55	66.86	-0.97	-2.12	1.94	0.71
N8	82.65	-0.12	0.45	81.16	-1.05	-0.78	2.06	80.26	-1.04	0.21	80.10	-0.92	0.07	2.06	0.25
N9.5	97.57	0.81	4.18	96.04	-0.06	2.19	2.30	95.18	-0.60	4.33	95.15	0.11	4.40	2.30	1.02
7.5P4/10	43.94	26.74	-26.00	44.69	30.54	-21.86	3.65	44.43	19.04	-27.80	45.81	20.15	-22.35	3.65	3.97
10PB4/6	41.13	8.07	-25.56	40.39	6.82	-25.70	1.30	42.29	6.77	-30.63	41.86	5.47	-28.18	1.30	0.89
2.5GY8/8	83.68	-10.04	62.29	81.96	-10.99	58.58	1.76	82.21	-9.84	70.67	81.12	-8.05	56.52	1.76	3.74
7.5GY7/10	71.41	-33.40	54.87	69.83	-34.64	50.96	2.06	70.24	-24.53	62.71	68.98	-23.62	55.19	2.06	2.38
10R6/8	66.70	37.43	39.61	66.16	33.99	37.78	1.45	64.98	26.30	29.38	65.73	23.67	30.04	1.45	1.93
7.5RP4/12	46.87	45.62	6.38	48.44	53.37	11.28	3.55	44.90	33.34	-4.55	47.75	37.35	2.80	3.55	5.32
10YR7/4	74.59	8.56	33.35	73.11	8.48	31.31	1.40	73.33	2.28	33.51	72.65	4.04	28.74	1.40	2.68
7.5B8/4	79.92	-13.97	-14.17	79.11	-14.59	-15.40	0.93	79.89	-9.54	-14.99	80.09	-9.52	-12.94	0.93	1.26
7.5PB4/6	40.01	1.61	-27.81	39.72	0.48	-27.56	0.91	39.61	3.02	-34.96	40.09	1.20	-31.09	0.91	1.03
5P4/10	41.43	25.04	-29.67	40.50	24.23	-27.75	1.23	40.25	20.60	-36.33	40.26	19.95	-32.01	1.23	2.25
5R4/10	49.24	45.41	33.78	48.37	48.68	32.78	1.94	46.28	33.06	23.31	47.79	35.48	23.32	1.94	1.88
10GY7/8	70.66	-32.40	34.24	68.99	-34.32	31.75	2.07	69.73	-25.24	38.68	69.65	-24.16	30.52	2.07	3.32
5YR7/6	75.80	22.58	36.74	74.20	21.00	35.19	1.44	72.74	13.29	30.86	73.24	13.90	29.55	1.44	1.01
7.5R4/10	49.30	45.04	43.46	47.62	46.31	41.65	2.13	45.99	33.54	36.28	46.71	34.42	36.02	2.13	0.89
5Y8/4	84.58	-1.43	35.57	81.94	-0.30	32.55	2.29	81.30	-3.77	37.27	80.66	-1.44	29.50	2.29	3.46
2.5BG7/4	70.69	-19.61	1.03	69.84	-20.74	-0.32	1.36	70.40	-13.81	-4.62	71.23	-13.66	-2.66	1.36	1.62
2.5G8/2	81.86	-9.27	6.60	80.90	-11.22	5.59	2.12	79.83	-6.84	2.23	80.53	-7.67	3.74	2.12	1.50
5RP4/12	46.72	44.04	-2.71	47.89	50.80	2.08	3.48	44.37	32.26	-12.45	47.70	35.20	-4.93	3.48	5.55
10BG8/2	80.86	-9.30	-3.06	80.09	-10.74	-4.76	1.81	78.86	-6.41	-5.78	79.54	-7.29	-3.80	1.81	2.04
5PB4/2	40.60	-1.39	-9.33	40.33	-1.74	-9.44	0.50	40.69	-0.41	-13.99	41.56	-1.08	-12.06	0.50	1.64
10Y8/4	83.85	0.05	34.52	82.97	-1.24	32.78	1.37	81.17	-1.59	29.39	82.11	-1.50	26.73	1.37	1.34
2.5B8/2	80.59	-8.58	-4.50	79.99	-9.30	-5.76	1.17	78.67	-5.74	-6.02	79.51	-5.97	-4.45	1.17	1.45
7.5G8/4	80.52	-23.50	6.16	79.61	-25.13	4.22	1.77	78.84	-15.31	2.61	79.20	-16.23	2.75	1.77	0.69
10P6/4	62.65	14.96	-5.00	62.10	13.75	-5.40	1.08	61.80	10.92	-10.88	62.62	9.18	-8.57	1.08	2.05
						Average:	1.73						Average:	1.73	Max 5.55

The average measured colorimetric differences for all wheel's colours between the A (incandescent) light sources and the average of the differences between the calculated CIELAB values in the 2 lights are equal, which means that the average difference in colour shifts from reference to test light source determined with the digital camera method is the same with the difference in colour shifts measured colorimetric. There are however 2 individual colours for that the difference of the differences exceed 5 ΔE_{00} units. They are marked with red in Table 6.16. Although they should not affect the general CRI, they might affect the special CRI. Usually, the special CRI for 4.5R4/13 is checked, which should be good because the difference of the differences for this colour is 1.93 ΔE_{00} units.

6.4. Final discussion about the results presented in this chapter

All results and intermediary conclusions on experimental data presented in this chapter formed the basis of the detailed methodology shown in 4.4. The experiments that led to these results followed the general outline described in subchapters 4.1 to 4.3 but the detailed description of the methodology from 4.4 emerged from experimentation. In the same time, the calculation processes and algorithms were improved step by step during the experiments, leading in the end to the algorithms and software code presented in chapter 5. During these experiments, the colour wheel mentioned in each session was created from uncut Munsell matt sheets assembled as shown in Figure 6.69, arranging each sheet so that it has approximately an equal surface in the wheel compared to the other sheets. Due to the high cost of Munsell sheets, assembling perfect wheels by cutting and gluing the Munsell sheets for each stage of the experiment was not an option. However, at the end of the experiments, such a wheel was created, therefore scene 23, which is the last presented in the results, uses a very well assembled colour wheel, having the Munsell patches cut and glued together, respecting a 12.4^{o} angle for each of the 29 Munsell sheets (N9.5 being in the middle) so that they cover equal surfaces in the wheel's geometry.

Figure 6.69 Temporary assembled colour-wheel during the colour selection process.

When taking pictures of the scenes, a circle corresponding to 12 cm diameter around the assembled wheel was cropped from the picture, as explained in chapter 4, the light of the light source was not viewed directly by the camera's objective and the pictures were containing exclusively the colours of the wheel.

The improvements obtained in the colorimetric outputs are presented in graphical form by plotting the evolution of the colour differences between calculated and measured CIELAB values averaged for the colours used in each scene (Figure 6.70). The graphic can be divided in 3 parts: scene 1-6, scene 7-15 and scene 16-23.

In the first part (scene 1 to 6), the 15 initially selected colours are corrected and the average colour difference drops from above 5 ΔE_{00} units to nearly 3. However, the improvement is done by the cost of eliminating the whole blue, buish-green and blue colour regions.

In the second part (scene 7 to 15), colours are added to fill the gap and other colours are added to cover more hue angles, which leads to a deterioration of the colorimetric output. This is corrected until scene 15, when the average colour difference between calculated and measured CIELAB values decrease to the same level as in scene 6, but having 24 colours now, instead of 15, which cover well the hue angles. The saturation of colours in the blue, bluish-green and green regions is however very low.

In the last part (scene 16 to 23), when starting to optimize the colours for both D65 light sources, the ΔE_{00} surges to around 4 units but then improves during the colour selection process to a better value than the one from which the optimization started.

Figure 6.71 shows how the maximum colour differences between calculated and measured CIELAB values for individual colours of the wheel evolve from scene 1 to scene 23. Reducing these differences is important for the aim of this work. Therefore, the graph in Figure 6.71 is important for completing the overall view on the colour selection process that is already given by Figure 6.70.

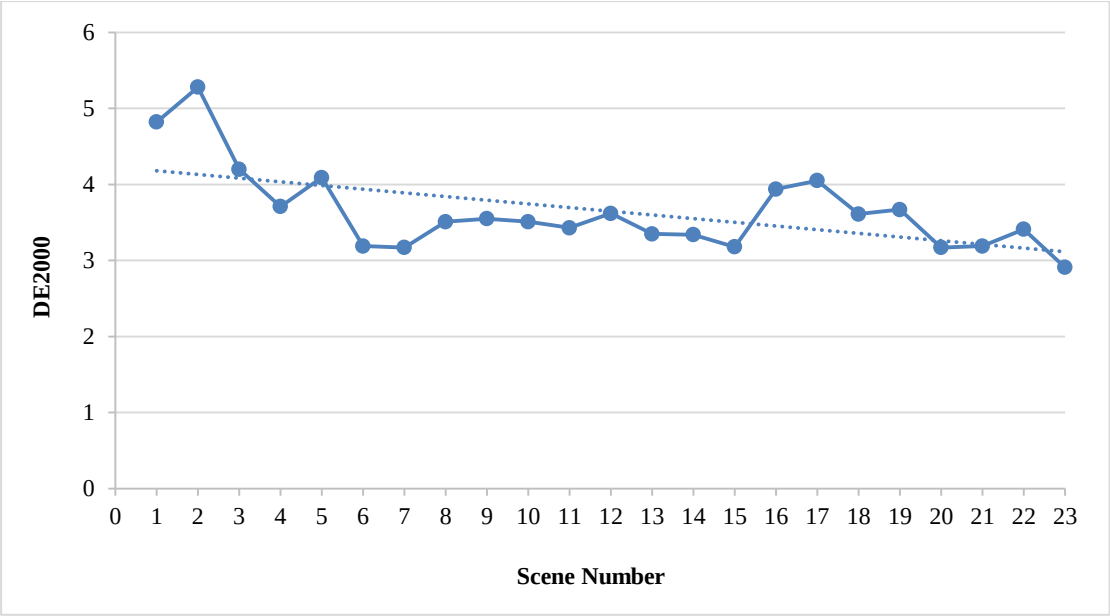

Figure 6.70 Average ΔE_{00} improvement between calculated and measured CIELAB values of all colour-wheel's colours across all scenes.

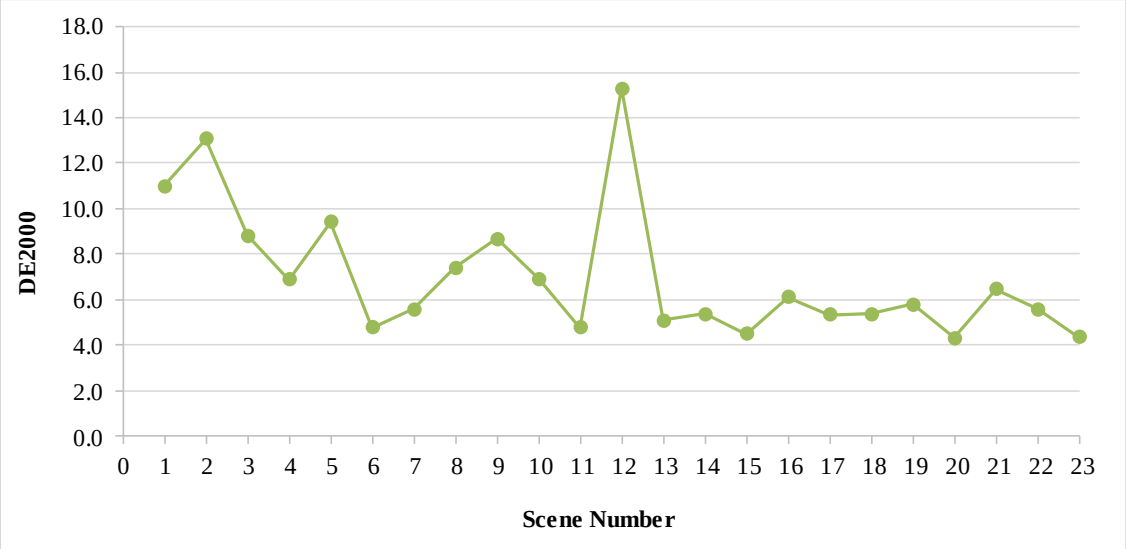

Figure 6.71 Maximum ΔE_{00} between calculated and measured CIELAB values of individual colours from the colour-wheel's from scene 1 to 23.

As can be seen in Figures 6.70 and 6.71, the average DE2000 between CIELAB calculated and measured values are reduced from almost 5 to less than 3 units and the maximum ΔE_{00} between CIELAB calculated and measured values of individual colours are reduced from almost 14 to about 4 units.

CHAPTER 7

CONCLUSIONS

The methodology in this work was developed using two low-cost SLR digital cameras with different architecture, produced by different manufacturers. The white balance of the cameras were left in automatic mode. Reproducibility of results were tested with 3 more SLR digital cameras with the white balance preset using an N9.5 Munsell sheet. The CIELAB values calculated from the 3^{rd} – 5^{th} camera digital images, obtained according to the described methodology, are listed in the Appendix D. These results prove that the method can be applied on various SLR digital cameras regardless of the white balance setup. Comparing the data obtained with all five cameras, the conclusion is that some cameras with automatic white balance on, can give better results than other cameras with a preset white balance. This means that across cameras the importance of sensors (CCD or CMOS) is overseeded by other factors strictly related to manufacturing (hardware and software).

Comparing the same colour from pictures taken with different low cost SLR digital cameras in sRGB mode, as shown in the described method, the differences can be seen with naked eye. The reason for these differences is that colour output is not stable across low-cost SLR cameras. However, if the camera is not cheaper than few hundred US dollars, the manufacturer tries to adhere best to the sRGB standards as a minimal request imposed by the price tag.

Therefore, in order to improve the colorimetric behavior across multiple SLR digital cameras in sRGB mode, the best guess was to maintain the standard linear transform between linearised RGB and XYZ, while finding an own linearization for the device dependent RGB data that are recalculated for every camera. This linearization can be adapted for each SLR camera and eventually can be recalculated even for every scene under the same light source, if, for some reason, the white balance of the digital camera cannot be used for establishing an absolute white point. The method treats the general case of using automatic white balance.

User grade SLR commercial digital cameras have different settings for the white balance, including a ‘custom’ option that allows setting an absolute white for multiple pictures. Considering the sRGB mode, it is logic to set the absolute white point with the N9.5 Munsell sheet because it is the highest white on the sRGB white scale. However, the sheet must be placed on the bottom of the box, in the center, while the camera is placed at 1 m distance. Low-cost SLR cameras, such as the cameras used in this work, do not have a zoom lens powerful enough to catch the N9.5 standard Munsell sheet on the entire screen while respecting the experimental setup. For this reason, the auto white balance was used during the described experiments and linearizations were recalculated for every scene. A powerful lens was used as optimal accessory for the Nikon cameras during the experiments.

The colour correction algorithm does not include custom coefficients for the linear transform because this would restrain the usage of the software for one particular camera. It is considered that the applied linearization corrects the RGB values within the sRGB colour space selected from the camera’s setup menu; therefore the standard sRGB transform is applied to the resulted linear RGB.

One may think that if random cameras are used for assessing different light sources, then it is hard to control the variables because both the light source and camera are changing. However, if the digital camera fulfills the minimal requirements of the sRGB standards, then the variables are constrained within limits by its manufacturing (hardware and software) and they can be controlled. The results presented in the previous chapters using two very different cameras and the results shown in the Appendix D using three more cameras, prove that the formulated assumptions are correct for the developed methodology.

The colour selection experiment performed in this work took into account only the D65 light sources. Results were tested later with the mentioned A light sources. Although the average colour differences between calculated and colorimetric measured CIELAB values under the A light sources for the entire wheel were acceptable (~4 ΔE_{00} units), the maximum ΔE_{00} for individual colours of the wheel was 9.5. The conclusion was that, for defining colour space regions where SLR digital cameras have a good response, CIELAB predictions for light sources having at least two other correlated colour temperatures should be taken into account when selecting

the Munsell colour codes for assembling the wheel. Because the method described in this work is a result of experimentation, the mentioned conclusion was included in the methodology.

If the detailed methodology is to be followed in a new experimental cycle, the colour selection process should be more straightforward and colour-codes with better colorimetric response, for light sources other than D65 type, should result from the colour selection process. However, the results shown in 6.4 show that the selected colours are acceptable for being used in light quality assessments that aim only the calculation of a general CRI. Better results could be obtained by using cameras with improved grey balance compared to the ones used in this work. Tables 7.1 and 7.2 show the grey balance for each camera, using the cameras' chromaticities.

Table 7.1 Grey balance for Canon EOS X4 camera.

Grey	R	G	B
N2	0.333	0.333	0.333
N3.5	0.328	0.336	0.336
N5	0.328	0.336	0.336
N6.5	0.326	0.339	0.336
N8	0.324	0.340	0.336
N9.5	0.329	0.342	0.329
	STDVA	0.006	

Table 7.2 Grey balance for Nikon D40x camera.

Grey	R	G	B
N2	0.338	0.338	0.324
N3.5	0.325	0.342	0.333
N5	0.326	0.340	0.334
N6.5	0.331	0.340	0.329
N8	0.327	0.338	0.335
N9.5	0.333	0.341	0.326
	STDVA	0.006	

Because the neutrals are new Munsell sheets, they have excellent neutrality, and the chromaticities of the cameras could be used for evaluating the grey balance of

each camera. For both cameras, the grey balance is quite good, having a standard deviation from the mean of 0.006 in both cases.

As future work, the methodology should be applied in the context of a colour wheel selection based on CIELAB predictions for Munsell patches under more light source types for defining the colour space region with greater accuracy.

Although the proposed method proves to work well for assessing the quality of light, this work should be viewed as a proposal for further research based on this work's findings.

REFERENCES

Agoston, G. A. (1989). "Colour theory and its application in art and design." Colour Research and Application **14**(5): 272.

Alesse, F. (2008). Philo of Alexandria and Post-Aristotelian Philosophy, BRILL.

Allen, R. (1999). David Hartley on human nature, SUNY Press.

Andrew, R. (2006). The last Man who Knew everything. New York, Pi press.

Bahadir, G. K., J. Glotzboch, Y. Altunbasak, W. R. Schafer and M. R. Mersereau (2005). "Demosaicking: colour filter array interpolation." IEEE signal Processing Magazine,: 44-54.

Barth, G. F., G. P. Deutsch and D. H. Klein (2012). Sensory Perception, Springer.

Benson, W. (1868). Principles of the Science of Colour: Concisely stated to aid and promote their useful application in the decorative art. London, Chapman and Hall.

Berns, S. R. (2010). "Designing White-Light LED Lighting for the Display of Art: A Feasibility Study." Colour Research and Application: 1-11.

Bezold, W. J. F. (1876). The theory of colour in its relation to art and art-industry. Boston, L. Prang & Company.

Blanc, C. (1867). Grammaire des arts du dessin architecture, sculpture, peinture. Paris, Librairie renouard.

Blanksby, J. A. and J. M. Loinaz (2000). "Performance analysis of a colour CMOS photogate Image Sensor." IEEE transactions on electron devices **47**: 55-64.

Blaszczyk, L. R. (2012). The colour revolution, MIT Press.

Blitzer, H., S. K. Ferguson and J. Huang (2008). Understanding Forensic Digital Imaging, Academic Press.

Boissard, S. and M. Fontoynont (2009). "Optimization of LED-based light blendings for object presentation." Colour Research and Application **34**(4): 310-320.

Bowers, B. (2009). "Lengthening the Day: History and technology of the invention of electric lamp." Annual Lecture 2009: Museum Year 2009.

Brusso, C. B. and G. Author (2008). "From crystallography to visible light." IEEE Industry Applications Magazine: 8-10.

Byrne, A. and R. D. Hillbert (1997). Reading on colour: The science of colour, MIT Press.

Caes, J. C. (2001). How do we know the speed of light, The Rosen Publishing Group.

Cheung, V. and S. Westland (2006). "Methods for optimal colour selection." J. Imaging Science and Technology **50**: 481-488.

Cheung, V., S. Westland and M. Thomson (2004). "Accurate estimation of the nonlinearity of input/output Response for colour cameras." Colour Research and Application **29**: 406-412.

Chevreul, E. M. (1858). The Laws of Contrast of Colour: And Their Application to the Arts of Painting, Decoration of Buildings, Mosaic Work, Tapestry and Carpet Weaving, Calico Printing, Dress, Paper Staining, Printing, Illumination, Landscape and Flower Gardening. London, G. Routledge & Co., Farringdon St.

CIE, I. C. o. I. (1995). Method of Measuring and Specifying Colour Rendering Properties of Light Source. CIE 13.3.

CIE, I. C. o. I. (2005). CIEDE2000 colour difference formula. Implementation Notes, supplementary test data, and mathematical observations CRA

Collett, E. (2003). Polarized light in fiber optic, SPIE Press.

Converse, S. (1856). The American Journal of Science and Art, NewYork: PUTNAM &CO.
Davis, W. and Y. Ohno (2006). Development of a Color Quality Scale. Proceeding of Light and color symposium: Sixth international LRO Lighting Research Symposium, Orlando , FL.
Davis, W. and Y. Ohno (2009). "Approaches to colour rendering measurement." Journal of Modern Optics **56**: 1412-1419.
Davis, W. and Y. Ohno (2010). "Development of a colour quality scale." Optical Engineering **49**(3).
De Lodyguine, A. (1897). Illuminant for incandescent lamps, Google Patents.
Dhanani, S. and M. Parker (2013). Digital video processing for engineers, Newnes.
Diels, H. and W. Kranz (1949). Vorsokratische Denker: Auswahl dem uberlicferten. Berlin, Weidmann.
DiLaura, D. (2008). A Brief History of Lighting. http://www.osa-opn.org
Đorđević, D., A. Hladnik. and A. Javoršek (2009). " Performance of five chromatic adaptation transforms using large number of colour patches." Acta graphica **20**(1-4): 9-19.
Dudda, B. (2013). Morphology of LEDs by Atomic Force Microscopy. Master in physics, University of Bologna.
Dyer, L. F. and C. T. Martin (2010). Edison: His life and invention, The Floating Press.
Enloe, L. C. (2001). Physical science : what the technology professional need to know, John Wiley & Sons.
Fairchild, D. M. (2013). Colour Appearance Model, John Wiley & Sons.
Fairman, S. H., M. H. Brill and H. Hemmendinger (1997). "How the CIE 1931 Colour-Matching Functions Were Derived from Wright–Guild Data." Colour Research and Application **22**: 11-23.
Fenna, D. D. (2002). A Dictionary of Weights Measures and Units, Oxford University Press.
Finger, S. (2004). Origins of Neuroscience: A History of explorations into brain function, Oxford University Press.
Gendre, F. M. (2003). "Two centuries of electric light sources innovations." Retrieved April 23, 2014.
Gross, G. C. (1999). "The five that comes from the eye." The neuro scientist **5**(1): 58-64.
Gulrajani, L. M. (2010). Colour measurement: principle, advances and industrial application, Academic Press.
Hain, R., J. C. Kahler and C. Tropea (2007). "Comparison of CCD, CMOS and intensified cameras." Exp Fluids **42**(3): 403-411.
Haralabidis, E. P. and C. Pilinis (2005). "Linear colour camera model for a skylight colourimeter with emphasis on the imaging pipeline noise performance." Journal of Electronic Imaging **14**(4): 1-20.
Hardin, L. C. and L. Maffi (1997). Colour categories in thought and language, Cambridge University Press.
Harris, M. (1766). The Natural System of Colours. Lailer's office, Princes-street, London, Licester-Fields.

Hatfield, C. G. (1990). The natural and normative: Theories of spatial perception from Kant to Helmholtz, MIT Press.
Hearnshaw, B. J. (2014). The Analysis of Starlight: Two Centuries of Astronomical Spectroscopy, Cambridge University Press.
Helmut, M. F. O. (2013). Sustainability, energy and architecture, Academic Press.
Hog, E. (2008). 650 Years of Optics: From Alhazen Fermet and Romer. Contribution to the symposium: "400 Years of Telescopes".
Hooke, R. (1757). Robert Hooke's Critique of Newton's Theory of Light and Colours. The History of Royal Society. London. **3:** 10-15.
Hullfish, S. (2013). The Art and Technique of Digital colour correction, Taylor&Francis.
Hunt, G. R. W. (1995). Measuring colour, Ellis Horwood.
Hunt, G. R. W., C. Li and R. M. Luo (2005). "Chromatic adaptation transforms." Colour Research and Application **30**: 69-71.
Hunter, S. R. (1987). The measurement of appearance, John Wiley & Sons.
Huxtable., J. M. (2013). "The relationship of light and colour in Medieval thought and imagination." On Light: 25-44.
Hytti, T. H. (2006). Characterization of digital image noise properties based on Raw data. Proc. SPIE 6059, Image Quality and System Performance III.
Jones, W. D. (2012). "A brief illustrated technical history punched card." Retrieved April 16, 2014.
Kelly, L. K. and B. D. Judd (1955). Colour: Universal language and dictionary of names. Washington.
Kim, K. J., H. Luo, F. E. Schubert, J. Cho, C. Sone and Y. Park (2005). "Strongly enhanced phosphor Efficiency in GaInN white light emitting diode using remote phosphor configuration and diffuse reflector cup." Japanese Journal of Applied Physic **44**(21): 649-651.
Kirk, S. G., E. J. Raven and M. Schofield (1983). The Presocrafic Philosophers: A critical history with a selection of texts, Cambridge University Press.
König, A. (1886). Die Grundempfindungen und ihre Intensitäts-Vertheilung im Spectrum (Fundamental sensations and their intensity distribution in the spectrum). Berlin, Sitzungsberichte der Akademie der Wissenschaften.
Kries, J. V. (1970). Influence of adaptation on the effects produced by luminous stimuli. Cambridge, MIT Press.
Kuehni, G. R. (2002). "The Early Development of the Munsell System." Colour Research and Application **27**: 20-27.
Kuehni, G. R. (2003). Colour space and its Division: Colour order from Antiquity to the present, John Wiley & Sons.
Kuehni, G. R. (2004). Colour: An introduction to practice and principles, John Wiley & Sons.
Kuehni, G. R. (2008). Colour vision & Technology, AATCC.
Kuehni, G. R. (2010). "A Brief history of disk colour mixture." Colour Research & Application **35**(2): 110-121.
Kuehni, G. R. and A. Schwarz (2007). A. Colour ordered: A survey of colour systems from Antiquity to the present, Oxford University Press.
Küller, R. (1997). Preferences for colour in urban spaces, colour and psychology. Stockholm International Colour Association**:** 104-105.

Lago, D. M., M. Meneghini, N. Trivellin, G. Mura, M. Vanzi, G. Meneghesso and E. Zanoni (2012). "Phosphors for LED-based light source: Thermal properties and reliability issues." Microelectronic Reliability **52**: 2164-2167.
Lambert, H. J. (1772). Beschreibung einer mit dem Calauschen Wachse ausgemalten Farbenpyramide. Berlin, Haude&Spener.
Langmuir, I. and H. K. Kingdom (1925). Thermionic effects caused by vapours of alkali metals. Proceeding of royal society A.
Lardner, D. (1846). Popular lectures on science and art, Greeley & McElrath.
Lowergard, S. (2006). The Creation of colour in 18th century Europe. http://www.gutenberg-e.org/lowengard/c_Chap14.html Columbia University Press.
Lui, Z., G. Xia, L. Ting, G. Xiaoling, Q. L. Ming and S. Guangdi (2007). "Colour rendering and luminous efficacy of trichromatic and tetrachromatic LED- based white LEDs." Microelectronics Journal **38**: 1-6.
Luo, R. M., G. Cui and C. Li (2006). "Uniform color space based on CIECAM02 color appearance model." Colour Research and Application **31**(40): 320-330.
Ma, W. and R. S. Wang (2010). "Luminescence properties of full colour single phased phosphors for white LEDs." Journal of Alloys and Compounds **503**: 118-121.
Mach, E. (2003). The Principles of physical Optic: An Historical and Philoophical Treatment, Courier Dover Publications.
Mahler, E., J. J. Ezarati and F. Viénot (2009). "Testing LED lighting for color discrimination and color rendering." Color Research and Application **34**(1): 8-17.
Marguier, J., N. Bhatti, H. Baker, M. Harville and S. Süsstrunk (2007). Assessment human skin colour from uncalibrated image, Wiley Periodicals Inc.
Marion, J. (1981). Physics in the modern world, Academic Press.
Martinez-Verdu, F., J. Pujol, M. Vilaseca and P. Capilla (2003). Characterization of a digital camera as an absolute tristimulus colourimeter. Proc. SPIE 5008, Colour Imaging VIII: Processing, Hardcopy, and Applications.
Maxwell, C. J. (1857). "Experiments on colour, as perceived by the eye, with remarks on Colour Blindness." Transactions of the Royal Society of Edinburgh **21**(2): 275-298.
Meneghini, M., S. Vaccari, D. M. Lago, S. Marconi, M. Barbato, N. Triuellin, A. Griffoni, G. Alfier, G. Verzellesi, G. Meneghesso and E. Zanoni (2014). "ESD degradation and robustness of RGB LEDs and modules: An investigation based on combined electrical and optical measurement." Microelectronic Reliability: 1-7.
Michelson, A. (1878). Experimental determination of Velocity of light. The Scientific Monthly**:** 563-565.
Montwil, A. and A. Breslin (2008). Let there be light: The story of light from atoms to galaxies, Imperial College Press.
Narendran, N. and L. Deng (2002). Color rendering properties of LED light sources. Proc Solid State Lighting II SPIE 4776.
Nassau, K. (1997). Colour for science art and technology, Elesvier.
Newton, I. (1730). OPTICKS or, A Treatise of the Reflections, Refractions, Inflections and Colours of Light. London, William Innys at the West-End of st. Paul's.
Ohta, N. and R. A. Robertson (2005). Colourimetry: fundamentals & application, John Wiley & Son.
Okamura, S. (1994). History of electron tube, IOS Press**:** 7-97.

Parkhurst, C. and L. R. Feller (1982). "Who invented the colour wheel?" Colour Research & Application **7**(3): 217-230.
Poljanc, K., G. Steinhauser, H. J. Sterba, K. Buchtela and M. Bichler (2007). "Beyond low-level activity: on a "non-radioactive" gas mantle." Science of the total environment **343**: 36-42.
Pope, A. (2011). The painter's terms: An introduction to the language of drawing and painting, Literary Licensing.
Porter, C. D. (1965). The new photograph. Opening address of the winter session at Royal Victoria Hospital**:** 117-127.
Poynton, C. (2012). Digital Video HD, Morgan Kaufmann.
Raizner, C. and D. Fritsch (2010). Stray light analysis of high-dynamic-range cameras based on digital image processing**.** DGaO Proceedings 2010.
Randall, L. D. (1983). Colour technology in the textile industry. NC, AATCC.
Rea, S. M. and P. J. Freyssinier-Nova (2008). "Color rendering: A tale of two metrics." Colour Research and Application **33(**3): 192-202.
Renner, E. (2008). Pinhole Photography: From Historic Technique to Digital Application, Taylor&Francis.
Riley, T. M. (1995). "Ptolemy's use of his predecessors' data." Transactions of the American philological association: 221-250.
Rood, O. N. (1892). On a colour system, New Haven.
Runge, O. P. (1810). Philipp Otto Runge's Colour Sphere. Hamburg, Friedrich Perthes.
Sarton, G. (1952). Ancient science through the golden age of Greece, Courior Dover Publication.
Schade, P. (2010). "100 years of doped tungsten wire." Int. Journal of refractory metals and hard materials **28**: 648-659.
Schiffermüller, I. (1772). Versuch eines Farbensystems. Vienna.
Schneider, W. (1986). "Do the "Double Slit" Experiment the way it was Original done." The Physics Teacher **29**.
Schubert, F. E. (2002). Light emitting diodes, Cambridge University Press.
Sharma, A. (2004). Understanding Colour Management, Cengage Learning.
Shevell, S. K. (2003). The Science of Color, Elsevier.
Silver, B. L. (2008). The ascent of science, Oxford University Press.
Silvestrini, N. (1994). Ideacolour. Zurich, Baumann & Stromer pubisher.
Solli, M., N. Anderson, R. Lenz and B. Kruse (2005). Colour measurements with a consumer digital camera using spectral estimation techniques, Springer-Verlag Berlin Heldelberg.
Stokes, M., M. Anderson, S. Chandrasehar and R. Motta. (1996). "A Standard Default Colour Space for the Internet – sRGB, Version 1.10."
Stoll, I. (2003). The long journey of Doppler's vision into modern physics. Proceeding of the Commemmorative Symposia Christian Doppler: Life and work, Principle and Applications, Austria.
Stratton, M. G. (1917). Theophrastus and the Greek physiological psychology before Aristotle, WC Brown Reprint Library.
Stratton, R. (1964). "Energy distributions of field emitted electron." Physical Review Letters **135**: 794-805.

Stroebel, D. L. and D. R. Zakia (2008). Basic Photographic Materials and Process, Taylor & Francis.
Süsstrunka, S., J. Holmb and D. G. Finlayson (2006). Chromatic Adaptation Performance of Different RGB Sensors. Proceedings for the 6th Light Research Office Symposium in Light and Color.
Taguchi, T. (2006). "Developing white LED lighting systems and its technological roadmap in Japan." J Light Vis Environ **30**: 177-182.
Thomas, C. N. (1991). "The early history of spectroscopy." Journal of chemical education **68**(8): 631-634.
Thompson, M. and M. U. O'Reilly (2007). An Investigation into the Perception of Color under LED White Composite Spectra with Modulated Color Rendering. International Conference on Solid State Lighting.
Topdemir, G. H. and F. A. Kamal (2007). "Kamal Al-Din Farisi's Explanation of the rainbow." Humanity &Social Sciences Journal **2**(1): 75-85.
Tsuei, H. C. and S. W. Sun (2011). "Momentary adjustment means for simulating the sunlight colour temperature, hues and brightness with RGB LEDs in indoor lighting." Physic Procedia **19**: 239-243.
Ware, C. (2013). Information Visualization, Morgan Kaufmann.
Whitcomb, A. M. and P. W. Benson (1968). Proceeding of Spring Meeting, National Academics.
Wolf, E. D. (2013). Methods in cell biology: The optics of microscope image formation, Academic Press.
Woods, W. J. (2012). Multidimensional signal, image and video processing and coding, Academic Press.
Wright, S. (2010). Digital compositing for film and video, Focal Press.
Wu, W., P. J. Allebach and M. Analoui (2000). "Imaging Colorimetry Using a Digital Camera." Journal of Imaging Science and Technology **4**: 267-279.
Wyszecki, G. and S. W. Stiles (2000). Colour Science Concepts and methods, quantitative data and formulae, Wiely.
Yam, K. F. and Z. Hassan (2005). "Innovative advances in LED technology." Microelectronics Journal **36**: 129-137.
Yang, H. S., S. J. Lin, S. F. Juang, C. D. Chu, H. M. Chung, M. C. Chen and C. L. Liu (2013). "White light emitting diodes (LEDs) with good colour rendering indices (CRI) and high luminous efficiencies by the encapsulation of mixed and double-deck phosphors." Current Applied Physic **13**: 931-934.
Yanoff, M. and S. J. Duker (2013). Ophthalmology, Elsevier Health Sciences.
Zappe, H. (2010). Fundamentals of Micro – Optics, Cambridge University Press.
Zewail, H. A. and M. J. Thomas (2010). "4D electron microscopy: Imaging in space and Time." World Scientific: 1-5.
Zheng, Y., S. Lin, C. Kambhamettu, J. Yu and B. S. Kang (2006). Single image vignetting correction. Proc. IEEE computer Society conference on Computer Vision and Pattern Recognition, New York, US.

APPENDIX

APPENDIX A

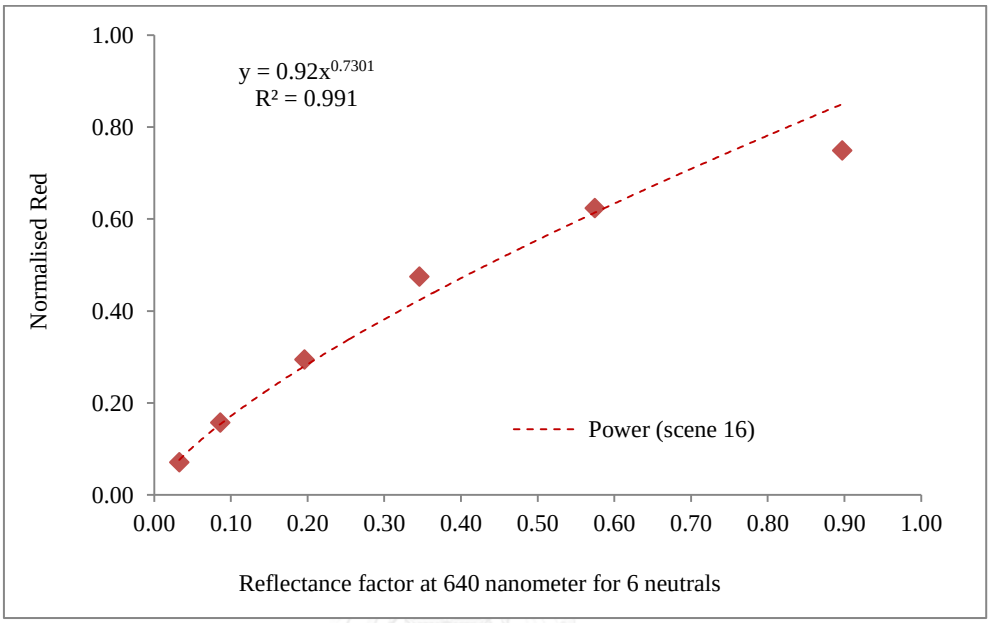

Figure A1 Correlation of the digital red values obtained for the 6 neutrals versus the 6 neutrals' reflection values at 640 nm, under the fluorescent D65 light source, for scene 16.

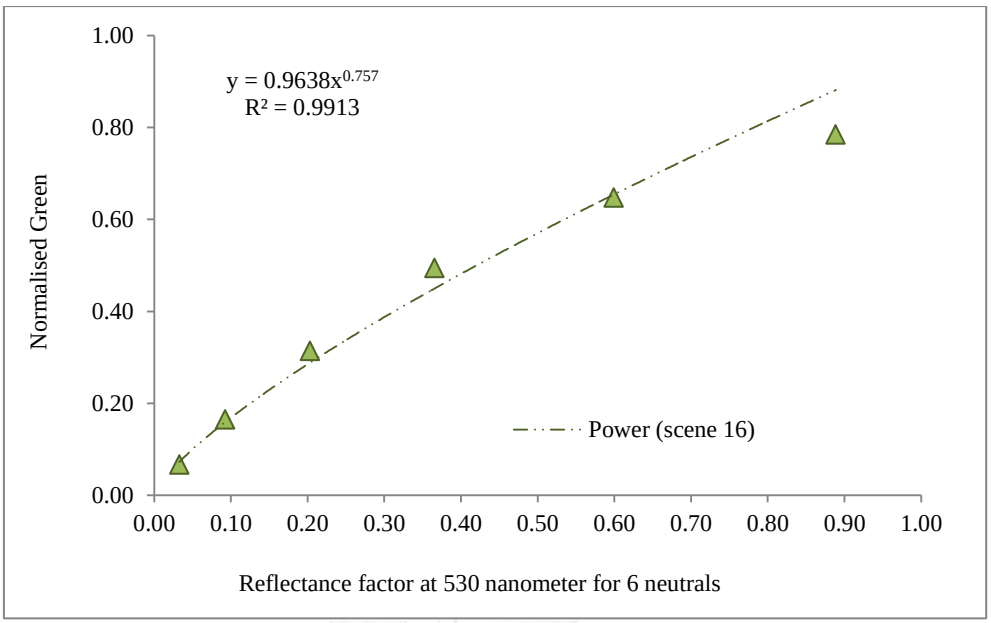

Figure A2 Correlation of the digital green values obtained for the 6 neutrals versus the 6 neutrals' reflection values at 530 nm, under the fluorescent D65 light source, for scene 16.

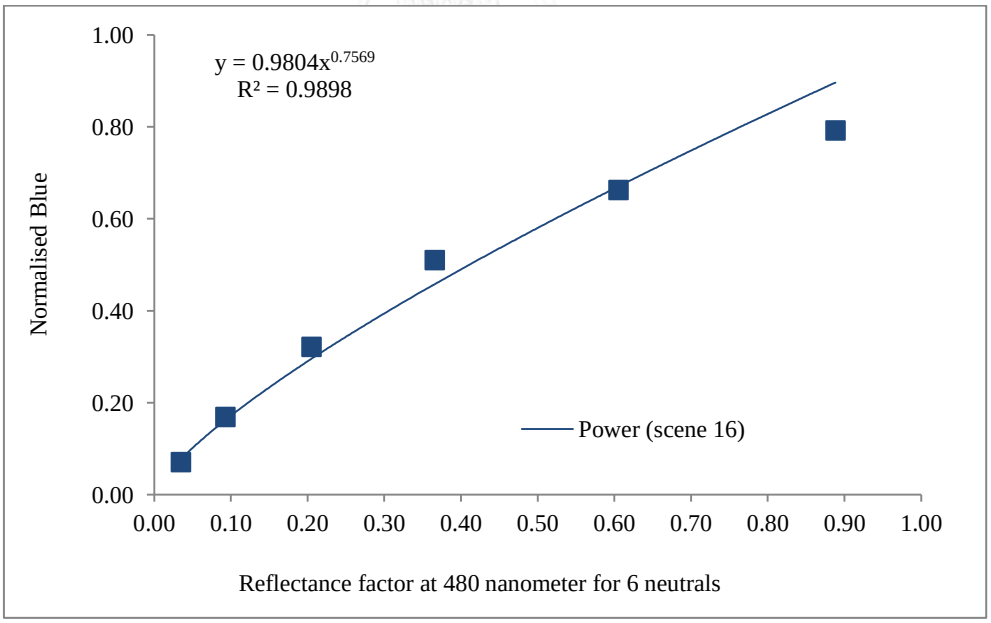

Figure A3 Correlation of the digital blue values obtained for the 6 neutrals versus the 6 neutrals' reflection values at 480 nm, under the fluorescent D65 light source, for scene 16.

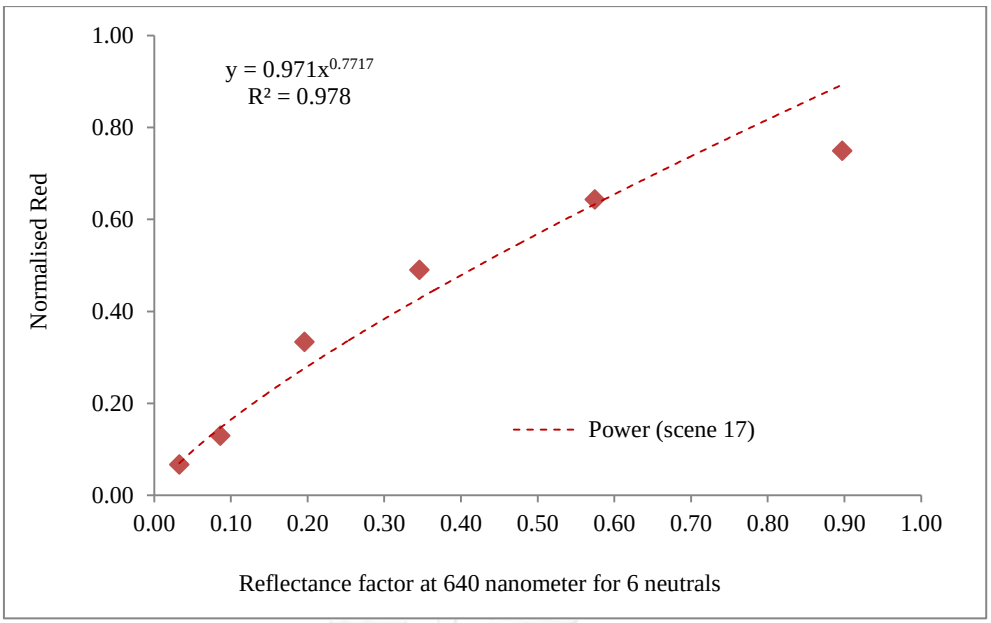

Figure A4 Correlation of the digital red values obtained for the 6 neutrals versus the 6 neutrals' reflection values at 640 nm, under the fluorescent D65 light source, for scene 17.

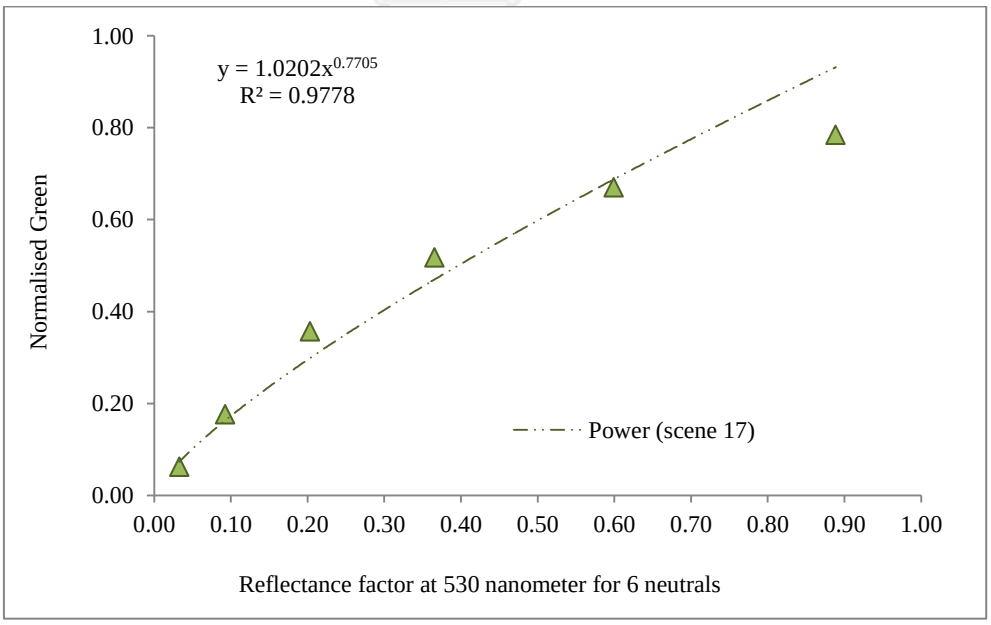

Figure A5 Correlation of the digital green values obtained for the 6 neutrals versus the 6 neutrals' reflection values at 530 nm, under the fluorescent D65 light source, for scene 17.

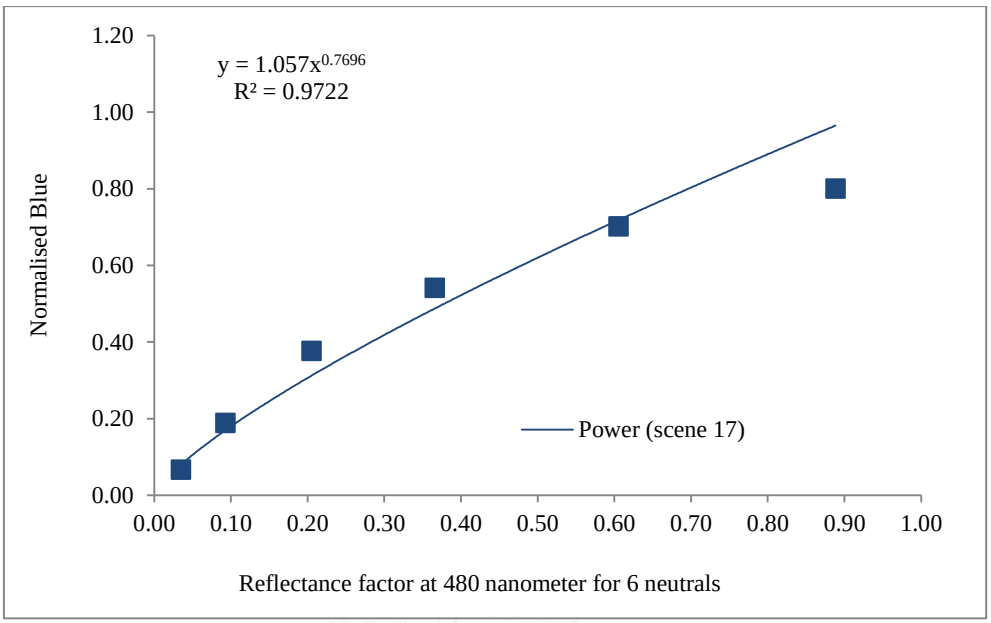

Figure A6 Correlation of the digital blue values obtained for the 6 neutrals versus the 6 neutrals' reflection values at 480 nm, under the fluorescent D65 light source, for scene 17.

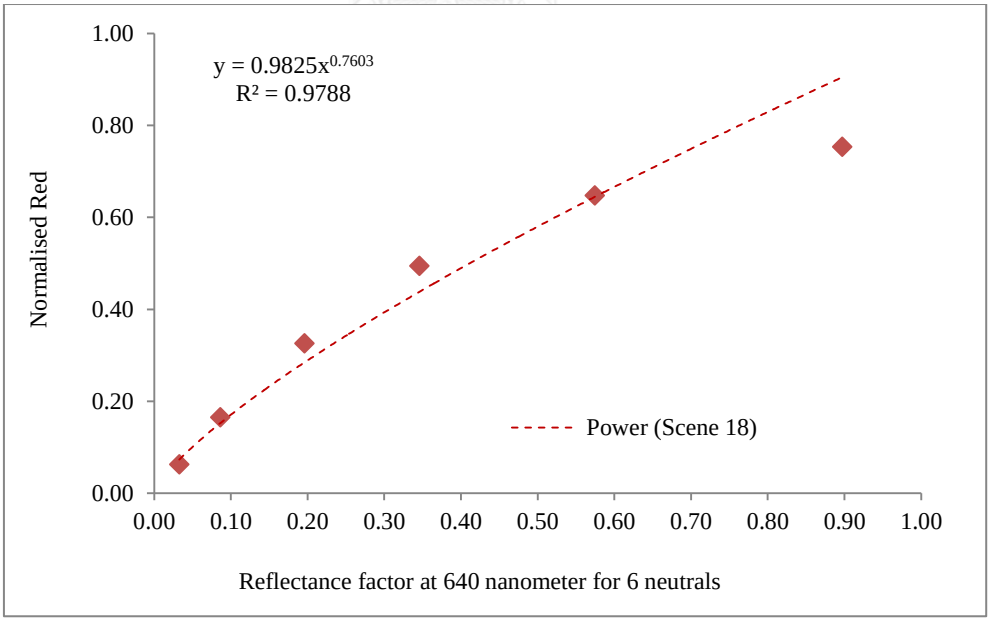

Figure A7 Correlation of the digital red values obtained for the 6 neutrals versus the 6 neutrals' reflection values at 640 nm, under the fluorescent D65 light source, for scene 18.

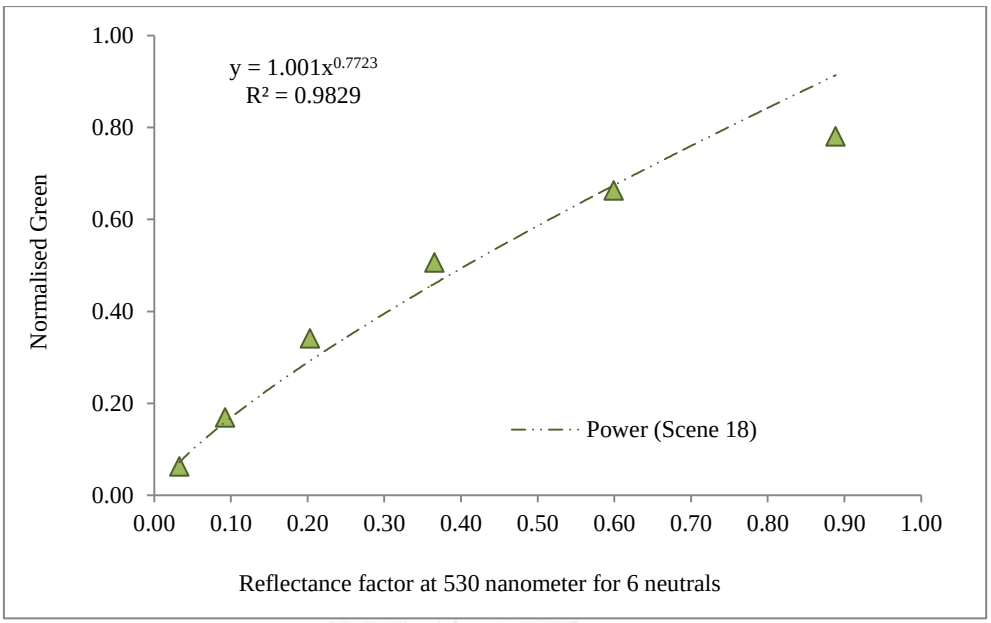

Figure A8 Correlation of the digital green values obtained for the 6 neutrals versus the 6 neutrals' reflection values at 530 nm, under the fluorescent D65 light source, for scene 18.

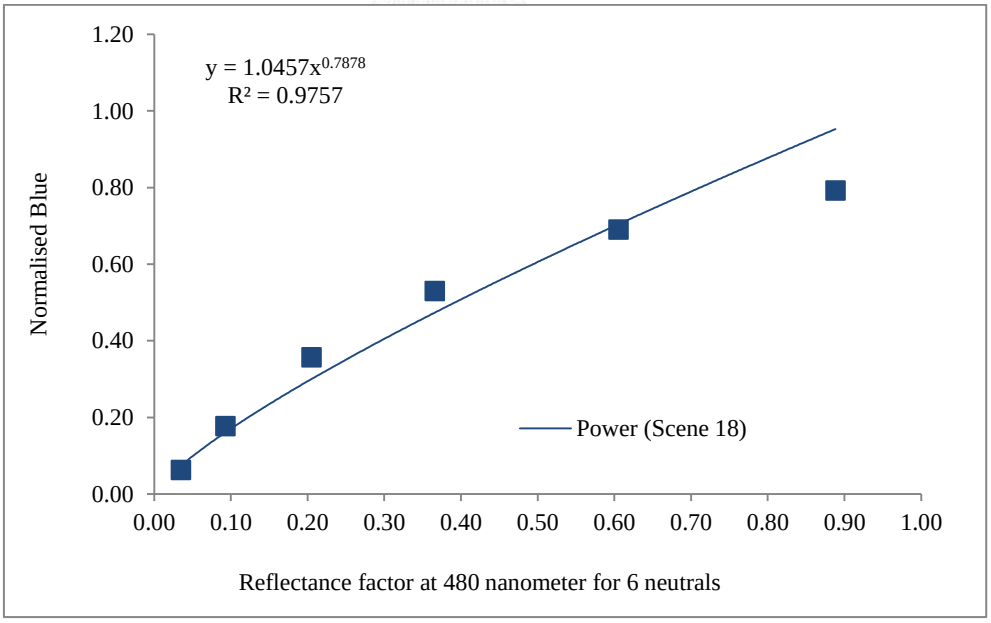

Figure A9 Correlation of the digital blue values obtained for the 6 neutrals versus the 6 neutrals' reflection values at 480 nm, under the fluorescent D65 light source, for scene 18.

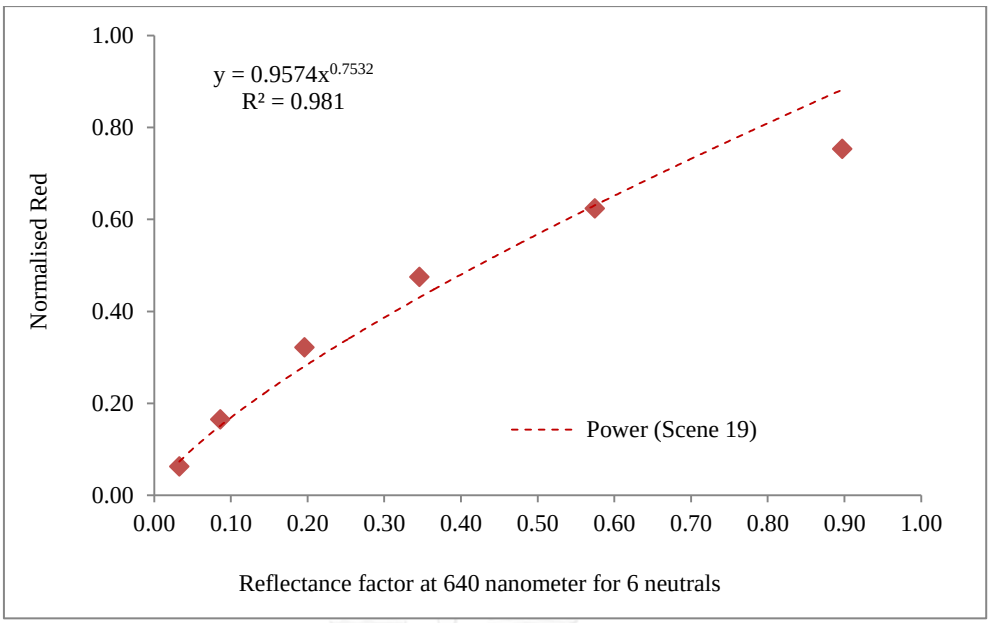

Figure A10 Correlation of the digital red values obtained for the 6 neutrals versus the 6 neutrals' reflection values at 640 nm, under the fluorescent D65 light source, for scene 19.

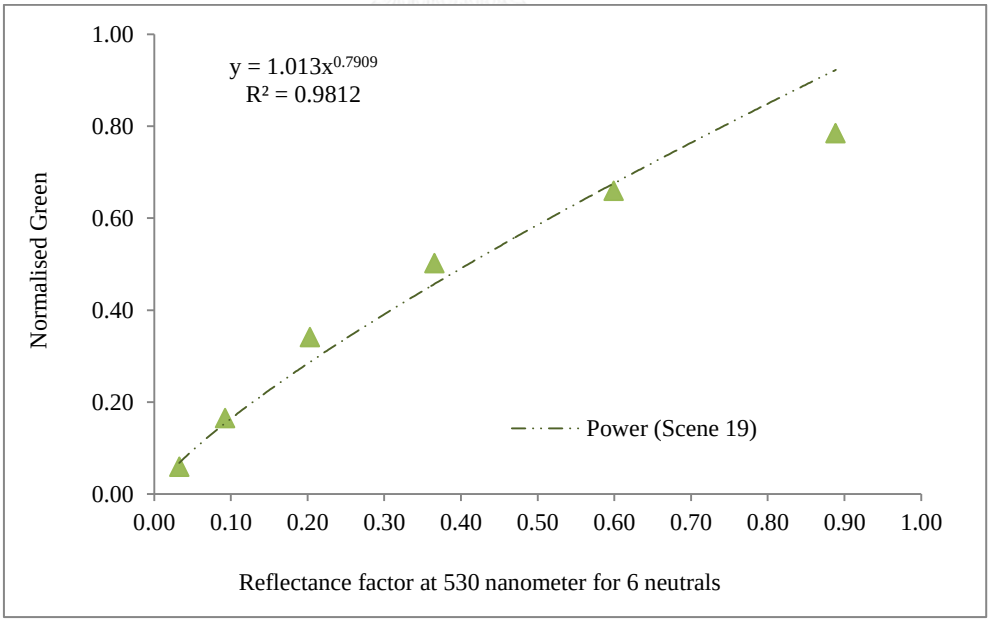

Figure A11 Correlation of the digital green values obtained for the 6 neutrals versus the 6 neutrals' reflection values at 530 nm, under the fluorescent D65 light source, for scene 19.

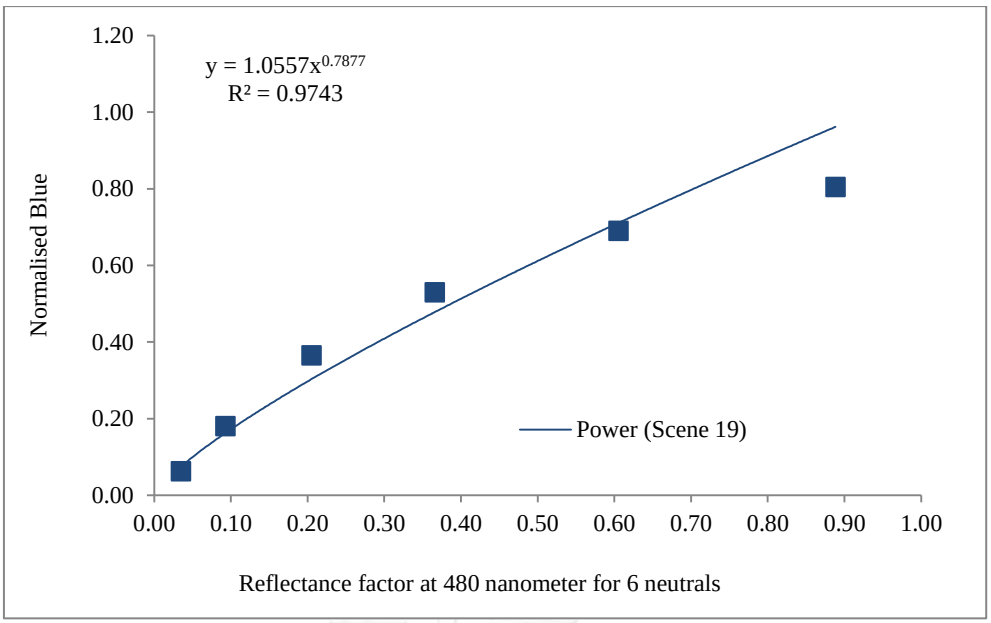

Figure A12 Correlation of the digital blue values obtained for the 6 neutrals versus the 6 neutrals' reflection values at 480 nm, under the fluorescent D65 light source, for scene 19.

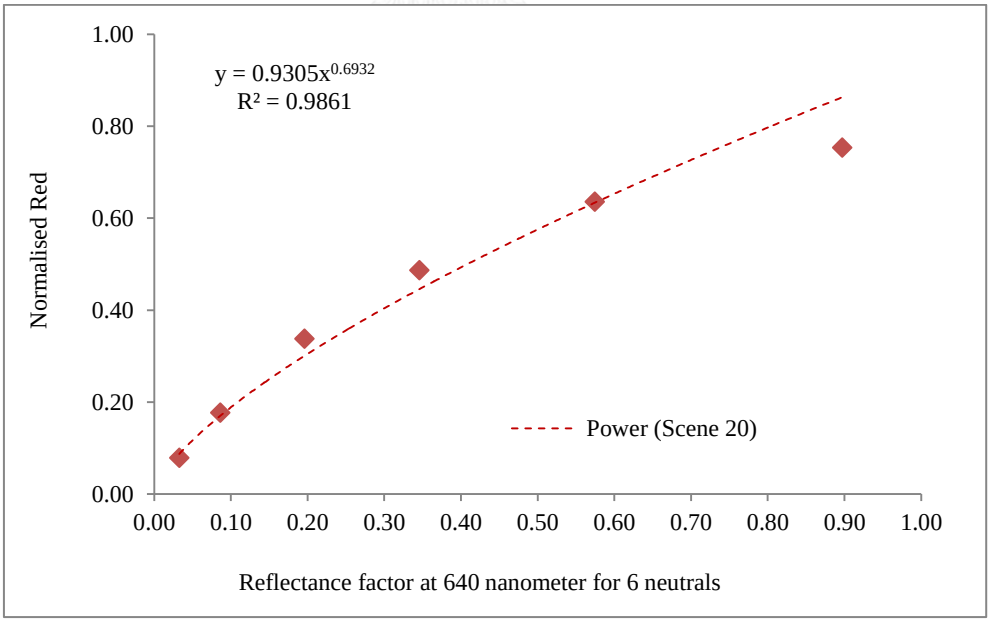

Figure A13 Correlation of the digital red values obtained for the 6 neutrals versus the 6 neutrals' reflection values at 640 nm, under the fluorescent D65 light source, for scene 20.

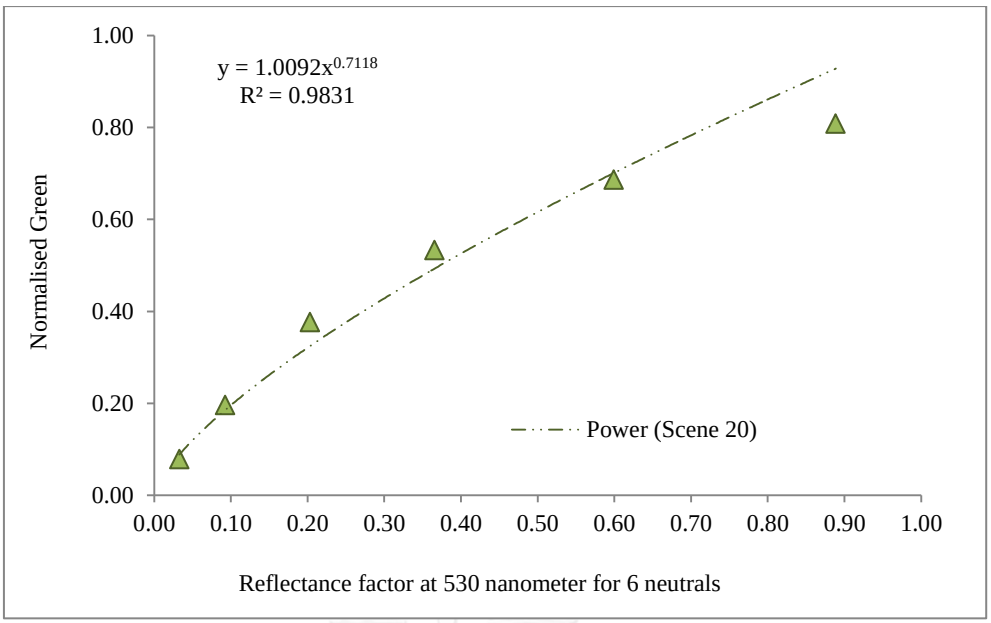

Figure A14 Correlation of the digital green values obtained for the 6 neutrals versus the 6 neutrals' reflection values at 530 nm, under the fluorescent D65 light source, for scene 20.

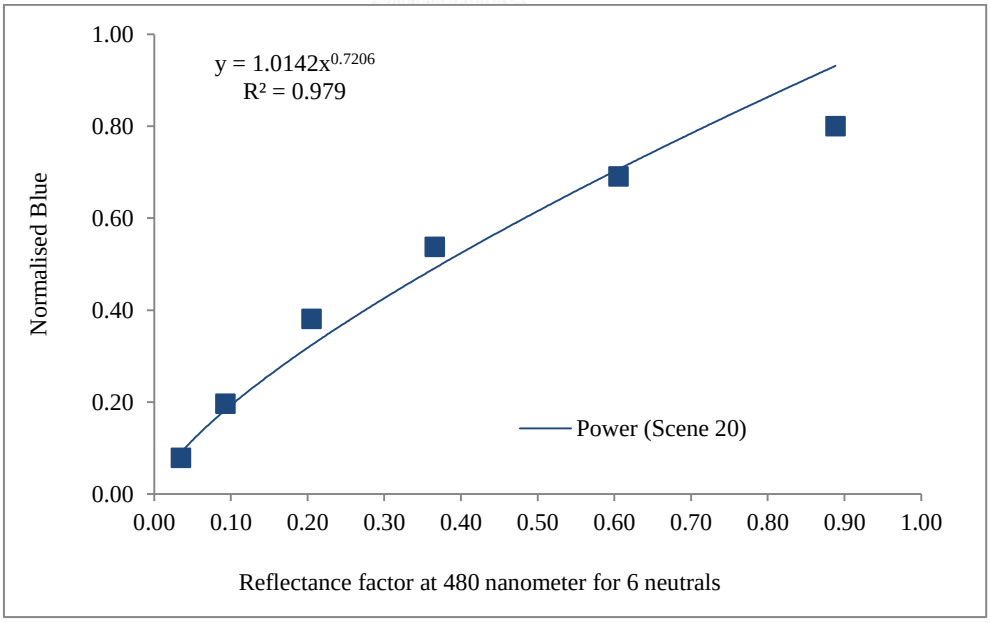

Figure A15 Correlation of the digital blue values obtained for the 6 neutrals versus the 6 neutrals' reflection values at 480 nm, under the fluorescent D65 light source, for scene 20.

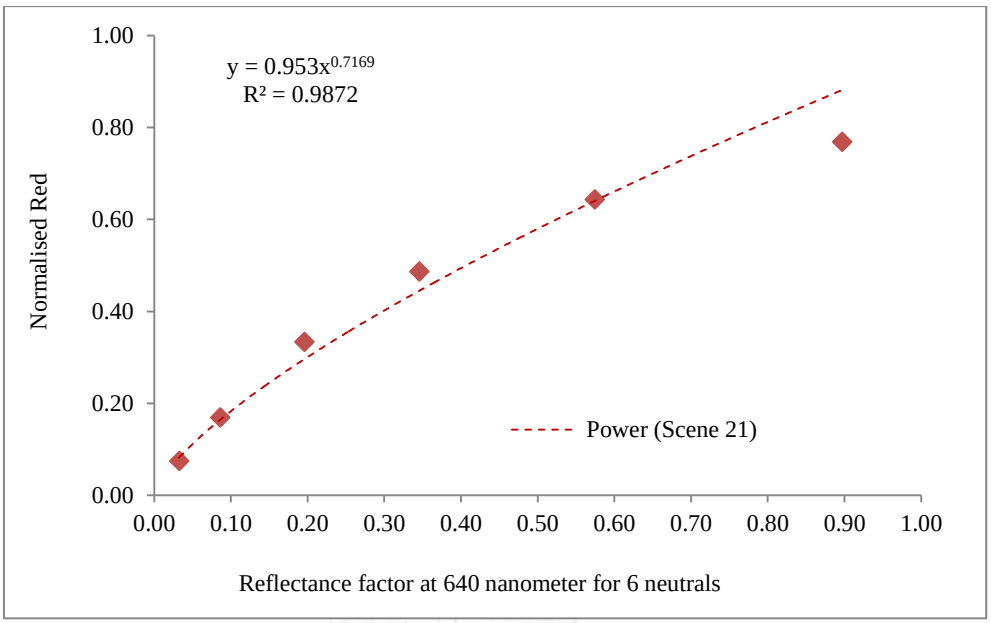

Figure A16 Correlation of the digital red values obtained for the 6 neutrals versus the 6 neutrals' reflection values at 640 nm, under the fluorescent D65 light source, for scene 21.

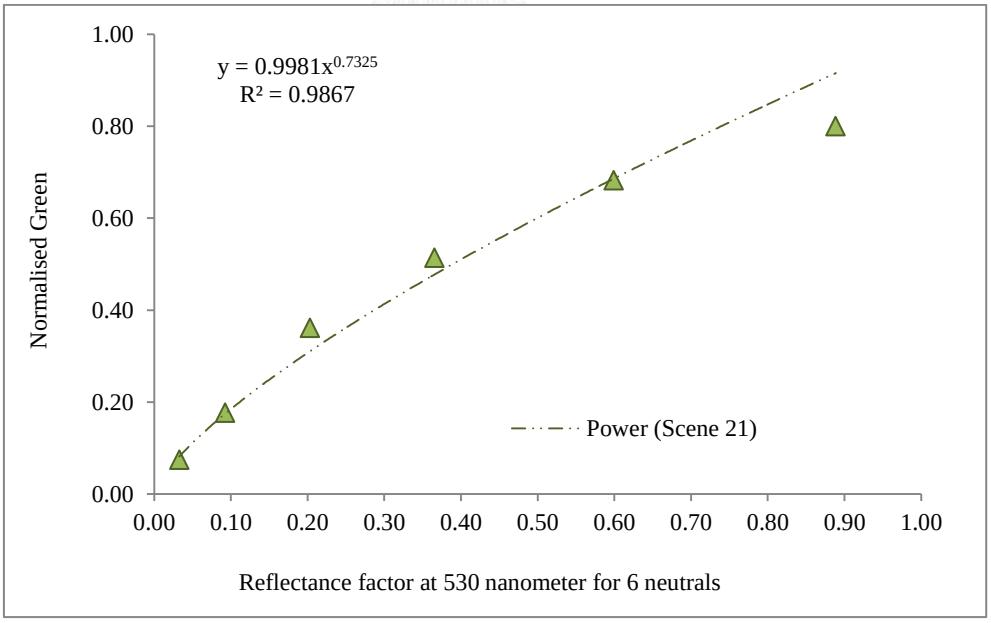

Figure A17 Correlation of the digital green values obtained for the 6 neutrals versus the 6 neutrals' reflection values at 530 nm, under the fluorescent D65 light source, for scene 21.

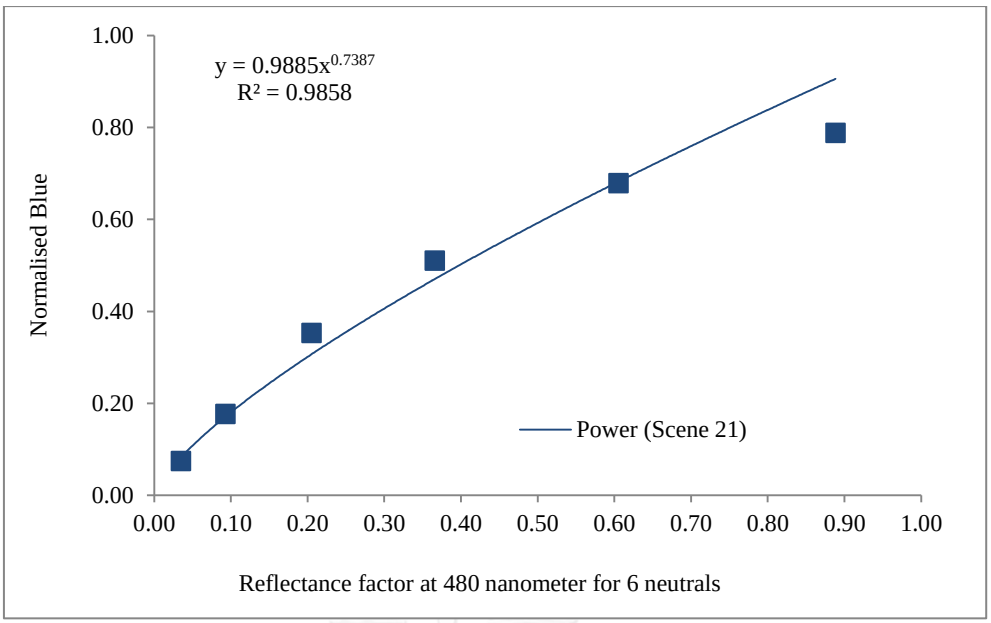

Figure A18 Correlation of the digital blue values obtained for the 6 neutrals versus the 6 neutrals' reflection values at 480 nm, under the fluorescent D65 light source, for scene 21.

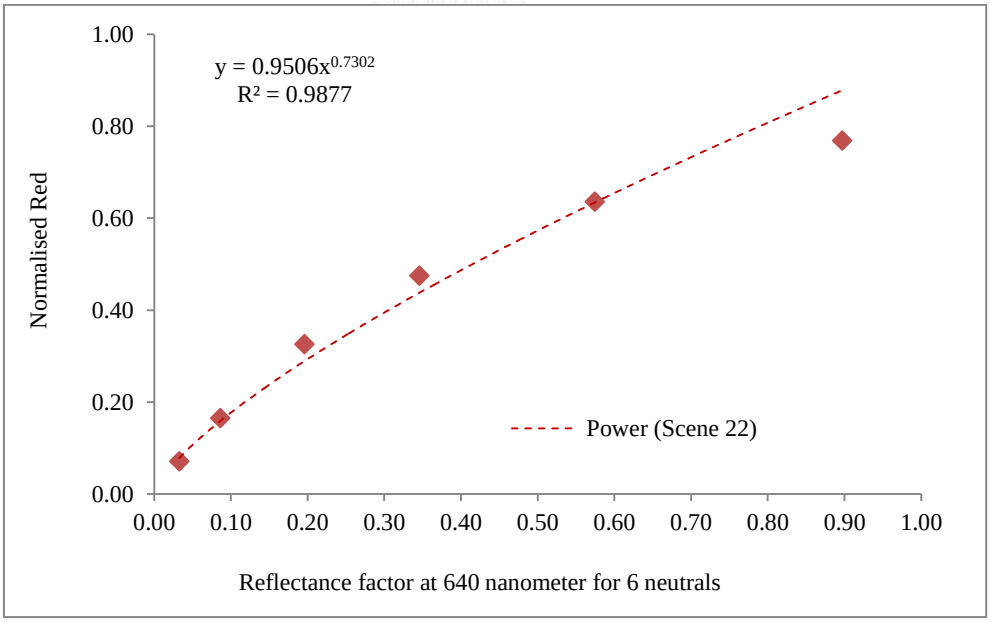

Figure A19 Correlation of the digital red values obtained for the 6 neutrals versus the 6 neutrals' reflection values at 640 nm, under the fluorescent D65 light source, for scene 22.

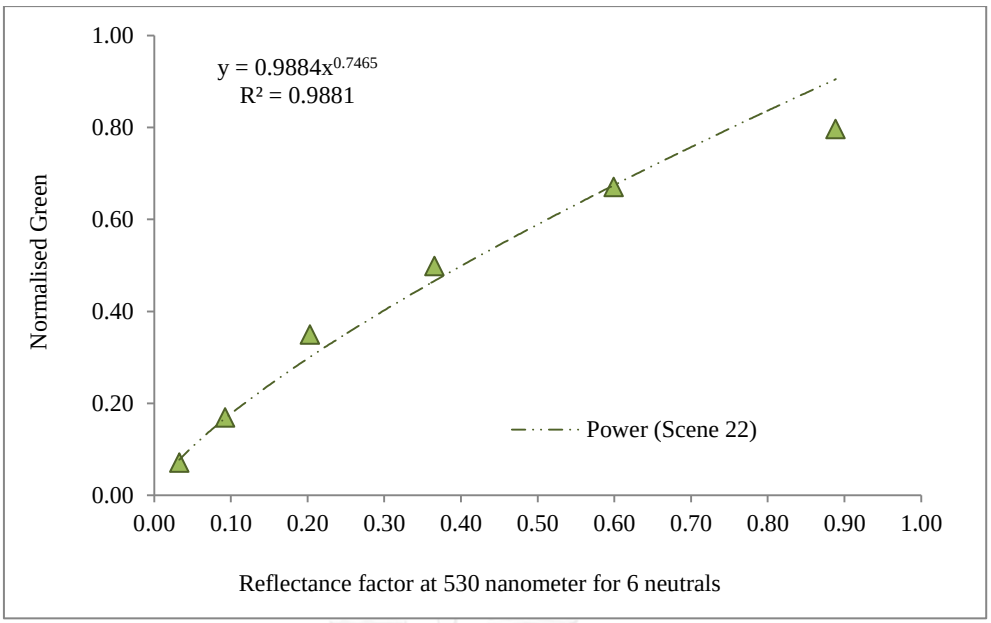

Figure A20 Correlation of the digital green values obtained for the 6 neutrals versus the 6 neutrals' reflection values at 530 nm, under the fluorescent D65 light source, for scene 22.

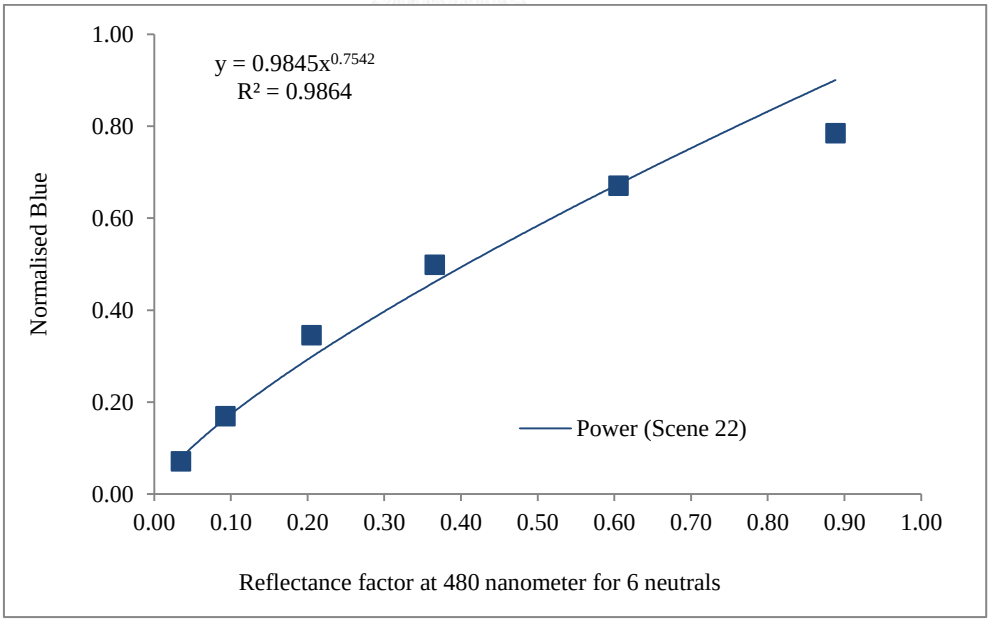

Figure A21 Correlation of the digital green values obtained for the 6 neutrals versus the 6 neutrals' reflection values at 480 nm, under the fluorescent D65 light source, for scene 22.

APPENDIX B

Table B1 Calculated CIELAB from Canon EOS X4's digital image scene 16 under Fluorescent D65 and ΔE_{00} toward measured CIELAB, D65/2°.

Calculated CIELAB from Canon's digital image scene 16 under Fluorescent D65 and DE00 toward measured CIELAB, D65/2										
Munsell Patches	Measured Spectrophotometer			R	G	B	Calculated CIELAB of scene 16			ΔE_{00}
	L*	a*	b*				L*	a*	b*	
N2	21.15	-0.15	-0.82	17	16	17	19.82	0.40	-0.96	1.24
N3.5	36.28	-0.45	-0.90	39	40	41	36.56	-0.95	-0.66	0.79
N5	52.15	-0.43	-0.62	76	82	83	55.12	-2.15	-0.59	3.73
N6.5	66.68	-0.93	-0.63	124	129	133	70.68	-0.36	-0.98	3.27
N8	81.55	-0.85	-0.97	164	171	174	81.74	-0.34	-0.22	1.04
N9.5	95.71	-0.59	1.54	193	201	205	88.77	0.02	-0.26	4.69
7.5 P 4/10	42.10	31.96	-21.37	89	41	112	45.66	34.20	-29.69	5.17
10 PB 4/8	40.87	18.36	-31.31	66	55	128	48.01	19.98	-33.64	6.78
2.5 GY 8/10	81.54	-22.10	70.22	154	178	54	80.58	-19.52	50.16	5.64
7.5 GY 7/10	68.01	-36.06	49.74	87	166	38	74.43	-39.19	51.25	5.01
10 R 6/8	61.66	31.08	30.41	175	75	61	61.54	30.78	22.39	4.55
7.5 RP 4/12	41.25	52.52	0.54	120	21	60	41.85	50.13	-5.71	3.21
10 YR 7/4	70.05	4.63	27.19	152	128	79	71.30	1.13	25.09	3.31
7.5YR7/6	71.22	12.54	34.09	167	120	68	70.54	7.68	30.14	3.49
7.5PB4/6	41.06	6.95	-24.74	49	54	108	45.32	10.44	-28.59	4.37
5P4/10	39.59	32.15	-27.96	74	38	113	43.05	32.17	-34.40	4.56
5 R 4/12	41.59	52.54	27.90	121	14	21	38.69	51.12	23.04	3.47
10GY7/8	70.09	-37.48	32.28	81	167	78	74.91	-35.84	29.65	3.77
5 YR 7/6	70.26	16.91	29.31	175	117	81	70.74	12.75	23.57	3.11
7.5R4/10	40.16	43.95	28.85	123	22	21	41.28	45.42	26.34	2.05
5Y8/4	79.56	-3.33	29.44	165	169	108	80.36	-7.27	23.74	4.69
2.5BG7/4	70.95	-20.57	0.42	101	165	152	76.84	-17.89	0.30	4.66
2.5G8/4	81.38	-22.31	13.49	131	184	153	81.91	-15.99	7.46	4.71
5RP4/12	41.72	51.19	-6.39	116	29	73	44.03	44.75	-10.85	3.84
10BG8/2	79.33	-9.23	-2.91	143	174	178	81.19	-6.19	-2.57	3.26
5PB4/2	40.8	0.34	-8.82	52	60	75	46.34	-0.39	-9.30	5.24
10Y8.5/6	86.51	-11.29	44.7	176	187	96	83.93	-11.71	33.96	4.57
2.5B8/2	79.01	-8.08	-3.50	150	179	183	82.53	-5.51	-2.31	3.64
7.5G8/4	79.79	-23.20	5.96	127	191	169	83.20	-17.20	3.44	4.40
10P4/6	41.22	25.07	-13.45	88	50	90	47.42	23.37	-15.76	6.10

Table B2 Calculated CIELAB from Canon's digital image scene 17 under Fluorescent D65 and ΔE_{00} toward measured CIELAB, D65/2°.

Calculated CIELAB from Canon's digital image scene 17 under Fluorescent D65 and DE00 toward measured CIELAB, D65/2										
Munsell Patches	Measured Spectrophotometer			R	G	B	Calculated CIELAB of scene 17			ΔE_{00}
	L*	a*	b*				L*	a*	b*	
N2	21.15	-0.15	-0.82	17	16	17	19.13	1.88	0.15	3.37
N3.5	36.28	-0.45	-0.90	33	45	48	37.23	-4.84	-2.66	5.78
N5	52.15	-0.43	-0.62	85	91	96	57.56	-0.21	-0.94	5.15
N6.5	66.68	-0.93	-0.63	125	132	138	70.48	0.04	-0.49	3.31
N8	81.55	-0.85	-0.97	164	171	179	80.84	0.57	-0.47	2.21
N9.5	95.71	-0.59	1.54	191	200	204	87.51	-0.16	1.02	5.12
7.5 P 4/10	42.10	31.96	-21.37	89	42	113	45.19	34.32	-27.95	4.22
10 PB 4/8	40.87	18.36	-31.31	66	56	129	47.42	20.20	-32.03	6.19
2.5 GY 8/10	81.54	-22.10	70.22	152	177	56	79.40	-18.77	49.67	5.85
7.5 GY 7/10	68.01	-36.06	49.74	86	162	39	72.67	-36.99	50.40	3.60
10 R 6/8	61.66	31.08	30.41	173	76	63	60.72	30.69	22.50	4.53
7.5 RP 4/12	41.25	52.52	0.54	120	23	61	41.89	49.26	-3.60	2.36
10 YR 7/4	70.05	4.63	27.19	150	128	81	70.25	1.59	25.13	2.76
7.5 YR 7/6	71.22	12.54	34.09	166	121	70	69.60	7.35	30.17	3.90
7.5PB4/6	41.06	6.95	-24.74	50	55	109	44.82	11.10	-26.91	4.30
5P4/10	39.59	32.15	-27.96	75	38	114	42.41	33.33	-32.90	3.41
5 R 4/12	41.59	52.54	27.90	121	13	21	38.08	52.40	24.31	3.60
10GY7/8	70.09	-37.48	32.28	80	164	79	73.34	-34.17	29.49	2.82
5 YR 7/6	70.26	16.91	29.31	172	116	80	69.34	12.94	24.68	2.82
7.5R4/10	40.16	43.95	28.85	124	19	23	40.19	48.95	24.94	3.64
5Y8/4	79.56	-3.33	29.44	163	166	108	78.74	-6.23	24.11	3.84
2.5BG7/4	70.95	-20.57	0.42	99	162	151	75.17	-17.00	1.06	3.90
2.5G8/4	81.38	-22.31	13.49	129	181	152	80.30	-15.20	8.29	4.83
5RP4/12	41.72	51.19	-6.39	117	29	74	43.56	45.78	-9.35	2.92
10BG8/2	79.33	-9.23	-2.91	143	173	178	80.04	-5.47	-1.42	3.90
5PB4/2	40.80	0.34	-8.82	52	60	75	45.41	0.69	-7.93	4.32
10Y8.5/6	86.51	-11.29	44.7	172	185	97	82.44	-11.54	33.97	4.99
2.5B8/2	79.01	-8.08	-3.5	148	176	182	80.91	-4.77	-1.52	3.93
7.5G8/4	79.79	-23.20	5.96	126	188	169	81.68	-16.09	4.03	4.52
10P4/6	41.22	25.07	-13.45	88	51	90	46.88	23.62	-13.73	5.34

Table B3 Calculated CIELAB from Canon EOS X4's digital image scene 18 under Fluorescent D65 and ΔE_{00} toward measured CIELAB, D65/2°.

Calculated CIELAB from Canon's digital image scene 18 under Fluorescent D65 and DE00 toward measured CIELAB, D65/2										
Munsell Patches	Measured Spectrophotometer			R	G	B	Calculated CIELAB of scene 18			ΔE_{00}
	L*	a*	b*				L*	a*	b*	
N2	21.15	-0.15	-0.82	16	16	16	19.03	-0.25	-0.38	1.54
N3.5	36.28	-0.45	-0.90	42	43	45	37.68	-0.25	-1.45	1.33
N5	52.15	-0.43	-0.62	83	87	91	56.64	-0.96	-1.47	4.43
N6.5	66.68	-0.93	-0.63	126	129	135	70.32	-0.23	-1.00	3.06
N8	81.55	-0.85	-0.97	165	169	176	80.99	-0.33	-0.48	0.95
N9.5	95.71	-0.59	1.54	192	199	202	87.90	-1.40	1.09	4.97
7.5 P 4/10	42.10	31.96	-21.37	85	41	107	44.36	32.00	-28.08	4.11
10 PB 4/6	41.21	13.96	-23.96	59	47	103	43.25	18.10	-28.05	3.02
2.5 GY 8/10	81.54	-22.10	70.22	152	175	53	79.51	-20.16	49.97	5.93
7.5 GY 7/10	68.01	-36.06	49.74	86	159	36	72.58	-37.99	50.79	3.59
10 R 6/8	61.66	31.08	30.41	170	73	58	59.84	29.55	22.59	4.39
7.5 RP 4/12	41.25	52.52	0.54	118	21	57	40.79	48.99	-4.45	2.75
10 YR 7/4	70.05	4.63	27.19	149	124	76	69.67	0.79	25.28	3.46
7.5YR7/6	71.22	12.54	34.09	165	118	66	69.35	6.94	30.41	4.24
7.5PB4/6	41.06	6.95	-24.74	48	53	105	44.19	10.14	-27.66	3.36
5P4/10	39.59	32.15	-27.96	74	36	108	41.57	32.77	-33.03	3.05
5 R 4/12	41.59	52.54	27.90	121	12	21	37.51	52.37	21.88	4.76
10GY7/8	70.09	-37.48	32.28	81	162	75	73.51	-35.14	30.17	2.78
5 YR 7/6	70.26	16.91	29.31	173	115	78	69.50	11.89	24.30	3.41
7.5R4/10	40.16	43.95	28.85	125	21	22	40.64	46.65	24.87	2.97
5Y8/4	79.56	-3.33	29.44	165	165	105	79.12	-7.26	24.42	4.40
2.5BG7/4	70.95	-20.57	0.42	102	161	148	75.64	-17.57	1.50	4.05
2.5G8/2	80.10	-10.98	5.90	153	176	166	81.43	-7.01	3.60	3.96
5RP4/12	41.72	51.19	-6.39	116	27	72	42.75	45.92	-11.23	3.21
10BG8/2	79.33	-9.23	-2.91	145	172	176	80.46	-6.35	-1.38	3.11
5PB4/2	40.80	0.34	-8.82	52	59	72	45.34	-0.31	-8.06	4.30
10Y8.5/4	86.29	-8.76	32.89	175	185	124	83.51	-9.44	22.56	5.37
2.5B8/2	79.01	-8.08	-3.5	149	175	180	81.28	-5.91	-1.55	3.06
7.5G8/4	79.79	-23.20	5.96	129	187	166	82.18	-16.84	4.53	4.13
10P4/4	41.42	15.68	-8.02	78	53	78	46.23	15.42	-9.97	4.66

Table B4 Calculated CIELAB from Canon EOS X4's digital image scene 19 under Fluorescent D65 and ΔE_{00} toward measured CIELAB, D65/2°.

Calculated CIELAB from Canon's digital image scene 19 under Fluorescent D65 and DE00 toward measured CIELAB, D65/2										
Munsell Patches	Measured Spectrophotometer			R	G	B	Calculated CIELAB of scene 19			ΔE_{00}
	L*	a*	b*				L*	a*	b*	
N2	21.15	-0.15	-0.82	16	15	16	18.92	-0.12	-0.32	1.62
N3.5	36.28	-0.45	-0.90	42	42	46	37.87	-0.16	-1.59	1.56
N5	52.15	-0.43	-0.62	82	87	93	57.01	-1.29	-1.49	4.85
N6.5	66.68	-0.93	-0.63	121	128	135	70.04	-1.00	-0.89	2.66
N8	81.55	-0.85	-0.97	159	168	176	80.60	-0.67	-0.49	0.84
N9.5	95.71	-0.59	1.54	192	200	205	88.11	-0.20	1.10	4.72
7.5 P 4/10	42.10	31.96	-21.37	82	39	108	43.95	32.01	-28.71	4.23
10 PB 4/8	41.21	13.96	-23.96	57	48	105	43.91	16.09	-27.51	3.04
2.5 GY 8/10	81.54	-22.10	70.22	148	174	55	79.21	-19.77	48.82	6.30
7.5 GY 7/10	68.01	-36.06	49.74	83	160	39	72.71	-38.52	49.32	3.78
10 R 6/8	61.66	31.08	30.41	168	72	60	60.10	30.03	22.10	4.71
7.5 RP 4/12	41.25	52.52	0.54	115	23	59	41.59	46.62	-4.25	3.07
10 YR 7/4	70.05	4.63	27.19	147	126	81	70.36	0.52	24.05	3.86
7.5YR7/6	71.22	12.54	34.09	163	119	69	69.87	6.91	29.83	4.16
7.5PB4/6	41.06	6.95	-24.74	48	52	107	44.39	10.29	-27.81	3.56
5P4/10	39.59	32.15	-27.96	71	37	110	42.10	30.51	-32.67	3.75
5 R 4/10	41.01	44.41	19.55	118	20	31	40.21	46.32	15.60	2.69
10GY7/8	70.09	-37.48	32.28	77	162	79	73.39	-35.51	28.37	2.95
5 YR 7/6	70.26	16.91	29.31	169	114	81	69.50	12.16	23.15	3.50
7.5R4/10	40.16	43.95	28.85	121	21	22	40.68	45.39	25.10	2.49
5Y8/4	79.56	-3.33	29.44	161	166	109	79.28	-7.31	23.35	4.84
2.5BG7/4	70.95	-20.57	0.42	97	161	151	75.48	-18.22	0.64	3.67
2.5G8/2	80.10	-10.98	5.90	149	176	168	81.31	-6.98	3.27	4.06
5RP4/12	41.72	51.19	-6.39	112	28	73	43.12	43.82	-10.87	3.69
10BG8/2	79.33	-9.23	-2.91	141	171	177	80.15	-6.21	-1.61	3.13
5PB4/2	40.80	0.34	-8.82	49	59	74	45.60	-1.95	-8.46	5.36
10Y8.5/4	86.29	-8.76	32.89	171	184	127	83.23	-8.69	21.47	5.78
2.5B8/2	79.01	-8.08	-3.5	143	174	181	80.85	-6.23	-1.94	2.51
7.5G8/4	79.79	-23.20	5.96	123	186	168	81.69	-17.12	3.66	3.96
10P4/4	41.42	15.68	-8.02	74	52	79	46.04	14.13	-10.40	4.80

Table B5 Calculated CIELAB from Canon EOS X4's digital image scene 20 under Fluorescent D65 and ΔE_{00} toward measured CIELAB, D65/2°.

Calculated CIELAB from Canon's digital image scene 20 under Fluorescent D65 and DE00 toward measured CIELAB, D65/2										
Munsell Patches	Measured Spectrophotometer			R	G	B	Calculated CIELAB of scene 20			ΔE_{00}
	L*	a*	b*				L*	a*	b*	
N 2	21.15	-0.15	-0.82	20	20	20	19.15	0.46	-0.53	1.69
N 3.5	36.28	-0.45	-0.90	45	50	50	37.53	-1.39	-1.10	1.70
N 5	52.15	-0.43	-0.62	86	96	97	56.74	-1.45	-1.47	4.68
N 6.5	66.68	-0.93	-0.63	124	136	137	69.83	-0.85	-0.97	2.52
N 8	81.55	-0.85	-0.97	162	175	176	80.79	-0.11	-0.46	1.28
N 9.5	95.71	-0.59	1.54	192	206	204	88.52	-0.02	0.86	4.54
7.5P4/10	42.10	31.96	-21.37	92	48	116	45.01	33.57	-28.97	4.58
10PB4/6	41.21	13.96	-23.96	63	59	113	44.88	15.54	-27.90	3.92
2.5GY8/8	79.24	-17.71	54.70	154	183	57	79.94	-19.65	51.59	1.84
7.5GY7/10	68.01	-36.06	49.74	86	170	41	73.17	-40.50	51.65	4.26
10R6/8	61.66	31.08	30.41	176	80	62	60.48	32.81	24.89	3.89
7.5RP4/12	41.25	52.52	0.54	126	25	63	41.61	51.26	-3.08	1.85
10YR7/4	70.05	4.63	27.19	152	136	82	70.76	0.59	26.81	3.59
7.5YR7/6	71.22	12.54	34.09	166	127	69	69.73	7.57	32.69	3.76
7.5PB4/6	41.06	6.95	-24.74	51	61	114	44.36	10.10	-29.30	3.57
5P4/10	39.59	32.15	-27.96	81	43	121	42.48	34.73	-35.53	4.23
5R4/10	41.01	44.41	19.55	126	26	33	40.90	47.17	19.10	1.15
10GY7/8	70.09	-37.48	32.28	79	171	79	73.55	-37.97	31.22	2.68
5YR7/6	70.26	16.91	29.31	173	122	81	69.45	13.34	25.88	2.39
7.5R4/10	40.16	43.95	28.85	129	25	24	40.89	47.85	27.62	2.14
5Y8/4	79.56	-3.33	29.44	163	172	108	79.11	-7.22	25.45	4.01
2.5BG7/4	70.95	-20.57	0.42	99	168	154	75.34	-18.63	-0.23	3.51
2.5G8/2	80.10	-10.98	5.90	150	182	169	81.25	-6.95	2.80	4.24
5RP4/12	41.72	51.19	-6.39	120	31	77	42.69	47.44	-10.63	2.64
10BG8/2	79.33	-9.23	-2.91	143	178	178	80.26	-6.18	-2.12	3.09
5PB4/2	40.80	0.34	-8.82	54	65	79	44.59	-0.09	-9.77	3.58
10Y8/4	80.25	-7.58	29.94	164	177	117	80.26	-7.71	22.97	3.37
2.5B8/2	79.01	-8.08	-3.5	146	181	181	81.05	-6.06	-2.07	2.67
7.5G8/4	79.79	-23.20	5.96	124	192	168	81.67	-17.93	3.61	3.52
10P6/4	60.60	13.53	-7.02	133	113	139	65.57	12.73	-8.06	4.32

Table B6 Calculated CIELAB from Canon EOS X4's digital image scene 21 under Fluorescent D65 and ΔE_{00} toward measured CIELAB, D65/2°.

Calculated CIELAB from Canon's digital image scene 21 under Fluorescent D65 and DE00 toward measured CIELAB, D65/2										
Munsell Patches	Measured Spectrophotometer			R	G	B	Calculated CIELAB of scene 21			ΔE_{00}
	L*	a*	b*				L*	a*	b*	
N 2	21.15	-0.15	-0.82	19	19	19	19.62	0.14	-0.77	1.15
N 3.5	36.28	-0.45	-0.90	43	45	45	36.58	-0.51	-1.12	0.33
N 5	52.15	-0.43	-0.62	85	92	90	56.61	-1.76	-0.46	4.66
N 6.5	66.68	-0.93	-0.63	124	131	130	69.57	-0.67	-0.74	2.32
N 8	81.55	-0.85	-0.97	164	174	173	81.38	-0.70	-0.78	0.30
N 9.5	95.71	-0.59	1.54	196	204	201	88.89	0.03	0.21	4.47
7.5P4/10	42.10	31.96	-21.37	91	46	110	45.17	32.79	-28.31	4.51
10PB4/6	41.21	13.96	-23.96	65	56	107	45.20	16.45	-26.92	4.01
2.5GY8/8	79.24	-17.71	54.70	161	185	53	81.35	-19.95	53.57	2.04
7.5GY7/10	68.01	-36.06	49.74	93	173	38	75.04	-39.92	53.95	5.54
10R6/8	61.66	31.08	30.41	178	79	59	61.01	31.43	25.13	3.17
7.5RP4/12	41.25	52.52	0.54	125	23	59	41.38	50.98	-3.26	1.93
10YR7/4	70.05	4.63	27.19	156	135	78	71.57	0.21	27.73	4.06
7.5B7/8	71.19	-19.62	-26.92	83	173	201	77.44	-17.12	-17.42	6.46
7.5PB4/6	41.06	6.95	-24.74	51	58	107	44.46	10.06	-28.17	3.56
5P4/10	39.59	32.15	-27.96	80	39	114	41.99	35.46	-35.43	3.86
5R4/10	41.01	44.41	19.55	126	24	30	40.82	47.08	19.50	1.01
10GY7/8	70.09	-37.48	32.28	81	172	75	74.74	-38.49	32.66	3.52
5YR7/6	70.26	16.91	29.31	173	117	74	69.01	12.85	26.74	2.76
7.5R4/10	40.16	43.95	28.85	123	20	19	39.00	47.95	28.41	2.04
5Y8/4	79.56	-3.33	29.44	164	167	102	78.83	-7.15	25.52	3.95
2.5BG7/4	70.95	-20.57	0.42	101	163	147	75.23	-17.66	0.09	3.67
2.5G8/2	80.10	-10.98	5.90	150	177	162	80.94	-6.97	2.72	4.22
5RP4/12	41.72	51.19	-6.39	118	26	71	41.58	48.65	-11.17	2.52
10BG8/2	79.33	-9.23	-2.91	146	177	176	80.98	-6.10	-2.62	3.29
5PB4/2	40.80	0.34	-8.82	51	59	70	43.36	-0.12	-8.67	2.40
10Y8/4	80.25	-7.58	29.94	165	173	111	80.17	-7.98	23.19	3.34
2.5B8/2	79.01	-8.08	-3.5	148	178	178	81.31	-5.66	-2.87	2.94
7.5G8/4	79.79	-23.20	5.96	128	189	164	82.03	-16.86	3.38	4.24
10P6/4	60.60	13.53	-7.02	129	106	129	64.42	12.25	-7.83	3.48

Table B7 Calculated CIELAB from Canon's digital image scene 22 under Fluorescent D65 and ΔE_{00} toward measured CIELAB, D65/2°.

Calculated CIELAB from Canon's digital image scene 22 under Fluorescent D65 and DE00 toward measured CIELAB, D65/2										
Munsell Patches	Measured Spectrophotometer			R	G	B	Calculated CIELAB of scene 22			ΔE_{00}
	L*	a*	b*				L*	a*	b*	
N 2	21.15	-0.15	-0.82	18	18	18	19.67	-0.02	-0.79	1.05
N 3.5	36.28	-0.45	-0.90	42	43	43	36.58	-0.24	-0.91	0.40
N 5	52.15	-0.43	-0.62	83	89	88	56.51	-1.58	-0.74	4.48
N 6.5	66.68	-0.93	-0.63	121	127	127	69.24	-0.66	-0.91	2.09
N 8	81.55	-0.85	-0.97	162	171	171	81.35	-0.78	-0.84	0.21
N 9.5	95.71	-0.59	1.54	196	203	200	89.27	-0.21	0.53	4.09
7.5P4/10	42.10	31.96	-21.37	89	43	107	44.81	33.42	-28.52	4.30
10PB4/6	41.21	13.96	-23.96	62	53	103	44.73	16.24	-26.78	3.57
2.5GY8/8	79.24	-17.71	54.70	157	182	51	81.20	-20.66	53.42	2.28
7.5GY7/10	68.01	-36.06	49.74	91	168	37	74.61	-39.24	53.09	5.17
10R6/8	61.66	31.08	30.41	174	75	59	60.48	31.73	23.10	4.53
7.5RP4/12	41.25	52.52	0.54	122	23	58	41.58	49.90	-3.69	2.26
10YR7/4	70.05	4.63	27.19	152	131	77	71.21	0.09	26.58	4.09
7.5B 7/6	71.58	-15.14	-20.64	97	166	188	77.19	-13.42	-13.68	5.58
7.5PB4/6	41.06	6.95	-24.74	50	56	105	44.59	10.22	-28.14	3.70
5P4/10	39.59	32.15	-27.96	76	39	111	42.24	33.29	-34.72	3.99
5R4/10	41.01	44.41	19.55	124	24	30	41.19	46.24	18.62	1.04
10GY7/8	70.09	-37.48	32.28	81	168	73	74.62	-37.53	32.43	3.41
5YR7/6	70.26	16.91	29.31	172	116	73	69.46	12.29	26.69	3.05
7.5R4/10	40.16	43.95	28.85	122	20	19	39.48	47.45	27.78	1.92
5Y8/4	79.56	-3.33	29.44	162	165	99	78.98	-7.71	26.04	4.18
2.5BG7/4	70.95	-20.57	0.42	104	166	150	76.79	-17.62	0.29	4.69
2.5G8/2	80.10	-10.98	5.90	151	179	164	82.07	-7.49	2.80	3.97
5RP4/12	41.72	51.19	-6.39	122	29	74	43.77	47.76	-11.07	3.22
10BG8/2	79.33	-9.23	-2.91	149	180	178	82.40	-6.48	-1.99	3.45
5PB4/2	40.08	0.34	-8.82	52	61	72	45.15	-0.78	-8.56	4.87
10Y8/4	80.25	-7.58	29.94	167	177	114	81.75	-8.84	23.00	3.89
2.5B8/2	79.01	-8.08	-3.5	152	182	181	82.98	-6.03	-2.22	3.52
7.5G8/4	79.79	-23.20	5.96	130	193	167	83.59	-17.46	3.71	4.36
10P6/4	60.60	13.53	-7.02	133	109	133	66.30	12.09	-7.80	4.98

APPENDIX C

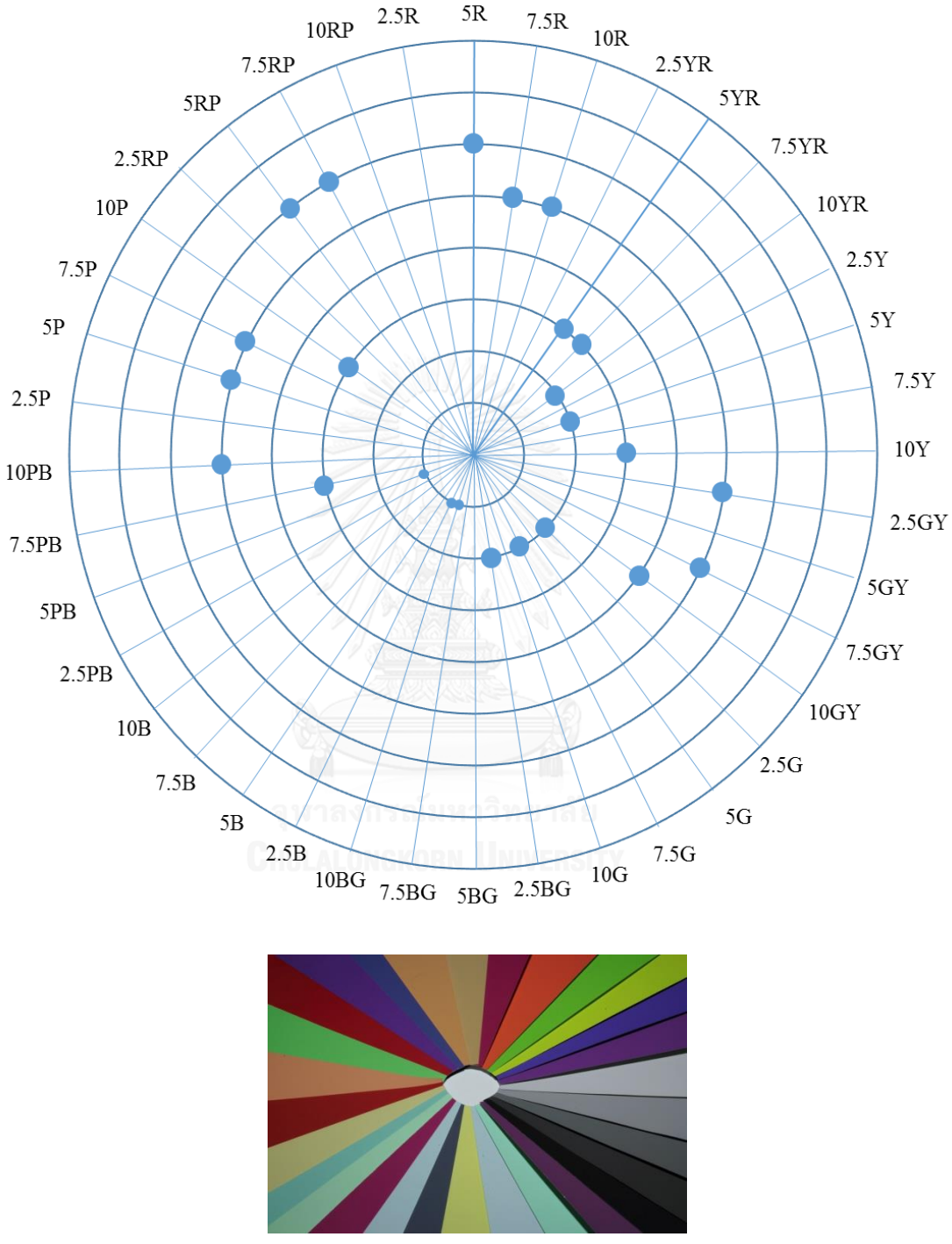

Figure C1 Hue-Chroma chart of the colours used in scene 15.

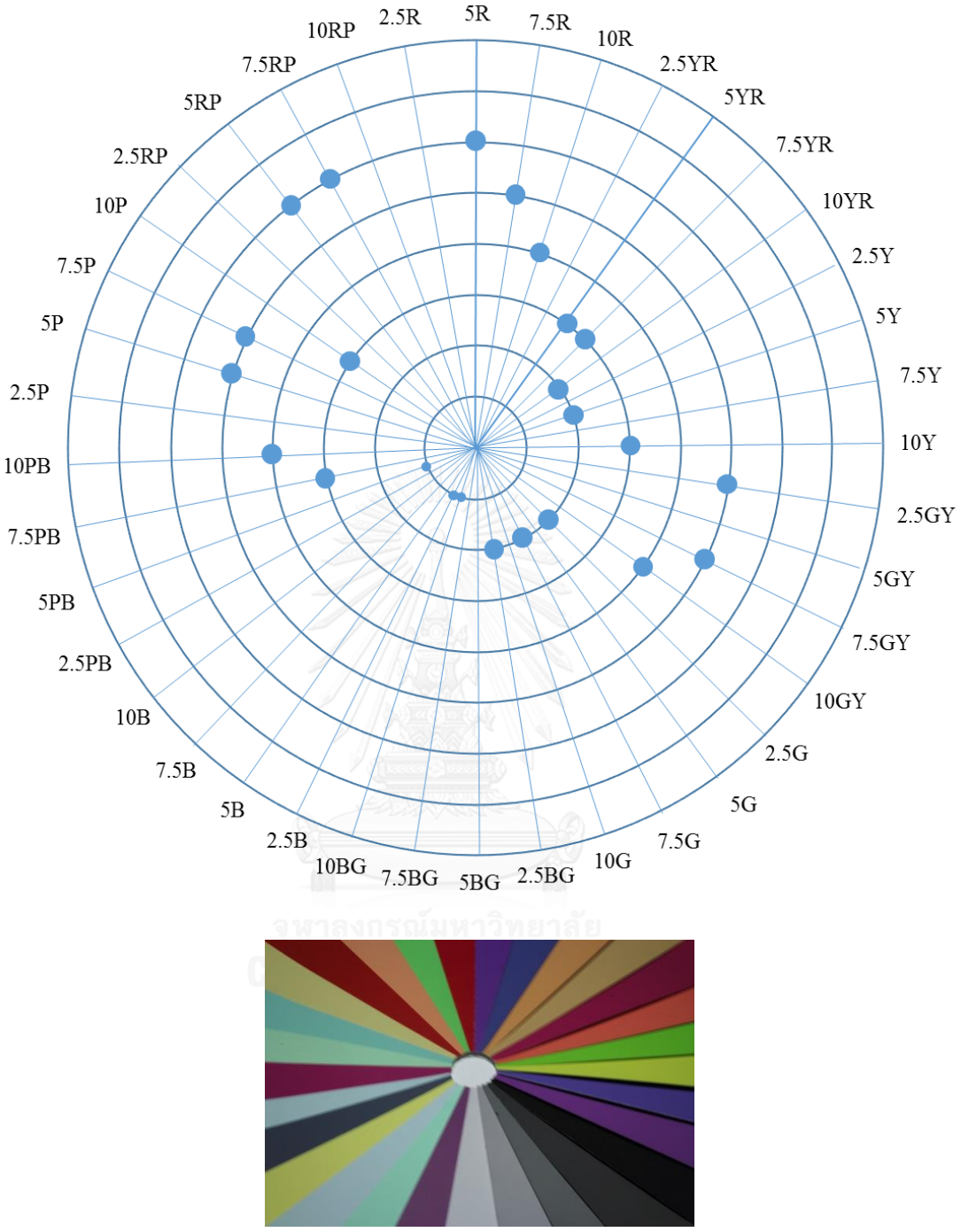

Figure C2 Hue-Chroma chart of the colours used in scene 16.

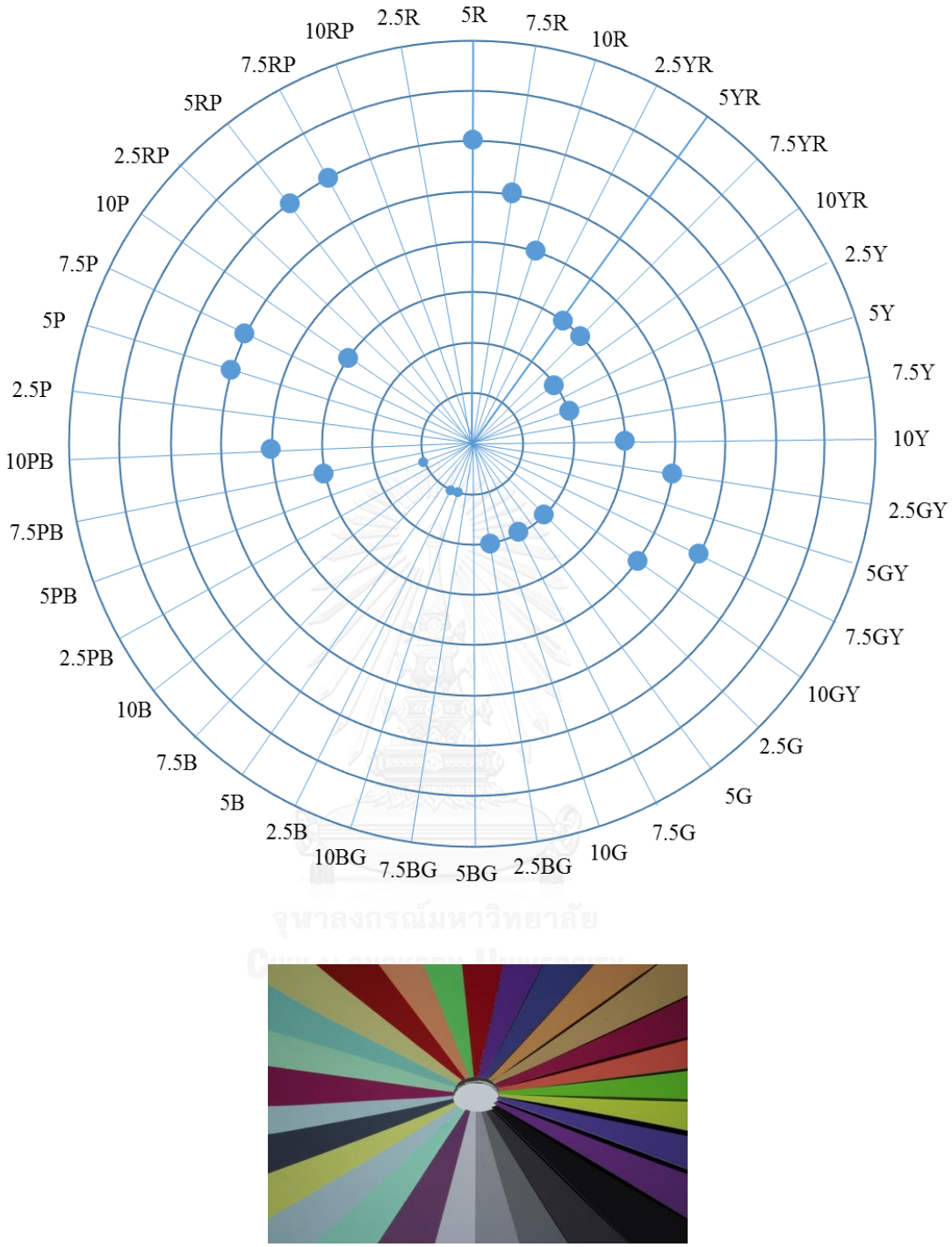

Figure C3 Hue-Chroma chart of the colours used in scene 17.

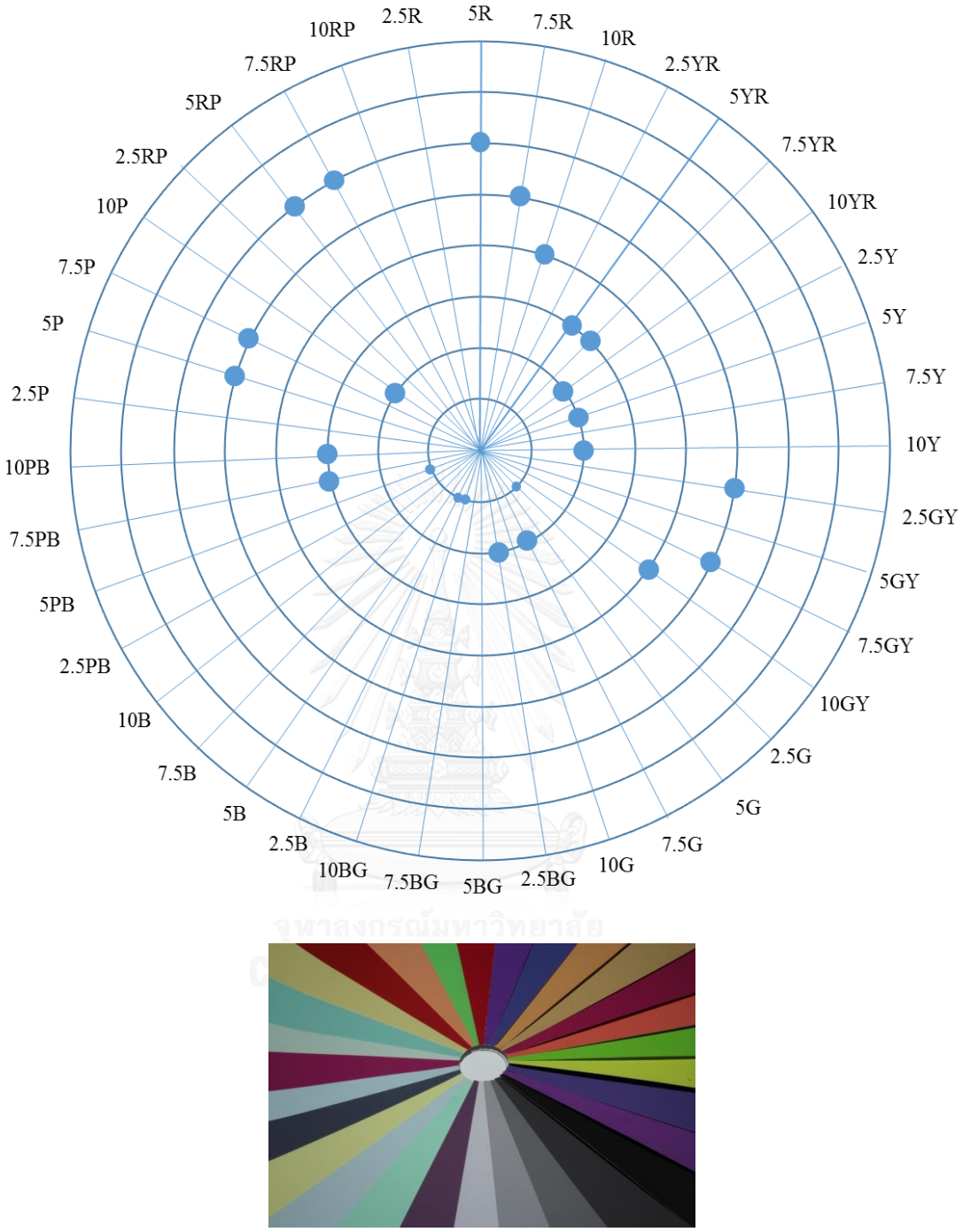

Figure C4 Hue-Chroma chart of the colours used in scene 18.

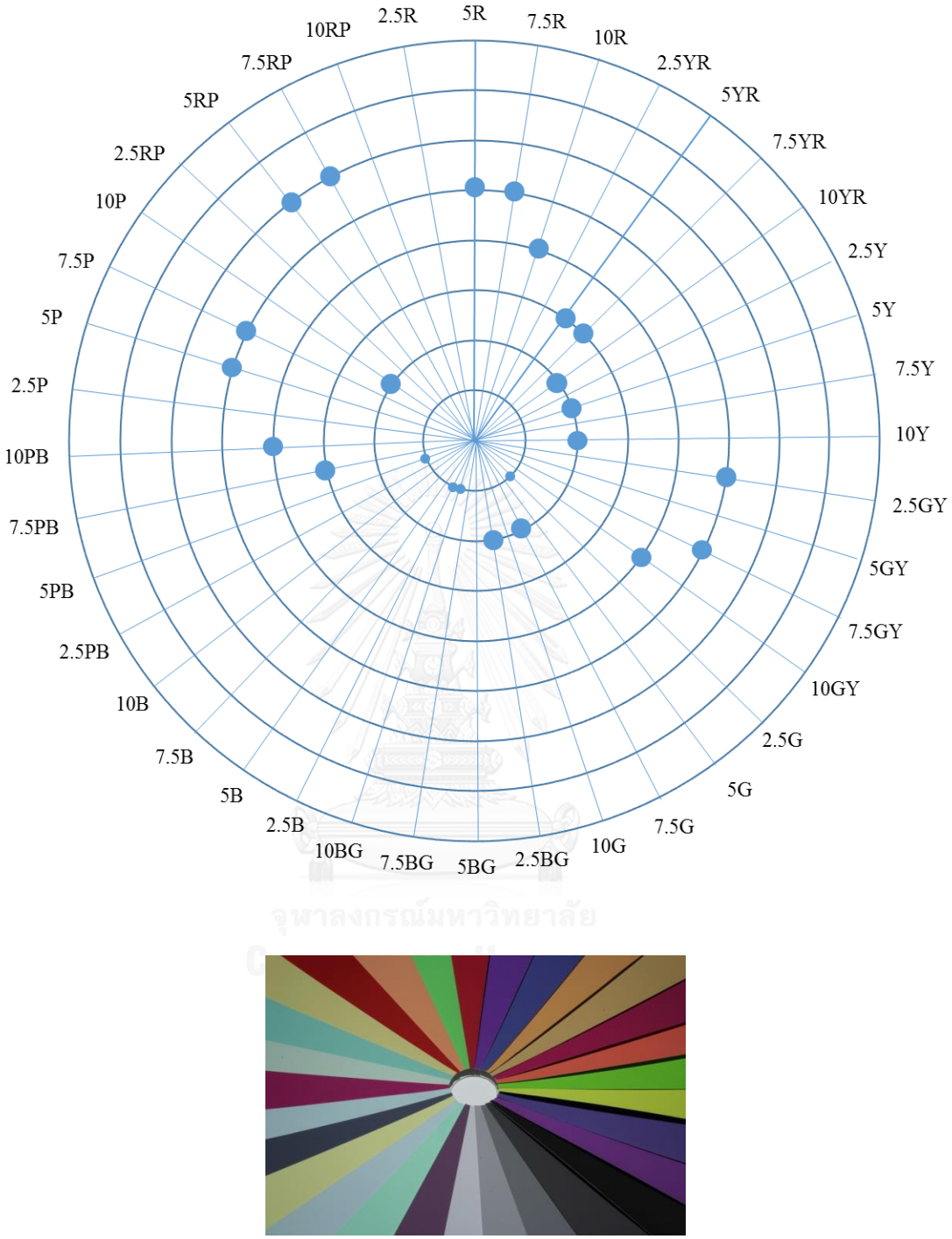

Figure C5 Hue-Chroma chart of the colours used in scene 19.

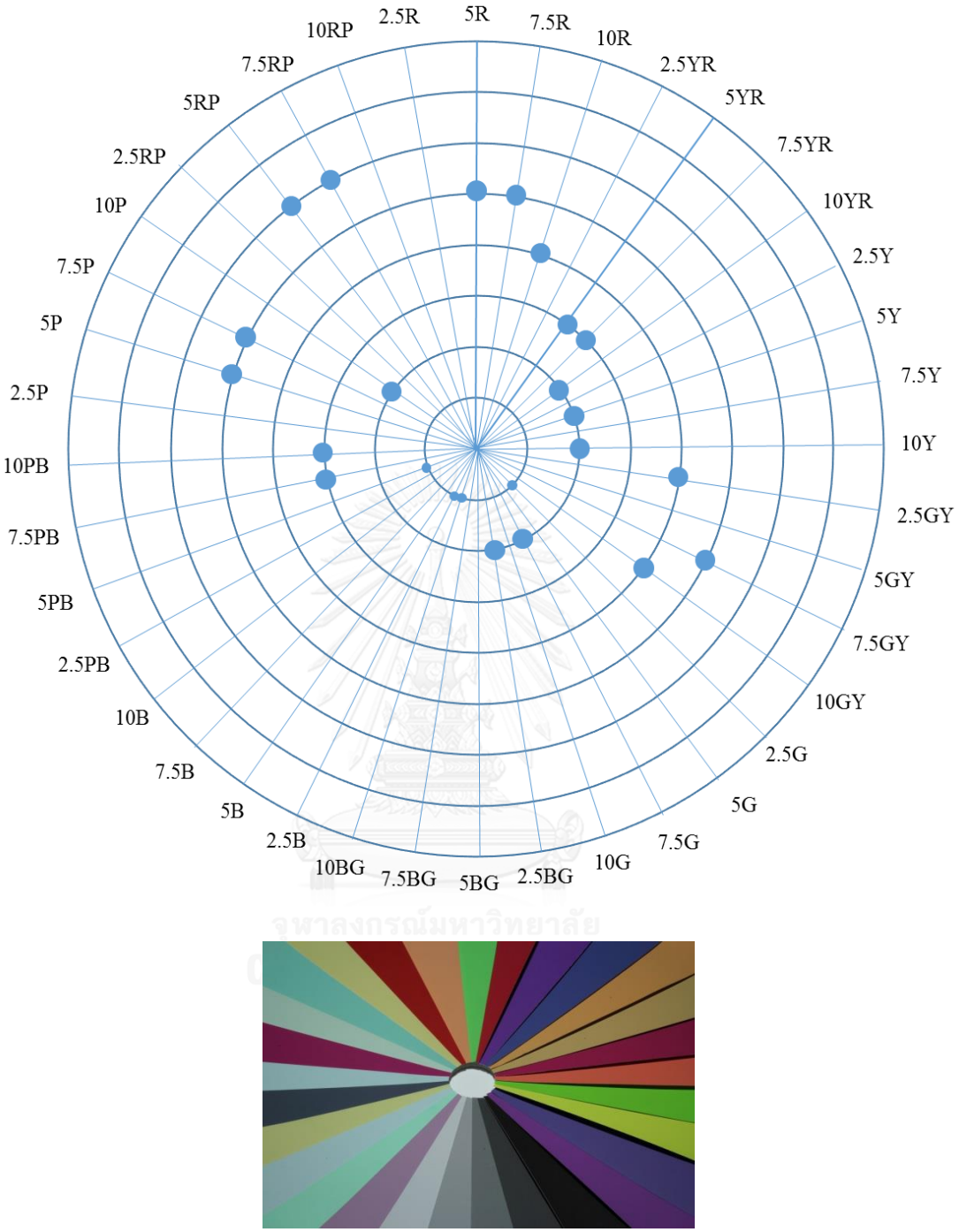

Figure C6 Hue-Chroma chart of the colours used in scene 20.

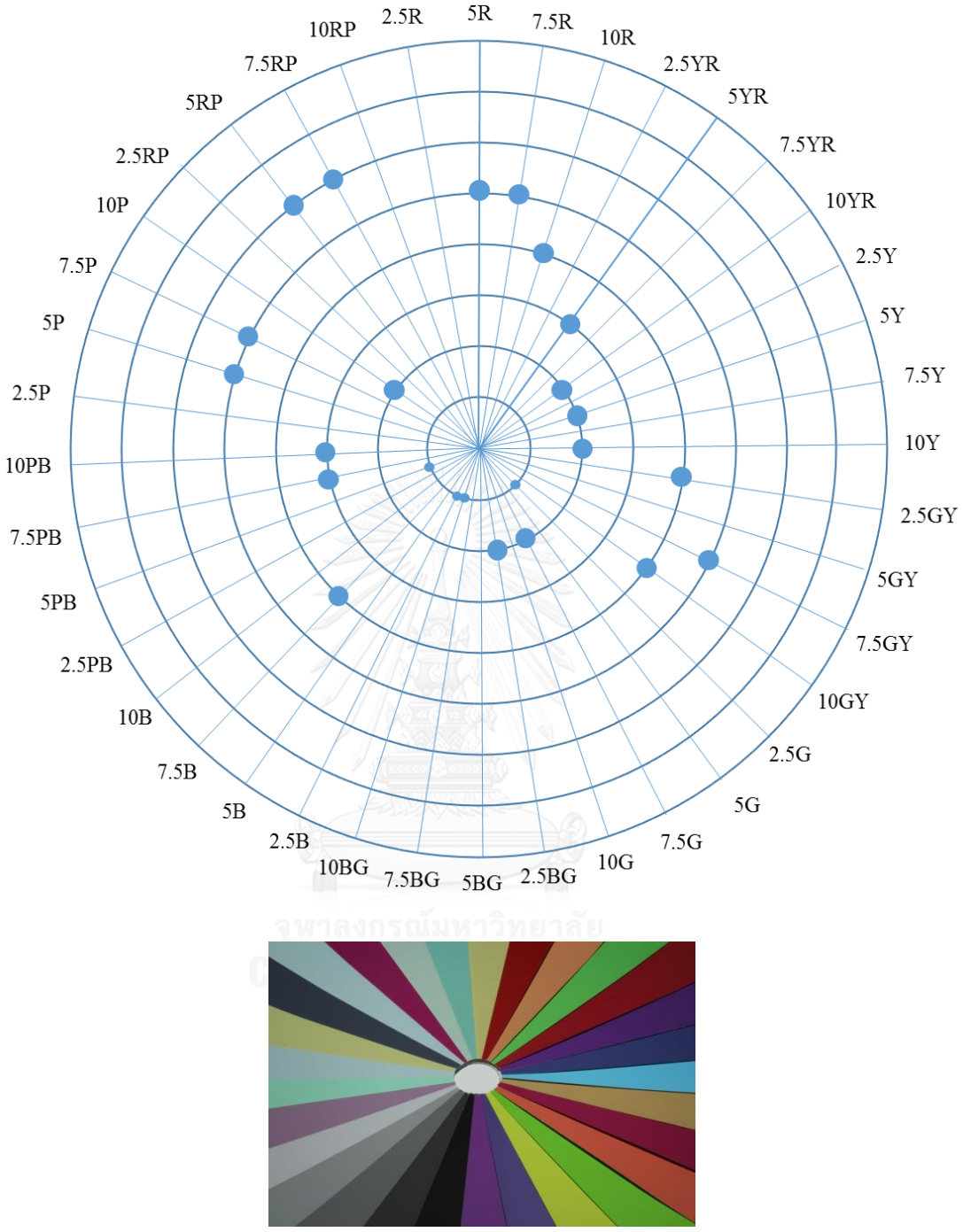

Figure C7 Hue-Chroma chart of the colours used in scene 21.

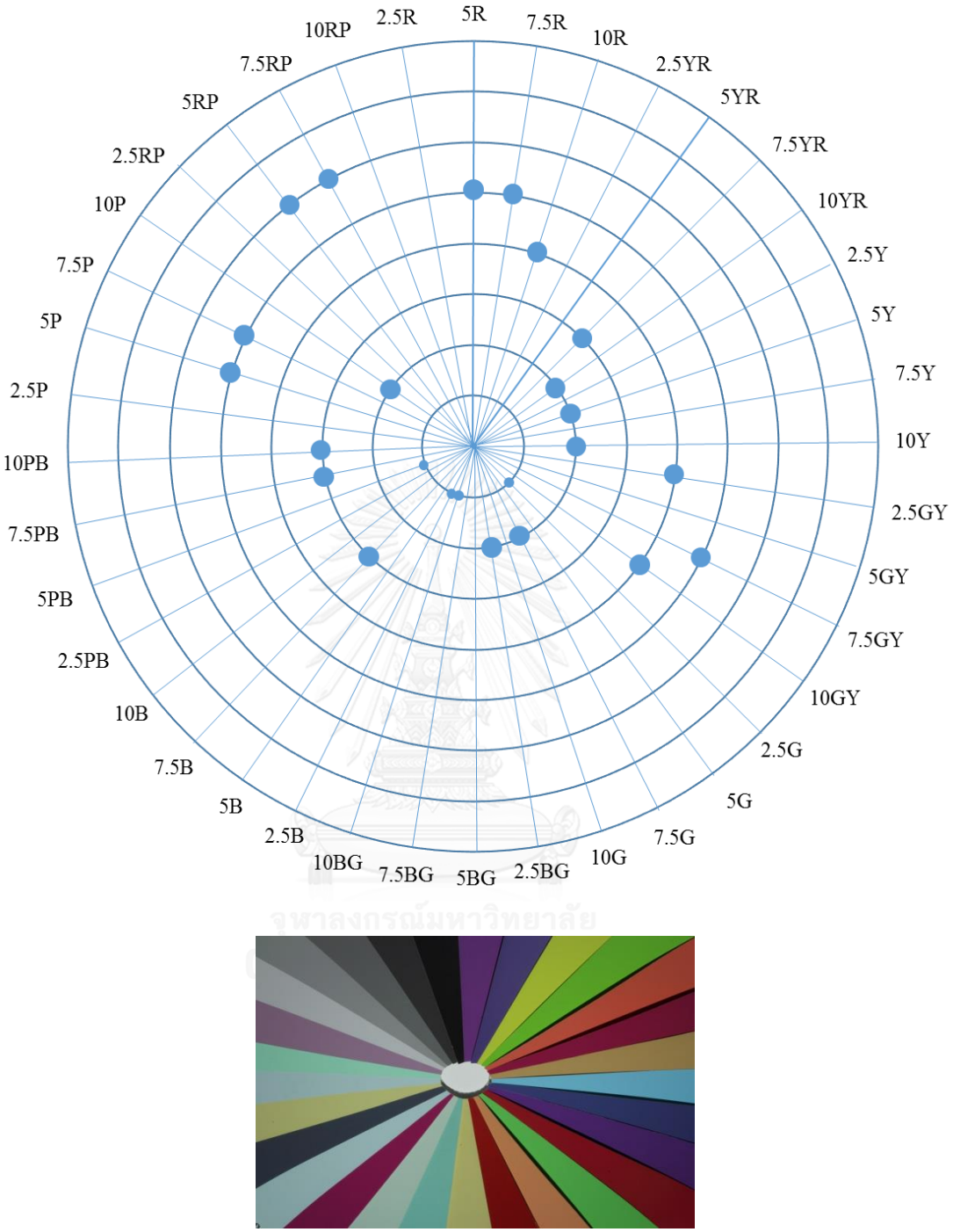

Figure C8 Hue-Chroma chart of the colours used in scene 22.

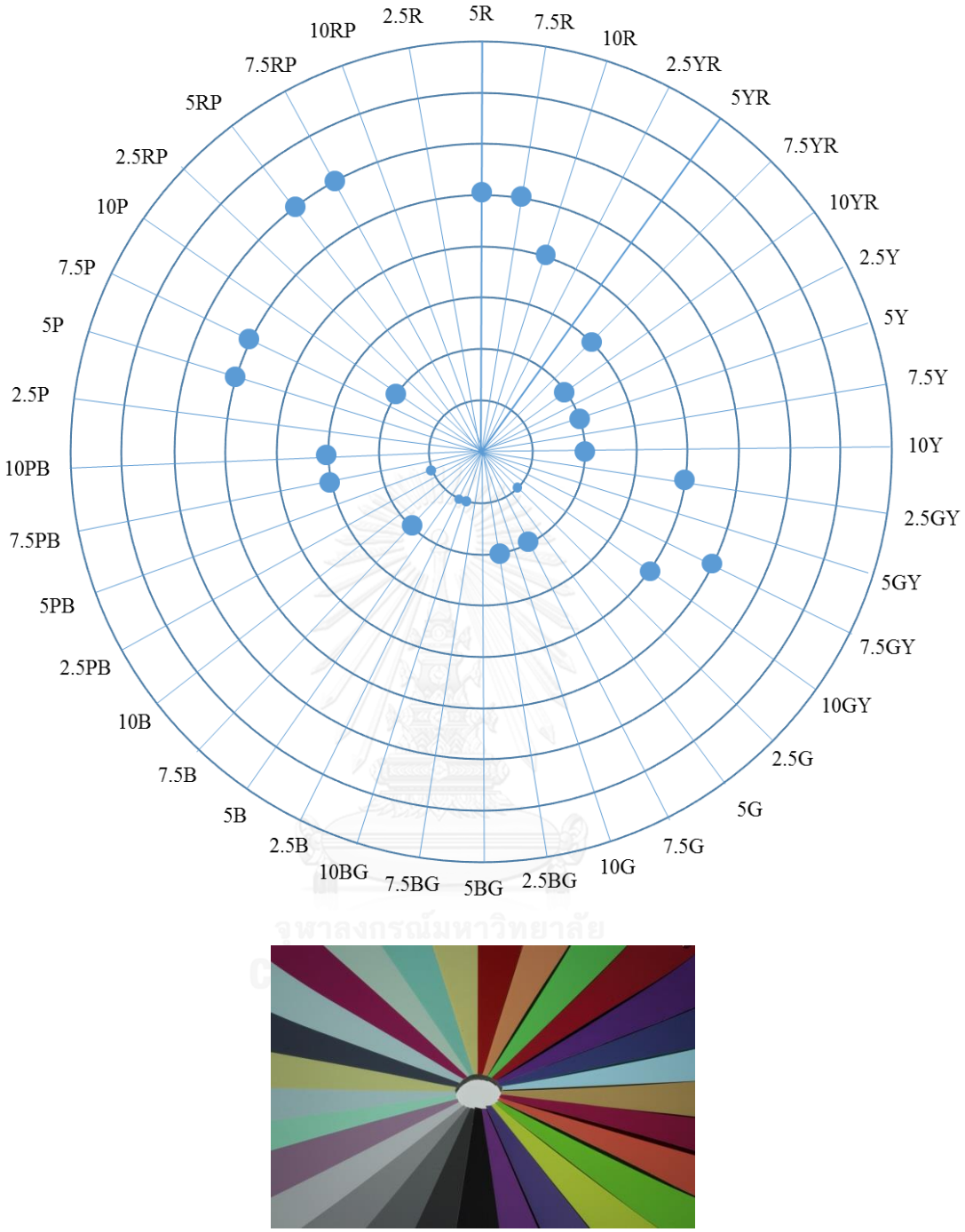

Figure C9 Hue-Chroma chart of the colours used in scene 23.

APPENDIX D

Table D1 Calculated CIELAB from Nikon D70's digital image under both light sources (Fluorescent D65 and LED D65) and ΔE00 toward spectroradiometric measured CIELAB, D65/2°.

Munsell Patches	Fluorescent D65							LED D65						
	R	G	B	L*	a*	b*	ΔE00	R	G	B	L*	a*	b*	ΔE00
N2	47	50	49	21.34	-0.52	-0.08	1.01	45	48	48	21.14	-0.46	-0.45	0.99
N3.5	77	81	83	35.90	0.05	-1.86	1.59	77	80	82	36.25	0.15	-1.43	0.61
N5	117	121	124	52.20	0.36	-1.88	2.40	117	120	122	52.34	0.03	-1.08	1.10
N6.5	155	162	163	66.86	-1.03	-0.79	1.32	155	161	163	66.78	-1.17	-1.13	1.37
N8	195	202	204	80.30	-0.87	-0.83	1.58	197	202	204	80.28	-1.09	-0.76	0.91
N9.5	248	255	251	96.68	-1.86	2.16	1.76	253	255	253	96.42	-1.23	1.42	1.16
7.5P4/10	117	74	133	40.15	30.33	-25.22	2.02	113	71	137	39.66	30.95	-28.74	1.27
10PB4/6	83	79	132	37.79	15.79	-28.60	3.56	83	75	133	37.36	18.18	-30.31	2.59
2.5GY8/8	202	214	91	81.80	-17.83	55.08	2.33	208	218	83	82.82	-18.96	59.36	2.31
7.5GY7/10	129	189	64	70.63	-36.26	53.60	2.93	141	190	57	71.59	-32.99	57.41	2.50
10R6/8	217	118	97	61.11	35.48	27.16	1.37	213	131	96	63.40	25.31	29.92	2.05
7.5RP4/12	154	58	92	40.33	45.01	0.11	1.86	146	57	95	39.29	42.27	-4.15	2.16
10YR7/4	196	172	120	71.64	2.40	28.36	1.30	197	176	120	72.63	-0.40	29.19	1.19
7.5B8/4	160	214	237	81.80	-10.91	-14.13	3.01	127	211	238	79.41	-17.81	-17.96	6.96
7.5PB4/6	70	84	134	38.23	8.99	-29.13	3.41	72	82	137	38.61	11.34	-30.68	2.64
5P4/10	108	67	136	37.51	32.44	-31.16	1.91	105	63	141	36.99	34.41	-35.26	1.10
5R4/10	162	63	62	41.81	42.24	21.61	1.77	151	64	62	40.60	36.57	18.92	2.36
10GY7/8	125	195	109	72.54	-35.16	34.17	2.14	135	195	102	73.03	-32.68	37.87	2.43
5YR7/6	220	162	119	71.41	16.04	28.95	2.02	219	169	119	72.78	10.51	30.21	1.90
7.5R4/10	164	62	49	41.72	42.55	30.04	1.43	153	65	48	40.85	35.63	28.50	2.36
5Y8/4	209	207	141	81.25	-7.29	30.83	1.21	213	208	142	81.55	-7.32	30.43	1.15
2.5BG7/4	131	189	177	72.56	-19.30	0.37	3.14	140	187	174	72.56	-16.36	1.78	2.47
2.5G8/2	184	213	198	82.04	-10.42	4.45	2.24	193	215	197	82.86	-9.31	6.19	1.83
5RP4/12	150	62	106	40.93	43.39	-7.71	2.17	145	61	110	40.45	41.83	-11.54	2.89
10BG8/2	176	209	212	80.91	-8.65	-3.82	1.75	183	209	212	81.20	-7.10	-3.20	0.83
5PB4/2	82	92	107	40.50	0.71	-9.77	1.37	84	91	108	41.04	1.97	-10.13	1.37
10Y8/4	215	214	150	83.45	-7.38	29.50	1.70	216	216	145	83.62	-9.55	31.79	2.16
2.5B8/2	177	209	212	80.97	-8.35	-3.72	0.98	182	207	212	80.67	-6.47	-3.97	2.66
7.5G8/4	158	221	196	82.45	-22.23	5.77	2.68	168	219	193	82.28	-19.08	7.02	3.64
10P6/4	164	139	163	61.89	14.11	-8.03	1.81	161	138	164	61.65	12.83	-9.16	3.02
						Mean	1.99						Mean	2.07
						Max	3.56						Max	6.96
						Min	0.98						Min	0.61
						STD	0.69						STD	1.20

Table D2 Calculated CIELAB from Canon 6D's digital image under both light sources (Fluorescent D65 and LED D65) and ΔE00 toward spectroradiometric measured CIELAB, D65/2°.

Munsell Patches	Fluorescent D65							LED D65						
	R	G	B	L*	a*	b*	ΔE_{00}	R	G	B	L*	a*	b*	ΔE_{00}
N2	13	13	15	20.94	0.46	-1.02	1.08	14	12	14	19.92	0.28	-1.44	0.97
N3.5	26	29	31	35.04	-2.07	-0.47	2.56	34	31	32	36.81	-1.01	0.87	2.42
N5	61	61	65	54.25	0.54	-0.29	2.67	66	64	68	55.06	-1.37	-0.97	3.95
N6.5	94	98	105	69.32	-0.32	-1.77	3.26	102	99	107	69.24	-0.38	-2.28	3.07
N8	127	135	140	81.26	-1.56	-0.86	1.53	138	135	141	80.81	-0.69	-0.94	0.50
N9.5	169	173	175	92.14	-0.48	0.77	3.58	177	171	173	90.83	-0.26	0.97	3.22
7.5P4/10	62	28	72	42.29	30.74	-23.11	2.03	64	29	78	42.37	29.02	-26.72	2.96
10PB4/6	37	32	70	40.23	14.68	-25.23	0.89	44	33	77	41.34	16.48	-27.88	1.72
2.5GY8/8	128	138	36	80.02	-17.45	54.98	2.93	138	147	28	81.34	-21.09	61.88	1.23
7.5GY7/10	66	123	29	72.12	-36.81	50.07	2.91	82	129	26	73.67	-35.11	54.05	2.60
10R6/8	138	51	38	58.77	33.49	27.94	2.38	144	66	35	62.34	21.66	34.73	4.65
7.5RP4/12	78	15	33	37.71	42.89	2.46	4.09	83	19	39	39.25	38.36	-1.44	3.87
10YR7/4	122	100	57	70.94	0.73	29.21	2.74	135	109	56	73.02	-2.28	32.68	2.64
7.5B8/4	106	150	172	83.86	-9.01	-10.65	3.49	121	147	173	82.97	-5.62	-10.99	3.17
7.5PB4/6	31	37	76	41.97	8.52	-26.64	1.01	42	38	82	43.48	12.19	-27.74	3.35
5P4/10	51	24	73	38.93	30.72	-29.17	1.42	55	27	85	40.64	29.39	-33.92	3.66
5R4/10	85	12	15	37.06	45.90	23.66	4.58	81	15	19	36.31	38.46	16.26	2.03
10GY7/8	63	129	58	73.98	-35.34	31.74	2.85	80	134	51	75.18	-33.80	37.98	3.50
5YR7/6	140	88	51	69.28	12.67	31.49	5.21	153	101	53	72.42	7.26	34.18	4.30
7.5R4/10	84	13	11	37.12	43.89	29.80	4.12	81	16	13	36.50	36.33	24.99	2.16
5Y8/4	135	133	77	80.08	-7.51	29.14	2.31	148	138	74	80.78	-8.47	32.07	0.40
2.5BG7/4	79	127	122	75.91	-16.44	-0.77	5.51	93	131	120	76.67	-16.02	2.14	4.84
2.5G8/2	122	147	139	83.49	-8.32	2.79	4.21	134	146	133	82.71	-7.62	5.27	2.92
5RP4/12	82	20	46	41.04	41.35	-4.81	3.48	78	19	51	39.00	38.88	-12.32	2.49
10BG8/2	114	145	149	82.78	-8.31	-2.66	1.39	130	143	148	82.14	-5.30	-2.03	2.30
5PB4/2	35	39	50	42.13	0.46	-7.32	1.30	41	41	54	43.34	0.64	-8.65	3.52
10Y8/4	137	139	85	81.67	-8.31	26.83	2.85	146	143	77	81.76	-10.74	31.66	0.97
2.5B8/2	117	144	151	82.80	-6.68	-3.47	2.34	130	143	151	82.21	-4.84	-3.20	4.12
7.5G8/4	97	153	135	83.19	-19.05	3.94	4.68	116	154	133	83.31	-16.07	6.01	5.61
10P6/4	99	76	102	63.72	13.51	-8.39	3.22	104	77	105	63.52	12.24	-9.69	4.24
						Mean	2.89						Mean	2.91
						Max	5.51						Max	5.61
						Min	0.89						Min	0.40
						STD	1.26						STD	1.30

Table D3 Calculated CIELAB from Canon 600D's digital image under both light sources (Fluorescent D65 and LED D65) and ΔE00 toward spectroradiometric measured CIELAB, D65/2°.

Munsell Patches	Fluorescent D65							LED D65						
	R	G	B	L*	a*	b*	ΔE_{00}	R	G	B	L*	a*	b*	ΔE_{00}
N2	17	15	16	20.84	0.59	-1.00	1.24	17	15	16	19.97	0.47	-0.97	0.88
N3.5	33	33	33	36.04	-1.75	-0.11	1.93	37	37	37	36.81	-2.04	-0.21	2.98
N5	61	61	63	52.96	-0.63	-1.36	1.99	75	71	74	54.82	0.41	-1.39	3.45
N6.5	93	96	98	68.53	-1.15	-1.28	2.43	110	110	112	69.38	-1.29	-1.06	2.98
N8	128	131	133	81.48	-0.24	-0.86	1.79	147	145	146	80.51	-0.66	-0.28	0.34
N9.5	164	168	166	93.11	-0.22	1.01	3.11	187	184	184	91.19	-0.31	0.24	3.37
7.5P4/10	60	31	73	41.48	28.06	-26.15	2.92	71	35	90	42.90	29.98	-29.41	3.09
10PB4/6	38	36	70	40.25	11.47	-26.11	3.17	49	39	86	41.49	17.02	-29.38	2.19
2.5GY8/8	121	138	43	80.80	-20.34	51.31	3.35	142	154	41	80.21	-20.37	54.42	3.00
7.5GY7/10	66	117	26	70.76	-37.96	51.68	2.76	91	138	30	73.28	-33.96	53.25	2.79
10R6/8	134	52	40	58.37	34.61	26.28	1.89	148	72	45	61.28	22.03	28.72	1.96
7.5RP4/12	83	15	38	37.38	46.52	-2.25	2.99	94	16	48	37.49	47.01	-7.98	0.79
10YR7/4	117	99	61	70.60	0.24	25.67	3.57	139	116	70	71.98	-1.30	25.94	2.12
7.5B8/4	108	148	163	84.82	-9.67	-10.29	3.26	132	158	177	82.96	-5.46	-9.54	3.59
7.5PB4/6	34	40	75	41.84	7.24	-27.32	2.21	45	44	91	43.23	12.42	-29.72	3.35
5P4/10	52	27	76	38.66	29.66	-32.84	3.10	65	31	94	40.85	32.54	-35.08	3.15
5R4/10	89	12	18	36.67	48.59	20.55	4.80	94	19	24	37.50	40.24	15.39	1.99
10GY7/8	71	125	60	74.04	-32.97	30.25	3.66	91	141	63	74.54	-30.03	32.96	4.27
5YR7/6	136	88	58	69.36	13.95	26.49	3.29	154	107	66	70.93	7.50	27.18	2.86
7.5R4/10	88	13	11	36.55	46.32	30.87	4.52	95	19	14	37.32	39.18	27.77	1.77
5Y8/4	132	130	81	80.38	-6.75	26.06	3.33	155	148	94	80.62	-7.00	24.46	3.49
2.5BG7/4	79	126	116	76.20	-18.71	-0.27	4.56	103	136	126	75.39	-13.09	0.90	5.58
2.5G8/2	120	142	131	83.47	-8.59	2.96	3.98	143	154	141	82.04	-6.28	4.07	4.26
5RP4/12	84	20	50	40.08	44.07	-9.56	1.98	93	19	61	38.98	46.16	-15.98	1.14
10BG8/2	117	141	142	83.28	-7.23	-2.73	2.47	139	153	154	81.86	-5.05	-1.78	2.46
5PB4/2	40	43	52	42.75	-0.38	-8.01	1.77	49	48	60	43.82	1.89	-8.48	3.78
10Y8/4	134	138	91	82.68	-8.26	23.32	4.52	154	153	94	81.60	-9.35	25.78	3.41
2.5B8/2	119	141	143	83.45	-6.38	-2.95	2.68	137	150	155	81.13	-4.21	-3.27	4.84
7.5G8/4	103	148	130	83.71	-17.41	3.65	5.57	127	161	140	82.53	-13.83	5.11	7.19
10P6/4	98	77	98	63.42	12.64	-8.77	3.64	113	87	109	63.71	11.44	-7.87	4.37
						Mean	3.08						Mean	3.05
						Max	5.57						Max	7.19
						Min	1.24						Min	0.34
						STD	1.04						STD	1.43

Table D4 Comparison of CRI obtained from using digital images, from using spectroradiometric measurements and from using Konica Minolta illuminance spectrophotometer.

Light Soures	Colour Rendering Index (CRI)							
	Digicam							
	Canon EOS X4	Nikon D40 x	Nikon D70	Canon 600D	Canon 6D	SPD from Spectroradiometer	illuminance Spectrophotometer	Manufacturer Specification
Philips Ambience fluorescent D65 Tornado	79.2 (ΔE^*_{ab})	86.1 (ΔE^*_{ab})	85.82 (ΔE^*_{ab})	79.55 (ΔE^*_{ab})	82.02 (ΔE^*_{ab})	83.24 (ΔE^*_{ab})		
	86.63 (ΔE^*_{00})	91.16 (ΔE^*_{00})	91.02 (ΔE^*_{00})	86.4 (ΔE^*_{00})	87.82 (ΔE^*_{00})	90.95 (ΔE^*_{00})	86	80 - 89
Osram Parathom Classic LED cool white A40	77.75 (ΔE^*_{ab})	80.56 (ΔE^*_{ab})	75.98 (ΔE^*_{ab})	72.15 (ΔE^*_{ab})	70.5 (ΔE^*_{ab})	76.09 (ΔE^*_{ab})		
	85.36 (ΔE^*_{00})	89.04 (ΔE^*_{00})	86.17 (ΔE^*_{00})	81.7 (ΔE^*_{00})	81.45 (ΔE^*_{00})	87.01 (ΔE^*_{00})	73	80

VITA

Teesit Varapaskul was born in Bangkok, Thailand on 13 July 1984. He graduated a Bachelor of Science at Chulalongkorn University, major of Imaging and Printing Technology in 2007. After the graduation he worked in the short period at Chriro Company Limited in position of Hasselblad camera technician. After that he decided to further study in Master degree in the same department, supporting by the fund of National Science and Technology Development Agency (NSTDA) in Palm Paper Packaging Project, and he graduated in the year of 2009. He later worked at Clariant (Thailand) Limited in position of colorant marketing research. After the contract ended, he enrolled in the Doctoral degree in department of Imaging and Printing Technology at Chulalongkorn University by receiving THE 90th ANNIVERSARY OF CHULALONGKORN UNIVERSITY FUND (Ratchadaphiseksomphot Endowment Fund) for funding source of materials and expense related to this Ph.D. research and received fund from Chulalongkorn graduation school titled Dussadee Bundit Pue Pattana-Sat for his study.